eISSN: 3108-5202

TRANSACTIONS ON

COMPUTATIONAL MODELING AND INTELLIGENT SYSTEMS

Volume 1, October 2025

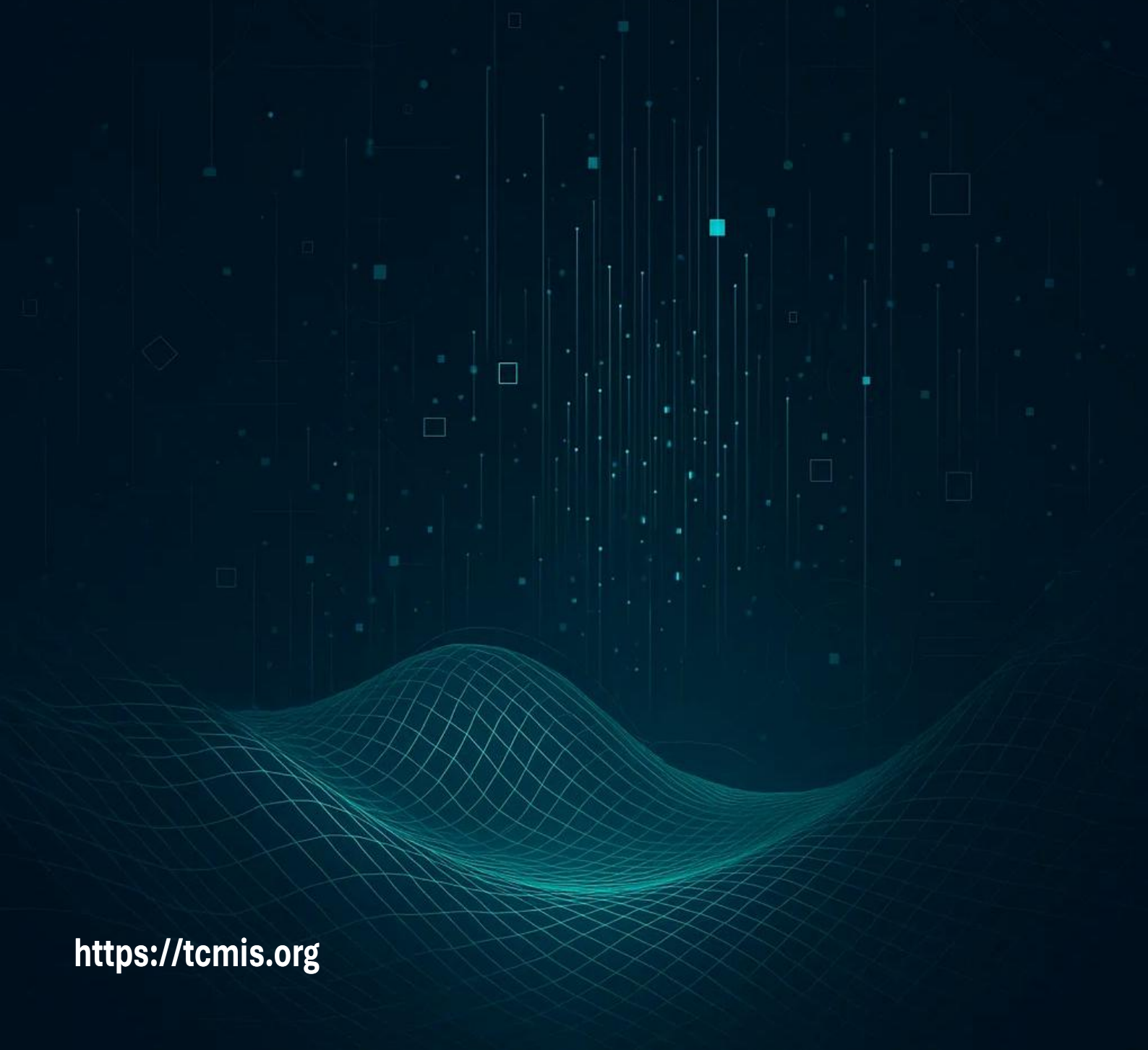

https://tcmis.org

Transactions on Computational Modeling and Intelligent Systems

Volume 1, October 2025

eISSN:

3108-5202

Editor-in-Chief:

Prof. Dumitru Baleanu, Institute of Space Sciences, Bucharest, Romania

Official Title:

Transactions on Computational Modeling and Intelligent Systems

Official Abbreviation:

Trans. Comput. Model. Intell. Syst.

Publisher:

Gülşen Yaman

Publication Period:

Quarterly (in January, April, July, October)

Webpage:

https://tcmis.org

Email:

editor@tcmis.org

Area Editors

Operational Research and Optimization

Gerhard W. Weber, Poznan University of Technology, Poland

Applied Mathematics and Control

Necati Ozdemir, Balikesir University, Turkiye
Zakia Hammouch, Moulay Ismail University, Morocco

Computational Modelling & Simulation

Guo-Cheng Wu, Chongqing University of Posts and Telecom., China

Intelligent Systems

Mukund N. Janardhanan, University of Warwick, United Kingdom

Editorial Board *(in alphabetical order)*

Ravi P. Agarwal, Texas A&M University-Kingsville, USA
Amar Debbouche, Guelma University, Algeria
Zakia Hammouch, Moulay Ismail University, Morocco
Hossein Jafari, Department of Mathematics, University of South Africa, South Africa
Amin Jajarmi, University of Bojnord, Iran
Mukund N. Janardhanan, University of Warwick, United Kingdom
Luis Vázquez Martínez, Universidad Complutense de Madrid, Spain
Necati Ozdemir, Balikesir University, Turkiye
Mirco Peron, NEOMA Business School, France
Anett Rácz, University of Debrecen, Hungary
Jocelyn Sabatier, Bordeaux Université, France
Achyut Shankar, Bennett University, India
Gerhard W. Weber, Poznan University of Technology, Poland
Guo-Cheng Wu, Chongqing University of Posts and Telecommunications, China

English Language Editor *(in alphabetical order)*

Dilek Inan, Izmir Democracy University, Turkiye

Abstracted & Indexed in:

Google Scholar, Harvard Hollis, OpenAIRE, Research Commons, Worldcat OCLC

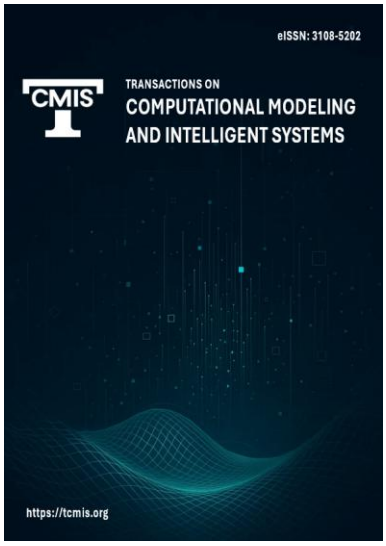

Volume 1, October 2025

Transactions on Computational Modeling and Intelligent Systems

eISSN: 3108-5202

Webpage: https://tcmis.org

CONTENTS (Article ID, Title and Authors)

Editorial

10015 A new journal on computational modeling and intelligent systems
Dumitru Baleanu

Systematic Review

10002 The logistic models and sigmoid functions: A variety of models and solution perspectives
Jordan Hristov

Research Articles

10008 Rebalancing of multi-manned mixed-model assembly lines with task relocation restrictions
Damla Camli, Ibrahim Kucukkoc, Zixiang Li

10011 Theoretical advances in two-step iterative schemes for nonlinear problems
Mudassir Shams

10013 Investigation of stability and oscillatory behavior of allelochemical influence on plants in time delay differential equation model
Mine Babaoglu, Dipesh, Pankaj Kumar

10014 Climate-based predictive modeling of malaria incidence using statistical and machine learning approaches
Oluwaseun Okundalaye, Necati Ozdemir, Bunmi Rotimi, Funmilola Akanbi

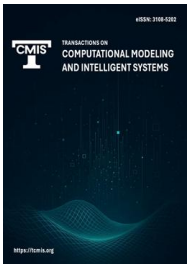

Transactions on
Computational Modeling and Intelligent Systems

Volume 1, October 2025, 10015
https://doi.org/10.65112/tcmis.10015

eISSN: 3108-5202
www.tcmis.org

EDITORIAL

A new journal on computational modeling and intelligent systems

Dumitru Baleanu

Institute of Space Sciences, Bucharest, Romania
Lebanese American University, Lebanon
Academy of Romanian Scientists, Bucharest, Romania
Email: editor@tcmis.org

The rapid development of artificial intelligence and computational technologies has initiated a radical transformation in the world of academic research and publishing. This transformation has not only increased the role of automation and intelligent algorithms but has also made the indispensable value of human thought, creativity, and interdisciplinary perspectives more evident. Particularly in the fields of system integration and intelligent systems design, the combination of computational models and human-centered thinking is more critical than ever.

This need was one of the primary motivations for the creation of the journal Transactions on Computational Modeling and Intelligent Systems (TCMIS): to provide an interdisciplinary academic platform for studies that are not limited to theoretical or algorithmic contributions but are also validated by real-world data, case studies, and industrial applications. The success of intelligent systems is determined not only by their algorithmic capabilities but also by the holistic integration of different components and the accurate modeling of the dynamics of complex systems.

In this first issue, we aim to strengthen the bridge between abstract models and practical applications by highlighting topics such as computational modeling, intelligent decision-making mechanisms, adaptive control, and simulation-based optimization. In this context, TCMIS aims to be not just a publication but a multidisciplinary forum that guides studies that will shape the future of science, engineering, and industry.

We believe that our journal will contribute to academic knowledge production and serve as an inspiring resource for researchers and practitioners.

We eagerly await all valuable contributions that will contribute to shaping this journey.

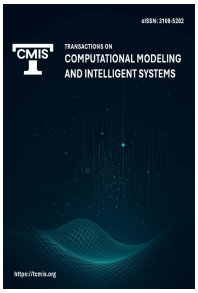

Transactions on
Computational Modeling
and Intelligent Systems

Volume 1, October 2025, Article 10002
https://doi.org/10.65112/tcmis.10002

eISSN: 3108-5202
www.tcmis.org

SYSTEMATIC REVIEW

The logistic models and sigmoid functions: A variety of models and solution perspectives

Jordan Hristov[1*]

[1]*Department of Chemical Engineering, University of Chemical Technology and Metallurgy, Sofia, Bulgaria.*
[*]*Corresponding Author. Email: jyh@uctm.edu, jordan.hristov@mail.bg (J. Hristov)*

Article Information

Received: 7 August 2025
Accepted: 1 October 2025
Published: 8 October 2025

AMS Classification:
62J12, 26A33, 34A08, 91B62

Abstract

A systematic review on logistic dynamics models and related sigmoidal functions has been developed, bringing together local and non-local interpretations. Special efforts were applied to show how non-locality can be implemented in logistic models, applying the Volterra approach and the causality concepts. An analysis of solutions of fractionalized logistic models is provided. Special attention is paid to logistic maps, both standard and fractional.

Keywords: Logistic models, sigmoidal curves, non-locality, fractional logistic models.

Contents

1. Introduction 2
2. Preliminaries: Sigmoid functions and logistic distributions 3
2.1. One-dimensional sigmoid function 3
2.2. Logistic and hyperbolic secant distributions 5
3. Growth and diffusion modeled by sigmoidal curves: Looking back at things 7
3.1. Growth curve modeling 8
3.2. Dynamic (kinetic) models of growth 8
3.3. Growth models for diffusion of products 15
4. Some computational and modeling aspects with sigmoidal functions 18
4.1. Approximations based on sigmoidal functions 18
5. Non-local approach to logistic models 20
5.1. The main idea towards the non-locality implementation 20
5.2. Non-local models based on Volterra equation of second kind 20
5.3. Other non-local formulations of the logistic model 21
6. Constructions of hereditary logistic models with fractional operators 25
6.1. Fractionalization based on the Volterra equation of second kind 25
6.2. Fractionalization based on the Volterra equation of the first kind 27
6.3. A fractionalization of the Volterra logistic model with an integral kernel: A good example 27

6.4. Fractionalization based on the causality principle 29
7. Surrogate fractional models (obtained by replacements) 30
7.1. Fractional models with singular memory kernels 31
7.2. Fractional models with non-singular memory kernels 36
7.3. Logistic dynamics in the Mittag-Leffler memory fractional framework 38
7.4. Logistic model with the Prabhakar fractional operator 42
8. Non-local operators related to the sigmoid function 44
8.1. Fractional derivative and integrals related to sigmoid function implementation 44
8.2. ψ-**Hilfer** fractional derivative: a specific case 45
8.3. Fractional derivative based on hyperbolic secant as a kernel 47
9. Discrete fractional-difference logistic equations 48
9.1. Some definitions 48
9.2. Fractional-difference logistic equation 48
9.3. Discrete fractional-difference logistic equation: Chaos 49
10. Logistic maps 50
10.1. Standard map 51
10.2. Fractional map 52
11. Final remarks 55
Acknowledgments 56
Funding 56
Conflict of interest 56
Author contributions 56
Declaration of using AI tools 56
References 56

1. Introduction

The logistic models of growth are almost 2 centuries old, starting from the seminal article of Verhulst in 1845 [1]. Their fascinating properties allow the modeling of various dynamic processes as well as fitting curves with experimental points in cases beyond the growth problems. Over the course of the last two centuries, numerous improvements and modifications have emerged. Moreover, in the modern era of the 21st century, fractional versions of the classical Verhulst model have been attacked by mathematicians. Commonly, in the literature, no studies are trying to link and compile various aspects of logistic models, starting from their basic definitions, exploring non-local versions, and other applications such as neural dynamics, control, modeling in rheology, material science, etc. One possible explanation of "separated islands of studies" could be found in the overly narrow specializations of people working with various versions of logistic models. This review is an attempt to bring together and compile closely related problems of logistic models, starting from a plethora of non-local versions with modified rate equations, through empirical modifications of the growth curves towards non-local formulations using Volterra's hereditary construction, and attempts to solve the basic logistic model (Verhulst version) in fractionalized versions. Moreover, concepts of how the local logistic models can be transformed to a non-local version and then this technology can be applied in cases when hereditaries are modeled by fractional operators are conceived.

Due to the limitations of the publication format, the focus is only on dynamic models, excluding statistical applications of logistic distributions, and applications in neural network dynamics, as well as modern trends of intelligent systems and artificial intelligence. To some extent, when considering statistical distributions, we can find similar sigmoidal behaviors. However, this is not the task of this study, and for completeness of the exposition, we refer only to two well-known distributions. (see Section 2.2). This introduction is short without exaggerating facts or historical observations because the sequel has sufficient comments, analyses, and thoughts on the topics covered.

In the end, the remarkable diversity of viewpoints, beginning with the straightforward but incredibly effective and powerful Verhulst's model and its "kids," which generated ideas in various directions and applied areas, motivated me to write this systematic review. I hope it will be a helpful source of information, establishing new connections between various fields and stimulating further research in them.

Note: In the following exposition, we try, to some extent, to unify the symbols used. However, often, this is impossible, and we especially mark such cases with comments *in original notations*. Hence, when reading equations, please focus attention on their meaning, but not on the formal use of similar or equal symbols.

2. Preliminaries: Sigmoid functions and logistic distributions

At the beginning we present the basic properties of the sigmoid function that enable further explanations of more complex problems involving it. These properties can be found in many articles and textbooks, but for the sake or clarity and well structuring of the exposition, we have to do that.

2.1. One-dimensional sigmoid function

The one-dimensional sigmoid function (hereafter named simply *sigmoid*) is a solution of the Verhulst equation (see further Eq.(35) in Section 3.2.1), namely

$$y(x) = \sigma(x, w) = \frac{e^{wx}}{1 + e^{wx}} = \frac{1}{1 + e^{-wx}} = \frac{1}{2} + \frac{1}{2}\tanh\left(\frac{x}{2}\right), \quad x \in \mathbb{R} \tag{1}$$

Note: We will use for the one-dimensional case (1) the symbol $\sigma(x)$ in contrast to all other versions of the sigmoidal family (see Section 3.2.1).

This function works in many applications, from population dynamics, where it was originally developed, to activation functions in neural dynamics [2, 3], variable transmuting parameters in transmutation transforms [4], relaxing boundary conditions in applied modeling [5, 6] and approximations in areas such as engineering and material science, where only its shape is the attractive fit to the data without any physical or modeling background (not considered here since we are oriented only towards dynamic models related to sigmoids).

From a pure mathematical point of view, $y(x) = \sigma(x)$ is a solution of the autonomous differential equation

$$\frac{dy}{dx} = y(1 - y), \quad x \in (-\infty, \infty), \quad y(0) = \frac{1}{2} \tag{2}$$

Moreover, we have the following relations satisfied by $\sigma(x)$ (for the sake of simplicity, we assume here $w = 1$)

$$\sigma(x) + \sigma(-x) = 1 \tag{3}$$

$$\lim_{x\to\infty}\sigma(x) = 1, \quad \lim_{x\to-\infty}\sigma(x) = 0, \quad \lim_{x\to 0}\sigma(x) = \frac{1}{2} \tag{4}$$

$$\int \sigma(x)\, dx = \ln(1 + e^x) + C \tag{5}$$

Note: The function $\ln(1 + e^x)$ is known as the Sofplus function [7], and the inequality $e^x - \ln(1 + e^x) > 0$ holds for all $x \in (-\infty, \infty)$.

Further, it is easy to check that

$$\sigma(x) + \sigma(y) = \sigma(x + y) \tag{6}$$

$$\frac{d}{dx}\left(\frac{d\sigma(x)}{dx}/\sigma^2(x)\right) = -e^{-x} < 0 \tag{7}$$

As well as, the Grünbaum-type inequality holds [7, 8]

$$1 + \sigma\left(z^2\right) \geq \sigma\left(x^2\right) + \sigma\left(y^2\right), \quad z^2 = x^2 + y^2, \quad x, y \in (0, \infty) \tag{8}$$

2.1.1. Derivatives of the sigmoid and its integral

The main attractive feature of the sigmoid is its monotonicity and simple form. Moreover, the form of its derivative makes its application attractive, for example, learning algorithms for back propagation (due to

the form of the lower derivatives and its Taylor series expansion). It is what follows in this section that we address the derivatives and the Taylor series expansion.

An interesting property of $\sigma(x, w)$ is that its derivatives concerning x can be written in terms of σ and w only [9], that is (for $x \in (-\infty, \infty)$)

$$\frac{d\sigma(x, w=1)}{dx} = \frac{e^x}{(1+e^x)^2} = \sigma(x)(1-\sigma(x)) \tag{9}$$

$$\frac{d^2\sigma(x, w=1)}{dx^2} = \frac{e^x(1-e^x)}{(1+e^x)^3} = \sigma(x)(1-\sigma(x))(1-2\sigma(x)) \tag{10}$$

$$\frac{d^3\sigma(x, w=1)}{dx^3} = e^x \frac{e^{2x} - 4e^x + 1}{(1+e^x)^4} \tag{11}$$

$$\frac{d\sigma(x)}{dx} = \frac{d\sigma(-x)}{dx} \tag{12}$$

$$\lim_{x\to\pm\infty}\left(\frac{d\sigma(x)}{dx}\right) = 0, \quad \lim_{x\to 0}\left(\frac{d\sigma(x)}{dx}\right) = \frac{1}{4} \tag{13}$$

$$\frac{d}{dx}\left(\frac{\sigma(x)}{x}\right) = \frac{e^{2x}}{x^2(1+e^x)^2} < 0 \tag{14}$$

and its integral were the rate constant w acts as a shifting factor (see Figure 1).

$$\int \sigma(x, w)\, dx = \int \frac{1}{1+e^{-wx}} dx = -\frac{1}{w}\ln\left(\frac{1}{1+e^{wx}}\right) \tag{15}$$

Illustrative plots of $\sigma(x)$, its integral, and its first 3 derivatives are shown in Figure 1

2.1.2. Taylor series expansion

The Taylor series expansions of (1) around x gives

$$\sigma(x+\Delta x) = \sigma(x) + \sum_{n=1}^{\infty} \frac{1}{n!}\frac{d^n\sigma}{dx^n}(\Delta x)^n \tag{16}$$

With the help of (9) and (10) it is possible to establish a recursive procedure for obtaining $\frac{d^n\sigma(x)}{dx^n}$ [9], namely

$$\frac{d^n\sigma(x)}{dx^n} = w^n\frac{d^n\xi}{dx^n}, \quad \frac{d^n\xi}{dx^n} = \sum_{k=1}^{n}(-1)^{k-1}C_k^{(n)}\sigma^k(1-\sigma)^{n+1-k} \tag{17}$$

The coefficients $C_k^{(n)}$ is equal to the Eulerian number $A_{n,k-1}$ from the recurrence

$$A_{r,q} = (q+1)A_{r-1,q} + (r-q)A_{r-1,q-1} \tag{18}$$

with integer $q, r > 0$, and therefore the Eulerian form of $d^n\xi/dx^n$ is [9])

$$\frac{d^n\xi}{dx^n} = \sum_{k=1}^{n}(-1)^{k-1}A_{n,k-1}\sigma^k(1-\sigma)^{n+1-k} \tag{19}$$

From Eq.(19) it is easy to see that with $n = 1$ we get $\frac{d\xi}{dx} = \sigma(1-\sigma)$ is what we already know. More details and analyzes are available in [9].

Remark 1 (Some versions of the sigmoids for practical use)**.** *Bearing in mind that for $x = 0$ we get $\sigma(0, w) = 1/2$ for any w, then a widely used version in the literature is the activation function [10]*

$$\sigma_{act}(x, w) = \frac{2}{1+e^{-wx}} - 1 \tag{20}$$

Moreover, a degenerate sigmoid function is defined as [11]

$$\sigma_\lambda(x) = \frac{(1+\sigma(x))^{\frac{1}{\lambda}}}{1+(1+\lambda x)^{\frac{1}{\lambda}}} = \frac{1}{1+(1+\lambda x)^{-\frac{1}{\lambda}}} = \frac{1}{2} + \frac{1}{2}\tanh_\lambda\left(\frac{x}{2}\right), \quad \lambda \in (0, \infty) \tag{21}$$

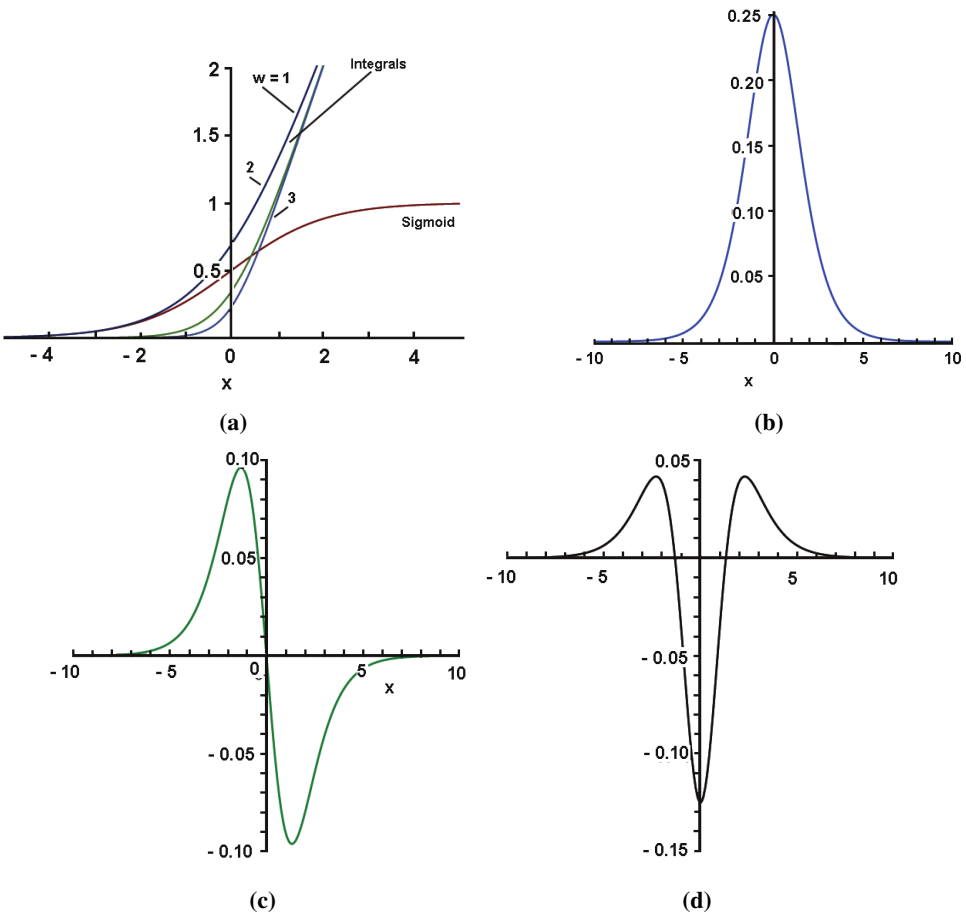

Figure 1. The sigmoid function and its integral with different values of w (a), and its first 3 derivatives: $1st$ derivative (b), $2nd$ derivative (c), and $3rd$ derivative (d), with $w = 1$.

For $\lambda \to 0$ we have $\sigma_x(x) \to \sigma(x)$.
The first derivative is

$$\frac{d\sigma_\lambda(x)}{dx} = \frac{(1+\lambda x)^{-\frac{1}{\lambda}-1}}{\left(1+(1+\lambda x)^{-\frac{1}{\lambda}}\right)^2} > 0, \quad x \in (-\infty, \infty) \tag{22}$$

The degenerate sigmoid obeys relations and inequalities to some extent, resembling those exhibited for the normal (non-degenerate) sigmoid (see more details in [11] since this problem is beyond the scope of this work).

2.2. Logistic and hyperbolic secant distributions

Here we present two distributions that, at least as formulas, resemble the logistic function. We do this especially for the sake of clarity of the exposition and to avoid confusion since they are different in nature and are applied in different fields to model data of different origins (see the Note below).

2.2.1. Logistic Distribution

The name of the logistic function is mainly taken from its cumulative distribution function (CDF) [12]

$$F_{cdf}(x,\mu,s) = \frac{1}{1+e^{-\frac{(x-\mu)}{s}}} = \frac{1}{1+e^{-(x-\mu)t}}, \quad \frac{1}{s} = t > 0 \tag{23}$$

Alternatively, it is called a hyperbolic tangent because [12]

$$F_{cdf-Log}(x,\mu,s) = 1 + \frac{\tanh\left(\frac{x-\mu}{2s}\right)}{2} = 1 + \frac{\tanh\left(\frac{x-\mu}{2}t\right)}{2}, \quad \frac{1}{s} = t > 0 \tag{24}$$

Note: As especially noted by Oliver [13], the logistic distribution should not be confused with the logistic function. The logistic distribution is occasionally used to represent data with patterns similar to the normal distribution because the ogives (the cumulative frequency polygons) are much the same.

The probability density function (PDF) is (hereafter, we prefer to use the variable t instead, s as it is more convenient in the development of further analyses in this article)

$$f_{pdf-Log}\left(x,\mu,t\right)=\frac{dF_{cdf-Log}\left(x\right)}{dx}= \\ =t\frac{e^{-(x-\mu)t}}{\left(1+e^{-(x-\mu)t}\right)^{2}}=t\frac{1}{\left(e^{\frac{(x-\mu)}{2}t}+e^{-\frac{(x-\mu)}{2}t}\right)^{2}}=\frac{t}{4}\mathrm{sech}^{2}\left(\frac{x-\mu}{2}t\right) \tag{25}$$

In the case when the location parameter μ (coinciding with the mean and the median) is zero, we get

$$F_{cdf-hypS}(x,0,t)=1+\frac{\tanh\left(\frac{x}{2}t\right)}{2} \tag{26}$$

$$f_{pdf-HypS}\left(x,0,t\right)==t\frac{e^{-xt}}{\left(1+e^{-xt}\right)^{2}}=t\frac{1}{\left(e^{\frac{x}{2}t}+e^{-\frac{x}{2}t}\right)^{2}}=\frac{t}{4}\mathrm{sech}^{2}\left(\frac{x}{2}t\right) \tag{27}$$

Plots of PDFs and CDFs of the logistic function for various parameters μ and t are shown in Figure 2.

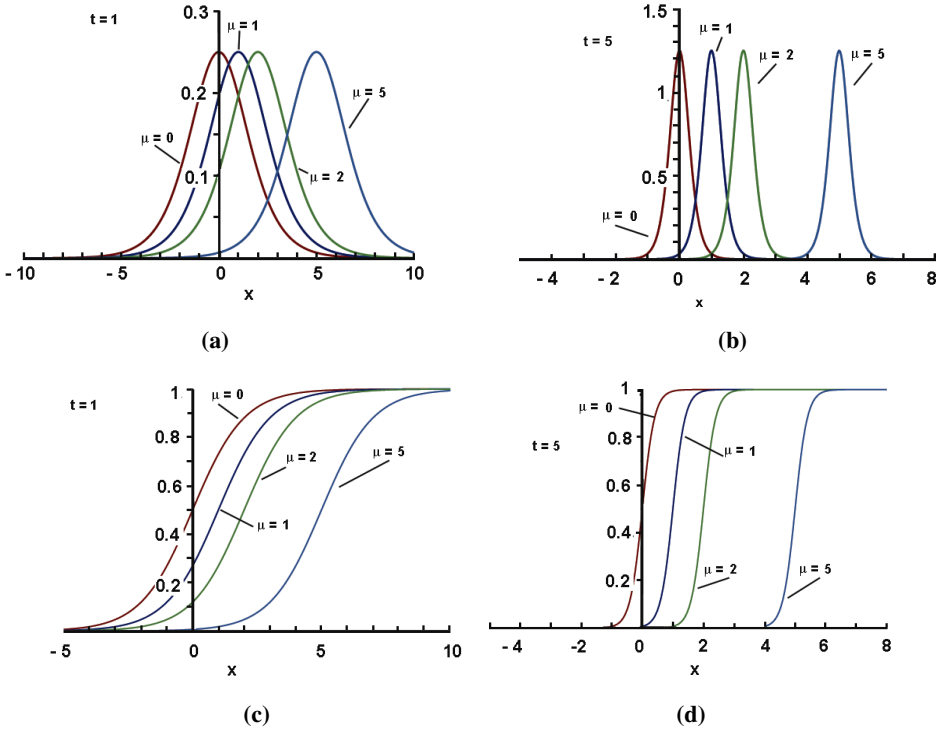

Figure 2. Logistic distributions for two values of t and various values of μ. Top raw-PDFs, Bottom raw-CDFs

2.2.2. Hyperbolic secant distribution

The hyperbolic secant distribution is a continuous probability distribution, as it is seen from the definitions (28) and (29) with PDF and CDF proportional to the hyperbolic secant function [12, 14, 15].

$$f_{pdf-\mathrm{sech}}\left(x\right)=\frac{1}{2}\,\mathrm{sech}\,\frac{\pi}{2}x \tag{28}$$

$$F_{cdf-\mathrm{sech}}\left(x\right)=\frac{1}{2}+\frac{1}{\pi}\arctan\left(\sinh\frac{\pi}{2}x\right)=\frac{2}{\pi}\arctan\left(\exp\left(\frac{\pi}{2}x\right)\right) \tag{29}$$

Here, both the median and the mean are zero (see Figure 3).

The distribution generalization can include a shifting (location) parameter μ and a scale parameter s

$$f_{pdf-\text{sech}}(x,\mu,s) = \frac{1}{2s}\,\text{sech}\left(\frac{\pi}{2}\left(\frac{x-\mu}{s}\right)\right) \tag{30}$$

$$F_{cdf-\text{sech}}(x,\mu,s) = \frac{2}{\pi}\arctan\left(\sinh\left(\frac{\pi}{2}\left(\frac{x-\mu}{s}\right)\right)\right) = \frac{2}{\pi}\arctan\left(\exp\left(\frac{\pi}{2}\left(\frac{x-\mu}{s}\right)\right)\right) \tag{31}$$

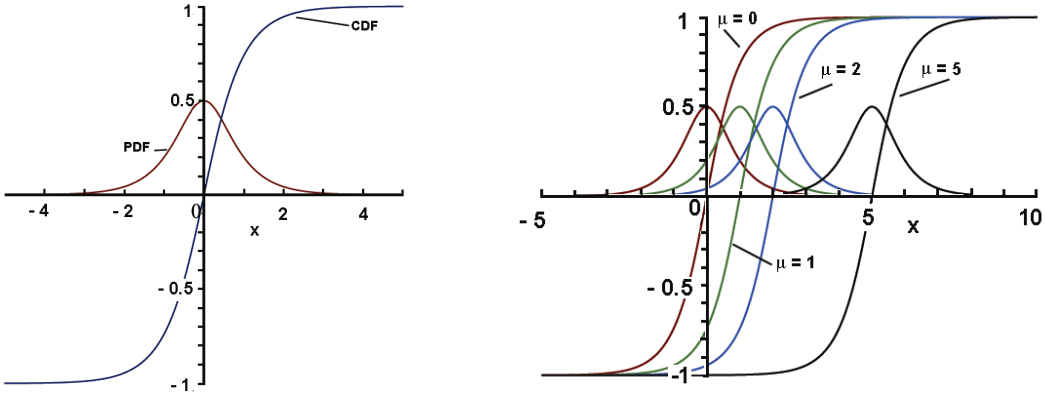

Figure 3. Hyperbolic secant distribution: (a) Non-shifted for $\mu = 0$ and (b) Shifted. In all cases $s = 1$

Remark 2 (The family of the logistic and hyperbolic secant functions)**.** *The hyperbolic secant distribution and the logistic distribution are special cases of the Chappernowne distribution [16, 17] with CDF and PDF defined as*

$$F_{cdf-Cham}(x,\mu,\lambda,x_0) = \frac{n}{\cosh(\mu(x-x_0))+\lambda}, \quad -\infty < x < \infty \tag{32}$$

$$f_{pdf-Cham}(x,\mu,\lambda,x_0) = \frac{n}{\frac{1}{2}e^{\mu(x-x_0)} + \frac{1}{2}e^{-\mu(x-x_0)} + \lambda} \tag{33}$$

because $x = \frac{1}{2}\left(e^{x} + e^{-x}\right)$ *and all parameters* μ, x_0, λ *are positive, while n it is a normalization constant. The Chapernowne distribution has a density* $f_{pdf-Cham}(x,\mu,\lambda,x_0)$ *that is symmetric concerning the median* x_0 *and exhibits a tail heavier than the normal distribution. For* $\lambda = 0$ *,* $\mu = \pi/2$ *and* $x_0 = 0$ *we get the hyperbolic secant distribution. For* $x_0 = 0$*,* $\lambda = 1$ *and* $\mu = 1$ *we get the logistic distribution*

$$f_{pdf-Cham}(x,1,1,0) = \frac{1}{2+e^{x}+e^{-x}} = \frac{e^{x}}{(1+e^{x})^{2}} = f_{pdf-Log} = \frac{dF_{pdf-Log}}{dx} \tag{34}$$

3. Growth and diffusion modeled by sigmoidal curves: Looking back at things

Many branches of applied research, including biology, economics, epidemiology, and demography, deal with growth and diffusion processes that are, in general, represented by growth curves. Diffusion can be considered a large subset of growth [18]. Since there are no natural phenomena with infinite growth, an upper limit is specified by the nature of the modeled process that finally leads to so-called S-curves, or sigmoidal curves, a term that we will use. The growths could be of two basic types: positive and negative [18]. The most well-known representatives of the positive growths are the logistic [1, 19, 20] and the Gompertz [21] models (see below).

Historically, growth modeling has been associated with some particular populations of humans or animals, virus propagation, cells, marketing, etc.(see more details in the sections developed during the course of this article). The diffusion, however, relies on the spreading of cells, viruses, people, or species in specified areas. That is, the growth is a manifestation of life or an action (process) leading to growing [18].

The main approach in growth curves to model some specific growths is the trend analysis, where fitting some known sigmoidal models is tested against experimental data collected. The methods applied in such tests are different, but the non-linear least squares fitting dominates.

3.1. Growth curve modeling

The growth is considered with the start of a natural process, exhibiting a maximum (maturity) and a final stage (death) [18]. In such processes, the describing functions are commonly referred to as sigmoid curves, but in some cases, they could be exponential curves saturating at high values of the arguments [18].

Considering a growth curve as a measure of how some quantities dominating the process increase over time. Hence, we may consider a dominant parameter or some secondary effects, but finally, we focus on the growth process. A dominant element could be birth, death, cell number, or biomass amount, exhibiting growth in time.

3.2. Dynamic (kinetic) models of growth

3.2.1. The logistic (Verhulst) model

The logistic growth law is a solution of the Verhulst [1] dynamic equation concerning the population size in time

$$\frac{dy(t)}{dt} = my(t) - ny^2(t), \quad y(0) = y_0 > 0 \tag{35}$$

where m and n are constants. Further, Eq.(35) came naturally as a solution to the Lotka model ([19]) when a growth rate is expressed as a series

$$\frac{dy(t)}{dt} = a_1 y + a_2 y^2 + a^3 y^3 + \dots \tag{36}$$

and truncated, for the sake of simplicity, at the quadratic term. The uniqueness of Eq.(35) was tested by Feller [22] and proved that the solutions (population trajectories) allow well to be fitted by either normal distribution curves with time-dependent arguments. Furthermore, Feller suggested a stochastic model describing the process as

$$\frac{dy(t)}{dt} = \left(ay(t) - by^2(t)\right) dt + c\sqrt{y(t)}dW \tag{37}$$

where $y(t)$ is a random population size time, while W denotes a standard Wiener process (all integrals related to it should be considered in the Ito sense). The random growth rate models related to the logistic model will not be further discussed here but a comprehensive analysis is available in [23].

Remark 3 (A non-conventional link of the Verhulst model to reaction-diffusion models)**.** *The Verhulst model can be considered as a diffusionless version of the so-called reaction-diffusion models (Fisher-type models [24, 25], also known as Fisher-Kolmogorov-Petrovsky-Piskunov models [26])*

$$\frac{\partial u}{\partial t} = D\frac{\partial^2 u}{\partial x^2} + mu^p - mu^{p+q} \tag{38}$$

when the spatial diffusion is neglected, that is the diffusion coefficient D in Eq.(38) is zero and the exponents p and q are set to 1*. As commented by Bacaër in Chapter 20 of [27], the initial step in Fisher's study was the equation $du/dt = au(1-u)$, where we recognize the Verhulst model. The diffusion term was added after that to account for the dispersion randomly in the neighborhood of spatial location x.*

3.2.2. Models of one-stage growths as variants of the logistic models

A more attractive approach that fits well with the context of this article is the modeling through dynamic models producing sigmoidal functions as solutions [18,28,29], resembling, to a greater extent, the solution of the Verhulst model, and we will address next some of them.

That is, considering the dynamic behavior of a certain differentiable variable $x\,(t)$, the simple kinetic (growth) equation is

$$\frac{dx\,(t)}{dt} = y\,(x)\,, \quad t > 0 \tag{39}$$

The function $y\,(x)$ should have non-negative values throughout its path, thus guaranteeing that the solution $x\,(t)$ demonstrates a sigmoidal behavior. Moreover, $x\,(t_2) \geq x\,(t_1)$, such that $\Delta x = x\,(t + \Delta t) - x\,(t) \geq 0$.

An example is the Rayleigh-Nordon (RN) equation [18, 29] (in original notations)

$$\frac{dF}{dt} = at\,(K - F\,(t)) \Rightarrow F\,(t) = K\left(1 - e^{-\frac{a}{2}t^2}\right) \tag{40}$$

As suggested by Berny [18] some factors could be of a power-law that correct the solution in a way that avoids the growth to be proportional to t^2 , that is

$$\frac{dF}{dt} = at^{w-1}\left(K - F\left(t\right)\right) \Rightarrow F\left(t\right) = K\left(1 - e^{-\frac{a}{w}t^w}\right), \quad w > 1, \quad t > 0 \tag{41}$$

Some commonly used sigmoidal models, which are variants of the powered logistic model (41), following Berny [18], commented further in this article, are, for instance:

- Logistic (auto-catalytic) model [1, 20]

$$\frac{dy}{dt} = ky\frac{(A-y)}{A} \Rightarrow y = \frac{A}{1+e^{-kt}}, \quad A = \lim_{t\to\infty} y\left(t\right), \quad t > 0 \tag{42}$$

  The growth curve is symmetrical around its point of inflexion, and its growth rate declines linearly proportional to x (see plots in Section 2)

- Monomolecular model [20]

$$\frac{dy}{dt} = p\left(A - y\right) \Rightarrow y = A\left(1 - be^{-pt}\right), \quad A = \lim_{t\to\infty} y\left(t\right), \quad t > 0 \tag{43}$$

- Brody's model [28]

$$\frac{dy}{dt} = pe^{-kt} \Rightarrow y(t) = A(1 - Be^{kt}), \quad t > 0, \quad p = ABk = \left(\frac{dy}{dt}\right)_{t=0}, \quad A = lim_{t\to\infty} y(t) \tag{44}$$

- Gompertz's model [20, 21]

$$\frac{dy}{dt} = ky\ln\left(\frac{A}{y}\right) \Rightarrow y = Ae^{-be^{-kt}}, \quad A = \lim_{t\to\infty} y\left(t\right), \quad t > 0 \tag{45}$$

  This growth curve, to some extent, resembles the logistic, but it is asymmetrical.

- Richards's model [20]

$$\frac{dy}{dt} = \frac{k}{s}y\left(1 - \left(\frac{y}{s}\right)^s\right) \Rightarrow y = \frac{k}{\left(1 + se^{(b-kt)}\right)^{1/s}}, \quad t > 0 \tag{46}$$

- Weibull model [30, 31]

$$\frac{dy}{dt} = sk^{1/s}\ (k-y)\left(\ln\frac{b}{k-y}\right)^{\frac{s-1}{s}} \Rightarrow y = k - be^{kt^s}, \quad t > 0 \tag{47}$$

- Morgan-Mercer-Flodin model [32, 33]

$$\frac{dy}{dt} = sk\left(k-b\right)\left(\frac{y-b}{k-b}\right)^{\frac{s-1}{s}}\left(1 - \frac{y-b}{k-b}\right)^{\frac{s-1}{s}} \Rightarrow y = \frac{b + k(pt)^s}{1 + (pt)^s}, \quad t > 0 \tag{48}$$

All parameters k, b, s, p in these growth models are positive constants.

Systematic analyzes of growth curves of the sigmoid family are available in [34–38] and other studies not quoted here. We refer also to the work of Savageau [41] where a general formulation and a survey of special cases are systematically developed.

3.2.3. Attempts to generalizations of the logistic model: The rate equation reconsidered

In most cases when complex systems and derived data have to be modeled, attempts to modify and generalize the logistic curve of growth have been carried out. Here, we will present some examples in this direction.

- Turner et al. model [42]

This model suggests the dynamic equation of growth as

$$\frac{dy}{dt} = \beta x\left(\frac{\phi\left(k\right) - \phi\left(y\right)}{\phi\left(k\right)}\right) \tag{49}$$

with proportional constant (intrinsic growth coefficient as defined in [42]) β to the population y.

The number of available spaces depends on the monotonically increasing function $\phi(.)$ of the population size [42]. If $\phi(.)$ it is the identity (i.e., a function mapping any variable into itself) we have $\phi(x) = x$ and we get the original logistic equation of Verhulst.

Turner et al. [42] suggested a power-law function $\phi(.)^m$ with a positive exponent $m > 0$ that led to

$$\frac{dy}{dt} = \beta k^{-m} x \left(k^m - y^m\right) \tag{50}$$

The integration of Eq. (49) yields a solution

$$y = \frac{k}{\left[1 + \left(\left(\frac{k}{y_0}\right)^m - 1\right) e^{-\beta m t}\right]^{\frac{1}{m}}} \tag{51}$$

A version known as a *generic model* was also developed by Turner et al. [43] where the rate equation is formulated as (in the original notations)

$$\frac{dy}{dt} = \frac{\beta}{k^n} x^{1-np} \left(k^n - y^n\right)^{1+p} \tag{52}$$

and the solution is

$$y = \frac{k}{\left\{1 + \left[1 + \beta n p \left(t - \tau\right)\right]^{-\frac{1}{p}}\right\}^{\frac{1}{n}}} \tag{53}$$

with τ as a constant of integration. In the special case where $p \to 0$ the model reduces to the construction of Richards [20]. It was discussed by Nelder [44] and can be expressed as

$$y = \frac{k}{\left[1 + e^{-\beta n (t-\tau)}\right]^{\frac{1}{n}}} \tag{54}$$

This is the same as Eq.(56) simply replacing n by $1/m$.

- Nelder's model [44]

Alternatively, Nelder [44] assumed that $\frac{1}{y^m}\left(\frac{dy}{dx}\right)^m = m\frac{1}{y}\frac{dy}{dx}$ and this allowed Eq.(50) to be transformed to the ordinary logistic equation in y^m. With some details, Nelder considered the equation (expressed in the common notations used here)

$$\frac{dy}{dt} = k y \left[1 - \left(\frac{y}{A}\right)^{\frac{1}{m}}\right] \tag{55}$$

With $m > 0$ the solution to Eq.(55) can be written as

$$y = \frac{A}{\left[1 + e^{-\left(\frac{\lambda + kt}{m}\right)}\right]^m} \tag{56}$$

with a constant of integration λ.

Further, A and k are positive because $y(t)$ increases monotonically in time. From Nelder's solution, it follows that $y^{1/m}$ satisfies the logistic equation, and the upper asymptote (for $t \to \infty$) is $A^{1/m}$.

The common problem in logistic law constructions is the definition of the coefficient k, which denotes the maximum of the population size (the plateau of the sigmoid curve). If we assume that the maximum population is a constant over a certain period, then considering a more global case suggests that we have a time-dependent $k(t)$ upper limit of the population growth; this physically means that the population growth passes through several steps (several saturations) towards the maximum of $k_{\max} = K$. Thus, the time-dependent $k(t)$ can be expressed as [42]

$$k(t) = \frac{K}{\left(1 + \alpha e^{Bmt}\right)^{\frac{1}{m}}} \tag{57}$$

As a result, the integration of Eq. (50) yields

$$y = K\left[1 + \left(\left(\frac{K}{y}\right)^m - 1 - \frac{\alpha\beta}{\beta - B}\right) e^{-\beta m t} + \frac{\alpha\beta}{\beta - B} e^{-Bmt}\right]^{\frac{1}{m}} \tag{58}$$

For $m = 1$, $\alpha = 0$ (or $B \to \infty$) Eq.(57) reduces to the ordinary logistic growth curve; with $m = 1$ and $B = 0$, the result is also a logistic curve but with modified constants.

- Levenbach's model [45]

Levenbach [45] addressed a generalization of the logistic models using the preceding model of Hotelling [46] where both the relative growth rate $\frac{1}{y}\left(\frac{dy}{dt}\right)$ and y (as a variable, an increasing monotone function) are related as

$$\frac{1}{y}\left(\frac{dy}{dt}\right) = \frac{d}{dt}\ln y\,(t) \tag{59}$$

Then, expressing the relative growth rate as a Taylor series about y and truncating to the first order term, we get

$$\frac{1}{y}\left(\frac{dy}{dt}\right) = a + by\,(t) \tag{60}$$

and the solution is the ordinary logistic curve.

Further, Levenbach [45] did a step ahead, considering the model (60) as a particular case of the Riccati equation

$$\frac{dy}{dt} = ay + by^2 + c \tag{61}$$

with a solution [45]

$$y\,(t) = \frac{(d+a) - C\,(d-a)\,e^{-dt}}{-2b\left(1 + Ce^{-dt}\right)} = \left(\frac{d+a}{d-a}\right)\frac{\left(1 - Ce^{-dt}\right)}{-2b\left(1 + Ce^{-dt}\right)} \tag{62}$$

were $d = \sqrt{a^2 - 4bc} > 0$, $b < 0$ and C as integration constant.

All solutions expressed as Eq.(62) can be presented as

$$y\,(t) = C + \frac{M}{1 + Ke^{-dt}}, \quad M = -\frac{d}{b}, \quad C = \frac{d-a}{2b} \tag{63}$$

From the result (63) it follows that the solution is bounded from below by $(d-a)/2b$ and attains a saturation for $-(a+d)/2b$

Since the solution of the Riccati model can start at zero initial state, it is convenient to model the so-called *diffusion growths of things*, such as spreading of telephones, cars, and other stuff in technological forecasting and marketing (see Section 3.3).

- Blumberg's model [47]

The Blumberg model [47] considers a rate equation as

$$\frac{dy}{dt} = ky^a(y_\infty - y)^b \Rightarrow \frac{dy}{dt} = k\frac{y^a}{y_\infty^b}\left(1 - \frac{y}{y_\infty}\right)^b \Rightarrow \int \frac{dy}{y^a(1-y)^b} = ky_\infty^{a+b-1}t + C \tag{64}$$

with the inflexion point at $y_{\inf}/y_\infty = a/(a+b)$ and C as a constant of integration.

For $1 - np = 2 - b$, $\beta = 1$ and $b < 2$ this model is consistent with the generic model of Turner et al. [43]. Also, for $a = b$ we get the Verhulst model.

The Blumberg model has not analytical solutions but the last version (the integral equation) allowed to formulate the function $F\,(b, a; y) = \int \frac{dy}{y^a(1-y)^b}$ with $F\,(a, b; y) = -F\,(a, b; 1-y)$. This allowed to create a set of special cases when analytical solutions are possible (see [47] and the analysis in [38]).

A growth form of the Blumberg type, in a hyperbolic form, represented by a sigmoid curve to a regenerative growth, was developed by Spencer and Coulombe [39] (see also comments of Tsoularis and Wallace in [38]).

$$\frac{dy}{dt} = ry^{\left(1-\frac{1}{n}\right)}\left(1 - \frac{y}{y_\infty}\right)^{\left(1+\frac{1}{n}\right)} \Rightarrow, \quad \frac{y\,(t)}{y_\infty} = \frac{(t+a)^n}{b + (t+a)^n}, \quad r = n\left(\frac{y_\infty}{b}\right)^{\frac{1}{n}} \tag{65}$$

where y_∞ is the final value and a, b, n are positive parameters. The inflexion point is $y_{\inf}/y_\infty = (n-1)/2n$.

- Tsoularis-Wallace model [38]

Tsoularis and Wallace [38] formulated a generalized logistic rate equation (autonomous equation)

$$\frac{dy}{dt} = ry^{\alpha}\left[1 - \left(\frac{y}{y_{\infty}}\right)^{\beta}\right]^{\gamma} \tag{66}$$

where α, β, γ are positive constant and $y_{t\to\infty} \to y_{\infty}$ (the carrying capacity). From (66) the relative growth rate attains its maximum at

$$\left(\frac{1}{y}\frac{dy}{dt}\right) = y_{\infty}\left(1 + \frac{\beta\gamma}{\alpha - 1}\right)^{-\frac{1}{\beta}} \tag{67}$$

The change in the variable as $x = (y/y_{\infty})^{\beta}$ allows Eq. (66) to be transformed as

$$\frac{dx}{dt} = \beta r y_{\infty}^{\alpha-1} x^{\frac{(\alpha-1)}{\beta}+1}(1-x)^{\gamma} \tag{68}$$

A detailed solution via separation of variables is available in [38] and we will skip its cumbersome expressions and relevant analyses.

It is important to note that in [38], there are systematic comparative analyses of known logistic models. Some of these models are discussed here, while others are not. This analysis, with many illustrative plots, facilitates a better understanding of the areas where different approaches compete to establish suitable models.

- Logistic model with a polynomial rate [40]

The idea of a polynomial rate function in the Verhulst model, earlier conceived empirically by Pearl and Reed (1922) [55] (see further Eq.(78) in Section 3.2.4) was explored by Kyurkchiev et al. in [40].

The starting model is the reaction network $S + X \overset{k=const.}{\to} 2X$ modified as

$$S + X \overset{k(t)}{\to} 2X, \quad k(t) = \sum_{i=0}^{n} b_i t^i \tag{69}$$

For example, the case with $n = 2$ is [40]

$$\begin{cases} \dfrac{ds}{dt} = -\left(b_0 + b_1 t + b_2 t^2\right) sx \\ \dfrac{dx}{dt} = \left(b_0 + b_1 t + b_2 t^2\right) xs \end{cases}, \quad s_0 = s(0), \quad x_0 = x(0) \tag{70}$$

For $s_0 = 1/2$, $x_0 = 1/2$ and with $ds/dt + dx/dt = 0$, the results is $s + x = C_{sx}$, where $C_{sx} = s_0 + x_0$. Then, the model (70) becomes [40]

$$\begin{cases} \dfrac{ds}{dt} = -\left(b_0 + b_1 t + b_2 t^2\right) s(1-s) \\ \dfrac{dx}{dt} = \left(b_0 + b_1 t + b_2 t^2\right) x(1-x) \end{cases} \tag{71}$$

and the solutions are [40]

$$s(t) = \frac{e^{-\left(b_0 t + \frac{b_1}{2}t^2 + \frac{b_3}{3}t^3\right)}}{1 + e^{-\left(b_0 t + \frac{b_1}{2}t^2 + \frac{b_3}{3}t^3\right)}}, \quad x(t) = \frac{1}{1 + e^{-\left(b_0 t + \frac{b_1}{2}t^2 + \frac{b_3}{3}t^3\right)}} \tag{72}$$

In general, for $n > 2$ we have [40]

$$s(t) = \frac{e^{-\left(b_0 t + \frac{b_1}{2}t^2 + \frac{b_3}{3}t^3 + \ldots \frac{b_n}{n+1}t^{n+1}\right)}}{1 + e^{-\left(b_0 t + \frac{b_1}{2}t^2 + \frac{b_3}{3}t^3 + \ldots \frac{b_n}{n+1}t^{n+1}\right)}}, \quad x(t) = \frac{1}{1 + e^{-\left(b_0 t + \frac{b_1}{2}t^2 + \frac{b_3}{3}t^3 + \ldots \frac{b_n}{n+1}t^{n+1}\right)}} \tag{73}$$

3.2.4. Attempts to generalizations of the logistic model: Logistic curve manipulations

- *Two-stage growth (Bi-logistic)*

Meyer [48] considers processes where the carrying capacity, such as in the simple logistic, is not constant but can change as the process evolves, that is, the monitored species at issue expand their niche (habitat). Therefore, there are two processes of logistic growth appearing consequently (as cascades) or in parallel.

This is the so-called Bi-logistic model defined as (in the original notations)

$$N(t) = \frac{k_1}{1 + \exp\left[\frac{\ln(81)}{\Delta t_1}(t - t_{m1})\right]} + \frac{k_2}{1 + \exp\left[\frac{\ln(81)}{\Delta t_2}(t - t_{m2})\right]} \tag{74}$$

as a superposition of two three-parameter logistic models, where $t_{m1}$and t_{m2} denote the upper times (the points of saturations) of each one-stage logistic sub-model.

A similar approach was used by Tissen et al. [49] with

$$y = \frac{a_1}{1 + \exp\left[-b_1(t - c_1)\right]} + \frac{f - a_1}{1 + \exp\left[-b_2(t - c_2)\right]} \tag{75}$$

For more details about the model parameters, meaning, and the asymptotic behavior of this model, we refer to section 2 in [49].

A close approach was applied by Jolicoeur and Pontier [50] with

$$N(t) = \frac{1}{C_1 e^{t/D_1} + C_2 e^{-t/D_2}}, \quad t > 0 \tag{76}$$

where the first exponential term with the rate constant $1/D_1$ corresponds to the population decrease, while the second one, with a rate constant $1/D_2$, measures to the population growth.

For $C_1 = 0$ we get an exponential growth model ; For $D_1 \to \infty$ (too large values) the model approaches the logistic curve. For $C_2 = 0$ we get an exponentially decreasing curve. For $D_2 \to \infty$ we get a logistically decreasing curve. A good analysis and design issues concerning data fitting with Eq. (76) were performed by Fidalgo et al. [51].

The Bi-logistic models can be considered as an attempt to decompose the overall growth process into one-stage (fine-grained) logistic sections following the idea developed in [52] . Modis [52] developed the idea of the analysis of any growth process in terms of sub-processes (cascades). The idea came from the Fourier analysis, the so-called “logistic harmonics”; an old mathematical concept that is frequently used to describe a function as a sum of terms that belong to a particular class of functions.

- Triple-logistic function

As an extension of the idea to create multi-term logistic functions, we refer to Bock and Tissen [53] (in the original notations)

$$y = \alpha\left(\frac{1 - p}{1 + \exp\left[-a(t - b)\right]} + \frac{p}{1 + \exp\left[-c(t - d)\right]}\right) + \frac{\beta}{1 + \exp\left[-b(t - g)\right]} \tag{77}$$

where $a, b, c, d, f, g, p, \alpha, \beta$are parameters; $t$is age (the time of individual growth).

An analysis of the accuracy and data fitting problems of Bi-logistic and Triple-logistic was performed by Fujii [54].

- *Pseudo-logistic model with a polynomial approximation of the growth exponents*

Following Pearl and Reed [55] the expression can be consequently transformed as

$$y = \frac{be^{ax}}{1 + ce^{ax}} \Rightarrow y = \frac{b}{c + e^{-ax}} \Rightarrow \frac{k}{1 + me^{k_a x}}, \quad k = b/c\,, \quad m = 1/c\,, \quad k_a = -a \tag{78}$$

and the dynamic equation of the rate of change dy/dx is

$$\frac{dy}{dx} = -k_a y(k - y) \tag{79}$$

Taking into account that the growth rate dy/dx is dependent on factors that are functions of x (in many cases, the variable x is the time), the factor k_a can be assumed as a function of x, too. Then, denoting, still an unknown, function $f_k(x)$ instead of k_a the rate equation can be expressed as

$$\frac{dy}{y(k - y)} = -f_k(x)\,dx \tag{80}$$

which is a separable equation with a solution

$$y = \frac{k}{1 + m^{-kF_k(x)}}, \quad F_k(x) = \int f_k(x)\,dx \tag{81}$$

Then, the principal step is to replace ax in (78) by $F_k(x)$ expressing it as a Taylor series. This step leads to

$$y = \frac{k}{1 + m\exp\left(a_1x + a_2x^2 + a_3x^3 \cdots a_nx^n\right)} \tag{82}$$

For $a_{i>1} = 0$, the model reduces to (78).

The approach increases the number of parameters that should be determined through the data fitting procedure; it was assumed to limit the number of terms in the Taylor series up to three, that is

$$y = \frac{k}{1 + m\exp\left(a_1x + a_2x^2 + a_3x^3\right)} \tag{83}$$

with $a_3 < 0$ in the case of growth and $a_3 > 0$ the case of decay.

As pointed in [55], the relation (83) results in curves resembling in shape the ordinary logistic curve, that is, there are no maximum and minimum points, but only a point of inflexion.

Buis [56] considered and analyzed this purely empirical modification of the logistic model and showed that *posteriori* assumption about the specific growth rate is

$$\frac{1}{y}\frac{dy}{dx} = k(x)(A - y)\left((1 - \frac{y}{A}\right) = c(t)\left(1 - \frac{y}{A}\right) \tag{84}$$

where $c(t) = Ak(t) = -df_k/dt$ is a polynomial with strictly positive real values, at least at $t > 0$.

With the case when $f_k(x)$ is cubic, as result of the sign change of a_3 in (83), we get $c(t)$ increasing and then decreasing: as result the rate equation is then a product of two quadratic polynomials in t and in y, namely

$$\frac{dy}{dt} = (-a_1 + 2a_2t - 3a_3t^2\left(1 - \frac{y^2}{A}\right) \tag{85}$$

In addition, there is a left-hand dissymmetry of the growth curve exists for $y < A/2$ [56] that breaks that well-established symmetry of the original logistic model.

In practical applications to fit data from engineering experiments, some versions of the sigmoid functions, or close to them, are widely used. Here we consider versions where the equation of the logistic curve (the CFD in terms of distributions) is modified (see many examples in [57]),among them:

- *Cumulative normal curve* [62, 63]

In the early studies on diffusions, the shape of the cumulative normal curve was widely used because its shape resembles that of the logistic curve (see Figure 7-3 in [63], see also [57])

$$X(t) = a\int_{-\infty}^{t}\frac{1}{\sqrt{2\pi\sigma}}\exp\left(-\frac{y-\mu}{2\sigma^2}\right)dy + \varepsilon(t) \tag{86}$$

where σ is the dispersion (do not mix it with $\sigma(t)$ used to denote the sigmoid function), and $\varepsilon(t)$ is a stochastic term.

- *Cumulative log-normal curve* [58] (see also [57] for comments)

$$X(t) = a\int_{0}^{t}\frac{1}{y}\frac{1}{\sqrt{2\pi\sigma}}\exp\left[-\frac{(\ln y - \mu)^2}{2\sigma^2}\right]dy + \varepsilon(t) \tag{87}$$

This resembles the Gompertz curve and is asymmetric.

In both (86) and (87), for a given μ, the value of σ controls the point of inflection (see, for example, similar effects in the preceding section about the logistic distribution).

- *Log-logistic curve* [59]

The replacement of time t by $\ln(t)$ leads to an asymmetric curve about the inflexion point, namely

$$X(t) = \frac{a}{1 + c\exp(-b\ln(t))} + \varepsilon(t) \tag{88}$$

The inflection point appears earlier than the cumulative sales reach half of the saturation level (the model (88) is related to the diffusion of products discussed in Section 3.3).

- *Non-symmetric responding curve* [60]

$$X(t) = \frac{a}{1 + c\exp\left(-bX^{\delta}t\right)} + \varepsilon(t) \tag{89}$$

where δ is a *non-uniform influencing factor*.

- *Flexible logistic curve (FLOG)* [61]

This is a four-parameter generalization of the logistic curve, and it is general enough to vary the position of the inflexion point between the top and the bottom bounds, as well as being symmetric about it [57]. On its basis, several models have been generated (see [57]), namely:
Inverse power transformation

$$X(t) = \frac{a}{1 + c\exp\left[-b(1+kt)^{\frac{1}{k}} - 1\right]} + \varepsilon(t) \tag{90}$$

Exponential logistic

$$X(t) = \frac{a}{1 + c\exp\left[-b\frac{\exp(kt-1)}{k}\right]} + \varepsilon(t) \tag{91}$$

Box-Cox transformation

$$X(t) = \frac{a}{1 + c\exp\left[-b\frac{(1+t)^{k}-1}{k}\right]} + \varepsilon(t) \tag{92}$$

As commented in [57], the choice of a given model to be applied depends on the log-likelihood, which should be higher than that of the others, and the requirement not to be degenerate.

3.3. Growth models for diffusion of products

Here we address applications of dynamic models that result in equations close to the logistic one, but are not related to biological populations. The common term for such models is *diffusion models*, which refers to the *diffusion (spreading) of technological innovations* or *logistic models for forecasting* [62], popularly known as *Bass models* [64–73]

Remark 4 (Diffusion of products: Rogers' definition [62])**.** *It is noteworthy to mention that the use of the term diffusion should be considered as spreading or increasing the population of something non-biological, such as goods, products, ideas, etc., and there is no spatial diffusions as in the well-known Fick or Fourier models of mass and heat diffusion. Here we provide two definition of Rogers [62] that will clarify the exposition.*

- *Chapter 1 in [62](p.5): Diffusion is the process by which an innovation is communicated through certain channels over time among the members of a social system. It is a special type of communication, in that the messages are concerned with new ideas. Communication is a process in which participants create and share information with one another in order to reach a mutual understanding. This definition implies that communication is a process of convergence (or divergence) as two or more individuals exchange information in order to move toward each other (or apart) in the meanings that they ascribe to certain events.*
- *Chapter 6 in [62] (pp.234-235): The diffusion effect is the cumulatively increasing degree of influence upon an individual to adopt or reject an innovation, resulting from the activation of peer networks about an innovation in a social system. For example, when only 5 percent of the individuals in a system are aware of a new idea, the degree of influence upon an individual to adopt or reject the innovation is quite different from when 95 percent have adopted. In other words, the norms of the system toward the innovation change over time as the diffusion process proceeds, and the new idea is gradually incorporated into the livestreams of the system.*

Note: Following Trajtenberg and Yitzhaki [74], historically, the use of the logistic in diffusion studies is a clear case of methodological *spill-over* from other disciplines, primarily from Biology (e.g., bio-assay) and Population Studies.

The analysis of the Bass model (Section 3.3.2) follows the direct application of the Riccati equation (Section 3.3.1) in the remainder of this section.

3.3.1. The Riccati equation applications

As mentioned by Levenbach [45], the first attempt to apply the Riccati equation to model a logistical growth curve of diffusion of Centrex telephones (a business customer telephone service introduced in 1961) in the 60s of the last century was done by Oliver [13] covering the period from 1961 till 1971.

Oliver's model is a Riccati equation (in the original notations)

$$R_t = \frac{dy(t)}{dt} = \alpha + \beta y(t) + \frac{\gamma}{y(t)} + \varepsilon(t) \tag{93}$$

where α, β and γ are empirical coefficients of effects, while $\varepsilon(t)$ denotes the statistical error.

The data fitting of Oliver's model to populations of cells [45] (the first application of this model to biological populations) yielded (the source data and the data fitting details are available in Table 3 of [45]) a logistic growth equation

$$y(t) = \frac{6452}{1 + 6.90e^{-2.36t}} - 616, \quad t = 1, 2, \ldots 10 \tag{94}$$

Levenbach [45] applied the method of Erkelens [75] and the technique presented previously in Section 3.2.3.

3.3.2. The Bass diffusion model of growth

The Bass model [64, 65] was based on the following assumptions:

- The initial product purchases are made by both *innovators* and *imitators*, and the difference between these two groups is *the buying influence*.
- The importance of innovators will be greater at the beginning but will vanish with time.
- In the following formulations, the coefficients and refer to the *coefficient of innovators* and the *coefficient of imitators*, respectively.

Therefore, the likelihood (the chances) of purchase $f(T)$ at time T given that *no purchase has not been made* is

$$\frac{f(T)}{1 - F(T)} = P(T) = p + \frac{q}{mY(T)} = p + qF(T) \tag{95}$$

with the integral condition $F(T) = \int_0^T f(t)dt$ and initial condition $F(0) = 0$.

The density function $Y(T)$ is constructed as an integral of the sales $S(t)$ over the interval $t \in [0, T]$, namely

$$Y(t) = \int_0^T S(t)dt = m\int_0^T f(t)dt = mF(T) \tag{96}$$

as the total number of product purchases from $t \in [0, T]$.

Then, the sales at $t = T$ are

$$\begin{aligned} S(T) = mf(T) = P(T)[m - Y(T)] = \left(\left[p + \frac{1}{m}q\int_0^T S(t)\,dt\right]\left[m - \int_0^T S(t)\,dt\right]\right) = \\ = pm + (q - p)Y(T) - \frac{q}{m}Y^2(T) \end{aligned} \tag{97}$$

The Bass model can be reformulated as [64]

$$\frac{1}{1 - F(t)}\frac{dF(t)}{dt} = p + qF(t), \quad F(0) = 0 \tag{98}$$

and expressed as an ordinary differential equation (as a Riccati equation-see the last version in Eq. (99))

$$\frac{dF(t)}{dt} = p(1 - F) + qF(1 - F) = p - F(p - q) - qF^2 \tag{99}$$

The analytical solution is

$$F(t) = \frac{1 - e^{-(p+q)t}}{1 + \frac{q}{p} e^{-(p+q)t}}, \quad F(0) = 0 \tag{100}$$

For the parameter mapping, Bass [64] suggested the case $p > q$, leading to a positive peak in time (for $p < q$ the peak is negative). Under this condition, the periodic sale peak is [64]

$$t^* = \frac{1}{p+q} \ln\left(\frac{q}{p}\right) \tag{101}$$

The inflection points are (two inflection points exist) [76]

$$t^{**} = \frac{\ln\left(\frac{q}{p}\right) - \ln\left(2 \pm \sqrt{3}\right)}{p+q} = t^* \pm \frac{\ln\left(2 \pm \sqrt{3}\right)}{p+q} \tag{102}$$

Hence, the time between the inflection point t^{**} and the peak t^* depends only on $(p+q)$ but not on p/q [76].

When the interest in the new products (goods, technologies, ideas,faxes, cellular phones, etc.) is low, the minimal limit (the initial condition) $F_{\min}(t) = F_0$ is assumed to be kept at $F_0 \approx |p|/q$ (if F_0 is higher, then the seed (the initial product release on the market) to the market is larger [76].

A cumulative adoption of the peak in time with seeding was developed by Jain et al. [77], with $F_0 \neq 0$, as

$$F(t) = \frac{1 - \frac{p(1-F_0)}{p+qF_0} e^{-(p+q)t}}{1 + \frac{q(1-F_0)}{p+qF_0} e^{-(p+q)t}} \tag{103}$$

$$t^* = \frac{1}{p+q} \ln\left[\frac{q(1-F_0)}{p+qF_0}\right] \tag{104}$$

With initial seeding on the market, i.e. for $F_0 = 0$ the model and its solutions, reduce to original Bass model. In addition, taking into account that Eq. (102) is valid for $p < 0$, then the condition to have two inflection points is [76]

$$\frac{q(1-F_0)}{p+qF_0} > 2 + \sqrt{3} \tag{105}$$

This condition is completely obeyed when the seed size $F_0 \approx |p|/q$ for any q/p [76] (Orbach summarizes 7 regions of q/p in Table 2 of his work with corresponding boundaries,peak, inflexion points and equilibrium).

The practical meaning of these results is that positive p can be released and at the same time, at least $F_0 \approx |p|/q$ the amount of goods is crucial for starting the market (that is, an initial critical mass is needed to start the product diffusion-see the following Remark 5). Moreover, for $p > |q|$ the product market will attain its 100 % potential in the long range of time (for regular values of $q > 0$). However, for $p < |q|$ the long-range prediction for cumulative sales follows from Eq.(100) as $F(t \to \infty) \to p/|q|$ [76]. Some computer simulations are presented in Figure 4: we can see the low level saturations for cases when $q < 0$ and the vertical shifts for cases with $F_0 \neq 0$.

Remark 5 (The critical mass appearance)**.** *According to Rogers [63], the critical mass occurs at the point at which enough individuals in a system have adopted an innovation so that the innovation's further rate of adoption becomes self-sustaining. For more detailed and expanded explanations, we refer to the 5th edition of the Rogers' book [63].*

The Bass model presents challenges related to data fitting, primarily due to the application of nonlinear least squares methods (see [78, 79] and the references therein). Although this issue is beyond the scope of this work, we must mention it for the sake of completeness in our exposition.

At the end of this section we refer to an extension of the model (98) as [66]

$$\frac{1}{1 - F(t)} \frac{dF(t)}{dt} = [p + qF(t)]\, x(t) \tag{106}$$

where the function $x(t)$ relies on percentage change in price and other emerging variables.

In contrast to the analytic solution of the original Bass model, the extended version (106) has no analytical solution and numerical procedures were applied [76].

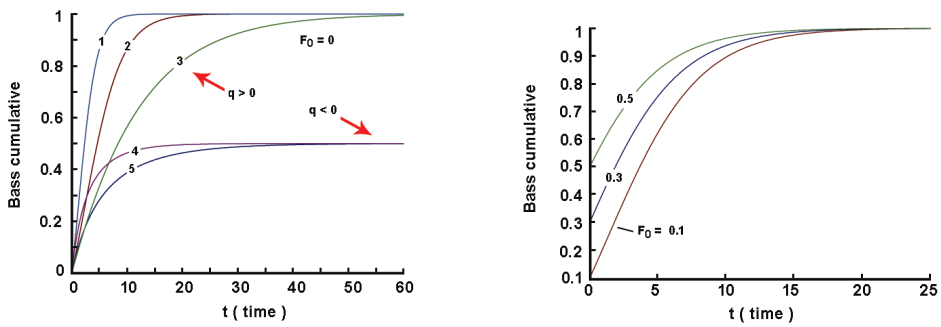

(a) **(b)**

Figure 4. Simulations of the Bass cumulative curve (the parameters p and q are taken from [76], but the plots are created by the author): (a) For $F_0 = 0$: 1-$p = 2, q = 0.4$; 2-$p = 0.1, q = 0.2$; 3-$p = 0.08, q = 0.01$; 4−p=0.1, $q = -0.2$; 5-$p = 0.1, q = -0.2$ and (b) $p = 0.1, q = 0.2$, and $F_0 \neq 0$:(the values of F_0 are chosen arbitrarily, only to show the effect on the separation of the plots.)

4. Some computational and modeling aspects with sigmoidal functions

Since the solutions of the analyzed logistic models revealed numerous sigmoidal functions, it is reasonable to question the computations involved, the related computational techniques, and the approximations that resulted from these applications. In this section, we credit [80–83] and many examples are available in [84]. We try only to show what happens and what can be found beyond the sigmoidal solutions; this is not a complete exposition of the computational problems but only a part of this study contributing to the coherence and more harmonic presentation.

4.1. Approximations based on sigmoidal functions

Now, we focus the attention on approximations based on the sigmoidal function and the computational problems thereof.

4.1.1. The logistic function

- Step (Heaviside) function approximation

The sigmoidal function (1) is a good tool for the approximation of the Heaviside step function $f = ah_0$ by the logistic function $g = s_0$ [80]. The basic problem emerging in such an approximation attempt is the Hausdorff distance, (between two functions f and g) denoted here as H and defined as [80, 85].

$$\rho(f,g) = \max\left\{\sup_{A\in F(f)} \inf_{B\in F(g)} \|A-B\|, \sup_{B\in F(f)} \inf_{A\in F(g)} \|A-B\|\right\} \tag{107}$$

Then, $H = \rho(f,g) = \rho(ah_0, s_0)$ should satisfy the relations $0 < H < a/2$, and $a - s_0(H)$, such that

$$\frac{a-H}{H} = e^{wH}, \quad 0 < H < a/2 \tag{108}$$

where w is the logistic rate constant.

It follows that for $w \to \infty$ that $H \to 0$. Moreover, the rate constant w as a function of H can be presented as [80]

$$w = w(H) = \frac{1}{H}\ln\frac{a-H}{H} = O\left(\frac{1}{d}\ln\frac{1}{d}\right) \tag{109}$$

For the sake of simplicity, we assume $a = 1$, so that the rate constant w is the only argument of the logistic sigmoid, which yields $s_0 = 1/(1+e^{-wt})$. Then, the Hausdorff distance H, for $w \geq 2$ is [80]

$$H(w) = \frac{\ln(w+1)}{w+1}\left[1 + O(\varepsilon(w))\right], \quad \varepsilon(w) = \frac{\ln(\ln(w+1))}{\ln(w+1)} \tag{110}$$

- Shifted logistic function

When the logistic sigmoid is shifted as $(t-\tau)$ we get the same (i.e., preserving the shape) function, but laterally translated (see, for example, the plots in Figure 2). Since the unit step function also preserves its shape under lateral translation, it follows that the approximation discussed above can be applied ; hence, $s_{w-\tau}(t) = s_0(t-\tau) = \left(1+e^{-w(t-\tau)}\right)^{-1}$, and at the point $-\tau$ we get $s_0(-\tau) == (1+e^{w\tau})^{-1}$ [80]. From a computational point of view, the shifted logistic sigmoid is a solution of

$$\frac{dy(t)}{dt} = wy(1-y), \quad y(0) = \frac{1}{1+e^{w\tau}} \tag{111}$$

With an increase in τ, for example, for $w\tau > 30$ the value of the Hausdorff distance is acceptable for the approximation of shifted step functions [80].

- Recurrence generated logistic sigmoids

Consider the recurrence generated sigmoids defined as [81]

$$y_{k+1}(t) = \frac{1}{1+w_{k+1}e^{-w(t+y_k(t))}}, \quad y_{k+1}(0) = \frac{1}{2}, \quad k = 1,2,\ldots \tag{112}$$

From Eq.(112) it follows that $w_{k+1} = e^{w/2}$, $k = 1,2,\ldots$.
In the special case, for example, with one step of recurrence, we have [81]

$$y_1(t) = \frac{1}{1+e^{\frac{w}{2}}e^{-wt}e^{\frac{-w}{1+e^{-wt}}}} \tag{113}$$

In such a case, the Hausdorff distance to the Heaviside function, for $w > e$, should satisfy the condition [81]

$$1 - H_1 = y_1(H_1) = \frac{1}{1+e^{\frac{w}{2}}e^{-wH_1}e^{\frac{-w}{1+e^{-wH_1}}}} \tag{114}$$

where H_1 is bounded as [81]

$$H_{1-low} = \frac{1}{\frac{1}{4}\left(w^2+4w+16\right)} < H_1 < \frac{\ln\left[\frac{1}{4}\left(w^2+4w+16\right)\right]}{\frac{1}{4}\left(w^2+4w+16\right)} \tag{115}$$

4.1.2. Blumberg's function

The Blumberg model (64), termed also as *hyper-log-logistic*, can be represented as [82]

$$\frac{dy}{dt} = ky^{1-\frac{1}{\beta}}(1-y)^{1+\frac{1}{\beta}} \tag{116}$$

This is the same as the formulation used by Tsoularis in [38], for the Spencer-Coulombe model [39] (see Eq.(65)). That is, regarding Eq.(64), the exponents are replaced as $a = 1-1/\beta$ and $b = 1+1/\beta$; for $\beta \to \infty$ we get $a = b = 1$ and Eq.(116) (the Verhulst model) . However, for $\beta = 1$, Eq.(116) is a second-order kinetic equation [82]

$$\frac{dy}{dt} = k(1-y)^2 \tag{117}$$

Hereafter, in this section, we preserve the notation used in [82] (i.e., we will use β instead n in Eq.(65).
The solution of Eq.(116) suggests that $y(t)$ is defined by the nonlinear equation [82]

$$\left(\frac{y}{1-y}\right)^{\frac{1}{\beta}} = 1 + \frac{kt}{\beta} \tag{118}$$

Differentiation of both sides of Eq.(118) and a rearrangement yields Eq.(116), which confirms Eq.(118) as its solution. Further, Eq. (118) can be represented as [82]

$$y(t) = 1 - \frac{1}{1+\left(1+\frac{kt}{\beta}\right)^{\beta}}, \quad y(0) = \frac{1}{2} \tag{119}$$

Now, concerning the approximation of the Heaviside function, the bounds of the Hausdorff distance to the function (119) is [82].

$$\frac{1}{2+k} < H < \frac{1}{1+\sqrt{k}} \tag{120}$$

The one-sided distance of the Blumberg function to the Heaviside function reduces to that established for the Verhulst model, because both models merge as $\beta \to \infty$ [82], which is obvious, as commented above. However, this is a special case, since as we saw the Blumberg model has no analytical solution but only some tabulated cases of an integral function.

The function (119) allows generation of a recurrence family [82]

$$y_{j+1}(t) = 1 - \frac{1}{1 + \left[1 + \frac{k}{\beta}\left(t - \frac{1}{2} - y_j(t)\right)\right]^{\beta}}, \quad j = 1, 2, \ldots \tag{121}$$

Remark 6. *Computational tasks of sigmoidal functions and their use to approximate other functions envisage a careful measure of the approximation accuracy, and as demonstrated above, the Hausdorff distance is an adequate approach to do that. We presented only a few examples, but the approach can be extended towards other sigmoidal functions; we refer to the quoted works and especially to [84], where detailed developed problems and pertinent computer codes are available.*

5. Non-local approach to logistic models

Now, we start with logistic models with heredity in their historical chain of development. This step is important and germane in light of modern trends to apply fractional (non-local) operators to what is already established in practice as models. Traces of this approach could be detected back to the 60s-70s of the last century [86–89, 91–96, 98–100] (see the comprehensive analysis of Frenkel and Choudhury [101]) and continued in the 21st century [102] .

The heredity effects incorporated in the mathematical models alter the formulations, since as a result, we get integro-differential equations [86, 87]. In this context, the most well-described examples of this approach exist in [86, 99] where the hereditary effects on the logistic models are systematically presented, and we will follow this style as a highly needed step towards the next level, implementing fractional operators.

5.1. The main idea towards the non-locality implementation

5.2. Non-local models based on Volterra equation of second kind

For a single-species the model with heredity, following Davis [86], as well as Frenkel and Choudhury [101], can be formulated as

$$\frac{dy}{dt} = ay - by^2 + \lambda y \int_{s=0}^{t} K(t, s)\, y(s) ds, \quad t \geq 0 \tag{122}$$

The population is assumed to be continuous and nonnegative in time. As in the Verhulst model, the parameters a and b are assumed positive, but λ can be either positive or negative. This model has a positive initial condition $\lim_{t\to 0} y(t) = y_0$.

The kernel $K(t, s)$ is the correlation function (memory), and the entire model is a Volterra non-linear integro-differential equation. The choice of the kernel $K(t, s)$ depends on the physical background of the modeled populations and is a matter of argument when the model has to be constructed. For example, in [101] it was decided, for the sake of simplicity, to perform the analysis assuming $K(t, s) = 1$, which was done in [86]

5.2.1. Transformation into a non-linear differential equation

The introduction of new variables [101] such as , $y(t) = (a/b)\,\Theta(t), t = \xi/a$ and $\Lambda = \lambda/(a/b)$, allows Eq. (122) to transformed as

$$\frac{d\Theta}{d\xi}(\xi) = \Theta(\xi)\left[1 - \Theta(\xi)\right] + \Lambda\Theta(\xi) \int_{\xi_0=0}^{\xi} \Theta(\xi_0)\, d\xi_0, \quad \xi \geq 0 \tag{123}$$

with the initial condition $\lim_{t\to 0}\Theta(\xi) = \Theta_0$, and $\Theta(\xi) \in C^{\infty}(\mathbb{R})$, $\xi \in [0, \infty)$ and $\Theta_0 \in (0, 1)$;Λ is a coefficient.

Now, the first idea coming to mind is to convert Eq.(123) into an equivalent non-linear differential equation. The first attempts in this direction [86, 99] (see also [101]) are by a direct differentiation and then eliminating the remaining integral term, which finally increases the order of the equation in $\Theta(\xi)$, namely

$$\Theta(\xi)\frac{d^2\Theta(\xi)}{d\xi^2}-\left(\frac{d\Theta(\xi)}{d\xi}\right)^2-\Theta^2(\xi)\frac{d\Theta(\xi)}{d\xi}+\Lambda\Theta^3(\xi) \tag{124}$$

The increase in the order of the new equation to the second order in time invokes two auxiliary conditions to be imposed: the first is $\lim_{t\to 0}\Theta(\xi)=\Theta_0$, but the second one is $\lim_{t\to 0}\frac{d\Theta(\xi)}{d\xi}=\Theta_0(1-\Theta_0)$ (obtained by setting $\xi=\xi_0$ in (123). This new formulation poses the problem posed (i.e., it is not ill-posed) [101, 104].

5.2.2. Transformation into an equivalent integral equation

The integration of Eq. (123) directly (with the condition $\lim_{t\to 0}\Theta(\xi)=\Theta_0$) with respect to ξ [87, 101], met computational difficulties. Alternatively, if we present Eq.(123) as [101]

$$\frac{d}{d\xi}\ln\Theta(\xi)=1-\Theta(\xi)+\Lambda\int_{\xi_0=0}^{\xi}\Theta(\xi_0)\,d\xi_0,\quad \lim_{t\to 0}\Theta(\xi)=\Theta_0,\quad 0\le\xi\le\xi_{\max} \tag{125}$$

and integrating the result is

$$\Theta(\xi)=\Theta_0 e^{\xi}\exp\left[\int_{\xi_0=0}^{\xi}K(\xi,\xi_0)\,\Theta(\xi_0)\,d\xi_0\right],\quad 0\le\xi\le\xi_{\max} \tag{126}$$

The kernels is $K(\xi,\xi_0)=-1+\Lambda(\xi-\xi_0)$ and it is non-singular [101]; not additional analyzes concerning the type of the kernel exist in [101].

5.2.3. Transformation into an alternative differential equation

Following Frenkel and Choudhury [101], the transformed model (124) , which is a hyperbolic integro-differential equation, is hard to analyze. Because of that, they suggest the function (as a cumulative population up to a current time ξ)

$$C(\xi)=\int_{\xi_0=0}^{\xi}\Theta(\xi_0)d\xi_0 \tag{127}$$

Then, Eq. (123), with $\lim_{t\to 0}\Theta(\xi)=\Theta_0$, can be presented as

$$\frac{d^2C}{d\xi^2}=\frac{dC}{d\xi}\left(1-\frac{dC}{d\xi}\right)+\Lambda C(\xi)\frac{dC}{d\xi},\quad \xi\ge 0 \tag{128}$$

with $lim_{\xi\to 0}C(\xi)=0$ and $lim_{\xi\to 0}\frac{dC(\xi)}{d\xi}=\Theta_0$

Frenkel and Choudhury [101] developed a detailed analysis of Eq.(128) with both analytical (through $\Theta(\xi)$ expansion as a series) and numerical (by a conventional Runge-Kutta method) solutions, and for a better understanding of the outcomes of this study, we suggest a thorough reading of all its sections.

5.3. Other non-local formulations of the logistic model

We now address other approaches to implement non-locality in the logistic model. To a greater extent, the models considered in this section are directly postulated (that is, there are no derivations from first principles, which can be easily explained by the tasks: mathematical analyses and solutions rather than model build-ups).

5.3.1. Cushing's studies

Cushing [93] considered the integro-differential equation

$$\frac{dN}{dt} = \lambda N(t)\left[1 - \frac{1}{c}\int_0^{\infty} N(t-s)\, d\alpha(s)\right], \quad t \in (-\infty, \infty) \tag{129}$$

modeling a single-species population growth when the rate of growth depends on (is affected by) the population size at previous times. The integral term is interpreted as the accumulated or hereditary effects of past population sizes. This is the model introduced by Volterra [103]; λ is a coefficient .

The integral term can be considered as a Stieltjes integral (due to the original formulation $d\alpha(s) = f(s)\, ds$), which can be easily transformed into a Riemann integral. That is, when $\alpha(s)$ represents a unit step function ($s = 0$) there are no memory effects, and we get the Verhulst logistic equation.

As commented by Cushing [93], Miller in the above mentioned work [87] considered the case when

$$\alpha(s) = bu_s(s) + \int_0^{s} f(\eta)\, d\eta, \quad f(s) \geq 0, \quad \int_0^{\infty} f(s) ds < \infty \tag{130}$$

which is equivalent to $d\alpha(s) = f(s)\, ds$.

From (130) it follows that $b > \int_0^{s} f(s)\, ds$ [87, 93]. As a result, all solutions approach c for long times ($t \to \infty$).

On the other hand, with $\alpha(s)$ as a unit step function and $s = \tau$ (delay) we get a constant time-lag formulation of the logistic model.

$$\frac{dN}{dt} = \lambda N(t)\left[1 - \frac{1}{c}N(t-\tau)\right] \tag{131}$$

The basic assumption considered by Cushing in [93] is

$$\int_0^{\infty} d\alpha(s) = 1, \quad s \in [0, \infty) \tag{132}$$

and it supports the Volterra hypothesis $d\alpha(s) = f(s)\, ds$, $f(s) > 0$, and $\int_0^{\infty} f(s) ds = 1$.

Further, if $N(t)$ is bounded (the main feature of the logistic model) and continuously differentiable with bounded derivative, and ω-periodic, then $\int_0^{\infty} N(t-s) d\alpha(s)$, and the differentiation can be taken under the integral [93] .

The further studies of Cushing [95, 96] considered cases when the net birth rate in the logistic model (the coefficient m in the ordinary Verhulst model (Eq.(35)) is a periodic function of time (as a result of biological or seasonal fluctuations). We will consider the final results of [95, 96] because this direction is outside the main line of the present work.

5.3.2. Brauers's analysis

Brauer [92] considered the Volterra equation (in the original notations)

$$x(t) = f(t) + \int_0^{t} g[x(x-s)] P(s)\, ds \tag{133}$$

In Eq. (133) $g(x)$ is the number of the members added to the population in unit time when the population size is x; that is ratio $g(x)/x$ is the relative rate of growth per unit time. The function $P(s)$ is the probability that a member of the population survives to age t. Hence, $g[x(x-s)]\, P(s)\, \Delta s$ and there is a change in the population from time $(t-s)$ to another $(t-s+\Delta s)$ with members surviving to age s at the time t.

Brauer [92,94] was interested in the boundedness of the solution (a fact we know about the ordinary logistic equation), assuming that $f(t)$ is nonnegative, continuous, and of bounded variation on $0 \leq t < \infty$, such that $f(\infty) = \lim_{t\to\infty} f(t)$. Also, $P(s)$ is nonnegative, nonincreasing, and differentiable on $0 \leq t < \infty$ obeying the condition $\int_0^\infty P(s)ds$, and is normalized, so that $P(0) = 1$.

With $g(0) = 0$ the assumption that $g(x)$ is continuous and nonnegative on $0 \leq x < \infty$ results that the limit of the solution c should satisfy the equation [92]

$$c = f(\infty) + g(c) \int_0^\infty P(s)ds \tag{134}$$

as a good support of this result, if the linear integral equation [92, 97] is considered

$$z(t) = F(t) + \int_0^{t-\tau} z(t-s)a(s)\,ds, \quad t \geq \tau \tag{135}$$

as well as $z(t)$, $F(t)$ ($F(0) = 0$) and $a(t)$ are continuous and differentiable on $0 \leq t < \infty$; also $a(t)$ is bounded variation such that $\int_0^\infty a(t)dt < \infty$.

Then, if $\int_0^\infty a(t)dt = 1$ and $\int_0^\infty ta(t)dt = m_1 < \infty$, as well as $\int_0^\infty t^2 a(t)dt < \infty$ with $\int_0^\infty F(t)dt = b < \infty$ we have a unique solution of Eq. (135), for $\tau \leq t < \infty$, which is nonnegative such that $\lim_{t\to\infty} z(t) = b/m_1$ yielding that

$$\lim_{t\to\infty} z(t)\, e^{-\sigma(t-\tau)} = \frac{\int_\tau^\infty e^{-\sigma(t-\tau)} F(t)\,dt}{\int_\tau^\infty te^{-\sigma(t-\tau)} a(t)\,dt} \tag{136}$$

Brauer demonstrated that with a change in the variable $t - \tau$ and defining $\upsilon(u) = z(u+\tau) = z(t)$ $\Phi(u) = F(u+\tau) = F(t)$, for $u > 0$ it is possible to represent Eq. (133) as

$$\upsilon(u) = \Phi(u) + \int_0^u z(t-s)a(s)\,ds = \Phi(0) + \int_0^u \upsilon(t-s)a(s)\,ds, \quad t \geq \tau, \quad u \geq 0 \tag{137}$$

which, to a greater extent, resembles the constructions we will consider further when fractional models are discussed.

5.3.3. Zwanzig's derivation of a non-local (generalized) Verhulst law

After the preceding analyzes, where properties of the modeling equations and their solution were briefly outlined, we would like to stress on the technology of model derivation. In this direction, we credit Zwanzig [89], whose model-building approach could be considered as a good template towards the development of new non-local logistic equations.

The Zwanzig derivation starts with a set of Volterra equations, raising the following question:

- What are the conditions under which the species' evolution would follow the Verhulst model ?

In answering this formulated problem, and considering a population of n species, Zwanzig suggested that at the time $t = 0$ all species (from 1 to n) with $N_j(0)$ are close to their equilibrium level Q_j, that is

$$N_j(0) \simeq Q_j, \quad j = 1, 2, \ldots n \tag{138}$$

However, the zeroth species may also be significantly out of equilibrium [89] and therefore a situation with $N_0(0) \neq Q_0$ is possible. Then, the rate of the zeroth species' evolution beyond the equilibrium is

$$\frac{dN_0(t)}{dt} = N_0(t) \sum_{j=1}^{n} a_{0j} \left(N_j(t) - Q_j\right) \tag{139}$$

The evolution of a certain j species ($j \neq 0$) can be represented as a sum of two terms

$$\frac{dN_j(t)}{dt} = N_j(t)\sum_{k=1}^{n} a_{jk}\left(N_k(t) - Q_k\right) + N_j(t)\, a_{j0}\left(N_0(t) - Q_0\right) \tag{140}$$

The linearization applied considered the deviation $N_j - Q_j$ (for $j \neq 0$) by introducing a new variable x_j so that $N_j = Q_j + \sqrt{Q_j}x_j(t)$. This generates a new matrix $c_{jk} = \sqrt{Q_j}a_{jk}\sqrt{Q_k}$, where $j,k \neq 0$. After these steps Eq.(140) can be presented as

$$\frac{dx_j(t)}{dt} = \left(1 + \frac{x_j}{\sqrt{Q_j}}\right)\sum_{k}^{n} c_{jk}x_k + \sqrt{Q_j}\left(1 + \frac{x_j}{\sqrt{Q_j}}\right)a_{j0}\left(N_0 - Q_0\right) \tag{141}$$

Zwanzig's hypothesis is that at the initial state, all values of x_j are negligibly small, and we can assume that $x_j(t) \ll \sqrt{Q_j}$, which are equivalent to $\log\left(Q_0/N_0(0)\right) \ll Q_1/2Q_0$. With this step Eq.(141) can be linearized as [89]

$$\frac{dx_j(t)}{dt} = \sum_{k}^{n} c_{jk}x_k + \sqrt{Q_j}a_{j0}\left(N_0 - Q_0\right) \tag{142}$$

Considering Eq.(142) as an initial value problem, Zwanzig's solution involved an exponential matrix operator $U_{jk} = \exp(ct)_{jk}$. Skipping details, the equation about $dN_0(t)/dt$ becomes [89]

$$\frac{dN_0(t)}{dt} = -N_0(t)\int_0^t K(t-s)\left[N_0(s) - Q_0\right]ds + N_0(t)\,F(t) \tag{143}$$

The kernel $K(t)$ represents the hereditary effects on the population and is explicitly defined as [89]

$$K(t) = -\sum_{j}\sum_{k} a_{0j}\sqrt{Q_j}U_{jk}(t)\sqrt{Q_k}a_{k0} \tag{144}$$

where the noise $F(t)$ is completely determined by all initial deviations of $x_k(0)$ as

$$F(t) = \sum_{j}\sum_{k} a_{0j}\sqrt{Q_j}U_{jk}(t)\,x_k(0) \tag{145}$$

As intermediate outcomes, the Zwanzig derivation of a hereditary population rate equation is based on a semi-linearization of the Volterra model, from which it starts. Further, when N_0 is enough smaller than the equilibrium value Q_0 we have $\log\left[Q_0/N_0(0)\right] \ll Q_1/2Q_0$. However, if $N_0(0)$ is much larger than Q_0 we have and $N_0(0)/Q \ll Q_1/2Q_0$.

- Zwanzig's assumptions about the heredity kernel

The hereditary kernel is determined by all interacting constants a_{jk} (see for clarity of this statement Eq.(144) and read the explanation in Remark 7). As commented by Zwanzig, the matrix c_{jk} is antisymmetric and if n is even, then its eigenvalue spectrum is a set of complex conjugate pairs $\pm i\omega_m$(the value of m is within the range $[1, n/2]$), but when n is odd, there is an additional eigenvalue [89]. Zwanzig decided that the kernel should be

$$K(t) = \sum K_m \cos(\omega_m t), \quad K(0) > 0 \tag{146}$$

An example provided by Zwanzig, is the case with the exponential kernel $K(t) = K(0)\exp(-t/T)$, where T is the relaxation time (in the original Zwanzig notation). Then, neglecting the noise, i.e. $F(t) = 0$, the generalized Verhulst equation, in Zwanzig's interpretation, becomes

$$\frac{dN_0(t)}{dt} = -K(0)\,N_0(t)\int_0^t e^{-\left(\frac{t-s}{T}\right)}\left[N_0(s) - Q_0\right] \tag{147}$$

As is it is well-known, and Zwanzig demonstrated that, by a change in variables $w(t) = \log\left[N_0(t)/Q_0\right]$ we get

$$\frac{dw(t)}{dt} = -K(0)\,Q_0\int_0^t e^{-\left(\frac{t-s}{T}\right)}\left[w(s) - 1\right] \tag{148}$$

Differentiating both sides of Eq. (148) concerning t , we obtain [89]

$$\frac{d^2w\left(t\right)}{dt^2}=-\frac{1}{T}\frac{dw\left(t\right)}{dt}-K\left(0\right)Q_0\left[e^w-1\right],\quad w\left(t=0\right)=\log\left[N_0\left(0\right)/Q_0\right],\quad \frac{dw\left(t=0\right)}{dt}=0 \tag{149}$$

Note: Just from a formal point of view, Eq.(149) is close to Eq.(124) and Eq.(128), concerning the second order derivatives in the left-hand sides.

Remark 7 (The appearance of the convolution in the Zwanzig model)**.** *Following Widder [90], the convolution of two series* $\{a_n\}_0^\infty$ *and* $\{b_n\}_0^\infty$ *is defined by a new series* $\{c_n\}_0^\infty$*, where*

$$c_n=\sum_{k=0}^{n}a_kb_{n-k}=\sum_{k=0}^{n}a_{n-k}b_k \tag{150}$$

This happens when the two series are multiplied together , i.e. $\sum\limits_0^\infty a_kz^k\sum\limits_0^\infty b_kz^k=\sum\limits_0^\infty c_kz^k$*. And, the convolution of two-sided series*

$$c_n=\sum_{-\infty}^{\infty}a_kb_{n-k}=\sum_{-\infty}^{\infty}a_{n-k}b_k \tag{151}$$

presents itself when two Laurent series are multiplied [90].
As especially mentioned by Widder, ***hardly less familiar is the continuous analogue*** *of (151)*

$$c\left(x\right)=\int_{-\infty}^{\infty}a\left(x-s\right)b\left(s\right)ds=\int_{-\infty}^{\infty}a\left(s\right)b\left(x-s\right)ds \tag{152}$$

If $a\left(x\right)$ *and* $b\left(x\right)$*, both vanish on* $(-\infty,0)$*, then Eq.(151) reduces to [90]*

$$c\left(x\right)=\int_{0}^{\infty}a\left(x-s\right)b\left(s\right)ds=\int_{0}^{\infty}a\left(s\right)b\left(x-s\right)ds \tag{153}$$

as a continuous analog of (150).

Remark 8 (Zwanzig's interpretation of Eq.(149))**.** *Zwanzig interpreted Eq.(149) as an equation of motion of a particle, where the coordinate is* w*, the mass is* T*, and the potential is defined as* $U\left(w\right)=K_0Q_0T\left[e^w-1\right]$*; the friction contributes with the term* $-dw\left(t\right)/dt$ *. From this point of view, if the relaxation time* T *is infinite, or we have a constant* $K\left(t\right)$*, the motion is periodic. However, with large* T*, the motion oscillates but is damped. Moreover, as mentioned by Zwanzig, the defined integral of* $K\left(t\right)$ *yields* $k=K\left(0\right)T$*, a constant corresponding to the rate constant in the Verhulst logistic curve. Further, last but not least, in the case with* $T\to0$ *(no relaxation of the motion process exists, we get directly the Verhulst model (in the light of the following discussion on non-locality in the logistic model, the Verhulst model is local in time, that is obvious by the use of local derivative* dy/dt *and no relaxation suggested in it derivation).*

6. Constructions of hereditary logistic models with fractional operators

In light of the general approach to constructing hereditary models, we emphasize applications of fractional operators and the main principles on which it is based. Developing the concept, we envisage two principal approaches:

- Volterra integral equations with memory kernels known from the fractional calculus
- Causality principle, taking into account the dynamic character of the logistic models

6.1. Fractionalization based on the Volterra equation of second kind

To develop this concept, let us go back to Eq.(122), rewriting it with a memory integral (a convolution term)

$$\frac{dy}{dt}=ay-by^2+\lambda\int_0^t R\left(t-s\right)y\left(s\right)ds \tag{154}$$

Since there is no restriction, from a mathematical point of view, we may consider that the memory kernel is singular and of Abel's type $R(t) = t^{1-\alpha}/\Gamma(\alpha)$. Then, we may construct a hereditary logistic equation in a Volterra manner as

$$\frac{dy}{dt} = ay - by^2 + \lambda \frac{1}{\Gamma(\alpha)} \int_0^t (t-s)^{1-\alpha} y(s)\, ds \Rightarrow \frac{dy}{dt} = ay - by^2 + \lambda^{RL} I_t^{\alpha} y(t) \tag{155}$$

where ${}^{Rl}I_t^{\alpha}[y(t);s] = \frac{1}{\Gamma(\alpha)} \int_0^t (t-s)^{1-\alpha} y(s)\, ds$, $0 < \alpha < 1$ is the Riemann-Liouville fractional integral.

Note: From the construction of eq.(155) it follows that when the second (convolution) term vanishes (since $R(t) \to 0$ for $t \to \infty$), we get the local logistic model with its asymptote $y(t) \to 1$ as $t \to \infty$.

Equation (155) can be transformed by differentiating on both sides for t, which yields

$$\frac{d^2y}{dt^2} = \frac{d}{dt}\left(ay - by^2\right) + \lambda \frac{1}{\Gamma(1-\alpha)} \frac{d}{dt} \int_0^t (t-s)^{-\alpha} y(s)\, ds \tag{156}$$

and we got an equation in terms of the Riemann-Liouville fractional derivative (the last damping term in Eq.(156)).

$${}^{RL}D_t^{\alpha} y(t) = \frac{1}{\Gamma(1-\alpha)} \frac{d}{dt} \int_0^t (t-s)^{-\alpha} y(s)\, ds \tag{157}$$

Further, rearrangements in (156) result in

$$\frac{d^2y}{dt^2} = \left(a\frac{dy}{dt} - 2by\frac{dy}{dt}\right) + \lambda^{RL} D_t^{\alpha} y(t) \tag{158}$$

Now, we can see that we got almost the same equation as (128) by Frenkel and Chodhury [101], where the coefficients $a = b = 1$, but now the last term is a convolution integral (a fractional derivative).

Moreover, bearing in mind that at zero initial condition, i.e., with $y(0) = y_0 = 0$, under the circumstances of the population models considered here, the Riemann-Liouville (158) and the Caputo derivative (160) are equivalent, then, for the sake of completeness of the exposition, we may write Eq.(158) as

$$\frac{d^2y}{dt^2} = \left(a\frac{dy}{dt} - 2by\frac{dy}{dt}\right) + \lambda^{C} D_t^{\alpha} y(t) \tag{159}$$

$${}^{C}D_t^{\alpha} y(t) = \frac{1}{\Gamma(1-\alpha)} \int_0^t (t-s)^{-\alpha} \frac{dy(s)}{dt} ds \tag{160}$$

Developing the technology to construct hereditary equations of Volterra type involving fractional operators, we may generalize it by setting the construction of the rate equation as

$$\frac{dy}{dt} = ay - by^2 + \lambda^{*} I_t^{\alpha} y(t) \tag{161}$$

where ${}^{RL*}I_t^{\alpha} y(t)$ is a convolution (constitutive fractional integral of Riemann-Liouville type [105]). The kernel considered should satisfy simultaneously the conditions to be used as memory and to be suitable to model the relaxation of the considered dynamic process (see examples of such constructions in [106] and [107].

Differentiating both sides of Eq.(161) we get a fractional differential equation

$$\frac{d^2y}{dt^2} = \left(a\frac{dy}{dt} - 2by\frac{dy}{dt}\right) + \lambda^{RL*} D_t^{\alpha} y(t) \tag{162}$$

That is, starting with a convolution integral as that in Eq.(154), we always obtain hyperbolic equations with damping terms expressed as fractional derivatives of a Riemann-Liouville type.

As a generalization of the above concept, if the growth model is of an autonomous type and local (of integer order), then the steps towards the hereditary construction of Volterra type involving fractional

operators (a generalized definition not related only the power-law memory kernel)

$$\frac{dy\left(t\right)}{dt}=F\left(y\left(t\right)\right)\Rightarrow hereditary\Rightarrow\frac{dy\left(t\right)}{dt}=F\left(y\left(t\right)\right)+\lambda^{RL*}I_{t}^{\alpha}y\left(y\right) \tag{163}$$

$$\frac{d^{2}y\left(t\right)}{dt^{2}}=\frac{d}{dt}F\left(y\left(t\right)\right)\Rightarrow hereditary\Rightarrow\frac{d^{2}y\left(t\right)}{dt^{2}}=\frac{d}{dt}F\left(y\left(t\right)\right)+\lambda^{RL*}D_{t}^{\alpha}y\left(y\right) \tag{164}$$

With this, we close this section, and it might be expected that future studies will accept this concept in model building, which is thermodynamically consistent and corresponds to the causality principle [106, 107]. The simple function $F\left(y\left(t\right)\right)=ay-by^{2}$ is only an example, but any other, as shown in Sections 3.2.2 and 3.2.3 could be considered.

6.2. Fractionalization based on the Volterra equation of the first kind

If the hereditary model is based on the Volterra equation of the first kind, then the general construction is

$$\frac{dy(t)}{dt}=\lambda\int_{0}^{t}R(t-s)\left[ay(s)-by^{2}(s)\right]ds \tag{165}$$

Then, we can see that assuming a kernel of Abel type, $R(t)=t^{1-\alpha}/\Gamma(\alpha)$ we get

$$\frac{dy(t)}{dt}=\lambda\frac{1}{\Gamma(\alpha)}\int_{0}^{t}(t-s)^{1-\alpha}\left[ay(s)-by^{2}(s)\right]ds \tag{166}$$

where the right-hand side is the Riemann-Liouville fractional integral.

Differentiating both sides with respect to t, we obtain

$$\frac{d^{2}y(t)}{dt^{2}}=\lambda\frac{1}{\Gamma(1-\alpha)}\frac{d}{dt}\int_{0}^{t}(t-s)^{-\alpha}\left[ay(s)-by^{2}(s)\right]ds\Rightarrow\frac{d^{2}y(t)}{dt^{2}}=\lambda^{RL}D_{t}^{\alpha}\left[ay(s)-by^{2}(s)\right] \tag{167}$$

In general, there is no restriction, from a mathematical point of view, to use a kernel different from the power-law, and then using Eq.(165), we can obtain

$$\frac{d^{2}y(t)}{dt^{2}}=\lambda\frac{d}{dt}\int_{0}^{t}R(t;\alpha)\left[ay(s)-by^{2}(s)\right]ds\Rightarrow\frac{d^{2}y(t)}{dt^{2}}={}^{RL*}D_{t}^{\alpha}\left[ay(s)-by^{2}(s)\right] \tag{168}$$

where ${}^{RL*}D_{t}^{\alpha}$ is a generalized form of a Riemann-Liouville derivative ireespective of the memory kernel.

These steps are one of the possible transformations of Eq.(165) into an equivalent differential equation, and we will see in the next Section 6.4 how this can be done in a different way using the causality principle.

6.3. A fractionalization of the Volterra logistic model with an integral kernel: A good example

A very good example supporting the general scheme of fractionalization presented above was developed by Monteiro et al. [108] based on the logistic equation in the Volterra convolution form [103] (see Eq.(129))

$$\frac{dy\left(t\right)}{dt}=ry\left(t\right)\left(1-\int_{0}^{t}R\left(t-s\right)y\left(s\right)ds\right) \tag{169}$$

The model assumes that the carrying capacity is delayed or is affected by the past [108]. Delays in the population dynamics can be due to many reasons, such as not enough food, diseases, insufficient stimuli, etc., and it can be performed at a time scale different from that of the relaxation process (concerning the relaxation of the memory kernel) [109].

The kernel is considered the generalized Gamma Mittag-Leffler probability distribution [110]

$$f\left(x\right)=\begin{cases}0, & elsewhere\\ Cx^{-\beta}e^{ax}E_{\alpha,\beta}\left(-\lambda x^{\alpha}\right), & x\geq0\end{cases} \tag{170}$$

where $C=a^{\beta}+a^{\beta-\alpha}\lambda$ is the normalizing factor; The Mittag-Leffler distribution does not have finite moments [108, 112] .

The following hypotheses have to be satisfied:

- $a=0,\quad\lambda>0,\quad0<\alpha=\beta\leq1$

- $-a^{\alpha} < \lambda \leq 0, \quad a > 0, \quad \alpha, \beta > 0$
- $0 \leq a^{\alpha}, \quad a > 0, \quad 0 < \alpha \leq 1, \quad \alpha \leq \beta$

Now, with $R(t) = f(t)$ Eq. (169) takes the form [108, 112]

$$\frac{dy(t)}{dt} = ry(t)\left(1 - \int_0^t C(t-s)^{\beta-1} e^{-a(t-s)} E_{\alpha,\beta}\left(-\lambda(t-s)^{\alpha}\right) y(s)\, ds\right) \tag{171}$$

Note: In such a case, we have the so-called integral kernel [108, 113].

Then, using the fractional Riemann-Liouville integral and derivative, as well as applying the Laplace transform, precisely that

$$\int_0^{\infty} Ct^{\beta-1} e^{-at} E_{\alpha,\beta}\left(-\lambda t^{\alpha}\right) dt = C\frac{a^{\alpha-\beta}}{a^{\alpha}+\lambda}, \quad 0 \leq \lambda < a^{\alpha}, \quad a > 0, \quad 0 < \alpha < 1, \quad \alpha \leq \beta \tag{172}$$

because, upon such conditions, $E_{\alpha,\beta}\left(-\lambda t^{\alpha}\right)$ is positive and completely monotonic [111].

Further, the logistic model can be written as [108, 112]

$$\frac{dy(t)}{dt} = ry(t) - ry(t)Ce^{-at}\mathcal{L}^{-1}\left\{\mathcal{L}\left[t^{\beta-1}E_{\alpha,\beta}\left(-\lambda t^{\alpha}\right)\right]\mathcal{L}\left[\left(e^{at}\right)y(t)\right]\right\} \tag{173}$$

Next, in terms of the Riemann-Liouville fractional integral, the result is

$$\frac{dy(t)}{dt} = ry(t) - ry(t)Ce^{-at}D_t^{1-\beta}\left[e^{at}W\right], \quad W = \int_0^t E_{\alpha}\left(-\lambda(t-s)^{\alpha}\right)e^{-a(t-s)}y(s)\, ds \tag{174}$$

With the help of the Leibniz rule, and that $E_{\alpha,\alpha}(x) = \sum_{n=0}^{\infty} \frac{n!}{\Gamma(\alpha n+1)}\frac{x^n}{n!} = \alpha E^2_{\alpha,1+\alpha}(x)$ we have [108, 112]

$$\begin{aligned} \frac{dW}{dt} &= y(t) - \int_0^t \left\{\lambda(t-s)^{\alpha-1}E_{\alpha,\alpha}\left[-\lambda(t-s)^{\alpha}\right]\right\} + \\ &+ aE_{\alpha}\left[-\lambda(t-s)^{\alpha}\right]e^{-a(t-s)}y(s)\, ds \end{aligned} \tag{175}$$

Compactly, the model can be presented as [108, 112]

$$\begin{cases} \dfrac{dy(t)}{dt} = \left\{ry(t)\left[1 - Ce^{-at}D^{1-\beta}\left(e^{at}W\right)\right]\right\}, \\ \dfrac{dW}{dt} = y(t) - \lambda e^{-at}D^{1-\alpha}\left(e^{at}W\right) - aW \end{cases} \tag{176}$$

It should be noted that for $\alpha > 1$ it followed $D^{1-\alpha}f(x) = I_t^{\alpha-1}f(x)$ (the fractional Riemann-Liouville integral of order $\alpha - 1$). Also, we have the same for $\beta > 0$. In terms of the Caputo derivative, instead of the fractional Riemann-Liouville derivative, it follows that $W(0) = 0$ (a logical result since both derivatives are identical at zero initial conditions).

In [108, 112] the authors especially stress the attention to the fact that the fractionalization process does not affect the time derivative $dy(t)/dt$ in contrast to the surrogate fraction mode commented in Section 7 where it is replaced mechanistically by a certain fractional derivative. This is in agreement with the general concept of implementing the non-locality in the logistic model, as we saw in all examples developed earlier. The idea of implementing the Gamma Mittag-Leffler function was also developed in [112, 114].

6.3.1. Some special cases

From the model developed, we may obtain some special cases :

- Mittag-Leffler distributed delay:

With $0 < \alpha = \beta < 1$ and $a = 0$, we have a fractional Poisson process, where the kernel is defined as the probability density function of the Mittag-Leffler distribution (alos termed as Mittag-Leffler PDF kernel).

Then, the model becomes

$$\frac{dy(t)}{dt} = ry(t)\,1 - \int_0^t \lambda(t-s)^{\alpha-1} E_{\alpha,\alpha}\left[-\lambda(t-s)^{\alpha}\right] y(s)\,ds \tag{177}$$

or

$$\begin{aligned} \frac{dy(t)}{dt} &= ry(t)\left(1 - \lambda D^{1-\alpha} W\right) \\ \frac{dW}{dt} &= y(t) - \lambda D^{1-\alpha} W \end{aligned} \tag{178}$$

For $\alpha \longrightarrow$ the model to recover an exponentially distributed delay.

- Erlang's probability distribution kernel :

Defining the probability density function of the Gamma distribution as a delay kernel when $\lambda = 0$ in Eq.(170), one obtains [115]

$$\frac{dy(t)}{dt} = ry(t)\,1 - \int_0^t \frac{a^{\beta}}{\Gamma(\beta)}(t-s)^{\beta-1} e^{-a(t-s)} y(s)\,ds, \quad \beta > 0 \tag{179}$$

If $\beta = n \in \mathbb{N}$, that is, we have the Erlang distribution. For $\beta = 1$ in Eq. (179) the following function can be defined

$$w(t) = \int_0^t a e^{-a(t-s)} y(s) ds \tag{180}$$

i.e, the memory kernel is ae^{-at} .
Since $\frac{dw(t)}{dt} = ay(t) - aw(t) = \frac{y(t)-w(t)}{\mu}$, with μ denoting the mean of the distribution, Eq.(179) is equivalent to the following system

$$\begin{cases} \dfrac{dy(t)}{dt} = ry(t)\,(1 - w(t)) \\ \dfrac{dw(t)}{dt} = \dfrac{y(t) - w(t)}{\mu} \end{cases} \tag{181}$$

- Gamma distributed delay:

With $\lambda = 0$ the model (179) reduces to

$$\begin{aligned} \frac{dy(t)}{dt} &= ry(t)\left[1 - Ce^{-at} D_t^{1-\beta}\left(e^{at} W\right)\right] \\ \frac{dW(t)}{dt} &= y(t) - aW(t) \end{aligned} \tag{182}$$

The model (182) lost Mittag-Leffler elements but remains fractional as long as $\beta \notin \mathbb{N}$ (as long as the kernel is Erlang's PDF) [108]

6.4. Fractionalization based on the causality principle

Now, consider the growth model as a dynamic system where the relation between the input and output, the causality principle [116], can be expressed as a convolution integral

$$y_{out}(t) = \int_{-\infty}^{\infty} R(t,s) y_{in}(s)\,ds \Rightarrow y_{out}(t) = \int_0^{\infty} R(t,s) y_{in}(s)\,ds \tag{183}$$

where $R(t)$ is a function of influence (memory function) relating the moment value of the function $y(t)$to its past; the recent moments have stronger effects than the distant ones, since the function $R(t)$ should decay and vanish as $t \longrightarrow \infty$
In the second form of Eq.(183), the lower terminal is set to zero, because in any population, in general, any dynamic growing process, *the time is not the chronological time*, *but the intrinsic time* (the time of process duration), starting at the point $t = 0$, because there is no growth before that [117, 118] ; the same principle, considering the memory kernel, needs $R(t)$ to be causal function, that is $R(t < 0) = 0$.

Hence, considering the dynamic growth models, in a local form, as

$$\underbrace{\frac{dy\left(t\right)}{dt}}_{output}=\underbrace{F\left(y\left(t\right)\right)}_{input} \tag{184}$$

we may construct a causal version as (this is a Volterra equation of first kind, as commented earlier)

$$\frac{dy}{dt}=\int_{0}^{t}R\left(t-s;\alpha\right)F\left(y\left(s\right)\right)ds\Rightarrow\frac{dy}{dt}={}^{*}I_{t}^{\alpha}F\left(y\left(t\right)\right),\quad 0<\alpha<1 \tag{185}$$

The right-hand side of Eq.(185), presented as ${}^{*}I_{t}^{\alpha}F\left(y\left(t\right)\right)$, can be considered as *a general construction of a memory integral*, where the kernel $R\left(t\right)$ could be of any type involved in the known fractional operators (we discussed this above).

Now, as in the preceding examples, let us consider that ${}^{*}I_{t}^{\alpha}F\left(y\left(t\right)\right)$ is of a Riemann-Liouville type, such that

$$\frac{dy}{dt}={}^{RL}I_{t}^{\alpha}F\left(y\left(t\right)\right)\Rightarrow\frac{dy}{dt}=\frac{1}{\Gamma\left(\alpha\right)}\int_{0}^{t}\left(t-s\right)^{1-\alpha}F\left(y\left(s\right)\right)ds \tag{186}$$

or more compactly as

$$\frac{dy}{dt}={}^{RL}I_{t}^{\alpha}F\left(y\left(t\right)\right)\Rightarrow\frac{dy}{dt}={}^{C}D_{t}^{1-\alpha}F\left(y\left(t\right)\right),\quad t>0,\quad 0<\alpha<1 \tag{187}$$

For the Caputo derivative and the fractional integral, we have: ${}^{C}D_{t}^{\alpha}I_{t}^{\alpha}f\left(t\right)={}^{C}D_{t}^{\alpha}{}^{C}D_{t}^{-\alpha}f\left(t\right)=f\left(t\right)$ and this allows us to transform Eq.(187) by applying to both sides the operator ${}^{C}D_{t}^{\alpha-1}$ (it is the left inverse to the fractional integral) , that is

$${}^{C}D_{t}^{\alpha}y\left(t\right)=F\left(y\left(t\right)\right),\quad t>0,\quad 0<\alpha<1 \tag{188}$$

Considering $F\left(y\left(t\right)\right)=ay-by^{2}$ we get a time-fractional logistic model with the Caputo derivative

$${}^{C}D_{t}^{\alpha}y\left(t\right)=ay-by^{2},\quad t>0,\quad 0<\alpha<1 \tag{189}$$

The development of Eq.(188) (and particularity Eq. (189)) was possible only because the Caputo derivative is left inverse to the fractional integral. *If such a property does not hold with other types of operators, where the kernels are not of power law type, the hereditary model is* Eq.(185), which a general hereditary construction.

Note: We can see now, in contrast to the fractionalized model using the construction of the Volterra equation of the second kind, when the kernel $R(t;\alpha)\rightarrow 0$ for $t\rightarrow\infty$ there is no asymptotic state $y(t)\rightarrow 1$; we will see such behaviors in the solution of the surrogate fractional models discussed in Section 7.

Remark 9. *The time-fractional growth model with the Caputo derivative (Eq.(185)) is the only case when the correctly derived model and the formal fractionalized equation (by replacing $dy\left(t\right)/dt$ by ${}^{C}D_{t}^{\alpha}y\left(t\right)$) coincide. We can see many examples in Section 7 and the results thereof.*

7. Surrogate fractional models (obtained by replacements)

Now, we stress the attention on various approaches to solve logistic equations when the time fractional derivative in the Verhulst model is replaced by different fractional operators (derivatives); but we do not discuss their origins (derivations). A standpoint about the renaming all models considered in this section as *surrogate*, and some additional details, is expressed in Remark 16. There are two groups, in accordance with the operator used: Models with singular memories (Section 7.1) and models with non-singular memories (Sections 7.2, 7.3 and 7.4).

7.1. Fractional models with singular memory kernels

7.1.1. Fractional logistic equation with Caputo derivative: Analytic techniques

We start considering the fractional logistic equation with Caputo derivative since this is the dominating case, irrespective of the solution method applied [119–139, 145–147]. We will try to encompass the more important results and to compile an expository text that would be useful for understanding the main lines of solutions and emerging problems. That is, we have the general construction of the fractional logistic equation with Caputo derivative [145].

As it was commented in the preceding section dynamic models with the Caputo derivative belong to a class of models where the constructions obtained from basic principles (causality concept) and by formal replacements coincide. That is, we have the general construction of the fractional logistic equation with Caputo derivative [145].

$$D_t^{\alpha} y(t) = y(t)(1 - y(t)), \quad y(0) = y_0, \quad t > 0, \quad 0 < \alpha < 1 \tag{190}$$

Note: Since the focus now is on the solution techniques applied, we accept, for the sake of simplicity, that all coefficients in Eq.(190) are equal to unity.

- Direct integration approach [145]

Nieto [145] applied the fractional integral (Riemann-Liouville integral) to both sides of Eq.(190) to get

$$I_t^{\alpha}\left[D_t^{\alpha} y(t)\right] = I_t^{\alpha}\left[y(t)(1 - y(t))\right] \tag{191}$$

and bearing in mind that $I_t^{\alpha}\left[D_t^{\alpha} y(t)\right] = y(t) + c$, where c is an arbitrary constant, the result of the integration is

$$y(t) - y_0 = (1 - \alpha)\left[y(t)(1 - y(t)) - y_0(1 - y_0)\right] + \alpha \int_0^t y(s)\left[1 - y(s)\right] ds \tag{192}$$

Then, differentiating both sides of Eq.(193) we obtain

$$y(t) - y_0 = (1 - \alpha)\left[y(t)\left(1 - y(t) - y(t)\frac{dy(t)}{d}\right)\right] + \alpha y(t)\left[1 - y(t)\right] \tag{193}$$

or more compactly as

$$\alpha \frac{dy(t)}{dt} + 2(1 - \alpha) y \frac{dy(t)}{dt} = \alpha y(t)\left[1 - y(t)\right] \tag{194}$$

From Eq.(194) we recover the ordinary Verhulst equation for $\alpha = 1$.

Equation (194) can be rearranged as (for $y \neq 0, 1$)

$$\alpha \frac{dy}{dt} - 2\alpha y \frac{dy}{dt} + 2y \frac{dy}{dt} = \alpha y(1 - y) \Rightarrow \frac{dy/dt - 2y dy/dt}{y - y^2} + \frac{2}{\alpha}\frac{dy/dt}{1 - y} \tag{195}$$

or

$$\frac{d}{dt}\ln\left|1 - y^2\right| - \frac{2}{\alpha}\ln|1 - y| = 1 \Rightarrow \ln\left|1 - y^2\right| - \ln\left(|1 - y|^{2/\alpha}\right) = t + c \tag{196}$$

Finally we get

$$\frac{y - y^2}{(1 - y)^{2/\alpha}} = \frac{y - y_0^2}{(1 - y_0)^{2/\alpha}} \exp(t) \tag{197}$$

- Power series solution [140]

Area and Nieto [140] developed a power series solution by the expansion, so that

$$y(t) = \sum_{n=0}^{\infty} a_n t^n \Rightarrow \frac{dy(t)}{t} = \sum_{n=0}^{\infty} n a_n t^{n-1} = \sum_{n=0}^{\infty} (n + 1) a_{n+1} t^n \tag{198}$$

Then, from the integer order model (the Verhulst equation), the following recurrence relation appears

$$a_{n+1} = \frac{1}{n + 1}\left[a_n - \sum_{j=0}^{n} a_j a_{n-j}\right], n \geq 1, a_0 = y_0 = \frac{1}{2} \tag{199}$$

That is, with $a_0 = 1/2$, $a_1 = 1/4$, $a_2 = 0$, $a_3 = -1/48$,$a_4 = 0$, $a_3 = 1/480$ ... we obtain the approximate solution of the Verhulst equation [140]

$$\frac{1}{1+e^{-t}} \approx \frac{1}{2} + \frac{1}{4}t - \frac{1}{48}t^2 + \frac{1}{480}t^3 \tag{200}$$

Remark 10 (On the recurrence relation (199))**.** *Area and Nieto [141] noted that the same relation can be obtained in a slightly different way, precisely as briefly explained next. It needs to be noted that the initial coefficient, $a_0 = 1/2$, is chosen from the local form of the logistic equation.*
With the assumption that the solution can be developed as a series (198), then with derivative $dy(t)/dt$ (from the same expression (198)) and with (a multiplication of infinite series (recall the remark 7 explaining the appearance of convolution on the Zwanzig solution)

$$y^2(t) = \sum_{n=1}^{\infty} n a_n t^{n-1} = \sum_{n=0}^{\infty} \left(\sum_{j=0}^{n} (n+1) a_j a_{n-j} \right) t^n \tag{201}$$

Then, substituting $y(t)$ and $dy(t)/dt$ in the classical Verhulst model, the recurrence (199) can be obtained. Alternatively, the same recurrence relation can be obtained by applying the Laplace transform [141] to the right-hand side of the logistic model, so that

$$\mathcal{L}\left[y(t) - y^2(t)\right] = \sum_{n=0}^{\infty} (a_n - b_n) \frac{n!}{s^{n+1}}, \quad b_n = \sum_{j=0}^{n} a_j a_{n-j} \tag{202}$$

as well as with

$$\mathcal{L}\left[\frac{dy(t)}{dt}\right] = sY(s) = \sum_{n=0}^{\infty} a_{n+1}(n+1)\frac{n!}{s^{n+1}} \tag{203}$$

The result in the Laplace domain is

$$\sum_{n=0}^{\infty} a_{n+1}(n+1)\frac{n!}{s^{n+1}} = \sum_{n=0}^{\infty} (a_n - b_n) \frac{n!}{s^{n+1}} \tag{204}$$

That directly leads to the recurrence (199); to start the recurrence, it is needed $a_0 = y(0)$ (see Eq.(199)).

- Power series solution in terms of the Euler polynomials [140]

If the Euler polynomials are considered (see Section 2.1.2 about the Taylor series expansion), i.e.,

$$\frac{2\exp(\xi t)}{\exp(t)+1} = \sum_{n=0}^{\infty} E_n(\xi)\frac{t^n}{n!} \tag{205}$$

and the series is convergent for $|t| < \pi$.
Thus, for $\xi = 1$,

$$\frac{2\exp(t)}{\exp(t)+1} = \frac{2}{1+\exp(-t)} = \sum_{n=0}^{\infty} E_n(1)\frac{t^n}{n!} \tag{206}$$

Hence, we have the approximation

$$\frac{1}{1+\exp(-t)} = \frac{1}{2}\sum_{n=0}^{\infty} E_n(1)\frac{t^n}{n!} \tag{207}$$

Therefore, the coefficients in the power series expansion can be represented by the Euler numbers as $a_n = \frac{1}{2}\frac{E_n(1)}{n!}$. Since, for the logistic function $a_n = y^{(n)}(0)/n!$, we have the relation $a_n = E_n(1)/2 = y^{(n)}(0)$ [140].
After the initial steps demonstrating the main logic of the power series solution, we look at the fractional logistic equation (190) and try to construct the solution as $x(t) = \sum_{n=0}^{t} b_n(\alpha)(t^\alpha)^n$. Skipping details, we get a recurrence relation [140]

$$b_{n+1}(\alpha) = \frac{\Gamma(n\alpha+1)}{\Gamma[(n+1)\alpha+1]}\left[b_n(\alpha) - \sum_{j=0}^{n} b_j(\alpha)\, b_{n-j}(\alpha)\right], \quad n > 0 \tag{208}$$

Hence, for example: $b_0(\alpha) = 1/2$, $b_2(\alpha) = 0$, $b_3(\alpha) = \Gamma(2\alpha+1)/\left[16\Gamma(\alpha+1)^2\right]\Gamma(3\alpha+1)$, $b_4(\alpha) = 0$.

- Logistic model with Caputo derivative and Allee effects

Now, consider a logistic model with Allee effect [142]

$$\frac{dy(t)}{dt} = y(t)(1-y(t))[y(t)-A], \quad A>0 \tag{209}$$

with constant solutions $0, 1, A$.

For $\frac{dy}{dt} > 0$ *and when* $A < y(0) < 1$ *we have an increasing* $y(t)$

For $\frac{dy}{dt} < 0$ *and when* $0 < y(0) < A$, *then* $y(t)$ is decreasing

With the assumption of developing a solution as a series (198) we have $y^2(t)$ approximated by Eq.(201) and $y^3(t)$ as

$$y^3(t) = \sum_{n=0}^{\infty}\left(\sum_{j=0}^{n}\left(\sum_{k=0}^{j} a_k a_{n-j}\right)\right)t^n \tag{210}$$

The substitution of these formal series approximations into Eq.(209) and bearing in mind that in such a case

$${}^{C}D_t^{\alpha} \approx \sum_{n=0}^{\infty} b_{n+1}(\alpha)\frac{\Gamma[(n+1)\alpha+1]}{\Gamma(n\alpha+1)}(t^{\alpha})^n \tag{211}$$

The following recurrence relation about the coefficients $b_n(\alpha)$ appears

$$b_{n+1} = \frac{\Gamma(n\alpha+1}{\Gamma[(n+1)\alpha+1]}\left[-Ab_n + (A+1)\sum_{j=0}^{n} b_j b_{n-j} - \sum_{j=0}^{n}\left(\sum_{k=0}^{j} b_k b_{j-k}\right)b_{n-j}\right] \tag{212}$$

valid for $n > 0$ and an initial condition $b_0 = y(0)$.

Note: A detailed analysis of stability and bifurcation behavior of a fractional logistic model with Allee effect was done in [143] oriented to thresholds to extinction of low-density populations (see also the references therein).

Remark 11 (On the exact solution of the fractional logistic equation)**.** *Area et al. [128] considered an analysis provoked by the preceding solution of West [127], who declared a development of an exact solution of Eq.(190) applying the Carleman embedding technique (see details about the solutions of a quasi Verhulst equation in [148]- Chapter 3.2) , as*

$$y(t) = \sum_{n=0}^{\infty}\left(\frac{y_0-1}{y_0}\right)^n E_{\alpha}(-nt^{\alpha}) \tag{213}$$

The detailed analysis of Area et. al. [128] demonstrated that the solution of West is valid only when $\alpha = 1$, *but suggested that Carleman techniques would be promising for solutions of fractional equations, although still undeveloped in this direction. D'Ovidio et al. [134] tested the function (213) but with a modified fractional logistic equation*

$$D_t^{\alpha} y(t) = y(t)(1-y(t)) + y_0\frac{t^{-\alpha}}{\Gamma(1-\alpha)} + \int_0^{\infty}\int_0^{\infty}\left[y(s)y(z) - y^2(s)\right]l_{\alpha}(z,t)\,dsdz \tag{214}$$

The additive term is related to the solution of the classical logistic equation. Also, the function obeys the conditions $l_{\alpha}(0,t) = t^{-\alpha}/\Gamma(1-\alpha)$ *and* $\int_0^{\infty} l_{\alpha}(s,t)ds = 1$, *as well as its Laplace transform, is* $\int_0^{\infty} e^{-\lambda s} l_{\alpha}(s,t)ds = E_{\alpha}(-\lambda t^{\alpha})$, $\lambda > 0$. *The tests in [134] demonstrated that (213) is a solution of Eq. (214), but not of Eq. (190).*

Ortigueira and Bengochea [130] were also attracted by the discussion on the solution of the fractional logistic equation raised by Area et al. [128] and solved the problem from a different point of view: they suggested that the fractional derivative is the Grunwald-Letnikov (GL) derivative, since, in contrast to the

Caputo derivative, there is no restriction the function to be differentiable. Assuming a solution as a Taylor series and the Pade approximation technique, a solution was developed.

Currently, since there are no exact solutions to the fractional logistic equation, many attempts are being made to develop approximate solutions using various techniques such as spectral methods [124, 132], as the series approximations discussed above. As an exception, Tarasov [137] developed exact solutions to Bernoulli and fractional logistic models in special cases where the coefficient is of power law, with examples from mechanics and economics.

Remark 12 (The Euler number approach to fractional logistic equation solution)**.** *Efficient solutions to the fractional logistic equations have been developed in [133, 138] by applying the Euler number approach, like that demonstrated earlier. A more advanced study in this direction was developed by Nieto [146].*

Remark 13 (Numerical techniques)**.** *Various numerical techniques have been applied to solve the fractional logistic equation Eq.(190), among them: Optimal HAM [125], iterative methods [119, 121], collocation methods [124, 129, 131], Chebishev approximations [123] , Adams-type predictor-corrector method [122], spectral methods [132, 136], Padé approximants [120], etc.; see for more details the quoted works and the reference therein. We do not develop analyzes of this trend in solutions of fractional logistic equations since it is beyond the framework of the study, but this does not mean you should neglect it.*

Note: For completeness of the reference information we refer to the thorough analysis and strong results concerning approximate analytical methods with Caputo fractional derivative developed by Aibinu and Momoniat [155].

7.1.2. Λ-fractional logistic equation

- Formulation and a simple series solution [150]

Recently, Jornet and Nieto [150] considered a fractional-logistic equation based on the Λ-fractional derivative [151–153]

$$ {}^{\Lambda}D^{\alpha}y = y\left(1-y\right) = y - y^2, \quad t > 0, \quad 0 < \alpha < 1 \tag{215} $$

where

$$ {}^{\Lambda}D^{\alpha}y = \frac{{}^{C}D^{\alpha}y\left(t\right)}{{}^{C}D^{\alpha}t} \tag{216} $$

is the Leibniz fractional derivative of an absolutely continuous function $y \in [0,T] \to \mathbb{R}$ [151]. In the nominator and denominator of ${}^{\Lambda}D^{\alpha}y$ there are Caputo fractional derivatives.

Equation (215) is equivalent to a non-autonomous Caputo equation [150]

$$ {}^{C}D_{t}^{\alpha}y = \frac{t^{1-\alpha}}{\Gamma\left(2-\alpha\right)}y\left(1-y\right) \tag{217} $$

The ${}^{\Lambda}D^{\alpha}y$ derivative defines a differential, and therefore, it has a geometrical meaning [150–152].

Assuming a solution as a formal series expansion $y\left(t\right) = \sum\limits_{0}^{\infty} a_n t^n$, a recursive relation was obtained

$$ a_{n+1} = \frac{\Gamma\left(n+2-\alpha\right)}{\Gamma\left(n+2\right)\Gamma\left(2-\alpha\right)}\left[a_n - \sum_{m=0}^{n} a_m a_{n-m}\right] \tag{218} $$

Besides, the solution in terms of ${}^{\Lambda}D^{\alpha}y$ is C^{∞} and real analytic, expanded in terms of t^n instead $t^{\alpha n}$, in contrast to the case when the logistic equation uses the Caputo derivative [150]. Further, as demonstrated by Jornet and Nieto [150]

$$ {}^{\Lambda}D^{\alpha}y = \frac{dy\left(0\right)}{dt} + \frac{1}{t^{1-\alpha}}\int_{0}^{t}\frac{1}{\left(t-s\right)^{\alpha-1}}\frac{d^2y\left(s\right)}{ds^2}ds \tag{219} $$

showing that it is with *a singular kernel*.

Since with $y = C$ (a constant) we have ${}^{\Lambda}D^{\alpha}C = 0$, the initial condition for Eq.(215) is the same as in the case when the Caputo derivative is applied [150] .

Last, but not least, considering the concept to represent the solution to Eq.(215) *via* the Euler numbers, the coefficients a_n of the series solution (defined by Eq.(218)) relate as

$$E_n^{\alpha} = 2a_n^{\alpha}\Gamma(2-\alpha)^n \prod_{j=1}^{n} \frac{\Gamma(j+1)}{\Gamma(j+1-\alpha)} \tag{220}$$

When ${}^{\Lambda}D^{\alpha}y(t)$ is applied to the population equation, there is a possibility that the local (integer-order) model to be extended to a non-local (fractional) version [150]. More interesting details about the properties of ${}^{\Lambda}D^{\alpha}y(t)$ are available in [150], especially the singularity of its kernel.

- More details on the Λ-fractional derivative and the logistic equation

The Λ-fractional derivative was defined above, but now, for the sake of clarity of exposition, we would like to present some additional details. As mentioned, in fact, it is the Leibniz fractional derivative defined by Eq.(216) as ${}^{\Lambda}D_t^{\alpha}y(t) = \frac{{}^{C}D_t^{\alpha}y(t)}{{}^{C}D_t^{\alpha}t}$ (see below)

With the Riemann-Liouville derivative of order $\alpha \in (0,1)$

$$D_t^{\alpha}u(t) = \frac{1}{\Gamma(1-\alpha)}\frac{d}{dt}\int_0^t \frac{u(s)}{(t-s)^{\alpha}}ds, \quad \alpha \in (0,1), \quad t \in [0,T] \tag{221}$$

and, as well as with $n \in N$, we have

$$D_t^{\alpha}t^n = \frac{\Gamma(n+1)}{\Gamma(n-\alpha+1)}t^{n-\alpha} \Rightarrow D_t^{\alpha}t^{\gamma}\frac{\Gamma(\gamma+1)}{\Gamma(\gamma-\alpha+1)}t^{n-\alpha}, \quad \alpha > 0, \quad \gamma > -1 \tag{222}$$

For $\gamma = 2$ we have $D^{\gamma}t^2 = \frac{\Gamma(3)}{\Gamma(3-\gamma)}t^{2-\gamma} = \frac{2t^{2-\gamma}}{\Gamma(3-\gamma)}$.

Now, if we need to differentiate a power-law function, i.e., to find ${}^{\Lambda}D_t^{\alpha}t^n$, applying the definition we have [154]

$${}^{\Lambda}D_t^{\alpha}t^n = \frac{\frac{\Gamma(n+1)}{\Gamma(n+1-\alpha)}t^{n-\alpha}}{\frac{t^{1-\alpha}}{\Gamma(2-\alpha)}} = \frac{\Gamma(n+1)\Gamma(2-\alpha)}{\Gamma(n+1-\alpha)}t^{n-1} \tag{223}$$

It is obvious that for $\alpha \to 1$ we have ${}^{\Lambda}D_t^{\alpha}t^n{}_{(\alpha\to 1)} \Rightarrow \frac{dt^n}{dt} = nt^{n-1}$. To make it clear, let us explain the transformation from the linear t space into the Λ-space [154], that is, this transformation is

$$t \to T = \frac{t^{2-\gamma}}{\Gamma(3-\gamma)} \tag{224}$$

Precisely, let us focus on the space transformation $u(t) \to U(T)$ as well as the power-law transform $t^b \to T^B$, which enables us to find a simple form of the logistic equation (see further Eq.(227). From the definition of T we have that $t = T\left(\Gamma(3-\gamma)^{\frac{1}{2-\gamma}}\right)$. Moreover,

$$\begin{aligned} T^B &= \frac{1}{\Gamma(1-\gamma)}\int_0^t \frac{s^b}{(t-s)^{\gamma}}ds = \frac{\Gamma(1+b)t^{1+b-\gamma}}{\Gamma(2+b-\gamma)} \Rightarrow \\ \Rightarrow T^B &= \frac{\Gamma(1-b)\left[\Gamma(3-\gamma)T\right]^{\frac{1+b-\gamma}{2-\gamma}}}{\Gamma(2+b-\gamma)} \end{aligned} \tag{225}$$

With these preliminaries, we may consider the Λ-logistic equation presented as (in the original notations of [154]) (for $T > 0$, $u \in AC[0,T]$)

$${}^{\Lambda}D_t^{\alpha}u(t) = t^b u(1-u) \tag{226}$$

where $0 < \gamma < 1$ in the initial t-space and take into account that the coefficient is t^b, i.e., time-dependent. Therefore, in the Λ-space, we have

$$\frac{dU(T)}{dT} = AT^B\left[U(T) - U^2(T)\right], \quad B = \frac{1+b-\gamma}{2-\gamma} \tag{227}$$

where $A = \frac{\Gamma(1-b)[\Gamma(3-\gamma)]^{\frac{1+b-\gamma}{2-\gamma}}}{\Gamma(2+b-\gamma)}$.

Then, the solution obtained (by Wolfram Mathematica) [154] in the Λ-space is

$$U(T)=\frac{1}{1+C\exp\left[-\left(\frac{A}{B+1}\right)T^{B+1}\right]} \tag{228}$$

where C is a constant.
Now, going back to the initial t space we have $\bar{U}(t)=U\left[T\to\frac{t^{2-\gamma}}{\Gamma(3-\gamma)}\right]$ and the solution is

$$\begin{aligned}u(t)&=D^{1-\gamma}\bar{U}(t)=\frac{1}{\Gamma(\gamma)}\frac{d}{dt}\int_0^t\frac{\bar{U}(s)}{(t-s)^{1-\gamma}}ds=\\&=\frac{\exp\left[\frac{A\left(\frac{t^{2-\gamma}}{\Gamma(3-\gamma)}\right)}{B+1}\right]\left\{\gamma t^{\gamma}\Gamma(3-\gamma)\left[\exp\left[\frac{A\left(\frac{t^{2-\gamma}}{\Gamma(3-\gamma)}\right)}{B+1}\right]+C\right]-AC(\gamma-2)t^2\left(\frac{t^{2-\gamma}}{\Gamma(3-\gamma)}\right)^B\right\}^B}{\gamma t\Gamma(3-\gamma)\Gamma(\gamma)\left[\exp\left[\frac{A\left(\frac{t^{2-\gamma}}{\Gamma(3-\gamma)}\right)}{B+1}\right]+C\right]^2}\end{aligned} \tag{229}$$

Remark 14 (Some comments on the Λ-fractional logistic equation)**.** *We can see that the transforms imposed by $D_t^{\alpha}y(t)$ allow us to obtain a logistic equation (227) very close to the original Verhulst model, which is easy to solve. However, the inverse transform into the original t space is not easy. Moreover, as also commented in [154], the solution of Eq.(229) it is to complicated and hard to interpret, compared with, for example, the series solutions, as was demonstrated above by the recursive relation (218). The solutions developed in [150] and [154], and discussed here, are examples of what we can do with a newly defined derivative. However, we have to expect more easy-to-understand applications of $D_t^{\alpha}y(t)$, since there is a serious background for this in [151–153].*

7.2. Fractional models with non-singular memory kernels

Now, we turn on non-local models with fractional operators with non-singular memories, a trend that began in 2015 when the Caputo-Fabrizio derivative was conceived [156]. This was the nuclei expanded towards the definition of the Atangana-Baleanu derivative (ABC) based on the Mittag-Leffler kernel [157] in 2016, and attempts to generalize these operators as special cases of the Prabhakar fractional calculus [158]. The following parts of this section consider models starting with a simple case with the Caputo-Fabrizio derivative and gradually passing through models with ABC and Prabhakar derivatives.

7.2.1. Logistic equations with the Caputo-Fabrizio operator

- Solution of Kumar et al. [159]

Kumar et al. [159] considered a fractional logistic equation with the Caputo-Fabrizio derivative (231) with a non-singular kernel [156]

$${}^{CF}D_t^{\alpha}y(t)=ky(t)(1-y(t)),\quad t>0,\quad y(0)=y_0=a\neq 0 \tag{230}$$

$${}^{CF}D_t^{\alpha}y(t)=\frac{M(\alpha)}{1-\alpha}\int_0^t e^{-\frac{\alpha}{1-\alpha}(t-\varepsilon)}\frac{dy(s)}{dt}ds \tag{231}$$

Stability issues:
The stability at the equilibrium points $y=0,1$, with

$$\frac{dg}{dt}(y(t))=k(1-2y(t))\Rightarrow\frac{dg}{dt}(0)=k,\quad\frac{dg}{dt}(1)=-k \tag{232}$$

Then, the solution of

$${}^{CF}D_t^{\alpha}\varepsilon(t)=g'\left(y_{eq}=0\right)\varepsilon(t)=k\varepsilon(t),\quad t>0,\quad\varepsilon(0)=y_0 \tag{233}$$

is

$$\varepsilon(t)=\frac{y_0}{1-k+k\alpha}\exp\left(\frac{k\alpha}{1-k+k\alpha}\right) \tag{234}$$

demonstrating that the point $y = 0$ is unstable. Otherwise, at $y = 1$, the solution of

$$ {}^{CF}D_t^{\alpha}\varepsilon(t) = g'\left(y_{eq} = 1\right)\varepsilon(t) = -k\varepsilon(t), t > 0, \varepsilon(0) = y_0 - 1 \tag{235} $$

is

$$ \varepsilon(t) = \frac{y_0 - 1}{1 - k + k\alpha}\exp\left(\frac{k\alpha}{1 - k + k\alpha}\right) \tag{236} $$

and reveals that the equilibrium point $y = 1$ is asymptotically stable.

Uniqueness of the solution:

The analysis in [159] reveals that if the condition (237) is satisfied (with $M(\alpha) = 1$)

$$ \left(1 - k\frac{2(1-\alpha)}{(2-\alpha)} - kt\frac{2\alpha}{(2-\alpha)}\right) > 0 \tag{237} $$

then, Eq.(230) has a unique solution.

A numerical solution based on the perturbation techniques and Pade approximation, with $y_0 = 1/2$ (two values of the coefficient k ($k = 1/2$ $k = 1/3$) was used to calculate plots showing the effect of the fractional order α.

- A hybrid solution of Jafari et al. [160]

Jafari et al. [160] also considered Eq.(230) and its solution, at least the initial steps applied, to some extent, resemble the approach used by Nieto (see above). Precisely, first rearranging Eq.(230) as

$$ \begin{aligned} &\frac{M(\alpha)}{1-\alpha}\int_0^t e^{-\frac{\alpha}{1-\alpha}(t-s)}\frac{dy(s)}{ds}ds = f(t, y(t)) \Rightarrow \\ &\Rightarrow \int_0^t e^{-\frac{\alpha}{1-\alpha}(t-s)}\frac{dy(s)}{ds}ds = \frac{1-\alpha}{M(\alpha)}e^{-\frac{\alpha}{1-\alpha}t}f(t, y(t)) \end{aligned} \tag{238} $$

Then, differentiation applied to both sides of Eq.(238) yields

$$ \frac{dy(t)}{dy} = \frac{1-\alpha}{M(\alpha)}\left[\frac{df(t, y(t))}{dt} + \frac{\alpha}{1-\alpha}f(t, y(t))\right] \tag{239} $$

With $f(0, y(0)) = 0$, the solution of Eq.(239) is

$$ y(t) = y(0) + \frac{1-\alpha}{M(\alpha)}f(t, y(t)) + \frac{\alpha}{M(\alpha)}\int_0^t f(s, y(s))ds \tag{240} $$

Further, expressing Eq.(240) for two different times $t = t_m$ and $t = t_{m+1}$, and subtracting them, side by side, the result (the difference) is

$$ y(t_{m+1}) - y(t_m) = \frac{1-\alpha}{M(\alpha)}\left(f(t_m, y(t_m)) - f(t_{m+1}, y(t_{m+1}))\right) + \frac{\alpha}{M(\alpha)}\int_{t_m}^{t_{m+1}} f(s, y(s))ds \tag{241} $$

Applying the three-step Adams-Bashforth technique to the integral term and using a Lagrange interpolation of $f(s, y(s))$on $[t_m, t_{m+1}]$, the solution was developed.

- A series solution of Area and Nieto [141]

Consider Eq.(230) with the series solution approximation (198), and applying the Laplace transform to both sides we get

$$ \sum_{n=1}^{\infty}\frac{\Gamma(n\xi + 1)}{(\alpha(1-s) + s)s^{n\xi}} = \sum_{n=0}^{\infty}(a_n - b_n)\frac{\Gamma(n\xi + 1)}{s^{n\xi+1}} \tag{242} $$

For example, if $\xi = \alpha$ and when $\alpha \to 1$ (from the left),), then we get the recursive relation (199).

The relationship (242) can be rearranged as (see the steps in [141])

$$\sum_{n=1}^{\infty}\Gamma(n\xi+1)\frac{a_n}{s^{n\xi}}=\alpha\sum_{n=0}^{\infty}(a_n-b_n)\frac{\Gamma(n\xi+1)}{s^{n\xi+1}}+ \\ +(1-\alpha)\sum_{n=0}^{\infty}(a_n-b_n)\frac{\Gamma(n\xi+1)}{s^{n\xi}} \tag{243}$$

When $\xi=1$, then Eq.(243) reduces to

$$a_n=\frac{1}{n}\left(a_{n-1}-b_{n-1}+nb_n\frac{\alpha-1}{\alpha}\right) \tag{244}$$

and for $\alpha\to 1$ we get the recurrence (199).

- Laplace transform solution by Kanth and Garg [144]

Consider again Eq.(230) in a simplified form [144]

$${}^{Cf}D_t^{\alpha}x(t)=k(1-x(t)),\quad 0<\alpha<1 \tag{245}$$

and applying the Laplace transform to both sides, we get

$$X(s)=\frac{x(0)-1}{(1+k-\alpha k)(s+\frac{\alpha k}{1+k-\alpha k})}+\frac{1}{s} \tag{246}$$

taking into account that $\mathcal{L}[{}^{Cf}D_t^{\alpha}x(t)]$ (see the definition (231)) is [156]

$$\mathcal{L}[{}^{Cf}D_t^{\alpha+n}x(t)]=\frac{s^{n+1}\mathcal{L}[x(t)]-x(0)S^n-x(0)s^{n-1}-\ldots x^{(n)}(0)}{s+(1-s)\alpha} \tag{247}$$

Then, the inverse transform of Eq.(246) yields

$$x(t)=\frac{x(0)-1}{1+k(1-\alpha)}exp\left[-\frac{\alpha k}{1+k(1-\alpha)}t\right]+1 \tag{248}$$

Now, with the substitutions $y(t)=1/x(t)$ and $x(0)=1/y(0)$ we obtain

$$y(t)=\left\{1+\frac{1-y(0)}{y(0)}\frac{1}{1+k(1-\alpha)}exp\left[-\frac{\alpha k}{1+k(1-\alpha)}t\right]\right\}^{-1} \tag{249}$$

For $\alpha\to 1$, Eq.(249) approaches to the integer-order Verhulst model, namely

$$y(t)_{\alpha\to 1}=\left[1+\left(\frac{1-y(0)}{y(0)}\right)exp(-kt)\right]^{-1} \tag{250}$$

Note: For completeness of the exposition, even though all published results cannot be encompassed here, we have to mention the work of Djeddi et al. [161] where a modified analytical approach to generalized logistic models with quadratic and cubic terms was developed. Attempts to solve the logistic models with the Caputo-Fabrizio derivative, by numerical solutions, applying a successive approximation method were reported by Adel and Khader [162]. Also, and use the compact finite difference scheme to solve this equation numerically was developed by Sattari and Ameri [163]; we mention these studies for completeness of the reference quotations since they also belong to the group of fractional models obtained by replacement.

7.3. Logistic dynamics in the Mittag-Leffler memory fractional framework

7.3.1. Logistic model with the Atangana-Baleanu derivative

- A solution by application of the Atangana-Baleanu integral [164]

Hassan et al. [164] considered the Verhulst logistic model

$${}^{ABC}D_{\alpha}^{t}=ky\left(t\right)\left(1-y\left(t\right)\right),\quad 0<\alpha\leq 1,\quad t\geq 0,\quad k>0,\quad y\left(0\right)=y_0>0 \tag{251}$$

by applying the Atangana-Baleanu fractional derivative of Caputo type [157]

$$
\begin{aligned}
{}^{ABC}D_{\alpha}^{t}f\left(t\right)=\frac{M\left(\alpha\right)}{1-\alpha}\int_{0}^{t}E_{\alpha}\left(-\frac{\alpha}{1-\alpha}\left(t-s\right)^{\alpha}\right)\frac{df\left(s\right)}{ds}ds= \\
=\frac{M\left(\alpha\right)}{1-\alpha}\frac{df\left(t\right)}{dt}*E_{\alpha}\left(-\frac{\alpha}{1-\alpha}t^{\alpha}\right), \qquad (252)\\
E_{\alpha}\left(-t^{\alpha}\right)=\sum_{0}^{\infty}\frac{\left(-1\right)^{n}t^{\alpha n}}{\Gamma\left(\alpha n+1\right)}
\end{aligned}
$$

where $E_{\alpha}\left(-t^{\alpha}\right)$ is the Mittag-Leffler function with one parameter, and the condition imposed on $M(\alpha)$ is $M\left(0\right)=M\left(1\right)=1$.

The Laplace transforms of ${}^{ABC}D_{\alpha}^{t}f\left(t\right)$ is

$$
\mathcal{L}\left[{}^{ABC}D_{t}^{\alpha}f\left(t\right)\right]=\frac{M\left(\alpha\right)}{1-\alpha}\frac{\left(s^{\alpha}F\left(s\right)-s^{\alpha-1}f\left(0\right)\right)}{s^{\alpha}+\frac{\alpha}{1-\alpha}} \qquad (253)
$$

Particularly, with a power-law function $f\left(t\right)=t^{n}$, pertinent to the series solution developed , is

$$
\mathcal{L}\left[{}^{ABC}D_{t}^{\alpha}t^{n}\right]=\frac{M\left(\alpha\right)}{\left(1-\alpha\right)}\frac{1}{s^{\alpha}+\frac{\alpha}{1-\alpha}}\frac{\Gamma\left(n+1\right)}{s^{n-\alpha+1}} \qquad (254)
$$

The model (251) was investigated in the Sobolev space. Moreover, a detailed analysis based on the fixed-point theory was done towards existence and uniqueness (see details in the original work).

As a first step of the solution technique, the Atangana-Baleanu Integral ${}^{ABC}I_{t}^{\alpha}$ (see Remark 15 for explanations)

$$
{}^{ABC}I_{t}^{\alpha}f\left(t\right)=\frac{1-\alpha}{M\left(\alpha\right)}f\left(t\right)+\frac{\alpha}{M\left(\alpha\right)}\frac{1}{\Gamma\left(\alpha\right)}\int_{a}^{t}\frac{f\left(s\right)}{\left(t-s\right)^{1-\alpha}}ds,\quad t>a \qquad (255)
$$

was applied to both sides of Eq.(251) to obtain

$$
y\left(t\right)=y_{0}+\frac{1-\alpha}{M\left(\alpha\right)}ky\left(t\right)\left(1-y\left(t\right)\right)+\frac{\alpha}{M\left(\alpha\right)}\frac{1}{\Gamma\left(\alpha\right)}\int_{0}^{t}ky\left(s\right)\left(1-y\left(s\right)\right)\frac{1}{\left(t-s\right)^{1-\alpha}}ds \qquad (256)
$$

Denoting $Y\left(t\right)=y\left(t\right)\left(1-y\left(t\right)\right)$, a more compact form of Eq.(255) for further analysis was used

$$
y\left(t\right)=y_{0}+\frac{1-\alpha}{M\left(\alpha\right)}\left[Y\left(t\right)\right]+\frac{\alpha}{M\left(\alpha\right)}\int_{0}^{t}Y\left(s\right)\frac{1}{\left(t-s\right)^{1-\alpha}}ds \qquad (257)
$$

Equation (257) was proved for the existence of unique solutions with $y_{0}\neq0$ following the Banach fixed point theorem (more details in the original work).

Remark 15 (On the Atangana-Baleanu integral)**.** *As was demonstrated by Atangana and Baleanu [157] the following fractional differential equation*

$$
{}_{0}^{ABR}D_{t}^{\alpha}\left[f\left(t\right)\right]=u\left(t\right) \qquad (258)
$$

where ${}_{0}^{ABR}D_{t}^{\alpha}f\left(t\right)$ *is the Atangana-Baleanu derivative in the Riemann-Liouville sense.*

$$
\begin{aligned}
{}^{ABR}D_{a+}^{\alpha}f\left(t\right)=\frac{M\left(\alpha\right)}{1-\alpha}\frac{d}{dt}\int_{0}^{z}f\left(z\right)E_{\alpha}\left[\frac{-\alpha}{1-\alpha}\left(t-z\right)^{\alpha}\right]dz,\quad 0<\alpha<1, \qquad (259)\\
a<t<b,\quad f\left(t\right)\in L^{1}\left[a,b\right]
\end{aligned}
$$

and

$$
{}^{ABC}D_{t}^{\alpha}\left[f\left(t\right)\right]={}_{0}^{ABR}D_{t}^{\alpha}\left[f\left(t\right)\right]-\frac{M\left(\alpha\right)}{1-\alpha}f\left(0\right)E_{\alpha}\left(-\frac{\alpha}{1-\alpha}t^{\alpha}\right) \qquad (260)
$$

Equation (258 has a unique solution

$$f(t)=\frac{1-\alpha}{M(\alpha)}u(t)+\frac{\alpha}{M(\alpha)}\frac{1}{\Gamma(\alpha)}\int_0^t u(\tau)(t-\tau)^{\alpha-1}d\tau \tag{261}$$

and from this, the associated Atangana-Baleanu integral was defined (with $M(\alpha)=1$, for the sake of simplicity of exposition)

$${}^{AB}I_{a+}^{\alpha}u(t)=(1-\alpha)u(x,t)+\alpha\,{}^{RL}I_{a+}^{\alpha}u(x,t)=f(x,t) \tag{262}$$

where for $\alpha=0$ we recover the initial function, while for $\alpha=1$ we get the ordinary Riemann integral.

Further, we have

$${}^{AB}I_{a+}^{\alpha}\left[{}^{ABR}D_{a+}^{\alpha}f(t)\right]=f(t),\quad {}^{ABR}D_{a+}^{\alpha}f(t)\left[{}^{AB}I_{a+}^{\alpha}f(t)\right]=f(t) \tag{263}$$

Note: *The derivative used in Eq.(252) and the operation resulting in Eq.(256) is of Caputo type, i.e., ${}_0^{ABC}D_t^{\alpha}$. A detailed analysis of the associated and constitutive Atangana-Baleanu integrals (as well as of the Caputo-Fabrizio operators) is available in [105].*

Two numerical approaches were applied to solve Eq.(251): Successive substitution algorithm (SSA) and the reproducing (RK) method, briefly presented next.

1) *Solution by the successive substitution algorithm (SSA):*

Representing Eq.(256) as an equivalent Volterra integral equation, the following recurrence formula was developed [164]

$$\begin{aligned}y_{n+1}(t)&=y_0+\frac{1-\alpha}{M(\alpha)}k\left[y_n(t)\left(1-y_n(t)\right)\right]+\\&+\frac{\alpha}{M(\alpha)}k\int_0^t y_n(s)\left(1-y_n(s)\right)\frac{1}{(t-s)^{1-\alpha}}ds\end{aligned},\quad n=0,1,2\ldots \tag{264}$$

with $y_{n=0}=y_0$

Note: It is easy for the reader to see the logical line to use the heredity of the logistic model expressed as Volterra integral equations, as we commented earlier.

2) *Reproducing kernel (RK) method:* As a first step, the initial condition was homogenized as $Z(t)=y(t)-y_0$. This allows us to get

$${}^{ABC}D_t^{\alpha}\left[Z(t)+y_0\right]=k\left(Z(t)+y_0\right)\left(1-Z(t)-y_0\right) \tag{265}$$

taking into account that ${}^{ABC}D_t^{\alpha}y_0=0$.

Then, the solution of the following initial value problem was developed

$${}^{ABC}D_t^{\alpha}Z(t)=k\left(Z(t)+y_0\right)\left(1-Z(t)-y_0\right),\quad Z(0)=0,\quad t>0 \tag{266}$$

Definition of the differential operator (in the original notations) ($L:W_2^2[a,b]\to W_2^1[a,b]$ (see the note below), such that $L[Z(t)]={}^{ABC}D_t^{\alpha}Z(t)$, allows to rewrite Eq.(266) as

$${}^{ABC}D_t^{\alpha}Z(t)=k\left[Z(t)+y_0\right]\left[1-Z(t)-y_0\right],\quad t>0 \tag{267}$$

Note: The operator L is bounded and linear from $W_2^2[a,b]$to $W_2^1[a,b]$, so that $L[Z(t)]={}^{ABC}D_t^{\alpha}Z(t)$ (the proof is provided by Theorem 4 in [164])

3) *Numerical simulations:*

Numerical solutions were carried out with different values of y_0, precisely $y_0=1/2$, $y_0=1/4$ and $y_0=0$,compared with exact solutions $y(t)=\frac{1}{1+e^{-y_0t}}$.

More details about the numerical procedures are available in the original work, but the results reveal that the plotted solutions are growing in time, and to some extent, resemble the original logistic function when $\alpha\to 1$, but no further analyzes are available, since the focus was on solution techniques, not on the physical relevance of the obtained results.

7.3.2. Solutions by the Laplace transform

As step towards a solution of Eq.(251), Bas and Ozarslan [165] considered the simple first-order kinetic model

$$^{ABC}D_t^{\alpha} = -ky(t), \quad t \geq 0, \quad 0 < \alpha < 1 \tag{268}$$

Applying the Laplace transform to both sides of Eq.(268), and rearranging the expressions to allow the inverse transform, the result is

$$y(t) = \frac{M(\alpha)}{1-\alpha}\frac{y(a)}{M(\alpha)-k(1-\alpha)}E_{\alpha}\left(\frac{k\alpha}{M(\alpha)-k(1-\alpha)}\right) \tag{269}$$

Note: In Eq.(269), the lower terminal in the convolution integral of (252) is defined as a .

The result (269) can be simplified, if $a = 0$ and $M(\alpha) = 1$, for the sake of simplicity, that is

$$y(t) = \frac{1}{1-\alpha}\frac{y(a)}{1-k(1-\alpha)}E_{\alpha}\left(\frac{k\alpha}{1-k(1-\alpha)}\right) \tag{270}$$

Then, the same approach was applied to Eq.(251) and the result (skipping the cumbersome expressions and transformations) is

$$\begin{aligned} y(t) = &-k\frac{1-\alpha}{1-k(1-\alpha)}E_{\alpha}\left(\frac{k\alpha}{1-k(1-\alpha)}\right)t^{\alpha}+ \\ &+\left[\frac{1-\alpha}{1-k(1-\alpha)}\right]^2\left(1-E_{\alpha}\frac{k\alpha}{1-k(1-\alpha)}t^{\alpha}\right)+\frac{y(0)}{1-k(1-\alpha)}E_{\alpha}\left(\frac{k\alpha}{1-k(1-\alpha)}t^{\alpha}\right) \end{aligned} \tag{271}$$

in a simplified form, with $M(\alpha) = 1$ and $y(a) = y(0)$, allowing a more unified presentation, as it was done in many cases considered in this work.

7.3.3. A solution by a series

Consider Eq.(251) and a formal series solution $y(t) = \sum_0^{\infty} a_n t^n$, and then applying the Laplace transform we have [154] (see similar operations with the power series approximation in the preceding parts of this text)

$$\mathcal{L}\left[^{ABC}D_t^{\alpha}y(t)\right](s) = \sum_{n=0}^{\infty}(a_n - b_n)\frac{\Gamma(n\xi+1)}{\xi^{n\alpha+1}} \tag{272}$$

Then, for $\xi = \alpha$

$$\frac{M(\alpha)}{(1-\alpha)\left(s^{\alpha}+\frac{\alpha}{1-\alpha}\right)}\sum_{n=1}^{\infty}a_n\frac{\Gamma(n\alpha+1)}{s^{(n-1)\alpha}+1} = \sum_{n=0}^{\infty}(a_n-b_n)\frac{\Gamma(n\alpha+1)}{s^{n\alpha}+1} \tag{273}$$

Further, with $b_n = a_0 a_n + \sum_{j=1}^{n-1} a_j a_{n-j}$, the recurrence relation is (we skip the intermediate steps that can be seen in details in [154])

$$a_n = \frac{(1-\alpha)\sum_{j=1}^{n-1}a_j a_{n-j} + \frac{\alpha\Gamma[\alpha(n-1)+1]\left[\sum_{j=1}^{n-1}a_j a_{n-j}+(2a_0-1)a_{n-1}\right]}{\Gamma(\alpha n+1)}}{(2a_0-1)(\alpha-1)-M(\alpha)} \tag{274}$$

For $\alpha \to 1$ the relation (274) converges to $a_n = \frac{\Gamma(n-1)\alpha+1}{\Gamma(n\alpha+1)}(a_{n-1}-b_{n-1})$ with $a_1 = \frac{a_0-b_0}{\Gamma(1+\alpha)}$.

7.3.4. A model accounting for the sex of the partners [166]

Alkahtani et al. [166] suggested a model

$$^{ABC}D_t^{\alpha}y(t) = ay^2(t) - by(t) - (1-p)\nu(t)y^2(t) = \\ = -by(t) + [a-(1-p)\nu]\,y^2(t) \tag{275}$$

where the time-dependent function $\nu(t)$ is a selection function giving individuals possibilities to choose partners of the same sex, that is it allows to account for non-reproductive couples.

Regarding the equilibrium point, and assuming, for the sake of simplicity, that the right-hand side Eq.(275) is time independent, it follows that [166]

$$ay^2 - by - (1-p)\nu y^2 = 0 \Rightarrow y = 0, \quad y = \frac{b}{1-(1-p)\nu}, \; a \neq (1-p)\nu \tag{276}$$

Hence, the real equilibrium point will be when the rate of death with the difference between the birth contribution and the factor accounting for the partner sex becomes zero [166]. Moreover, if the inequality $a - (1-p)\nu < 0$ holds, then the living individuals will become extinct. However, when $a = (1-p)$, then the population will quickly vanish if the number of individuals is not quite enough to reproduce themselves and survive. Probably if the number of individuals is too big (beyond a certain threshold number of the population members), it could survive, thus suppressing, to some extent, the negative effect of the selection function $\nu(t)$ on the biological growth [166].

A numerical solution by the forward-corrector method was performed by presenting the model (275) in an equivalent Volterra version, namely

$$\begin{aligned} y(t) - y(0) &= \frac{1-\alpha}{M(\alpha)}\left[ay^2(t) - by(t) - (1-p)\nu(t)y^2(t)\right] + \\ &+ \frac{\alpha}{M(\alpha)\Gamma(\alpha)}\int_0^t \frac{1}{(t-s)^{\alpha-1}}\left[ay^2(st) - by(s) - (1-p)\nu(s)y^2(s)\right]ds \end{aligned} \tag{277}$$

Here, we can see the application of the ABC integral (see Remark 15) as well as [167]), where such an expansion of the model was related to the fading memory concept (a form close to the Volterra approach as discussed in Sections 6.2). Thus, this solution approach could be, to some extent, related to method used by Hassan et al. in [164] (see the preceding Section 7.3.1). More details about the numerical approximations applied are available in [166], and we will skip this point.

7.4. Logistic model with the Prabhakar fractional operator

7.4.1. Prabhakar function

The three-parameter Mittag-Leffler function is defined as [170]

$$E^{\gamma}_{\alpha,\beta} = \sum_{n=0}^{\infty} \frac{(\gamma)_n}{\Gamma(n\alpha+\beta)\, n!} \tag{278}$$

For $\alpha = \beta = \gamma = 1$ we recover the exponential function. And, $E^{\gamma}_{\alpha,\beta}$ is an entire function. The Prabhakar kernel is defined as

$$e^{\gamma}_{\alpha,\beta}(\lambda; t) = t^{\beta-1}E^{\gamma}_{\alpha,\beta}(\lambda t^{\alpha}) \tag{279}$$

Thus, the Prabhakar fractional integral with a lower terminal 0 is defined as

$${}^{P}I^{\gamma}_{\alpha,\beta,\lambda}[f(t)] = \int_0^t e^{\gamma}_{\alpha,\beta}(\lambda; t-s) f(s)\, ds, \quad \alpha \in (0,1) \tag{280}$$

For $f(t) \in L^1(0,1)$ we have a relation to the Riemann-Liouville fractional integral as

$${}^{P}I^{\gamma}_{\alpha,\beta,\lambda}[f(t)] = \sum_{n=0}^{\infty} \frac{(\gamma)_n \lambda^n}{n!} {}^{RL}I_t^{\alpha n+\beta} f(t) \tag{281}$$

Moreover, ${}^{P}I^{\gamma}_{\alpha,\beta,\lambda}$ is linear and bounded from $L^p(0,1)$ into $L^p(0,1)$ for any $1 < p < \infty$ [154]. ${}^{P}I^{\gamma}_{\alpha,\beta,\lambda}$ allows definitions of two fractional derivatives [158]:

Prabhakar fractional derivative in Riemann-Liouville sense

$${}^{P}_{RL}D_{\alpha,\beta,\lambda} f(t) = \frac{d}{dt}\, {}^{P}I^{-\gamma}_{\alpha,1-\beta,\lambda} f(t) \tag{282}$$

Prabhakar fractional derivative in Caputo sense

$${}^{P}_{C}D_{\alpha,\beta,\lambda} f(t) = {}^{P}I^{-\gamma}_{\alpha,1-\beta,\lambda} \frac{df(t)}{dt} \tag{283}$$

The Laplace transform of ${}_C^P D_{\alpha,\beta,\lambda} f(t)$ when $f(t) = t^n$ is [154, 158] is

$$\mathcal{L}\left[{}_C^P D_{\alpha,\beta,\lambda} t^n\right](s) = s^{\beta-\alpha\gamma}(s^\alpha - \lambda)^\gamma \frac{\Gamma(n+1)}{s^{n+1}} \tag{284}$$

7.4.2. Prabhakar fractional logistic equation

After these preliminaries, let us consider the Prabhakar fractional logistic equation constructed in [154]

$$\Lambda(\alpha,\beta,\gamma,\lambda)\, {}_C^P D^\gamma_{\alpha,\beta,\lambda} y(t) = y(t)(1 - y(t)) \tag{285}$$

where the factor $\Lambda(\alpha,\beta,\gamma,\lambda)$ is defined as: $\Lambda(\alpha,\beta,\gamma,\lambda) = 1 - \frac{\lambda}{1-\lambda}$, for $\alpha = 1$ and $\Lambda(\alpha,\beta,\gamma,\lambda) = \left[\frac{M(\alpha)}{1-\alpha}\right]^{\frac{(1-\alpha)}{\alpha}\gamma\lambda}$ when , $\alpha \neq 1$.

With the formal power series $y(t) = \sum\limits_{n=0}^{\infty} a_n t^n$, suggested as a solution, and leading to $y(t)(1 - y(t)) = \sum\limits_{n=0}^{\infty} (a_n - b_n) t^{n\xi}$, with $b_n = \sum\limits_{j=0}^{n} a_j a_{n-j}$, as many times demonstrated here, and applying the Laplace transform to both sides of Eq.(285), we have

$$\Lambda(\alpha,\beta,\gamma,\lambda)\, s^{\beta-\alpha\gamma}(s^\alpha - \lambda)^\gamma \sum_{n=0}^{\infty} a_n \frac{\Gamma(\xi n+1)}{s^{\xi n+1}} = \sum_{n=0}^{\infty} (a_n - b_n) \frac{\Gamma(\xi n+1)}{s^{\xi n+1}} \tag{286}$$

Further, we skip this point; the recurrence relation about the coefficients $a_{n+1} = R(a_n, \alpha, \beta, \gamma, \lambda, n)$ is already demonstrated, and the reader can develop it himself.

Remark 16 (On the model constructions and solutions developed: a standpoint)**.** *As mentioned at the beginning of this section, the models considered are obtained by replacing the time derivative in the Verhulst model with various fractional derivatives. There are no derivations based on some first modeling principles. Because of that, they are considered surrogate models, replacing but not the same because of the missing starting concepts of their build-ups.*

Furthermore, as we see, in each particular case, when a certain fractional derivative is used by replacement, the authors change (modify) the basic birth-death function on the right-hand side to accommodate the model to the solution they desire to develop because each type of derivative imposes new conditions that should be taken into account; however, these are not conditions imposed by the physics behind the model equation. As a result, we have different models providing different solutions that are not ready to compare. Nevertheless, the solutions developed reveal a wide range of techniques allowing for solving them but we did not compare the efficiencies and exactness of the final solutions since neither empirical data nor benchmarking solutions are available in the literature; such a trend in the model brush-up draws a new study direction beyond the horizon of this work.

However, it is noteworthy to see that the solutions suggested as formal power series [140–142, 150, 154] lead to efficient recursive relationships. This amazing result, tracing it back to the classic series solution of integer-order differential equations, is quite efficient because all fractional operators (derivative) in the considered examples can differentiate power-law functions (see, for instance the analysis in [168]. In this context, it might be expected that this approach would also be efficient when hereditary models involving fractional operators are constructed, avoiding derivative replacements.

Remark 17 (The forgotten inflection point)**.** *We can see from the analyzed solutions that the problem of the inflection points of the sigmoid-like solutions developed by different technologies was forgotten. Since the solutions are primarily power series with recurrences in the coefficient determination rather than continuously differentiable functions, this can be partially understood and explained. For example, if we consider the formal power series solution $y(t) = \sum\limits_{0}^{\infty} a_n t^n$, the second-order derivative condition*

$\frac{d^2y(t)}{dt^2} = 0$, *defining the inflection point, is*

$$\begin{aligned} &\frac{d^2y\left(t\right)}{dt^2} = \sum_{n=0}^{\infty} n\left(n-1\right)a_n t^{n-2} = 2a_2 + 6a_3t^2 + a_n n\left(n-1\right)t^{n-2} = 0 \Rightarrow \\ &\Rightarrow 2a_2 + \sum_{n=3}^{\infty} a_n n\left(n-1\right)t^{n-2} = 0 \end{aligned} \tag{287}$$

Hence, it is obvious that we cannot define the inflexion point if the solution is as a power series. For the other solutions developed, similar tests can be done too.

Remark 18 (An open problem in fractional logistic modeling)**.** *As commented above and from the analyzes of the models discussed, it is evident that real data fitting by the solution developed is practically missing, which, to a greater extent, makes the validations and comparative analyzes difficult to carry out. In this context, the estimation of the fractional order in the models, using experimental data, as a serious inverse problem, is an open problem still undeveloped. Especially for the cases of the fractional logistic model, for instance, we refer to [169], where a Bayesian approach was applied. Hence, there is a new area where efforts might be directed to allow real validation of what in fractional population dynamics was developed as models.*

8. Non-local operators related to the sigmoid function

8.1. Fractional derivative and integrals related to sigmoid function implementation

8.1.1. From the Riemann-Liouville fractional derivative with respect to another function to the Hilfer construction

If the function $\psi\left(u\right) > 0$ is monotonically increasing on $[a, b]$ and its derivative $d\psi/du > 0$ is continuous on (a, b), where $a, b \in \mathbb{R}$, then with $\alpha > 0$ we may represent the Hilfer fractional derivative of order α , $0 < \alpha < 1$ and type β , $0 \leq \beta \leq 1$ concerning x as [171, 172]

$$D_{a+}^{\alpha,\beta} f\left(x\right) = {}^{1-\alpha}J_{a^+}^{\beta}\frac{d}{dx}\left({}^{1-\alpha}J_{a^+}^{1-\beta} f\left(x\right)\right) \tag{288}$$

if the right-hand side of Eq.(288) exists.
The Hilfer definition, Eq. (288), allows generalization of the so-called ψ fractional integral and derivative, namely

$${}^{H}D_{a^+}^{\alpha,\beta;\psi} f\left(x\right) = I_{a^+}^{\beta(n-\alpha);\psi}\left(\frac{1}{\frac{d\psi}{dx}}\frac{d}{dx}\right)^n I_{a^+}^{(1-\beta)(n-\alpha);\psi} f\left(x\right) \tag{289}$$

$${}^{H}D_{b^-}^{\alpha,\beta;\psi} f\left(x\right) = I_{b^-}^{\beta(n-\alpha);\psi}\left(\frac{1}{\frac{d\psi}{dx}}\frac{d}{dx}\right)^n I_{b^-}^{(1-\beta)(n-\alpha);\psi} f\left(x\right) \tag{290}$$

where $n = [\alpha] + 1$. Then, the corresponding fractional integrals are

$$I_{a^+}^{\alpha;\psi} f\left(x\right) = \frac{1}{\Gamma\left(\alpha\right)}\int_a^x \frac{d\psi\left(t\right)}{dt}\frac{f\left(t\right)}{\left(\psi\left(x\right) - \psi\left(t\right)\right)^{1-\alpha}} \tag{291}$$

$$I_{b^-}^{\alpha;\psi} f\left(x\right) = \frac{1}{\Gamma\left(\alpha\right)}\int_x^b \frac{d\psi\left(t\right)}{dt}\frac{f\left(t\right)}{\left(\psi\left(x\right) - \psi\left(t\right)\right)^{1-\alpha}} \tag{292}$$

Napoles-Valdes suggested the *k-generalization* of the $\psi - Hilfer$ integral as [172]

$$I_{G,a^+}^{\alpha,k;\psi} f\left(x\right) = \frac{1}{k\Gamma_k\left(\alpha\right)}\int_a^x \frac{d\psi\left(t\right)}{dt}\frac{f\left(t\right)}{G\left(\left(\psi\left(x\right) - \psi\left(t\right)\right), \frac{\alpha}{k}\right)}, \quad k > 0 \tag{293}$$

$$I_{G,b^-}^{\alpha,k;\psi} f\left(x\right) = \frac{1}{k\Gamma_k\left(\alpha\right)}\int_n^b \frac{d\psi\left(t\right)}{dt}\frac{f\left(t\right)}{G\left(\left(\psi\left(x\right) - \psi\left(t\right)\right), \frac{\alpha}{k}\right)}, \quad k > 0 \tag{294}$$

where $G(z,t) \in AC[a_1, a_2]$.
The corresponding $\psi - Hilfer$ fractional derivatives are

$$ {}^{H}D_{G,a^+}^{\alpha,k;\psi} f(x) = I_{G,a^+}^{\beta(n-\alpha);\psi} \left(\frac{1}{\frac{d\psi}{dx}} \frac{d}{dx} \right)^n I_{G,a^+}^{(1-\beta)(n-\alpha);\psi} f(x), \quad k > 0, \quad n = [\alpha] + 1 \tag{295} $$

$$ {}^{H}D_{G,b^-}^{\alpha,k;\psi} f(x) = I_{G,a^+}^{\beta(n-\alpha);\psi} \left(\frac{1}{\frac{d\psi}{dx}} \frac{d}{dx} \right)^n I_{G,b^-}^{(1-\beta)(n-\alpha);\psi} f(x), \quad k > 0, \quad n = [\alpha] + 1 \tag{296} $$

From these general definitions, we may see the following reductions (specific definitions) [172], for instance:

- For $k = 1$ and $G(z,\alpha) = z^{1-\alpha}$ as well as $d\psi(t)/dt = 1$ we get the fractional Riemann-Liouville operator
- For $k = 1$ and $G(z,\alpha) = z^{1-\alpha}$, but $d\psi(t)/dt = 1/t$, then we get the Hadamar fractional operator (see [171].

More such examples are available in [172].
At the end of this section, we refer to a particular case [172] that can be useful in the rest of this article, namely:
Using the definition of the sigmoid $\sigma(x) = \frac{1}{1+e^{-x}}$ and its derivative $d\sigma(x)/dx = \sigma(x)(1-\sigma(x))$, and with $k = 1$, $G(z,\alpha) = z^{1-\alpha}$, as well as with $\psi(u) = \sigma(u)$ the following fractional integral can be constructed

$$ I_{a^+}^{\alpha;\sigma} f(x) = \int_a^x \frac{\sigma(t)(1-\sigma(t))}{(\sigma(x)-\sigma(t))^{1-\alpha}} f(t)\, dt \tag{297} $$

and the corresponding derivative is

$$ {}^{H}D_{a^+}^{\alpha,\beta} f(x) = I_{a^+}^{\beta(n-\alpha);\sigma} f(x) = \left(\frac{1}{\frac{d\sigma(x)}{dx}} \frac{d}{dx} \right)^n I_{a^+}^{(1-\beta)(n-\alpha);\sigma} f(x) \tag{298} $$

In the context of applications of the sigmoid function, Napoles-Valdes [172] suggested, but not developed, a generalized version as

$$ \sigma(x) = \frac{1}{1+e^{-g(x)}} \tag{299} $$

with a smooth function $g(x)$. We will see how this idea is developed further in Section 8.2.

8.2. ψ-Hilfer fractional derivative: a specific case

If we define $\psi(x) = \sigma(x) = \frac{1}{1-e^{-x}}$ [173], as suggested in [172], and using the definitions of left and right fractional integrals (see Eq.(291) and Eq.(292)), and concerning an increasing and positive monotone function on the real axis, we may construct [173]

$$ \begin{aligned} I_{a^+}^{\alpha,\sigma} f(x) &= \frac{1}{\Gamma(\alpha)} \int_a^x \frac{e^{-t}}{(1+e^{-t})^2} \left(\frac{1}{1+e^{-x}} - \frac{1}{1+e^{-t}} \right)^{\alpha-1} f(t)\, dt = \\ &= \frac{1}{\Gamma(\alpha)} \int_a^x \sigma(t)(1-\sigma(t))(\sigma(x)-\sigma(t))^{\alpha-1} f(t)\, dt \end{aligned} \tag{300} $$

assuming that $\frac{d\psi(x)}{dx}$ is continuous on the interval (a,b).
Now, let us recall that the definitions of the left and $\psi - Hilfer$ derivatives are Eq.(289) and Eq.(290). Then, using these constructions, fractional derivatives with a sigmoid function as a kernel can be defined as [173]:

$$ {}^{H}D_{a+}^{\alpha,\beta;\psi} f(x) = \frac{1}{\Gamma((1-\beta)(n-\alpha))} \int_a^t \sigma(\tau)(1-\sigma(\tau))(\sigma(x)-\sigma(\tau))^{1-\alpha} f(\tau)\, dt d\tau \tag{301} $$

From this general definition, the following special cases can be developed, namely.

- For $\beta \to 0$,$n = 1$

$$ {}^{H}D_{a+}^{\alpha,0;\psi} f(x) = \frac{1}{\Gamma(1-\alpha)} \int_a^t \sigma(\tau)(1-\sigma(\tau))(\sigma(x)-\sigma(\tau))^{1-\alpha} f(\tau)\, dtd\tau \tag{302} $$

- For $\beta \to 1$,$n = 1$

$$ {}^{H}D_{a+}^{\alpha,0;\psi} f(x) = \frac{1}{\Gamma(1-\alpha)} \int_a^t \frac{1}{(\sigma(x)-\sigma(\tau))^{\alpha}} \frac{d}{dt} \int_a^t \sigma(\tau)(1-\sigma(\tau)) f(\tau)\, dtd\tau \tag{303} $$

- For $\beta \to 0$,$n \neq 1$

$$ \begin{aligned} {}^{H}D_{a+}^{\alpha,0;\psi} f(x) = \frac{1}{\Gamma^2(n-\alpha)} \int_a^t (\sigma(\tau)(1-\sigma(\tau)))^{1-n} \times \\ \times \left(\frac{d}{dt}\right)^n \int_a^t \sigma(\tau)(1-\sigma(\tau))(\sigma(x)-\sigma(\tau))^{n-\alpha} f(\tau)\, dtd\tau \end{aligned} \tag{304} $$

- For $\beta \to 1$,$n \neq 1$

$$ \begin{aligned} {}^{H}D_{a+}^{\alpha,0;\psi} f(x) = \frac{1}{\Gamma(n-\alpha)} \int_a^t (\sigma(\tau)(1-\sigma(\tau)))^{1-n} (\sigma(x)-\sigma(\tau))^{n-\alpha-1} \times \\ \times \left(\frac{d}{dt}\right)^n \int_a^t \sigma(\tau)(1-\sigma(\tau)) f(\tau)\, dtd\tau \end{aligned} \tag{305} $$

8.2.1. Some properties

Based on the boundedness of the sigmoid kernel, Eq.(301) defines a bounded operator for all $n-1 < \alpha < n$ and $0 \leq \beta \leq 1$, that is [173]

$$ \left\| {}^{H}D_{o^+}^{\alpha,\beta} \right\|_{C,\gamma,\sigma} \leq K \|f\|_{C,\gamma,\sigma}, \quad K = \left(\frac{1-e^{-b}}{2\left(1+e^{-b}\right)}\right)^{n-\alpha} \frac{1}{\Gamma(n-\gamma+1)\Gamma(\gamma-\alpha+1)} \tag{306} $$

Then, from ${}^{H}D_{a^+}^{\alpha,\beta} f(x) = I_{a^+}^{\gamma-\alpha;\sigma} D_{a^+}^{\gamma;\sigma} f(x) = I_{a^+}^{\gamma-\alpha;\sigma} D_{a^+}^{\gamma;\sigma} (\sigma(x)-\sigma(a))^{\delta-1}$ (from Lemma 1 and Lemma 2 in [173]). Further, Liu et al. [173] suggested that the simple sigmoid function defined by Eq.(300) can be controlled by a parameter α such that

$$ \sigma_\alpha(x) = \frac{1}{1+e^{-\alpha x}} \Rightarrow \frac{d\sigma_\alpha(x)}{dx} = \alpha \frac{e^{-\alpha x}}{(1+e^{-\alpha x})^2} = \alpha \sigma_\alpha(x)(1-\sigma_\alpha(x)) \tag{307} $$

That is, this is a particular version of the idea of Napoles-Valdes presented byEq. (299) with $g(x) = \alpha$, $0 < \alpha < 1$. Then, a fractional operator on this basis was formulated as [173]

$$ \begin{aligned} {}^{H}D_{a^+}^{\alpha,\beta} f(x) = \frac{1}{\Gamma(\beta(n-\alpha))} \frac{1}{\alpha^{n-2}} \int_a^x \sigma(t)(1-\sigma(t))(\sigma(x)-\sigma(t))^{\beta(n-\alpha)-1} \left(\frac{1}{\sigma(t)(1-\sigma(t))} \frac{d}{dt}\right)^n \times \\ \times \frac{1}{\Gamma((1-\beta)(n-\alpha))} \int_a^t \sigma(\tau)(1-\sigma(\tau))(\sigma(x)-\sigma(\tau))^{(1-\beta)(n-1)} f(\tau)\, dtd\tau \end{aligned} \tag{308} $$

Applying this derivative to a simple population growth model [173] as

$$ \left({}^{H}D_{a^+}^{\alpha,\beta} f \right)(t) = s_0 \exp(\lambda t) \tag{309} $$

$$f(t)=s_0\sum_{k=0}^{\infty}\frac{\lambda^k}{\Gamma(k\mu-\chi+1)}\left(\frac{1}{1+e^{-t}}-\frac{1}{1+e^{-\alpha}}\right)^{k\mu-\chi},\qquad \mu=n(1-\beta)+\alpha\beta,\quad \chi=(1-\beta)(n-\alpha) \tag{310}$$

For $\lambda>0$ and $n-1<\alpha<n$, and $0\leq\beta\leq 1$ the result can be expressed through the one-parameter Mittag-Leffler function as [173]

$$f(t)=s_0E_{\alpha}\left(\lambda\left(\left(\frac{1}{1+e^{-t}}-\frac{1}{1+e^{-\alpha}}\right)^{\alpha}\right)\right) \tag{311}$$

Similarly, versions of the Korteweg-deVries equation, Burger's equation, the shallow water model, and the reaction-diffusion equation were suggested by simple replacements of the time derivatives in the original models by ${}^{H}D_{a^+}^{\alpha,\beta}f(x,t)$; however, no solutions and consequent analyses were provided.

8.3. Fractional derivative based on hyperbolic secant as a kernel

A fractional, Caputo-type, and left-sided derivative with a hyperbolic secant-based kernel was proposed by Rezapour et al. [174] (with $0<\alpha<1$, $f(t)\in H^1(a,b)$, $t>a$)

$${}^{\sigma}D_a^{\alpha}f(t)=C_1(\alpha)\int_a^t\operatorname{sech}^2\left(\frac{s-t}{1-\alpha}\right)\left\{\frac{df(s)}{ds}\right\}ds \tag{312}$$

where the term $\left\{\frac{df(s)}{ds}\right\}$ denotes a H^1 a distributional derivative as defined in general as [175]

$$\int T'(t)\,\phi(t)\,dt=-\int T(t)\,\phi(t)\,dt \tag{313}$$

The definition (312) reduces to H^1 derivative for $\alpha\to 1$. Moreover, if $f(t)$ is at least twice differentiable, then ${}^{\sigma}D_a^{\alpha}f(t)$ is differentiable, too, and if $(df/dt)_{t=0}=0$ we have

$${}^{\sigma}D_a^{\alpha}f(t)\left[{}^{\sigma}D_a^{1}f(t)\right]={}^{\sigma}D_a^{1}\left[{}^{\sigma}D_a^{\alpha}f(t)\right],\quad 0<\alpha<1 \tag{314}$$

It is important to mention that ${}^{\sigma}D_a^{\alpha}f(t)$ does not satisfy the memory principle (see Remark 19) but can be approximated by a corresponding fractional derivative with a lower terminal $t-L$ (see the complete exposition of this theorem in [174]).

Remark 19 (The memory principle for fractional derivative)**.** *If we have a fractional operator of Caputo-type [174]*

$$D_K^{\alpha}f(t)\equiv\int_a^t K(t-s)\frac{df(s)}{ds}ds,\quad f\in H^1(a,b) \tag{315}$$

Then the memory principle describes the history of $f(t)$at the proximity of the lower terminal, i.e. for $t\to a$. In such a situation, if the memory length (distance) is defined as Lso that $a+L<t+b$ the errors in approximation of the fractional operator are defined as

$$Er_{L,a,\alpha}(t)=\left|{}_aD_K^{\alpha}f(t)-{}_{t-L}D_K^{\alpha}f(t)\right| \tag{316}$$

If $df/dt<M$ for $t\in(a,b)$ and with $0<\alpha<1$, then, for instance, in the case of the Caputo derivative, the error is

$$Er_{L,a,\alpha}(t)=\left|\frac{1}{\Gamma(1-\alpha)}\int_{t-L}^{t}\frac{1}{(t-s)\,\alpha}\frac{df(s)}{ds}ds\right|\leq M\frac{L^{1-\alpha}}{|\Gamma(2-\alpha)|} \tag{317}$$

Now, if $Er_{L,a,\alpha}(t)\leq\varepsilon$, $\varepsilon>0$ and $a+L\leq t\leq b$ the memory distance should be

$$L>\left(\frac{M}{\varepsilon\,|\Gamma(2-\alpha)|}\right)^{\frac{1}{\alpha-1}} \tag{318}$$

Remark 20. *We can see that these are only initial attempts to construct fractional operators, precisely to demonstrate that the $\psi-Hilfer$ derivative works with the sigmoid function. The works of Napoles-Valdes [172] and Liu et al. [173] were published around the same time at the end of 2020, and they provide nearly similar results; however, the formulation in [172] is more fundamentally rigorous. The fractional*

operator with a hyperbolic secant as a kernel is still at the beginning level. The literature browsing, however, did not detect any development of these operators.

9. Discrete fractional-difference logistic equations

9.1. Some definitions

Let us now consider the discrete logistic equation (map) conceived by May [176,177] (see further Eq.(343) in Section 10)

$$x_{n+1} = Kx_n\left(1 - x_n\right) \tag{319}$$

demonstrating chaotic behavior for K ranging from 3.57 and 4.

Following Edelman [177], the simplest construction of a discrete fractional equation is

$$\Delta^{\alpha}{}_{a,h}x\left(t\right) = f\left(x\right) \tag{320}$$

where the discrete forward h-difference operator acts as $\Delta_h f\left(x\right) = f\left(x + h\right) - f\left(x\right)$, and commonly its step h is accepted $h = 1$.

Since working in the area of fractional operators, we have dealt with integral convolution integral, which are, in fact, summation operators, thus jumping into the field of discrete models, we have summation-difference operators with an initial point a (commonly accepted as $a = 0$). It is important to stress the attention on the fact that, despite the term fractional, when $0 < \alpha \leq 1$, really the operators are defined for any real $\alpha \in \mathbb{R}$ [177].

Hence, the discrete fractional difference Caputo-like equation is [177]

$${}^{C}\Delta^{\alpha}x\left(n\right) = -G_K\left(n + \alpha - 1,\, x\left(n + \alpha - 1\right)\right), \quad 0 < \alpha < 1, \quad x\left(0\right) = x_0, \quad n \in \mathbb{N} \tag{321}$$

where $K$is a parameter (a coefficient, see more about it in Section 10).

Equation (321) can be presented as a fractional–difference map with failing factorial-law memory [177], namely

$$x_n = x_0 - \frac{1}{\Gamma\left(\alpha\right)}\sum_{s=0}^{n-1}\left(n - s - 2 + \alpha\right)^{(\alpha-1)}G_K\left(s, x_s\right) \tag{322}$$

The equivalent form of Eq.(322) , through the Bernoulli numbers $B\left(n, \alpha; s\right)$, is [177, 178]

$$x_n = x_0 - \sum_{s=0}^{n-1} B\left(n - 1, \alpha; s\right)G_K\left(s, x\left(s\right)\right), \quad B\left(n, \alpha; s\right) = \binom{n - s + \alpha - 1}{n - s}, \quad 0 \leq s \leq n \tag{323}$$

Then, the failing factorial function is defined as

$$t^{(\alpha)} = \frac{\Gamma\left(t + 1\right)}{\Gamma\left(t + 1 - \alpha\right)t^{\alpha}}, \quad t \neq -1, -2, -3, \ldots \tag{324}$$

It is worth noting that the failing factorial-law memory function is asymptotically power-law memory [177], that is

$$\lim_{t\to\infty}\left(\frac{\Gamma\left(t + 1\right)}{\Gamma\left(t + 1 - \alpha\right)t^{\alpha}}\right) = 1, \quad \alpha \in \mathbb{R} \tag{325}$$

9.2. Fractional-difference logistic equation

Equation (319) was reconsidered as [179]

$$\Delta x_n = \mu x_n\left(1 - x_n\right) \Rightarrow \Delta x_{n+1} = \left(1 + \mu\right)x_n - \mu x_n^2, \quad x\left(0\right) = c \tag{326}$$

and formulated through the left Caputo-like difference in the form [179]

$${}^{C}\Delta_a^{\alpha}x\left(t\right) = \mu x\left(t + \alpha - 1\right)\left(1 - x\left(t + \alpha - 1\right)\right), \quad \Delta^k x\left(a\right) = x_k \tag{327}$$

with $t \in \mathbb{N}_{a+1-\alpha}, x\left(a\right) = c$, and a difference order $\alpha \in \left(0, 1\right]$, where ${}^{C}\Delta_a^{\alpha}x\left(t\right)$ is the left Caputo-like difference and $\mathbb{N} = \left(a, a + 1, a + 2, \ldots\right)$ $a \in \mathbb{R}$ fixed .

Note: To clarify the above construction, recall (see the comments about Eq.(320)) that the action of the delta difference operator $\Delta_{h=1}$ on a function $f\left(n\right)$ is $\Delta f\left(n\right) = f\left(n + 1\right) - f\left(n\right)$

With the Caputo-like delta difference for $x(t)$ defined on $\mathbb{N}_a$ [180]

$$ {}^{C}\Delta_a^{\alpha} x(t) := \Delta_a^{-(m-\alpha)} \Delta^m x(t) = \frac{1}{\Gamma(m-\alpha)} \sum_{s=a}^{t-(m-\alpha)} (t-\sigma(s))^{(m-\alpha-1)} \Delta_s^m x(t) \tag{328} $$

for $0 < \alpha \notin \mathbb{N}$ and $t \in \mathbb{N}_{a+m-\alpha}$, $m = [\alpha] + 1$.

A fractional sum of order $0 < \alpha$, $(\mathbb{N}_a \to \mathbb{R})$ with a starting point a is defined by

$$ \Delta_a^{-\alpha} x(t) := \frac{1}{\Gamma(\alpha)} \sum_{s=a}^{t-\alpha} (t-\sigma(s))^{(\alpha-1)} x(s), \quad \sigma(s) = s+1, \quad t \in \mathbb{N}_{a+\alpha} \tag{329} $$

where $t^{(\nu)} = \frac{\Gamma(t+1)}{\Gamma(t+1-\nu)}$ is the *failing function*.

And, therefore,

$$ {}^{C}\Delta_a^{\alpha} x(t) := \Delta_a^{-(m-\alpha)} \Delta^m x(t) = \frac{1}{\Gamma(m-\alpha)} \sum_{s=a}^{t-(m-\alpha)} (t-\sigma(s))^{(m-\alpha-1)} \Delta_s^m x(t) \tag{330} $$

for $0 < \nu \notin \mathbb{N}$ and $t \in \mathbb{N}_{a+m-\alpha}$, $m = [\alpha] + 1$.

Now, for Eq.(327) with $m = [\alpha] + 1$ and $k = 0, \ldots, m-1$, the equivalent discrete integral equation is [179]

$$ \begin{aligned} x(t) &= x_0(t) + \frac{1}{\Gamma(\alpha)} \sum_{s=a+m-\alpha}^{t-\alpha} (t-\sigma(s))^{(\alpha-1)} f(s+\alpha-1, x(s+\alpha-1)) \\ x_0(t) &= \sum_{k=0}^{m-1} \frac{(t-a)^{(k)}}{k!} \Delta^k x(a) \end{aligned} \quad , \quad t \in \mathbb{N}_{a+m} \tag{331} $$

In Eq.(331) the discrete kernel function is $\frac{(t-\sigma(s))^{(\alpha-1)}}{\Gamma(\alpha)}$ and $(t-\sigma(s))^{(\alpha-1)} = \frac{\Gamma(t-s)}{\Gamma(t-s+1-\alpha)}$.

Note: During the transition from Eq.(328) to Eq.(331) there is a change in the time domain from $t \in \mathbb{N}_{a+m-\alpha}$ to $t \in \mathbb{N}_{a+m}$, but the function $x(t)$ is preserved to define on the isolated time scale $t \in \mathbb{N}_a$, when the summation Eq.(328) is carried out [179].

9.3. Discrete fractional-difference logistic equation: Chaos

9.3.1. Chaos in fractional sine

Wu et al. [182] considered a version of the integer-order sine map $x_{n+1} = x_n + \mu \sin(x_n)$ (see more detailed analysis on this problem and its fractionalized counterparts in the next Section 10). With ${}^{C}\Delta_a^{\alpha} x(t)$, defined above, it was reformulated as

$$ {}^{C}\Delta_a^{\alpha} x(t) = \mu \sin(x(t+\alpha-1)), \quad 0 < \nu < 1 \tag{332} $$

Then, the two-dimensional standard map (as used by the authors)

$$ \begin{aligned} x_{n+1} &= x_n - K \sin(z_n) \\ z_{n+1} &= z_n + x_{n+1} \end{aligned} \tag{333} $$

was modified as

$$ \begin{aligned} {}^{C}\Delta_a^{\alpha} x(t) &= -K \sin(z(t+\alpha-1)) \\ z_n &= z_{n-1} + x_n \end{aligned} , \quad 0 < \alpha < 1, \quad t \in \mathbb{N}_{a+1-\alpha} \tag{334} $$

For Eq.(332), with the discrete kernel $(t-\sigma(s))^{(\nu-1)}$, the explicit numerical formula is [182]

$$ x_n = x(a) + \frac{\alpha}{\Gamma(\alpha)} \sum_{j=1}^{n} \frac{\Gamma(n-j+\alpha)}{\Gamma(n-j+1)} \sin(x(j-1)) \tag{335} $$

Consequently for (334) the numerical version is

$$ \begin{aligned} x_n &= x(a) + \frac{\mu}{\Gamma(\mu)} \sum_{j=1}^{n} \frac{\Gamma(n-j+\alpha)}{\Gamma(n-j+1)} \sin(z(j-1)) \\ z_n &= z_{n-1} + x_n \end{aligned} , \quad n \geq 1 \tag{336} $$

9.3.2. Chaos and synchronization

For $a = 0$ and $\alpha = 1$, Eq.(327) reduces to Eq.(326) [179]. Applying the transformation

$$x_n = \frac{1+\mu}{\mu}\alpha_n \tag{337}$$

Equation (326) can be transformed as

$$\alpha_{n+1} = (1+\mu)\left(\alpha_n - \alpha_n^2\right), \quad \alpha_0 = \frac{\mu}{1+\mu}u_0 \tag{338}$$

Note: In Eq.(337) the function $(1+\mu)/\mu$ is the simplest form of a sigmoidal transformation because $(1+\mu)/\mu = 1/(1+1/\mu) \to 1$ for $\mu \to \infty$ [181], so that for large values of μ we have $x_n \to \alpha_n$ and $\alpha_0 \to u_0$.

With Eq.(328) and Eq.(329), defined above, the following discrete integral form of Eq.(326) can be formulated [179]

$$x(t) = u_0 + \frac{\mu}{\Gamma(\alpha)}\sum_{s=1-\alpha}^{t-\alpha}(t-s-1)^{(\alpha-1)}x(t-s-1)(1-x(t-s-1)), \quad t \in \mathbb{N} \tag{339}$$

with a corresponding numerical scheme, using $(t-\sigma(s))^{(\alpha-1)} = \frac{\Gamma(t-s)}{\Gamma(t-s+1-\alpha)}$, expressed as

$$x_n = x_0 + \frac{\mu}{\Gamma(\mu)}\sum_{j=1}^{n}\frac{\Gamma(n-j+\alpha)}{\Gamma(n-j+1)}x(j-1)(1-x(j-1)) \tag{340}$$

Hence, Eq.(340) has a discrete kernel function $(t-\sigma(s))^{(\nu-1)}$ in contrast to the integer-order Eq.(326) and, therefore, x_n is a function (depends on) of its past values.

On the basis of the results commented on above, precisely Eq.(327) considered as *a master system*. Wu and Baleanu [183] suggested *a coupled slave logistic map* (a term used by the authors), namely

$${}^{C}\Delta_a^{\alpha} z(t) = \mu z(t+\alpha-1)(1-z(t+\alpha-1)) + Hx(t+\alpha-1), \quad x(t+\alpha-1), \quad x(a) = x_0 \tag{341}$$

So, for a long time we have $|x(t)-z(t)|_{t\to\infty} \to 0$. Then, Eq.(327) and Eq.(341) form a synchronized system, namely

$$\begin{aligned} x(t) &= u_0 + \frac{\mu}{\Gamma(\alpha)}\sum_{s=1-\alpha}^{t-\alpha}(t-s-1)^{(\alpha-1)}x(t-s-1)(1-x(t-s-1)) \\ z(t) &= z(a) + \frac{\mu}{\Gamma(\alpha)}\sum_{s=a+1-\alpha}^{t-\alpha}(t-s-1)^{(\alpha-1)}\left[z(t-s-1)(1-z(t-s-1)) + H\right], \quad t \in \mathbb{N}_{a=1} \\ H &= Hx(t-s-1)z(t-s-1) \end{aligned} \tag{342}$$

Remark 21 (Some comments on the terminology used)**.** *Here, we refer to the term fractional discrete map used in [179, 182, 183]. As commented by Edelman (Section 3.1 in [177]) they are the only solutions of the discrete fractional-difference logistic equation, but not logistic maps. However, the results in [179, 182, 183] show chaotic behaviors with bifurcations clearly demonstrated and visualized. At this point, we hope the reader may see the differences in the positions of these authors and that of Edelman [177] (see the next Section 10) and take the right answer to the emerging terminology discrepancies.*

10. Logistic maps

The regular logistic map used in population dynamics, economics, and descriptions of other dynamic processes is simply defined as [176, 177, 191]

$$x_{n+1} = Kx_n(1-x_n) \tag{343}$$

and its simplest generalization is [184, 191]

$$x_{n+1} = Kx_n^p\left(1-x_n^q\right), \quad x \in [0,1], \quad p,q > 0 \tag{344}$$

For more versions see [191] and the references therein.

In this section, we credit the results of Zaslavsky, Tarasov, and Edelman [185–190], which form a solid background to understand the creation of logistic maps and their fractionalized versions.

10.1. Standard map

Following Tarasov and Zaslavsky [185], the mapping $x_{n+1} = f(x_n)$ is memoryless because x_{n+1} depends only on x_n. To construct a map with memory, we need to connect the discrete value x_{n+1} to its preceding values $x_n, x_{n-1}, \ldots, x_1$. This functionally can be expressed as $x_{n+1} = \sum_{k=1}^{n} f(x_k)$where $f(x)$ is a function describing a discrete map. Since the number of the preceding values is limited (finite), the memory described in this way is not complete as we desire it to be [185]. The map with long-time memory is defined as [185] $x_{n+1} = \sum_{k=1}^{n} V_\alpha(n,k) f(x_k)$, where $V_\alpha(n,k)$ are weighting functions and they should be determined through solutions of differential equations, as explained further in Remarks 22 and 23.

Let us consider, for instance, the equation of motion perturbed by a periodic sequence of kicks (delta function-type of pulses) with amplitude K [187, 188]

$$\frac{d^2x}{dt^2} + K\sin(x)\sum_{n=0}^{\infty}\delta\left(\frac{t}{T} - n\right) = 0 \tag{345}$$

With a period $T = 1$ (for the sake of simplicity) we read

$$\frac{d^2x}{dt^2} + K\sin(x)\sum_{n=0}^{\infty}\delta(t-n) = 0 \tag{346}$$

The transformation into a Hamiltonian form by $dx/dt = p$, yields

$$dx/dt = p, \quad \frac{dp}{dt} + K\sin(x)\sum_{n=0}^{\infty}\delta(t-n) = 0 \tag{347}$$

and allows (347) to be presented as a discrete map [187, 188]

$$x_{n+1} = x_x + p_{n+1}, \quad p_{n+1} = p_n - K\sin(x_n) \tag{348}$$

This is the *universal map* and it can be generalized as [185]

$$x_{n+1} = x_x + p_{n+1}, \quad p_{n+1} = p_n - G(x_n) \tag{349}$$

With $G(x) = \sin(x)$ we get the *Chirikov-Taylor map* [185], also known as a standard map [187] or *Chirikov map* [193].

Remark 22 (Cauchy-type problem and universal map equivalence)**.** *The Cauchy-type problem [186] (in the original notations)*

$$\frac{dx(t)}{dt} = p(t), \quad \frac{dp(t)}{dt} = -KG[x_k]\sum_{k=1}^{\infty}\delta\left(\frac{t}{T} - k\right), \quad x(0) = x_0, \quad p(0) = p_0 \tag{350}$$

is equivalent to a universal map with a period T, expressed as

$$x_{n+1} = x_0 + p_0(n+1)T - kT^2\sum_{k=1}^{n}G[x_k](n+1-k), \quad p_{n+1} = p_0 - KT\sum_{k=0}^{n}G[x_k] \tag{351}$$

Further, if (350) is presented as

$$\frac{d^2x(t)}{dt^2} = G[t, x(t)], \quad 0 \le t \le t_{final}, \quad x(0) = x_0, \quad \frac{dx(0)}{dt} = p(0) \tag{352}$$

It is equivalent to the Volterra equation of the second kind [186]

$$x(t) = x_0 + p_0 t + \int_0^t G[s, x(s)](t-s)\,ds \tag{353}$$

With $G[t, x(t)] = KG[x_k]\sum_{k=1}^{\infty}\delta\left(\frac{t}{T} - k\right)$ *we get (350).*

Remark 23 (On the equivalent Volterra equations of second kind)**.** *We saw that in many cases discussed here, there are equivalent models as Volterra equations of the second kind. Thus, we can see the common ground of memory in both continuous and discrete models. Precisely, working with discrete models and recalling the above comments about the functionality* $x_{n+1} = \sum_{k=1}^{n} f(x_k)$*, where the past values are weighted by* $V_\alpha(n,k)$*, we can look back at the models in Section 5, and especially in Section 6, where the weighting of the past values is by the correlation (memory) function. In all cases, discrete and continuous, the summation is a performance of memory. Referring to the beginning paragraph of Section 10.1, we can see that the incomplete memory due to the truncated series of past values has its analog in the convolution integrals when the memory functions can affect (weights) only the closest values rather than all in the past.In cases, discrete and continuous, the starting point (the point* $t = 0$*) is the moment where the process starts and is counted during the entire process duration (not the chronological time): Recall the comments in Section 6.4, precisely referring to the concept expressed by Hilfer [117, 118].*

10.1.1. Dissipative standard map

The dissipative standard map is defined as

$$X_{n+1} = X_n + \mu Y_{n+1} + \Omega, \quad Y_{n+1} = e^{-q}\left(Y_n + \varepsilon \sin\left(X_n\right)\right), \quad \mu = \frac{\left(e^{-q}-1\right)}{q} \tag{354}$$

and also known as the Zaslavsky map [187]. The shift Ω can be assumed as zero since it does not play a significant role in the map dynamics [187], and then

$$X_{n+1} = X_n + P_{n+1}, \quad P_{n+1} = -bP_n - Z\sin\left(X_n\right), \quad Z = -\varepsilon\mu e^{-q}, \quad P_n = \mu Y_n, \quad b = -e^{-q} \tag{355}$$

For $b = -1$ and $Z = K$ from the map (355) we recover the standard map (348). When $q \to \infty$ and $b \to 0$ as well as with $Z = -K$, the map (355) reduces to the one-dimensional Arnold's map [187, 194].

$$X_{n+1} = X_n + K\sin\left(X_n\right) \tag{356}$$

10.2. Fractional map

10.2.1. Fractional standard map with dissipation

A fractional generalization of Eq.(345) was conceived by Nigmatulin [195] as a discrete map corresponding to a fractional equation of order $0 < \alpha \leq 2$ and as a generalization of the standard map, *via* a Riemann-Liouville derivative ${}^{RL}D_t^\alpha x$, namely

$${}^{RL}D_t^\alpha x + K\sin\left(x\right)\sum_{n=0}^{\infty}\delta\left(t-n\right) = 0, \quad {}^{RL}D_t^\alpha x = \frac{1}{\Gamma\left(2-\alpha\right)}\frac{d}{dx^2}\int_0^t \frac{x\left(s\right)}{\left(t-s\right)^\alpha}ds, \quad 1 < \alpha \leq 2 \tag{357}$$

Through the momentum $p\left(t\right) = {}^{RL}D_t^{\alpha-1}x(t)$ and the initial conditions ${}^{RL}D_t^{\alpha-1}x\left(0+\right) = p_1$, [187] ${}^{RL}D_t^{\alpha-2}x\left(0+\right) = b$, the fractional standard map can be built [187, 188]

$$x_{n+1} = \frac{1}{\Gamma\left(\alpha\right)}\sum_{k=0}^{n} p_{k+1}V_\alpha\left(n-k+1\right), \quad 1 < \alpha \leq 2, \quad p_{n+1} = -bp_n - Z\sin\left(x_n\right) \tag{358}$$

where $Z = -\varepsilon\mu e^{-q}$, $P_n = \mu Y_n$, $b = -e^{-q}$ (see Eq.(355)). As mentioned in [187] for $b = -1$ and $Z = K$, then the map (358) reduces to a fractional dissipative standard map with $T = 1$. The map (358) is not a result of a fractional differential equation but from $p_n \to -bp_n$ in the fractional standard map [187].

10.2.2. A map with a fractional derivative in the kicked term

The equation of a kicked damped rotator is defined as [187, 188]

$$\frac{d^2x}{dt^2} - q\frac{dx}{dt} - K\sin\left(x\right)\sum_{n=0}^{\infty}\delta\left(t-n\right) = 0 \tag{359}$$

It can be fractionalized by applying the Caputo derivative ${}^{C}D_t^\alpha x(t)$ (see Eq.(361)), namely

$$\frac{d^2X\left(t\right)}{dt^2} - q\frac{dX\left(t\right)}{dt} - \varepsilon^{C}\sin\left({}^{C}D_t^\beta X\right)\sum_{n=0}^{\infty}\delta\left(t-n\right) = 0, \quad 0 \leq \beta < 1 \tag{360}$$

$$ {}^{C}D_{t}^{\beta}X=\frac{1}{\Gamma\left(1-\beta\right)}\int\limits_{0}^{t}\frac{1}{\left(t-s\right)^{\beta}}\frac{dX\left(s\right)}{ds}ds \tag{361} $$

This is *the first fractional dissipative standard map* [187, 188].

The fractional equation (359) is equivalent to the discrete map [187, 188]

$$ X_{n+1}=X_{n}+\frac{1-e^{-q}}{q}Y_{n+1},\quad Y_{n+1}=e^{q}\left\{ Y_{n}+\varepsilon\sin\left[\frac{1}{\Gamma\left(1-\beta\right)}\sum_{k=0}^{n-1}Y_{k+1}W_{2-\beta}\left(q,k-n\right)\right]\right\} \tag{362} $$

where the function is defined through the incomplete gamma function $\Gamma\left(a,b\right)$

$$ W_{2-\beta}\left(q,k-n\right)=a^{\beta-1}e^{a(b+1)}\left[\Gamma\left(1-\beta,ab\right)-\Gamma\left(1-\beta,a\left(b+1\right)\right)\right],\quad\Gamma\left(a,b\right)=\int\limits_{b}^{\infty}y^{a-1}e^{-y}dy \tag{363} $$

10.2.3. A map with a fractional derivative in the unkicked term

If the fractionalization Eq.(359) is done by replacements of both integer-order time derivatives (in the left-hand side) by Riemann-Liouville fractional derivatives of different fractional orders, then

$$ {}^{RL}D_{t}^{\alpha}X\left(t\right)-q{}^{RL}D_{t}^{\beta}X\left(t\right)-\varepsilon\sin\left(X\right)\sum_{n=0}^{\infty}\delta\left(t-n\right)=0,\quad1<\alpha\leq2,\quad0\leq\beta<1,\quad q\in R \tag{364} $$

and it is equivalent to the following discrete map [187, 188]

$$ X_{n+1}=\frac{1}{\Gamma\left(\alpha-1\right)}\sum_{k=0}^{n}Y_{k+1}W_{\alpha}\left(q,k-n-1\right),\quad Y_{n+1}=e^{q}\left[Y_{n}+\varepsilon\sin\left(X_{n}\right)\right] \tag{365} $$

with $W_{\alpha}\left(q,k-n-1\right)=a^{1-\alpha}e^{a(b+1)}\left[\Gamma\left(\alpha-1,ab\right)-\Gamma\left(\alpha-1,a\left(b+1\right)\right)\right]$. This can be considered as a fractional generalization of the dissipative standard map (348) with $\Omega=0$ [187]. For $\alpha=2$, the map (365) reduces to the discrete map (348).

With the variables $P_{n}=\mu Y_{n}$, $b=-e^{q}$ and $Z=-\mu\varepsilon e^{q}$ we get a new form of the map (365), namely

$$ X_{n+1}=\frac{1}{\mu}\frac{1}{\Gamma\left(\alpha-1\right)}\sum_{k=0}^{n}P_{k+1}W_{\alpha}\left(q,k-n-1\right),\quad P_{n+1}=-bP_{n}-Z\sin\left(X_{n}\right) \tag{366} $$

Note: In Eq.(359), Eq. (360) and Eq.(364), the second (damping) terms are with negative signs because the coefficients q could be positive or negative [187, 188].

10.2.4. Fractionalized standard map: Riemann-Liouville or Caputo derivative?

Here we refer to [189] where a comparative analysis of the fractional standard map with the two most used derivatives with power-law kernels was done. In more detail, considering the initial condition problem, we have a standard map [189]

$$ p_{n+1}=p_{n}-K\sin x_{n},\quad x_{n+1}=x_{n}+p_{n+1},\quad\left(\mathrm{mod}\,2\pi\right) \tag{367} $$

which can be derived from

$$ \frac{d^{2}x}{dt^{2}}=-K\sin\left(x\right)\sum_{n=0}^{\infty}\delta\left(\frac{t}{T}-\left(n+\varepsilon\right)\right),\quad\varepsilon\rightarrow0+ \tag{368} $$

A fractionalization by applying the Riemann-Liouville derivative leads to [186, 189]

$$ {}^{RL}D_{t}^{\alpha}x=-K\sin\left(x\right)\sum_{n=0}^{\infty}\delta\left(\frac{t}{T}-\left(n+\varepsilon\right)\right),\quad1<\alpha\leq2,\quad\varepsilon\rightarrow0+ \tag{369} $$

with initial conditions ${}^{RL}D_{t}^{\alpha-1}x\left(0+\right)=p_{1}$ and ${}^{RL}D_{t}^{\alpha-2}x\left(0+\right)=b$.

Otherwise, with the application of the Caputo derivative, we get [189]

$$ {}^{C}D_{t}^{\alpha}x = -K\sin\left(x\right)\sum_{n=0}^{\infty}\delta\left(\frac{t}{T}-\left(n+\varepsilon\right)\right), \quad 1<\alpha\leq 2, \quad \varepsilon\to 0+ \tag{370} $$

with initial conditions $p\left(0\right)={}^{C}D_{t}^{\alpha-1}x\left(0\right)=\frac{dx(0)}{dt}=p_{0}$ and ${}^{RL}D_{t}^{\alpha-2}x\left(0+\right)=b$, where $x\left(0\right)=x_{0}$.
The integration of Eq.(367) yields [189]

$$ p_{n+1}=p_{n}-K\sin\left(x_{n}\right), \quad x_{n+1}=\frac{1}{\Gamma\left(\alpha\right)}\sum_{k=0}^{n}p_{k+1}V_{\alpha}^{1}\left(n-k-1\right), \quad \left(\mathrm{mod}\,2\pi\right) \tag{371} $$

with $V_{\alpha}^{K}=m^{\alpha-k}-\left(m-1\right)^{\alpha-k}$ and $p\left(t\right)={}^{RL}D_{t}^{\alpha-1}x\left(t\right)$; $T=1$, and $1<\alpha\leq 2$.
Similarly, the integration of Eq.(370) , with $p=dx/dt$, $T=1$ and $1<\alpha\leq 2$, results in

$$ p_{n+1}=p_{n}-K\frac{1}{\Gamma\left(\alpha-1\right)}\left[\sum_{k=0}^{n-1}V_{\alpha}^{2}\left(n-k+1\right)\sin\left(x_{k}\right)+\sin\left(x_{n}\right)\right], \quad \left(\mathrm{mod}\,2\pi\right) \tag{372} $$

$$ x_{n+1}=x_{n}-K\frac{1}{\Gamma\left(\alpha\right)}\left[\sum_{k=0}^{n}V_{\alpha}^{1}\left(n-k+1\right)\sin\left(x_{k}\right)\right], \quad \left(\mathrm{mod}\,2\pi\right) \tag{373} $$

An alternative form of the map (372)-(373) is

$$ x_{n+1}=\sum_{k=0}^{n-1}\frac{c_{k}}{k!}h^{k}(n+1)^{k}-\frac{h^{\alpha}}{\Gamma\left(\alpha\right)}\sum_{k=0}^{n}G_{k}\left(x_{k}\right)(n-k+1)^{\alpha-1} \tag{374} $$

which can be obtained from a version of Eq.(370) related to a periodically kicked system (T is the period) [177, 185, 190]

$$ {}^{C}D_{t}^{\alpha}x\left(t\right)+G_{k}\left[x\left(t-\Delta t\right)\right]\sum_{n=-\infty}^{\infty}\delta\left(\frac{t}{T}-\left(n+\varepsilon\right)\right)=0 \tag{375} $$

where $\varepsilon>\Delta>0$, $\varepsilon\to 0$, $\alpha\in\mathbb{R}$, $0\leq n-1<\alpha<n$. It is easy to obtained from Eq.(374) with $G_{k}\left(x\right)=x-Kx\left(q-x\right)$ [189].

10.2.5. Stable fixed point

The standard map as well as the fractionalized versions with ${}^{C}D_{t}^{\alpha}x$ and ${}^{RL}D_{t}^{\alpha}x$ have the same fixed point at $(0,0)$ [185,189]. For the standard map, this point is stable for $K<K_{critical}<4$. With the fractionalized map involving ${}^{RL}D_{t}^{\alpha}x$the evolution trajectories near the fixed point are [189]

$$ \delta p_{n+1}=\delta p_{n}-K\delta x_{n}, \quad \delta x_{n+1}=\frac{1}{\Gamma\left(\alpha\right)}\sum_{k=0}^{n}\delta p_{n+1}V_{\alpha}\left(n-k+1\right) \tag{376} $$

With ${}^{C}D_{t}^{\alpha}x$ the evolution trajectories near the fixed point are [189]

$$ \begin{aligned} \delta p_{n+1}&=\delta p_{n}-K\frac{1}{\Gamma\left(\alpha-1\right)}\left[\sum_{k=0}^{n-1}V_{\alpha}^{2}\left(n-k+1\right)\delta x_{k}+\delta x_{n}\right] \\ \delta x_{n+1}&=\delta x_{n}+\delta p_{0}-K\frac{1}{\Gamma\left(\alpha\right)}\sum_{k=0}^{n-1}V_{\alpha}^{1}\left(n-k+1\right)\delta x_{k} \end{aligned} \tag{377} $$

More detailed analysis and numerical simulations are available in [189].

Remark 24 (On the fractionalization of the maps)**.** *We see that the fractionalization of the map is made directly by the replacement of the integer-order derivatives by fractional ones. For example, the case with Eq.(367) was developed through (see the explanation in [186]) a solution to the Cauchy problem [192]*

$$ {}^{RL}D_{t}^{\alpha}=G\left[t,x\left(t\right)\right] \tag{378} $$

with initial conditions ${}^{RL}D_{t}^{\alpha-k}\left(x\right)\left(0+\right)=c_{k}$, $k=1,2,\ldots n-1$.
Precisely, ${}^{RL}D_{t}^{\alpha-k}\left(x\right)\left(0+\right)=\lim_{t\to 0+}{}^{RL}D_{t}^{\alpha-k}x\left(t\right)$ *and* ${}^{RL}D_{t}^{\alpha-n}\left(x\right)\left(0+\right)=\lim_{t\to 0+}{}^{RL}I_{t}^{n-\alpha}x\left(t\right)$, *that is the limit taken at almost all points of the right-sided vicinity* $\left(0,0+\varepsilon\right),\varepsilon>0$ *[186]. The problem (378)*

can be reduced to a nonlinear Volterra integral equation of the second kind [186, 192]

$$x(t)=\sum_{k=1}^{n}\frac{c_k}{\Gamma(\alpha-k+1)}t^{\alpha-k}+\frac{1}{\Gamma(\alpha)}\int_0^t\frac{G[s,x(s)]}{(t-s)^{1-\alpha}}ds,\quad t>0 \tag{379}$$

For $\alpha=2$, Eq. (379) reduces to Eq.(350) (see Remark 22).

For understanding the background of all these results, we recommend a thorough reading of [186, 192] as well as [185, 187–189]. Moreover, we discuss the power-law memory constructions of logistic maps in the next Section 10.2.6

10.2.6. The Power-law memory kernel in the fractional logistic map construction

According to Edelman [191], the logistic map is a very simple discrete non-linear model of dynamical evolution accounting for the whole history of its development. Now, we focus our attention on the problem concerning the memory kernel function used in the basic non-local differential equation from which the corresponding discrete map can be constructed. Precisely, we address the power-law memory, as it was used in all preceding points of this section, and the main idea is to justify its origin in the fractional logistic maps.

Edelman demonstrates that the direct way to construct a map with a power-law memory is through a convolution, that is, (in the original notations) [191]

$$x_n=\sum_{k=0}^{n-1}(n-k)^{\alpha-1}G_K(x_k,h) \tag{380}$$

where K is a parameter, while h is the time step between the time instant t_n and t_{n+1}.

The more general construction is [191] (recall Eq.(379))

$$x_n=\sum_{k=1}^{[\alpha]-1}\frac{c_k}{\Gamma(\alpha-k+1)}(nh)^{\alpha-k}+\sum_{k=0}^{n-1}(n-k)^{\alpha-1}G_K(x_k,h),\quad \alpha\in\mathbb{R} \tag{381}$$

Note: Remember the elegant appearance of the convolution in the Zwanzig model (Section 5.3.3 and the explanations in Remark 7).

Assuming $G_K(x_k,h)=\frac{1}{\Gamma(\alpha)}h^{\alpha}G_K(x)$, where $G_K(x)$ is continuous, as well as with $dx/dt=x(t)$, $x_k=x(t_k)$, $t_k=a+kh$, $nh=t-a$, where $0\leq k\leq n$, when $h\to 0$, we get an equivalent Volterra equation of the second kind [191]

$$x_n=\sum_{k=1}^{[\alpha]-1}\frac{c_k}{\Gamma(\alpha-k+1)}(t-a)^{\alpha-k}+\frac{1}{\Gamma(\alpha)}\int_0^t\frac{G_K(s,x(s))}{(t-s)^{1-\alpha}}ds \tag{382}$$

Also, Eq.(382) is eqauivalento the fractional differential equation [191]

$${}^{RL}D_t^{\alpha-k}(x)(a+)={}^{GL}D_t^{\alpha-k}(x)(a+)=G_K(t,x(t)),0<\alpha \tag{383}$$

with initial conditions ${}^{RL}D_t^{\alpha-k}(x)(a+)={}^{GL}D_t^{\alpha-k}(x)(a+)=c_k$, $k=1,2,\ldots[\alpha]$, valid with the Riemann-Liouville ${}^{RL}D_t^{\alpha-k}(x)$ and Grunvald-Letnikov ${}^{GL}D_t^{\alpha-k}(x)$ derivatives.

11. Final remarks

This systematic review went through many points pertaining to problems involving logistic models and sigmoid functions. Looking at many available texts on logistic models with various applications, we saw that such a compilation of classical expositions of dynamic logistic-type models and non-local formulations has never been created before. Indeed, some topics, such as logistic chaotic maps, fractional Riccati equations related to processes of control, or Bass diffusion models, were not considered, but from a personal perspective, this would be a task for a project bigger than a systematic review. The point on fractional operators involving the sigmoid function was hard to be created due to insufficient published information, but now we hope the collected information will motivate somebody to work on similar problems.

We were interested and highly motivated to demonstrate the links from classical local models to the non-local ones based on the Volterra equations, where the problem of the choice of the memory kernel was not the primary issue. However, in the modern era, where fractional calculus is widely spread in mathematical modeling, the concept of how logistic models could be formulated in terms of fractional operators was highly necessary, and we took a step ahead to explain the basic rules. To this point, we believe that the explanation of how this could be done would be fruitful and will allow a better understanding of how fractionalization of logistic models should be done and, therefore, permit discovering the origins of discrepancies between the solutions developed; we hope the present analys will usefull.

Finally, I would like to recommend further readings on many aspects of dynamic growth models, covering both mathematical aspects and philosophical issues, two systematic studies driven by Elliot Montroll [196, 197] that might enlarge the perspective on logistic modeling despite the fact that are about 50 years old, but still young as expressions and ideas.

The motivation to create a well-structured and comprehensive exposition, as we suggested, showing the links between subjects commonly discussed separately but having common ground at the origin, allowed for the creation of this text. I would be pleased if this systematic approach would create new horizons and new motivations for research.

Acknowledgments

The author highly acknowledges the invitations of the editors of TCMIS to contribute to the inaugural issue of the journal and the opportunity to express his point of view on old but forever young and intriguing topics of logistic models and sigmoid functions.

Funding

This work is developed as part of contract No: BG-RRP-2.004-0002-C01, project name: BiOrgaMCT, Procedure BG-RRP-2.004 "Establishing of a network of research higher education institutions in Bulgaria", funded by Bulgarian National Recovery and Resilience Plan.

Conflict of interest

There is no conflict of interest to disclose.

Author contributions

Jordan Hristov is the sole author of this text, including all parts of it, starting from the concept, analysis, data collection, and interpretations, as well as graphical illustrations.

Declaration of using AI tools

The authors declare that they have not used any type of generative artificial intelligence for the writing of this manuscript, nor for the creation of images, graphics, tables, or their corresponding captions.

References

[1] P. Verhulst, "Recherches mathématiques sur la loi de d'accrooissement de la population", *Nouv.Mem. Acad.R. Soc.Belle-Lettr., Bruxelles*, vol.18,pp.1-38,1845.

[2] S. Haykin, *Neural networks*,2nd Ed., Upper Saddle River: Prentice Hall PTR, 1998.

[3] K. Basterretxea, J.M. Tarela and I. del Campo, "Approximation of sigmoid function and the derivative for hardware implementation of artificial neurons", *IEE Proc. Circuits Devices Syst.*, vol.151, pp.18-24, 2004. https://doi.org/10.1049/ip-cds:20030607.

[4] J. Hristov, "On a new approach to distributions with variable transmuting parameter: The concept and examples with emerging problems", *Math. Model.Num. Sim. Appl.*, vol.2, pp.73-87,2022. https://doi.org/10.53391/mmnsa.2022.007.

[5] J. Hristov, " On a nonlinear diffusion model of wood impregnation: Analysis, approximate solutions and experiments with relaxing boundary conditions", in: *Advances in Mathematical Modelling, Applied Analysis and Computation*, J.Singh, G.A. Anastassiou, D. Baleanu, C. Cattani and D. Kumar, Eds., Lecture Notes in Networks and Systems, vol 415. Singapore: Springer, 2023, pp.25-53. https://doi.org/10.1007/978-981-19-0179-9_2.

[6] S. M. Filipov, A. Avdzhieva, I. Faragó and J. Hristov, "Implicit time discretization and quasilinearization for numerical solution of transient nonlinear heat transfer problems", *Int. J. Num. Meth. Heat & Fluid Flow*, vol. 35, pp.2398-2436, 2025. https://doi.org/10.1108/HFF-11-2024-0862.

[7] K. Nantomah, " On some properties of the sigmoid function", *Asia Mathematica*, vol.3, pp.79-90,2019.

[8] B. Grünbaum, "Partitions of mass-distributions and of convex bodies by hyperplanes", *Pac. J. Math.*, vol. 10, pp.1257–1261,1960. https://doi.org/10.2140/pjm.1960.10.1257.

[9] A.A. Minai and R.D. Williams, "On the derivatives of the sigmoid", *Neural Networks*, vol.6, pp.845-853, 1993. https://doi.org/10.1016/S0893-6080(05)80129-7.

[10] J. Kilian and H.T. Siegelmann," The dynamic universality of sigmoidal neural networks", *Inf. Comp..*, vol.128, pp.48-56,1996. https://doi.org/10.1006/inco.1996.0062.

[11] T.A. Akugre, K. Nantomah and M.M. Iddrisu, "On certain properties of degenerate sigmoid functions", *Eur. J.Math. Anal.*, vol. 3, 17; 2023. https://doi.org/10.28924/ada/ma.3.17.

[12] N. Balakrishnan, *Handbook of the logistic distribution*, NY:Marcel Dekker, 1992.

[13] F.R. Oliver, "Method of estimating the logistic growth function", *J. R. Stat. Soc*, vol.13, pp.57–66, 1964. https://doi.org/10.2307/2985696.

[14] M. Abramowitz and I.A. Stegun, Eds., "Hyperbolic functions" , in *Handbook of mathematical functions with formulas, graphs, and mathematical tables* , 9th ed. Reading, New York: Dover,1972, pp.83-86.

[15] J. Spanier and K.B.Oldham,"The hyperbolic Secant $sech(x)$ and Cosecant $csch(x)$ functions" , in *Atlas of functions*,Washington: Hemisphere,1972, pp.273-278.

[16] D.G. Chapernowne, "The graduation of income distributions", *Econometrica* , 1952. https://doi.org/10.2307/1907644.

[17] D.G. Chapernowne, "A model of income distribution", *The Economic Journal* , vol.63, pp.318-351, 1953.https://doi.org/10.2307/2227127.

[18] J. Berny, "New concepts and applications in growth phenomena", *J. Appl. Stat.*, vol.21, pp.161-190, 1994. https://doi.org/10.1080/757583654.

[19] A.J. Lotka, *Elements of physical biology*, Baltimor:Williams and Wilkins, 1925.

[20] F.J. Richards, "A flexible growth function for empirical use", *J. Exp. Botany*, vol.10, pp.290-300,1959. http://www.jstor.org/stable/23686557.

[21] B. Gompertz, "On the nature of the function expressive of the law of human mortality, and on a new model of determining the value of life contingencies", *Philos.Trans.R. Soc.Lond.*, vol.115, pp.513-583, 1825. https://www.jstor.org/stable/107756.

[22] W. Feller, "On the logistic law of growth and its empirical verification in biology", *Acta Biotheor.*, vol.5, pp.51-56,1940. https://doi.org/10.1007/BF01602862.

[23] H.C. Tuckwell and J.M. Koziol, "Logistic population growth under random dispersal", *Bull.math. Biol.*, vol.49., pp.495-506, 1987. https://doi.org/10.1007/BF02458866.

[24] R.A. Fisher, "The wave of advance of advantageous genes", *Ann.Eugenics*, vol.7, pp. 353-361, 1937. https://doi.org/10.1111/j.1469-1809.1937.tb02153.x

[25] A.I. Kolmogorov, I. Petrovskii and N. Piskunov, "Etude de l'equation de la diffusion avec croissance de la quantite de la matiere e son application a un problem biologique", *Moscow Univ.Bull. Math.*, vol.1, pp.1-25, 1937.

[26] J. Hristov, "Approximate solutions to a degenerate reaction-diffusion model: A pragmatic sharp front approach", *J. Math. Chemistry*, vol.63, pp.1126–1153, 2025. https://doi.org/10.1007/s10910-025-01713-0.

[27] N. Bacaër,"The diffusion of genes (1937)", Chapter 20 in: *A short History of mathematical Population Dynamics*, pp. 111–116, London: Springer-Verlag, 2011.

[28] S. Brody, "Time relations of growth:I. Genetic growth constants of animals", *J. Gen.Physiol.*,vol. 8, pp.233–251, 1926. https://doi.org/10.1085/jgp.8.3.233.

[29] P.V. Nordon, “On the anatomy of development projects”, *IRE Trans.Eng. Mngm.* , vol.EM-7, pp.34-42, 1960. https://doi.org/10.1109/IRET-EM.1960.5007529.

[30] W. Weibull,”A statistical distribution function of wide applicability”, *J. Appl. Mech.*, vol.18, pp.293–297, 1951. https://doi.org/10.1115/1.4010337.

[31] R. Jiang and D.N.P. Murthy, ”A study of Weibull shape parameter: Properties and significance”, *Reliability Engineering and System Safety*, vol.96, pp.1619–1626, 2011. https://doi.org/10.1016/j.ress.2011.09.003.

[32] P.H. Morgan, L.P. Mercer, and N.W. Flodin, ”General model for nutritional responses of higher organisms”, *Proc. Nat. Acad. Sci. USA*, vol. 72, pp. 4327–4331,1975.https://doi.org/10.1073/pnas.72.11.4327.

[33] F. Louzada,P. H. Ferreira and C.A.R. Diniz, ”Skew-normal distribution for growth curve models in presence of a heteroscedasticity structure”, *Journal of Applied Statistics*, vol.41, pp. 1785–1798, 2014. https://doi.org/10.1080/02664763.2014.891005.

[34] L.G.M. Baas Becking, ”On the analysis of sigmoid curves”, *Acta Biotheor*, vol. 8,pp. 42–59, 1946. https://doi.org/10.1007/BF01555951.

[35] R.S. Zotina and A.I. Zotin, ”Towards a phenomenological theory of growth”, *J. Theor.Biol.*, vo.35, pp.213–225, 1972. https://doi.org/10.1016/0022-5193(72)90034-3.

[36] C.P.D. Birch, ”A new generalized logistic sigmoid growth equation compared with the Richards growth equation”, *Annals of Botany*, vol.83, pp.713–723,1999. https://doi.org/10.1006/anbo.1999.0877.

[37] M. Peleg, M.G. Corradini and M.D. Normand, ”The logistic (Verhulst) model for sigmoid microbial growth curves revisited”, *Food.Res.Int.*, vol.40, pp.808–818, 2007. https://doi.org/10.1016/j.foodres.2007.01.012.

[38] A. Tsoularis and J. Wallace, ”Analysis of logistic growth models”, *Math. Biosci.*, vol 179, pp.21–55, 2002. https://doi.org/10.1016/S0025-5564(02)00096-2.

[39] R.P. Spencer and M.J. Coulombe, ”Quantitation of hepatic growth and regeneration”, *Growth*, vol.30, pp.277–284, 1966.

[40] N. Kyurkchiev, A. Iliev and A. Rahnev, “On the Verhulst growth model with polynomial vrable transfer. Some applications”, *Int. J. Diff. Eqs. Appl.*, vol.19, pp.19-32, 2020. http://dx.doi.org/10.12732/ijdea.v19i1.2.

[41] M.A. Savageau, ”Growth equations: A general equation and s survey of special case”, *Math. Biosci.*, vol.48, pp.267–278, 1980. https://doi.org/10.1016/0025-5564(80)90061-9.

[42] M.E. Turner Jr, B.A. Blumenstein and J.L. Sebaugh, “ A generalization of the logistic law of growth”, *Biometrics*, vol.25, pp.577-580, 1969. https://doi.org/10.2307/2528910.

[43] M.E.Turner Jr, E.L. Bradley Jr, and K. Kirk, ”A theory of growth”, *Math Biosciences*, vol 29, pp.367–373, 1976. https://doi.org/10.1016/0025-5564(76)90112-7.

[44] J.A. Nelder, “The fitting of a generalization of the logistic curve”, *Biometrics*, vol. 17, pp.89–110,1961. https://doi.org/10.2307/2527498.

[45] H. Levenbach, “A generalization of the logistic growth function and its estimation”, *Statistica Neederlandica*, vol.27, pp.47–54, 1973.

[46] H. Hotelling, ”Differential equation subject to error, and population estimates”, *J. Am.Stat. Asoc*, vo.22,pp.283–314, 1927. https://doi.org/10.2307/2276800.

[47] A.A. Blumberg, ”Logistic growth rate functions”, *J. Theoret. Biol.*, vol.11, pp.42–44,1968. https://doi.org/10.1016/0022-5193(68)90058-1.

[48] P.S. Meyer, “Bi-logistic growth”, *Techol.Forecast.Soc. Change*, vol.47, pp.89–102, 1994. https://doi.org/10.1016/0040-1625(94)90042-6.

[49] D. Thissen, D. Bock, H. Wainer and A.F. Roche, “Individual growth in stature: a comparison of four growth studies in the U.S.A”, *Annal of Human Biology*, vol.3., pp.529–542, 1976. https://doi.org/10.1080/03014467600001791.

[50] P. Jolicoeur and J. Pontier, ”Population growth and decline: a four parameter generalization of the logistic curve”, *J.Theor. Biol.*, vol.141, pp.563–571, 1989. https://doi.org/10.1016/S0022-5193(89)80237-1.

[51] J. Lopez Fidalgo, I.M. Ortiz Rodriguez and W.K. Wong, "Design issues for population growth models", *J. Appl. Stat.*, vol.38, pp.501–512, 2011. https://doi.org/10.1080/02664760903521419.

[52] T. Modis, "Fractal aspects of natural growth", *Techol.Forecast.Soc. Change*, vol.47, pp.63–73,1994. https://doi.org/10.1016/0040-1625(94)90040-X.

[53] R.D. Bock and D. Tissen, "Statistical problems of fitting individual growth curves", in *Human Physical Growth and Maturation: methodologies and factors*, F.E., Jonston, A.F. Roche and C. Susanne, Eds., New York and London: Plenum Press, 1980, pp. 265–290.

[54] K. Fujii, "Connection between growth/development and mathematical function", *Int. J.Sport and Health Sci.*, vol.4, pp.216–232, 2016. https://doi.org/10.5432/ijshs.4.216.

[55] R. Pearl, L.J. Reed, "A further note on the mathematical theory of population growth", *Proc. Nat. Acad. Sci. USA*, vol.8., pp.365–368, 1922. https://doi.org/10.1073/pnas.8.12.36.

[56] R. Buis, "On the generalization of the logistic law of growth", *Acta Bioteoretica*, vol.39, pp.185–195, 1991. https://doi.org/10.1007/BF00114174.

[57] N. Meade and T. Islam, "Forecasting with growth curves: An empirical comparison", *Int. J. Forecasting*, vol.11, pp.199–215, 1995. https://doi.org/10.1016/0169-2070(94)00556-R.

[58] A.D. Bain, "The growth of demand for new commodities. *J. R.Stat.Soc.,Ser.A*, vol.126, pp.285–299, 1963. https://doi.org/10.2307/2982371.

[59] J.C. Tanner, "Long term forecasting of vehicle ownership and road traffic", *J. R. Stat. Soc., Ser. A*, vol.141, pp.14–63, 1978. https://doi.org/10.2307/2344775.

[60] C.V. Easingwood, V. Mahajan and E. Muller, "A non-symmetric responding logistic model for forecasting technological substitutions", *Technological Forecasting and Social Change*, vol.20, pp.199-213, 1981. https://doi.org/10.1016/0040-1625(81)90021-4.

[61] R. Bewley and D. Fiebig, "Flexible logistic growth model with applications in telecommunications", *Int.J. Forecasting*, pp.177–192, 1988. https://doi.org/10.1016/0169-2070(88)90076-3.

[62] E.M. Rogers, *Diffusion of Innovations*, 1st ed. New York: The Free Press, 1962.

[63] E.M. Rogers, *Diffusion of Innovations*, 5th ed. New York: The Free Press, 2003.

[64] F.M. Bass, "A new product growth for model consumer durables", *Management. Sci.*, vol.15, pp. 215–227, 1969. https://doi.org/10.1287/mnsc.15.5.215.

[65] F.M. Bass, "A new product growth for model consumer durable", *Management. Sci.*, vol.50, pp.1825–1832, 2004. https://doi.org/10.1287/mnsc.1040.0264.

[66] F.M. Bass, T. Krishnan and D.C. Jain, "Why the Bass model fits without decision variables", *Marketing Sci.*, vol.13, pp.203–223, 1994. https://doi.org/10.1287/mnsc.13.3.203.

[67] V. Mahajan and S. Sharma, "A simple algebraic estimation procedure for innovation diffusion models of new product acceptance", *Technological Forecasting and Social Change*, vol.30, pp.331-345,1986. https://doi.org/10.1016/0040-1625(86)90031-4.

[68] D. Sahal, "A generalized logistic model for technolocal forecasting", *Technological Forecasting and Social Change*, vol.7, pp.81–97, 1975. https://doi.org/10.1016/0040-1625(75)90007-4.

[69] V. Mahajan, E. Muller and F.M. Bass, "Diffusion of new products: Empirical generalization and managerial uses", *Marketing Sci.*, vol.14, pp. G79–G88, 1995. https://doi.org/10.1287/mksc.14.3.G79

[70] P.A. Geroski, "Models of technology diffusion", *Research Policy*, vol.29, pp.603–625, 2000. https://doi.org/10.1016/S0048-7333(99)00092-X.

[71] Z. Jiang, F.M. Bass and P.I. Bass, "Virtual Bass model and the left-hand data truncation bias in diffusion of innovation studies", *Int. J. Res. Marketing*, pp. 93–106, 2006. https://doi.org/10.1016/j.resmar.2006.01.008

[72] P.C. Jha, A. Gupta, and P.K. Kapur, "Bass model revisited", *J. Stat.Management Syst.*, vol. 11, pp. 413–437, 2008. https://doi.org/10.1080/09729510.2008.10701320

[73] H.P. Boswijk and P.H. Franses, "On the econometrics of the Bass diffusion model", *J. Business and Exonomic Statistics*, vol.23, pp.255–268, 2005. https://doi.org/10.1198/073500104000000604.

[74] M. Trajtenberg and S. Yitzhaki, "The Diffusion of innovations: A Methodological reappraisal", *National Bureau of Economic Research, Working Paper 1008*, 1982.

[75] J. Erkelens, "Eeen berekeningasmethode voor de logisrische curve", *Statistica Neederlandica*, vol.22, pp.213–216, 1968.

[76] Y. Orbach, "Parametric analysis of the Bass model", *Innovative Marketing*, vol.12, pp. 29–40, 2016. http://dx.doi.org/10.21511/im.12(1).2016.03.

[77] D.Jain, V.Mahajan and E. Muller, " An approach for determining optimal sampling for the diffusion of a new product", *J. Product. Innov.Management*, vol.12, pp. 124–135, 1995. https://doi.org/10.1016/0737-6782(94)00042-E.

[78] V. Srivanasan and Ch. H. Mason, "Nonlinear least squares estimation of new product diffusion models", *Marketing Sci.*, vol.5, pp.169–178, 1986. https://doi.org/10.1287/mksc.5.2.16.

[79] D. Jukic, "Total least squares fitting Bass diffusion model", *Mat.Comp. Modelling*, vol.53, pp.1756–1770, 2011. https://doi.org/10.1016/j.mcm.2010.123.054.

[80] N. Kyurkchiev and S. Markov, "Sigmoidal functions: Some computational and modeling aspects", *Biomath Commun.*, vol.1, pp.1-19, 2014. http://dx.doi.org/10.1145/j.bmc.2015.03.81.

[81] N. Kyurkchiev, "A family of recurrence generated sigmoidal functions based on the Verhulst logistic functions. Some approximation and modeling aspects", *Biomath Commun.*, vol.3, pp.1-4, 2016. https://doi.org/10.11145/bmc.2016.12.171.

[82] R. Anguelov, N.Kyurkchiev and S. Markov, "Some properties of the Blumberg's hyper-log-logistic curve", *Biomath*, vol.7, 1807317, 2018. https://doi.org/10.11145/j.biomath.2018.07.317.

[83] N. Kyurkchiev, "A look at the smooth approximation to using some sigmoidal functions: Applications", *AIP Conf.Proc.*, 2459, pp.030020-1-030020-13, 2021. https://doi.org/10.1063/5.0083553.

[84] N. Kyurkchiev and S. Markov, *Sigmoid functions: Some approximations, and modelling aspects*, Saarbrucken: LAP Lambert Academic Publishing, 2015.

[85] B.Sendov, *Hausdorff Approximations*, Boston: Kluwer, 1990.

[86] H.T. Davis, *Introduction to Nonlinear Differential and Integral Equations*, New York: Dover Press Inc., 1962.

[87] R.K. Miller, "On Volterra's population equation", *SIAM J. Appl.Math.*, vol.14, pp. 446–452, 1977. https://doi.org/10.1137/0114039.

[88] C.C.Shilepsky, "The asymptotic behavior of an integral equation with an application to Volterra's population equation" , *J. Math. Anal.Appl.*, vol. 486, pp. 764–779, 1974. https://doi.org/10.1016/0022-247X(74)90150-4.

[89] R. Zwanzig, "Generalized Verhulst law for population growth" , *Proc.,.Nat. Acad. Sci., USA*, vol. 70, pp.3048–3051, 1973. https://doi.org/10.1073/pnas.70.11.3048.

[90] D.V. Widder, "The convolution transform", *Bull. Amer. Math. Soc.*, vol. 60, pp.444–456, 1954. https://doi.org/10.1090/S0002-9904-1954-09828-2.

[91] S-O. Londen, "On a nonlinear Volterra integral equation", *J. Diff. Eqs.*, vol.14, pp.106–120, 1973. https://doi.org/10.1016/0022-0396(73)90080-6.

[92] F. Brauer, "On a nonlinear integral equation for population growth problems", *SIAM J. Appl.Math.*, vol.6, pp. 312–317, 1975. https://doi.org/10.1137/0506031.

[93] J.M. Cushing, "Periodic solutions of Volterra's population equation with hereditary effects", *SIAM J. Appl.Math.*, vol.31, pp. 251–261, 1976. https://doi.org/10.1137/0131020.

[94] F. Brauer, "Constant rate harvesting of population governed by Volterra integral equations", *J. Math. Anal.Appl.*, vol. 56, pp. 18–27, 1976. https://doi.org/10.1016/0022-247X(76)90004-4.

[95] J.M. Cushing, " Stable positive periodic solutions of the time-dependent logistic equation under possible hereditary influences", *J. Math. Anal.Appl.*, vol. 60, pp. 747–754, 1977. https://doi.org/10.1016/0022-247X(77)90014-2.

[96] J.M. Cushing," Periodic time-dependent predator-prey systems", *SIAM J. Appl.Math.*, vol.32, pp. 82–95, 1977. https://doi.org/10.1137/0132006.

[97] W. Feller, "On the integral equation of renewal theory", *Ann. Math. Stat.*, vol.12, pp.243–267, 1941.

[98] P.J. Wangersky, " Lotka-Volterra population models", *Ann.Rev.Ecol.Syst.*, vol.9, pp.189–218, 1978. https://doi.org/10.1146/annurev.es.09.110178.001201.

[99] T.L. Saaty, *Modern Nonlinear Mathematics*, New York: Dover Press Inc., 1981.

[100] J. Furter and M.Grinfeld, " Local vs. non-local interactions in population dynamics", *J. Math. Biol.*, vol. 27, pp.65–80, 1989. https://doi.org/10.1007/BF00276081.

[101] J.J. Frankel and S.R.Choudhury, "Some new observations on the classical logistic equation with heredity" , *App. Math. Comp.* , vol.58, pp. 275–308, 1993. https://doi.org/10.1016/0096-3003(93)90140-A.

[102] J.A.D. Appleby, I. Gyori and D.W. Reynolds, "History-dependent decay rates for logistic equation with infinite delay", *Proc.R.Soc.Edinburgh*, vol.141, pp.23–44, 2011. https://doi.org/10.1017/S0308210510000016.

[103] V. Volterra, *Lecons sur la Theorie Matematique de la Lute pour la View*, Paris: Gauthier-Villars, 1931.

[104] R. Grimshaw, *Nonlinear Ordinary Differential Equations*, Oxford: Blackwell Scientific, 1990.

[105] J. Hristov , "The integrals of fractional operators with non-singular kernels: a conceptual approach, formulations, and normalization functions", *Prog. Frac. Diff. Appl.*, vol. 10, pp:627-662, 2024. https://doi.org/10.18576/pfda/100409.

[106] J.Hristov , "The fading memory formalism with Mittag-Leffler-type kernels as a generator of non-local operators", *Appl.Sci.*,vol. 13, 3065, 2023. https://doi.org/10.3390/app13053065.

[107] J.Hristov, "Fractional modeling approaches to transport phenomena: Causality, Fading memory and Volterra equations", in: Computational and Modeling for Fractional Order Systems, S. Chakraverty and R. M. Jena, Eds. , pp.41-71, USA: Academic Press, 2024. https://doi.org/10.1016/B978-0-44-315404-1.00008-4.

[108] N. Z. Monteiro, R. W. dos Santos and S. R. Mazorche. "Bridging the gap between models based on ordinary, delayed, and fractional differential equations through integral kernels", *Proc. Nat. Acad. Sci.*, vol. 121, e2322424121, 2024. https://doi.org/10.1073/pnas.2322424121.

[109] J. M. Cushing, *Integrodifferential Equations and Delay Models in Population Dynamics*, Berlin, Heidelberg: Springer Science & Business Media, 2013.

[110] S. S. Nair, "An overview of generalized gamma Mittag-Leffler model and its applications", *Axioms* , vol.4, pp. 365–384, 2015. https://doi.org/10.3390/axioms4030365.

[111] R. Gorenflo, A. A. Kilbas, F. Mainardi and S. V. Rogosin, *Mittag-Leffler Functions, Related Topics and Applications*, Berlin: Springer,2014),

[112] N. Z. Monteiro, R. W. dos Santos and S. R. Mazorche. "Constructive fractional models through Mittag-Leffler functions", *Comp. Appl. Math.*, vol 43, 177, 2024. https://doi.org/10.1007/s40314-024-02680-z.

[113] R.Hilfer and L.Anton, "Fractional master equations and fractal time random walks", *Phys. Rev. E*, vol. 51,848, 1995. https://doi.org/10.1103/PhysRevE.51.R848.

[114] S. R. Mazorche and Th. S. Oliveira, "Modelos Populacionais: Da Teoria de Lotka com o uso das Funcoes de Mittag-Leffler" , *Proc. Series of the Brazilian Soc. of Comp. Appl. Math.*, vol. 11, 010437, 2025. https://doi.org/10.5540/03..2025.011.01.0437.

[115] S. Miller and D. Childers, *Probability and Random Processes*, Elsevier Science, 2004.

[116] H. Nussenzveig, H. *Causality and dispersion relations*,New York: Academic Press, 1972.

[117] R.Hilfer, "Fractional Time evolution", in: *Applications of Fractional Calculus in Physics*, Hilfer,R., Ed.,pp. 89–116, Singapore: World Scientific,2000.

[118] R. Hilfer, "Mathematical and physical interpretations of fractional derivatives and integrals", in: Ĥandbook of fractional calculus with applications, vol.1, A. Kochubei and Y. Luchko, Eds., pp.,47-85,2019. https://doi.org/10.1515/9783110571622-003.

[119] V. Daftardar-Gejji and H. Jafari, "An alternative method for solving nonlinear functional equatins", *J. Math. Anal. Appl.*, vol.316, pp.753-763,2006. https://doi.org/10.1016/j.jmaa.2005.05.009.

[120] S. Momani and R. Qaralleh, " Numerical approximations and Padé approximants for a fractional population growth model", *Appl.Math. Model.*, vol.31, pp.1907-1914. https://doi.org/10.1016/j.apm.2006.06.015.

[121] S. Bhalekar and V. Daftardar-Gejji, " Solving fractional-order logistic equation using a new iterative method", *Int. Diff. Eqs*, vol.2012, 975829, 2012. https://doi.org/10.1155/2012/975829.

[122] A.M.A. El-Sayed, A.E.M.El-Mesry and H.A.A. El-Saka, "On the fractional order logistic equation", *Appl./ Math. Lett.*, vol.20, pp.817—823, 2007. http://dx.doi.org/10.11648/j.acm.20140301.14.

[123] N.H. Sweilam, M.M. Khader and A.M.S. Mahdy , "Numerical studies for fractional-order logistic differential equation with two different delays, *J. Appl. Math*, vol.2012, 764894, 2012. http://dx.doi.org/10.1155/2012/764894.

[124] M.M. Khader and M.M. Babatin, " On approximate solutions for fractional logistic differential equation", *Math Problem Eng.*, vol.2013, 391901, 2013. http://dx.doi.org/10.1155/2013/391901.

[125] M.S. Mohamed, " Application of optimal HAM for solving the fractional order logistic equation", *App. Comp. math*, vol.3, pp.27-31, 2014. http://dx.doi.org/10.1016/j.aml.2006.08.013.

[126] Z,F. El Raheem and S.M. Salman, "On a discretization process of fractional-order logistic differential equation", *J. Egypt Math. Soc.*, vol. 22,pp..407-412, 2014. http://dx.doi.org/10.1016/joems.2013.09.001.

[127] B. West, "Exact solution to fractional logistic equation", *Physica A*, vol. 4294, pp.103—108, 2016. http://dx.doi.org/10.1016/j.physa.2015.10.037.

[128] I.Area, J. Losada and J.J. Nieto, " A note on the fractional logistic equation", *Physica A*, vol. 444, pp.182—167, 2016. http://dx.doi.org/10.1016/j.physa.2015.02.073.

[129] S. Yuzbasi, " A collocation method for numerical solutions of fractional order logistic population method", *Int.J.Biomath.*, vol./9, 165031, 2016. http://dx.doi.org/10.1142/S1793524516500315.

[130] M. Ortigueira and G. Bengochea, " A new look at the fractionalization of the logistic equation", *Physica A*, vol.467, pp.554-561, 2017. http://dx.doi.org/10.1016/j.physa.2016.10.052.

[131] F. Pitolli and L.Pezza, "A fractional spline collocation method for the fractional order logistic equations", in: *Approximation Theory XV: San Antonio 2016*, G.E. Fasshauer and L.L. Schumaker, Eds., AT 2016. Springer Proceedings in Mathematics and Statistics, vol. 201, pp.307-318, 2017, Cham: Springer. https://doi.org/10.1007/978-3-319-59912-0_15.

[132] M. Turalska and B. West, "A search for a spectral technique to solve fractional differential equations", *Chaos, Solitons, Fractals*, vol.102, pp. 387-395, 2017. https://doi.org/10.1016/j.chaos.2017.04.022.

[133] M.D'Ovidio and P. Loreti, " Solutios of fractional logistic equations by Euler's numbers", *Physica A*, vol.506, pp.1081-1092, 2018. http://dx.doi.org/10.1016/j.physa.2018.05.030.

[134] M.D'Ovidio, P. Loreti and S.S.Ahrabi, " Modified fractional logistic equation", *Physica A*, vol.505, pp.818-824, 2018. http://dx.doi.org/10.1016/j.physa.2018.04.011.

[135] Y.Y.Y.Noupoue, Y.Tandoglu and M.Awadalfa, "On numerical techniques for solving the fractional logistic differential equation", *Adv. Diff. Eqs.*,vol. 2019, 108, 2019. http://dx.doi.org/10.1186/s13662-019-2055-y.

[136] M. Izadi and H.M. Srivastava, "A discretization approach for the nonlinear fractional logistic equations, *Entropy*, vol.22, 1328, 2020. http://dx.doi.org/10.3390/e22111328.

[137] V. E. Tarasov, "Exact solutions of Bernoulli and logistic fractional differential equations with power law ciefficients", *Mathematics*, vol. 8,2231, 2020. http://dx.doi.org/10.3390/math8122231.

[138] L.N.Kaharuddin, C.Piang and S.S.Jamaian, " Solution of the fractional logistic equations by modified Eulerian numbers", *Eur.Phys. J. Plus*, vol.135, 229, 2020. http://dx.doi.org/10.1140/epjp/s13360-020-00135-y.

[139] E. Pelinovsky, A. Kurkin, O.Kurkina and M.Kokoulina, " Logistic equation and COVID-19", *Chaos, Solitons Fractals*, vol.140, 110241, 2020. http://dx.doi.org/10.1016/j.chaos.2020.11024.

[140] I. Area and J.J. Nieto, "Power series solution of the fractional logistic equation", *Physica A*, vol. 573, 125947, 2021. http://dx.doi.org/10.1016/j.physa.2021.125947.

[141] I. Area and J.J. Nieto, " Fractional-order logistic differential equations with Mittag-Leffler-type kernel", *Fractal Fract*, vol.5, 273, 2021. http://doi.org/10.3390/fractalfract5040273

[142] I. Area and J.J. Nieto,"On the fractional Allee logistic equation in the Caputo sense", Êxamplesa and Counterexamples, vol.4, 100121, 2023. http://doi.org/10.1016/j/exco.2023.100121.

[143] F. Bozkurt and A. Yousef, "Flip bifurcation and stability analysis of a fractional-order poulation dynamics with Allee effect", *J. Interdisciplinary math*, vol.22, pp.1009-1029. http://doi.org/10.1080/09720502.2019.1698403.

[144] A.S.V. Ravi Kanth and N.Garg, "Computational simulations for solving a class of fractional models via Caputo-Fabrizio fractional derivative", *Procedia Comp. Sci.*, vol.125, pp.476-482, 2018. http://doi.org/10.1016/j.procs.2017.12.063.

[145] J.J. Nieto, "Solution of fractional logistic ordinary differential equation", *Appl. Math. Lett.*, vol.123, 107558, 2022. http://dx.doi.org/10.1016/j.aml.2021.107568.

[146] J.J. Nieto, "Fractional Euler numbers and generalized proportional fractional logistic differential equation", *Frac, Calc. Appl. Anal.*, vol.25, pp.876-886, 2022. http://dx.doi.org/10.1007/s13540-022-00044-0.

[147] P. Kalra and N. Malhotra, "Modeling and analysis of fractional order logistic equation incorporating additive Allee effect", *Contemporary Math.*, vol.5 , pp.380-401, 2024. https://doi.org/10.37256/cm.5120243183.

[148] K. Kowalski and W-H. Steeb, *Nonlinear Dynamical Systems and Carleman Linearization*, Singapore:World Sientific Publ., 1991.

[149] B. Shiri, Z.Alijani and Y. Karaca, "A power series method for the fuzzi fractional logistic differential equations", *Fractals*, vol.31, 2340086, 2023. https://doi.org/10.1142/S0218348X23400868.

[150] M. Jornet and J.J. Nieto, "Power-series solution of L-fractional logistic equation", *Appl. Math. Lett.* , vol.154, 109085, 2024. https://doi.org/10.1016/j.aml.2024.109085.

[151] K.A.Lazopoulos and A.K. Lazopoulos, "Fractional vector calculus and fractional continuum mechanics", *Prog. Fract. Differ. Appl.*, vol.2, pp.67-85, 2016. http://dx.doi.org/10.18576/pfda/020107.

[152] K.A.Lazopoulos and A.K. Lazopoulos, "Fractional differential geometry of curves and surfaces" *Prog. Fract. Differ. Appl.*,vol.2, pp.169-186, 2016. http://dx.doi.org/10.18576/pfda/020302

[153] K.A.Lazopoulos and A.K. Lazopoulos, "Equilibrium of –fractional liquid crystals", *Mech. Res. Commun.*, vol.136,104243, 2024. https://doi.org/10.1016/j.mechrescom.2024.104243.

[154] I. Area, K.A Lazaropoulos and J.J. Nieto, " Λ-Fractional logistic equation" , *Prog.Frac. Differ.Appl.*, vol.9, pp.345-350, 2023. https://doi.org/10.18576/pfda/090301.

[155] M.O. Aibinu and E.Momoniat,"Approximate analytical solutions and applications to logistic models with fractional derivatives", *Part.Diff. Eqs. Appl. Math*, vol.13, 101043,2025. https://doi.org/10.1016/j.padiff.2024.101043.

[156] M. Caputo and M. Fabrizio, "A new definition of fractional derivative without singular kernel" *Prog. Fract. Differ. Appl.*, vol.1, pp.73-85, 2015. http://dx.doi.org/10.12785/pfda/010201.

[157] A.Atangana and D. Baleanu, "New fractional derivatives with non-local and non-singular kernel: theory and application to heat transfer model", *Thermal Sci.*, pp.763-769, 2016. http://doi.org/10.2298/TSCI160111018A.

[158] A. Giusti, I. Colombaro, R. Garra , R. Garrappa, P. Polito, M.Popolizo and F. Mainardi, "A practical guide to Prabhakar fractional calculus", *Frac.Calcul.Appl.Anal.* , vol. 23, pp.9-54, 2020. https://doi.org/10.1515/fca-2020-0002.

[159] D. Kumar, J. Singh, M.Al Qurashi and D. Baleanu, "Analysis of logistic equation pertaining to a new fractional derivative with non-singular kernel", *Adv.Mech.Eng*, vol.9, 2017. https://doi.org/10.1177/1687814017690069.

[160] H. Jafari, R.M. Ganji, N.S. Nkomo and Y.P. Lv, "A numerical study of fractional order population dynamics model", *Results in Physics*, vol.27, 104456, 2021. http://dx.doi.org/10.1016/j.rinp.2021.104456.

[161] N.Djeddi, S.Hasan, M.Al-Smadi and S.Momani," Modified analytical approach for generalized quadratic and cubic logistic models with Caputo-Fabrizio fractional derivative", *Alexandia Eng. J.*, vol.59, pp.5111-5122, 2020. http://doi.org/10.1016/j.aej.2020.09.041.

[162] M.Adel and M. M. Khader, "Numerical treatment by implementing a successive approximation method for fractional Riccati and logistic differential equations", *J.Appl.Math. Comput. Mech.*, vol.23, pp.5-17, 2024. http://doi.org/10.17512/jamcm.2024.4.01.

[163] M. Sattari and M. A Ameri, "Compact finite difference scheme sor numerical solution of Caputo-Fabrizio Fractional Riccati Differential Equations", *Comp. Meth. Diff. Eqs.*,pp.1-14,*in press*, 2025. https://doi.org/10.22034/cmde.2025.60832.2602

[164] S.Hasan, A. El-Ajou, S. Hadid, M. Al-Smadi and S. Momani, "Atangana-Baleanu fractional framework of reproducing kernel technique in solving fractional population dynamic system", *Chaos, Solitons, Fractals*, vol.133, 109624, 2020. http://doi.org/10.1016/j.chaos.2020.109624.

[165] E. Bas and R. Ozarslan, " Rear world applications for fractional models by Atangana-Baleanu fractional derivative", *Chaos, Solitons and Fractals*, vol.116, pp.121-125, 2018. http://doi.org/10.1016/j.chaos.2018.09.019

[166] B.S.T. Alkahtani, A. Atangana and I. Koca, "New nonlinear model of population growth, *PLoS ONE*, vol.12, e0184728,2017. https://doi.org/10.1371/journal.pone.0184728.

[167] J. Hristov, "On the Atangana-Baleanu derivative and its relation to the fading memory concept: The diffusion equation formulation", in: *Fractional Derivatives with Mittag-Leffler Kernel*, 1st ed., J. F. Gómez et al. (eds.), Springer Nature Switzerland AG, **2019**, pp. 175-193, 2019. https://doi:10.1007/978-3-030-11662-0_11.

[168] D. Caratelli and P.E. Ricci, "A note on fractional -type models of population dynamics", *Math. Model. Anal.*, 29, pp.480-492, 2024. https://doi:10.3846/mma.2024.19588.

[169] F.J.Ariza-Hernadez, M.P.Arciga-Alejandre, J.Sanchez-Ortiz and A.Fleitas-Imbert, "Bayesian derivative order estimation for fractional logistic model", *Mathematics*, vol.8, 109, 2020. https://doi:10.3390/math8010109.

[170] R. Prabhakar, "A singular integral equation with a generalized Mittag-Leffler function in the kernel", *Yokohama Math. J.*, vol.19, pp.7-15, 1971.

[171] S.G., Samko, A.A. Kilbas, and O.I. Marichev, *Fractional Integrals and Derivatives: Theory and Applications*, Yverdon:Gordon and Breach,1993.

[172] J.E.Napoles Valdes, "Generalized fractional Hilfer integral and derivative", *Contrib.Math.*, vol.2, pp.55–60, 2020. https://doi.org/10.47443/cm.2020.0036.

[173] J-G. Liu and X-J Yang, " New derivative with sigmoid function as the kernel and its models",*Chinese Journal of Physics*, vol.68, pp.533–541, 2020. https://doi.org/10.1016/j.cjph.2020.10.001

[174] M.Rezapour, A. Sijuwade and A.Asaki, "A sigmoidal fractional derivative for regularization", *AIMS Mathematics*, vol.5, pp. 3284-3297, 2020. https://doi.org/10.3934/math.2020211.

[175] A.H.Zemanian, *Distributional theory and transform analysis*,New York: Dover Pub. Inc.,1987.

[176] R.M.May, "Simple mathematical models with very complicated dynamics", *Nature*, vol.261. pp.459-467, 1976. https://doi.org/10.1038/261459a0.

[177] M.Edelman, "On fractional generalizations of the logistic map and their applications", eprint arXiv:2503.13256,2025. https://doi.org/10.48550/arXiv.2503.13256.

[178] M.Edelman," Maps with power-law memory: direct introduction and Eulerian numbers, fractional maps, and fractional difference maps", in:*Handbook of fractional calculus with applications: Theory*, Kochubei, A. and Lucko , Y. Eds., vol.2,pp.47-64, Berlin: De Gruyter, 2019.

[179] G-C. Wu and D. Baleanu, " Discrete fractional logistic map and its chaos", *Nonlinear Dyn*,vol.75,pp.283-287,2014 https://doi.org/10.1007/s11071-013-1065-7 .

[180] T. Abdeljawad, " On Riemann and Caputo fractional differences ", *Comp. Math.Appl.*, vol.62, pp.1602-1611, 2011.https://doi.org/10.1016/j.camwa.2011.03.036.

[181] M.Abundo, L.Accardi, A.Finazzi Agro, G. Mei, and N.Rosato, "A stochastic model for the sigmoidal behaviour of cooperative biological systems", *Biophys. Chem.*, vol.58, pp.313-323., 1996. https://doi.org/10.1016/0301-4622(95)00111-5.

[182] G-C. Wu, D. Baleanu and S-D Zeng, " Discrete chaos in fractional sine and standard maps", *Phys.Lett. A*, vol.378, pp.484-487, 2014. https://doi.org/10.1016/j.physleta.2013.12.010.

[183] G-C. Wu and D. Baleanu, "Chaos synchronization of discrete fractional logistic map", *Signal Proc.*, vol.102, pp.96-99,2014 https://doi.org/10.1016/j.sigpro.2014.02.022.

[184] R.Rak and E.Rak, "Route to Chaos in Generalized Logistic Map", *Acta Physica Polonica A*,vol.127,pp.A-113-117, 2015. https://doi.org/10.12693/APhysPolA.127.A-113.

[185] V. E. Tarasov and G. M. Zaslavsky, "Fractional equations of kicked systems and discrete Maps", *J. Phys. A, Math. Theor.*, vol.41, 435101, 2008. https://doi.org/10.1088/1751-8113/41/43/435101.

[186] V. E. Tarasov, "Differential Equations with Fractional Derivative and Universal Map with Memory", *J. Phys. A, Math. Theor.*, vol.42, 465102, 2009. https://doi.org/10.1088/1751-8113/42/46/465102.

[187] V.E. Tarasov and M. Edelman, "Fractional dissipative standard map", *Chaos*, 023127, 2010. https://doi.org/10.1063/1.3443235

[188] M. Edelman and V.E. Tarasov, "Fractional standard map", *Phys. Lett. A*, vol.374, pp.279-385, 2009. https://doi.org/10.1016/j.physleta.2009.11.008.

[189] M. Edelman, "Fractional standard map: Riemann-Liouville v. Caputo", *Comm. Nonlinear Sci. Numer. Simulat.*, vol.16, pp.4573-4580, 2011. https://doi.org/10.1016/j.cnsns.2011.02.007.

[190] M.Edelman, "Universal fractional map and cascade of bifurcations type attractors ", *Chaos*, vol.23, 033127, 2013. https://doi.org/10.1063/1.4819165.

[191] M.Edelman, "Universality in systems with power-law memory and fractional dynamics", in: *Chaotic, Fractional and Complex Systems: New Insights and Perspectives. Understanding Complex Systems*, M.Edelman, E.Macau, and M.Sanjuan, Eds., Cham: Springer, pp.147-171. https://doi.org/10.1007/978-3-319-68109-2_8.

[192] A.A.Kilbas, B.Bonnila and J.J.Trujillo, "Nonlinear differential equations of fractional order in the space of integrable functions", *Dokl. Math.*, vol.62, pp.222-226, 2000. (English Translation).

[193] B.V. Chirikov, "A universal instability of many-dimensional oscillator systems", *Phys. Rep.*, vol. 52, pp. 263-379, 1979. https://doi.org/10.1016/0370-1573(79)90023-1.

[194] V.Arnold, Small denominators. I: On the mappings of the circumference onto itself, Amer. Math. Soc. Transl.,vol. 46,pp. 213-284,1965.https://doi.org/10.1007/978-3-642-01742-1_10.

[195] R.R. Nigmatulin, "Fractional integral and its physical interpretation",*Theor.Math.Phys.*, vol.90, pp.242-251,1992. https://doi.org/10.1007/BF01036529

[196] N.S.Goel, S.C. Maitra and E. Montroll , "On the Volterra and other nonlinear models of interacting populations ", *Rev. Mod. Phys.*, vol.43, pp.231-276, 1971. https://doi.org/10.1103/RevModPhys.43.231.

[197] E. Montroll, "On the dynamics and evolution of some sociotechnical systems", *Bull. Amer. Math. Soc.*, vol.16, pp. 1-46, 1987. https://doi.org/10.1090/S0273-0979-1987-15462-0.

All open access articles published in Transactions on Computational Modeling and Intelligent Systems (http: //tcmis.org) are distributed under the terms of the CC BY-NC 4.0 license (Creative Commons Attribution Non-Commercial 4.0 International Public License as currently displayed at http:// creativecommons.org/li censes/by-nc/4.0/legalcode) which permits unrestricted use, distribution, and reproduction in any medium, for non-commercial purposes, provided the original work is properly cited.

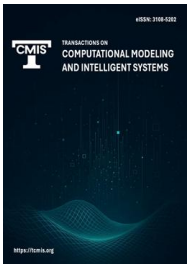

Transactions on
Computational Modeling and Intelligent Systems

Volume 1, October 2025, Article 10008
https://doi.org/10.65112/tcmis.10008

eISSN: 3108-5202
www.tcmis.org

RESEARCH ARTICLE

Rebalancing of multi-manned mixed-model assembly lines with task relocation restrictions

Damla Camli[1*], Ibrahim Kucukkoc[2] and Zixiang Li[3,4]

[1] *Continuous Improvement Department, Önen Food Company, Çanakkale, Turkiye.*
[2] *Department of Industrial Engineering, Balikesir University, Balikesir, Turkiye.*
[3] *Key Laboratory of Metallurgical Equipment and Control Technology of Ministry of Education, Wuhan University of Science and Technology, Wuhan, Hubei, China.*
[4] *Hubei Key Laboratory of Mechanical Transmission and Manufacturing Engineering, Wuhan University of Science and Technology, Wuhan, Hubei, China.*

[*] *Corresponding Author. Email: damla.camli@dardanel.com.tr (D. Camli)*

Article Information

Received: 15 August 2025
Accepted: 2 October 2025
Published: 3 October 2025

AMS 2020 Classification: 90B10, 90B35

Abstract

Increasing competition and customized demands have led companies to use assembly lines more flexible and efficiently. Companies need to frequently rebalance their lines to adapt changes either in the product model demand or task processing times. During which, some tasks will be required to assign a different workstation (causing a change in the task allocation) due to the nature of the rebalancing procedure. However, as the number of relocations made during rebalancing increases, the likelihood of costs and quality errors will also arise. This study aims to efficiently balance mixed-model assembly lines while restricting the number of relocations to a limited value. A mixed-integer program is proposed to maximize line efficiency (minimising both cycle time and number of workstations, called type-E) considering the number of task relocations up to a certain value. An iterative algorithm is also developed for solving large-sized problems. The model allows lower and upper bounds to be imposed on the cycle time and aims to avoid 'substantial' changes in task assignments during rebalancing. The multi-manned workstation case is also integrated, which gives the advantage of determining the number of operators, i.e., increasing line efficiency. Tests have shown that the heuristic algorithm achieves competitive solutions in compare with the mixed-integer programming model within short periods of time, including large-size problems.

Keywords: Mixed-model assembly line, type-E, task relocation restrictions, rebalancing, mixed-integer programming, multi-manned workstations.

1. Introduction

Assembly lines ensure efficient use of resources which usually yields in cost reduction. At the same time, it increases the efficiency of the system and the production per unit time by minimising the number of workstations and/or cycle time. An assembly line consists of a set of workstations connected to each other by a transportation mechanism (conveyor or moving belt) [1, 2]. Each workstation is responsible from executing a set of tasks within the cycle time determined. The allocation of tasks to the workstations aiming to minimise or maximise an objective function under certain constraints is called the assembly line balancing problem [3]. The precedence relationship constraints and cycle time constraints are mandatory while some other constraints might be added based on the work environment, and the objectives sought.

Due to customized demands and increasing competition, companies have utilised mixed-model assembly lines, where similar models of a product are assembled on the same line with no need for set-up [4, 5]. It is of great strategic importance for companies to quickly adapt to changing market conditions, increase customer satisfaction and gain global competitive advantage. At this point, mixed model assembly lines provide many advantages to

companies. Improving the processes increases productivity by producing more products in a shorter time and thus resource utilisation is minimised. This helps to control and reduce the costs of companies. In this sense, there are operational decisions that companies should make in order to maximise line efficiency. Some of them are the number of operators to be assigned to stations, cycle time and the number of stations to be opened [6].

In this study, a mathematical model that maximises line efficiency by minimising the multiplication of the number of stations and cycle time of mixed model assembly lines is developed. In this way, the aim is to meet rapidly changing customer demands in the fastest way possible by minimising idle time and optimising production capacity and resources with a balanced production line. At the same time, the mathematical model is formulated by allowing multi-manned workstations. Multi-manned workstations allow the utilisation of a cycle time lower than the maximum task processing time by multiplying the workstation capacity. In the assembly line rebalancing problem, the assignment of jobs to completely different stations implies major changes to the existing assembly line. Due to this situation, the number of allowed task relocations is added as a new constraint to the model. In the developed model, by imposing lower and upper limits on the cycle time (C_{min} and C_{max} respectively) flexibility is provided to the model in order to maximise the line efficiency. The method we propose provides high-quality solutions for the companies, even for large size problems with the iterative algorithm integrated into the mathematical model.

The rest of the article is organised as follows: Section 2 provides the classification of assembly line balancing problems and a comprehensive literature review on the subject under consideration. Section 3 describes the mixed-integer programming model as well as the iterative algorithm, following a basic introduction of the notation and definitions. Section 4 presents the data set on which the model is tested, followed by the test results and their interpretation. Finally, Section 5 concludes the work with a discussion and potential topics for future studies.

2. Literature review

A review of the literature on assembly line balancing problems shows that assembly line balancing (ALB) problems are classified as follows according to the objective sought [3]:

- Type-1 ALB: To minimise the number of stations when the cycle time is given.
- Type-2 ALB: To minimise the cycle time when the number of stations is given.
- Type-E ALB: To maximise line efficiency minimising both the number of stations and the cycle time.
- Type-F ALB: To find a feasible solution given both the number of stations and the cycle time.

One might see Boysen et al. [7], Battaïa and Dolgui [8], and Li et al. [9] for the recent surveys and different classification schemes.

2.1. Literature review on MALBP

The literature on mixed-model assembly line balancing problem (MALBP) is rather extensive. The preliminary works in the literature are done by Thomopoulos [10, 11] who presented the first methods for mixed-models and worked on workload balancing. Subsequent research focused on multi-objective approaches and various optimisation techniques. Thomopoulos [11] and Gökçen [12] developed multi-objective models, while Emde [13] investigated workload smoothing methods. Belkharroubi and Yahyaoui [14] developed methods to reduce the number of workstations. In a later work by the same authors, Belkharroubi and Yahyaoui [15] aimed to minimise the number of workstations in mixed models where a greedy search procedure was employed.

Mönch et al. [16] emphasise the importance of adopting a single and flexible assembly line to gain competitive advantage in challenging conditions such as changing customer demands and short product lifetimes and show that variable takt times (average cycle time) increase labour productivity and simplify complex assembly lines. Meng et al. [17] aimed to minimise the number of stations by considering ergonomic conditions in mixed-model lines. Zhang et al. [18] proposed a MINLP model that aims to minimise the cost of opening station and the recruitment cost of operators. The study is important in terms of economic sustainability. Nourmohammadi et al. [19] aimed to minimise the cycle time at a certain number of stations. They developed a multi-objective MILP model to minimise cycle time, maximum ergonomic risks of stations and total ergonomic risks. Li et al. [20] focused on a mixed model type-2 assembly line balancing problem. They developed a mixed integer-based heuristic with a cost-oriented objective function and a customised neighbourhood search algorithm. Delice et al. [21] aimed to minimise the sum of workstation setup cost, supermarket setup cost and transportation cost in mixed-model assembly lines. The aim of the model developed in Dalle Mura and Dini [22] is to minimise the number of workstations, while balancing noise exposure and energy expenditure of operators. Çil et al. [23] addressed the type-2 MALBP (i.e. MALBP-2) and multiple operator assignment problem. They optimised the number of operators to be assigned to stations while minimising the cycle time. Workers and robots can work together as operators at stations. Alakas and Toklu [24] also considered the MALBP-2 and proposed a constraint programming approach as a solution method. Yuwei et al. [25] considered the type-1 MALBP (i.e. MALBP-1) and used genetic algorithm as the solution method. Yaphiar et al. [26] considered a mixed model type-1 assembly line balancing and operator assignment problem. Each workstation may contain only humans as operators, only robots, or humans

and robots simultaneously. Lalaoui and Afia [27] considered the MALBP-2 and used simulated annealing algorithm as a solution method. Sadeghi et al. [28] considered the MALBP-1. Variable neighbourhood descent and sequential positional weighting algorithms were used as solution methods. With one operator at each station, given the available time, it minimises the number of workstations while smoothing the workload of the operators. Naderi et al. [29] developed a mathematical model to minimise the number of operators to work for a given cycle time and number of stations and used a linear relaxation method. An efficient logic-based Benders decomposition algorithm is also developed. Kucukkoc et al. [30] considered the underground workstations in mixed-model two-sided lines and proposed a mathematical model as well as an ant colony optimization algorithm for solving the problem. Tanhaie et al. [31] addressed the MALBP-1. The developed mathematical model aims at both minimising the number of stations and minimising the total cost of task repetition and operator assignment to perform assembly tasks. Anh and Van Hop [32] studied the mixed model assembly line balancing problem of type-1, task processing time is defined and modelled as fuzzy stochastic processing times considering the natural uncertainties occurring in production. Schibelbain et al. [33] addressed a robotic assembly line problem under practical constraints, focusing on the challenges of mixed-model manufacturing. Two main issues are highlighted, namely the computational costs increasing with the problem size and the difficulties in developing a practical performance model using mathematical programming. Sikora [34] proposed an exact method and heuristic algorithm for mixed-model assembly lines, taking into account the random production sequence. Branch-and-bound algorithm using Markov chains is proposed to optimize the assignment of tasks, the length of the stations. Zhang et al. [35] addressed MALBP with a focus on human and robot co-operation in the context of Industry 5.0, together with the challenges arising from uncertainties and dynamic market demands.

Overall, this review of the literature shows that the MALBP covers a wide range of research, and various solution strategies have been used.

2.2. Literature review on type-E ALB problem

Studies on type-E assembly line balancing in the literature are rather limited. Recently, El Machouti et al. [36] reviewed the literature of simple assembly line balancing problems of type-E. Going back to the earlier studies, Plans and Corominas [37] developed MILP and heuristics for type-E ALB problem to improve efficiency. Then Wei and Chao [38] developed a new exact solution method to solve the type-E ALB problem based on solving several SALBP-2 formulations. Zacharia and Nearchou [39] proposed a direct solution method based on triangular fuzzy numbers without solving several type-1 or type-2 ALB problems [40]. Esmaeilbeigi et al. [40] developed a mixed-integer linear programming model to minimise cycle time, number of stations and smoothness index. Jusop and Rashid [41] solved the type-E ALB problem using genetic algorithm and also considered resource constrained scenarios. Khalid et al. [42] proposed a method to improve line efficiency with artificial immune systems. These studies addressed various aspects of the type-E ALB problems and presented different solution methods.

Manavizadeh et al. [43] conducted one of the preliminary works on type-E MALBP (i.e. MALBP-E), minimising both cycle time and the number of workstations as well as other objectives. A multi-objective genetic algorithm was proposed for this aim. Su et al. [44] proposed a combination of Petri net and binary search using a two-stage heuristic algorithm to solve the MALBP-E. Legesse et al. [45] presented metaheuristics to minimise cycle time and number of stations in stochastic environments.

Rebalancing studies usually focussed on cost minimisation and can be performed for straight line, parallel line, U-shaped and two-sided lines [46]. Çimen et al. [47] reviewed the related studies in the literature for assembly line rebalancing problems. According to Çimen et al. [47], the objective function of most of the studies for assembly line rebalancing problems are maximising the workload balance, minimising the rebalancing costs, and minimising task relocation. Also, a small proportion of the existing studies address to mixed-model assembly line rebalancing. Agpak [48] aimed to minimise cycle time fluctuations caused by rebalancing. Yang et al. [49] aimed to reduce the number of stations and minimised the total processing time for reassigned tasks with a cost function in mixed-model lines. Serin et al. [50] minimised the workload change and rebalancing cost. Oliveira et al. [51] developed mathematical and heuristic models for minimising the number of stations and average workload in an environment of arbitrarily mixed-models of products. Makssoud [52] developed a model to minimise changes and costs in an existing assembly line.

As seen in the survey given above, there are quite limited number of studies in the literature studying the type-E mixed-model assembly line rebalancing problem. This study contributes to literature addressing a mixed-model assembly line rebalancing problem allowing multi-manned operators under task relocation constraints. Different from the literature, the number of task relocations is not minimised but restricted to a certain number which can be decided by the line manager. In this way, companies will be able to easily adapt the newly balanced task allocation with minimal change requirements for operators and/or equipment. Moreover, managers will have the flexibility to determine the magnitude of the change based on the infrastructure they have. Hence, the mathematical model to be presented in the following section provides the decision maker with the advantage of maximising the

line efficiency by adding the maximum task relocation limit (B), which can be made in the existing assembly line considering the multi-operator conditions in mixed-model lines.

3. Problem description and mathematical model

More than one product model ($m \in M$) is assembled on a mixed-model assembly line in an intermixed way. Each task is re-assigned to exactly one workstation ($k \in K$) considering the precedence relationship constraints caused by technological requirements. S represents the set of precedence relationships, where $(r, s) \in S$ if task r immediately precedes task s in the precedence relationships diagram. The precedence relations by different models are constituted to a common diagram to ensure that common tasks between models are assigned to the same workstation. Each task ($i \in I$) needs a deterministic processing time (t_{im}) and the sum of the processing times of tasks assigned to a workstation cannot exceed the cycle time (C) on a model basis.

The existing task allocation of the line (called 'current state') is also considered during line balancing (rebalancing) and the total number of task relocations is restricted up to a certain value. M_{ik} shows the current allocation of tasks to workstations in the current state. If task i was assigned to workstation k, M_{ik} gets the value 1; otherwise it gets 0. If task i is assigned to a different workstation than the current state, this is considered as a 'relocation' and is expressed by the decision variable f_i. Thus, if the workstation to which task i is assigned has changed, f_i gets the value 1; otherwise, it gets the value 0. The developed model rebalances the line in compliance with the maximum number of relocations allowed, represented by B. To reflect the real-world conditions, more than one operator can be assigned to a workstation. OP denotes the total number of operators allowed while RP denotes the maximum number of operators that can be assigned to a workstation.

The notation used in the developed model is given in Table 1.

Table 1. Notation used in the mathematical model.

Sets	
Stations	$k \in K$
Tasks	$i, r, s \in I$
Models	$m \in M$
Parameters	
Maximum number of stations	K_{max}
Minimum cycle time	C_{min}
Maximum cycle time	C_{max}
Processing time of task i for model m	t_{im}
Set of precedence relationships	S
A precedence relationship; task r immediately precedes task s	$(r, s) \in S$
The maximum number of relocations allowed	B
If task i is assigned to station k in the current state, 1; otherwise, 0	M_{ik}
Decision Variables	
Cycle time	C
If task i is assigned to station k, 1; otherwise, 0	x_{ik}
The number of operators assigned to workstation k	z_k
If the station where task i is assigned has changed, 1; otherwise, 0	f_i

The MINLP model developed for the mixed-model type-E assembly line rebalancing problem (built over the work by [53]) is as follows [54]:

Objective function:

$$Minimise \ C \sum_{k=1}^{K_{max}} z_k \tag{1}$$

Subject to:

$$\sum_{k=1}^{K_{max}} x_{ik} = 1 \quad \forall i \tag{2}$$

$$\sum_{i=1}^{N} t_{im} x_{ik} \leq C z_k \quad \forall m, k \tag{3}$$

$$\sum_{k=1}^{K_{max}} k(x_{rk} - x_{sk}) \leq 0 \quad \forall (r,s) \in S \tag{4}$$

$$C \geq C_{min} \tag{5}$$

$$C \leq C_{max} \tag{6}$$

$$z_k \leq RP \quad \forall k \tag{7}$$

$$\sum_{k=1}^{K_{max}} z_k \leq OP \tag{8}$$

$$\sum_{i=1}^{N} f_i \leq B \tag{9}$$

$$x_{ik} - M_{ik} \leq f_i \quad \forall i,k \tag{10}$$

$$z_{k-1} \geq z_k \quad \forall k \mid k \neq 1 \tag{11}$$

$$x_{ik}, f_i \in \{0,1\} \quad \forall i,k \tag{12}$$

$$C, z_k \in \mathbb{Z}^+ \tag{13}$$

The objective (given in Eq. (1)) is to allocate tasks to workstations for maximising the line efficiency (type-E ALB), which equivalents to minimising the multiplication of the cycle time and the number of workstations considering that the total task time ($\sum_i \sum_m t_{im}$) is constant. Since tasks cannot be split, Constraint (2) guarantees that each task is assigned to exactly one workstation. Constraint (3) ensures that the total processing time of the tasks assigned to each workstation for each model cannot exceed the cycle time. For this, it is important whether the workstation is open or not, because tasks are only assigned to open workstations. Constraint (4) ensures that priority relationship constraints are not violated. If task r is an immediate predecessor of task s, then task s cannot be assigned to an earlier workstation than task r. Constraints (5) and (6) ensure that the cycle time gets a value within the minimum and maximum values allowed. Constraint (7) restricts that the number of operators assigned to a station should not exceed RP, given as a parameter. Constraint (8) ensures that the total number of operators assigned to workstations across the line does not exceed the total number of operators available in terms of operational resources. The total number of changes in the task assignments during rebalancing cannot the maximum number of relocations allowed, this is expressed by Constraint (9). Constraint (10) is to check whether each task is assigned to the same station both in the current state and rebalanced solution. If a task is assigned to a different workstation rather than the one to which it was currently assigned, it means a change. Constraint (11) ensures that workstations are utilised sequentially starting from 1. Constraints (12) and (13) define the sign constraints regarding the decision variables.

3.1. rMILP

Due to the nonlinearity (owing to the multiplication of endogenous variables in the objective function) and complexity of the proposed model, an optimal solution cannot be obtained in a reasonable time for large size problems. Only small size problems can be solved with the MINLP model. Therefore, an iterative algorithm is integrated into the MINLP model in order to solve large size problems. This approach is commonly referred to as ε-constraint method in the literature (see [55], [56] and [57]). The notation, sets, parameters and decision variables used for the rMILP model are generally the same as those used for the MINLP model. The major difference is that the cycle time is not defined as a decision variable in the rMILP model. Defining the cycle time as a parameter rather than a decision variable transforms the model into a type-I assembly line balancing problem. The mathematical model is run iteratively for each value of C between C_{min} and C_{max}. This also linearises the objective function of the model. The flow chart of the utilised algorithm is shown in Figure 1.

Variables used during the procedure are C_{best} which is best cycle time value found, K_{best} which is best number of stations found, $Model_{best}$ which is the best objective function value found. Firstly, C_{min} and C_{max} are determined for the given problem. C_{min} is determined in such a way that it is not lower than the processing times of the tasks. C_{max} is taken within a certain range in order not to reduce the production speed significantly. The maximum number of relocations that can be made to the existing assembly line is also determined based on the characteristics of the problem and the resources available. The current state M_{ik} is also gathered based on the existing line configuration of the line to be rebalanced. After initialising all parameters and variables, the developed model is solved by setting the cycle time to C_{min}. It is checked whether the line efficiency of the obtained solution is better than the line efficiency of the current best. If a better solution is found, the algorithm continues with the obtained

solution by increasing the cycle time by C_{step}. This loop continues until the cycle time reaches the maximum cycle time limit, C_{max}, and the algorithm terminates reporting the best solution with the highest line efficiency.

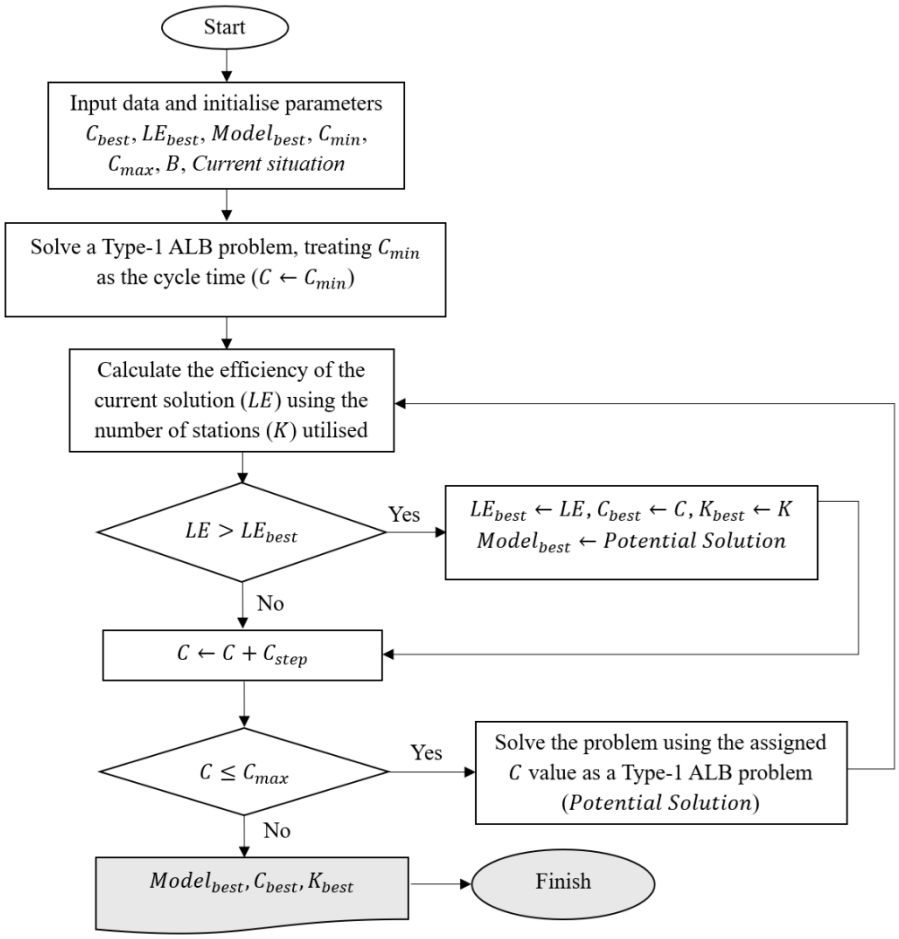
Start
Input data and initialise parameters $C_{best}, LE_{best}, Model_{best}, C_{min}, C_{max}, B$, Current situation
Solve a Type-1 ALB problem, treating C_{min} as the cycle time ($C \leftarrow C_{min}$)
Calculate the efficiency of the current solution (LE) using the number of stations (K) utilised
$LE > LE_{best}$
Yes
$LE_{best} \leftarrow LE, C_{best} \leftarrow C, K_{best} \leftarrow K$
$Model_{best} \leftarrow$ Potential Solution
No
$C \leftarrow C + C_{step}$
$C \leq C_{max}$
Yes
Solve the problem using the assigned C value as a Type-1 ALB problem (Potential Solution)
No
$Model_{best}, C_{best}, K_{best}$
Finish

Figure 1. Flow chart of the rMILP [58].

3.2. Numerical example

A numerical example, obtained from the P19 Thomopoulos, composed of 19 tasks and three different models [63] will be solved using the proposed models. The problem was solved using rMILP. The parameters (C_{min}, C_{max}, K_{max}, and OP) used for the problem are assumed to be 1.5, 3.0, 5 and 5, respectively. The model was tested for different B values by starting from 0, i.e. the current state for verification, and increasing by $C_{step} = 1$ up to the number of tasks (considering an extreme case that all tasks may be assigned to a different workstation). Thus, the algorithm was run through 19 iterations (except verification phase) in total and outputs were obtained. The optimum solution was found within 0.029 seconds for $RP = 1$ and 0.019 seconds for $RP = 2$.

Figure 2 shows the number of workstations cycle time and line efficiency for each B value. When reporting the B values, as mentioned before, only the B values that create a break (causing an increase in the line efficiency) are reported for the length constraints.

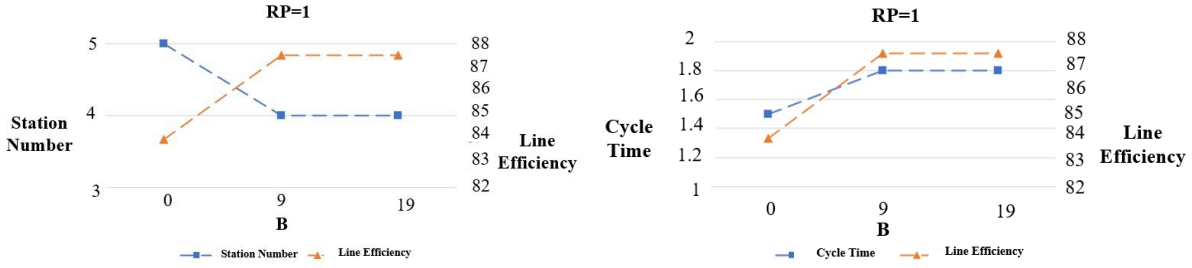

Figure 2. Change in the number of stations, cycle time and line efficiency across different B values when RP=1.

When Figure 2 is analysed, it is seen that the number of workstations is 5, the cycle time is 1.5 time-units and the line efficiency value is 84% for $B = 0$ (current state). Line efficiency increases as the B value increases indicating that a more effective line balancing solution is obtained as more changes are allowed. For example, when $B = 9$ (allowing up to nine task assignment relocations), the optimum solution requires four workstations with a cycle time value of 1.8 time-units, achieving a line efficiency of 87.50%. This indicates that a balancing solution with a line efficiency of as high as 87.5% can be achieved with changing the assignments of nine tasks. The line efficiency does not improve more even it is allowed to change the assignments of all tasks (see the situation of $B = 19$). These results show the effect of the proposed approach. Figure 3 shows the current situation, and the best solution obtained by rMILP when $RP = 1$.

(a)

Workstation No	WS1	WS2	WS3	WS4	WS5
Task Assignments	2,3,4,5	15	3,7,11,13,17	6,9,10,12,14,18	15,16,19
Workload Model 1	1.0	0.5	1.29	1.2	1.1
Workload Model 2	1.0	0.5	1.5	1.3	1.4
Workload Model 3	1.4	1.5	1.4	1.4	1.5

(b)

Workstation No	WS1	WS2	WS3	WS4
Task Assignments	2,3,4,5	1,8,11,16	7,9,10,12, 13,14,17	6,15,18,19
Workload Model 1	1.0	0.8	1.7	1.6
Workload Model 2	1.2	0.9	1.8	1.8
Workload Model 3	1.8	1.8	1.8	1.8

Figure 3. (a) Current situation and (b) the best solution obtained by rMILP when RP=1.

In the second scenario, it is allowed that two operators can be assigned to a workstation ($RP = 2$) for the same test problem. Figure 4 shows the change in the number of workstations, cycle time and line efficiency for each B value in the case of $RP = 2$. When calculating the line efficiency, the number of operators (OP) should be taken into account instead of the number of stations since some of the workstations might be allocated more than one operator. For example, if two operators are assigned to a workstation, the capacity of the station is doubled (see the column OP in Table 2).

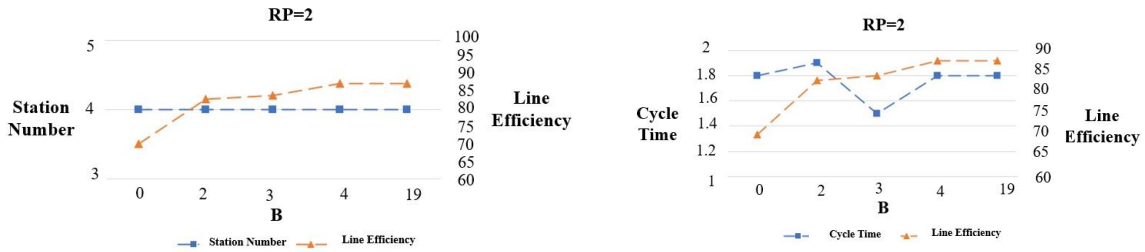

Figure 4. Combinations of cycle time and number of stations across varying B values when RP=2.

As seen in Figure 4, for $B = 0$, the number of workstations is four and the cycle time is 1.8 time-units corresponding the 70% of line efficiency. When the results are analysed, it is seen that the line efficiency improves with the increase in the B value. For example, when only two relocations are allowed (i.e. $B = 2$), line efficiency increases to 82.89% with $K = 4$ ($also\ OP = 4$) and $C = 1.9$. When $B = 4$, cycle time can be reduced to 1.8 time-units while keeping the number of workstations constant, which increases the line efficiency to 87.50%. Beyond this point, line efficiency does not improve even more relocations are allowed for the task assignments. Table 2 presents the best solutions across different B values. Decision makers can decide which solution to utilise based on their resources taking into account the extent of change they will be exposed to.

Table 2. Best results for P19 across different B values when RP=2

B	Cycle Time	OP	Number of Stations	OP*C	LE (%)
0	1.8	5	4	9	70.00
2	1.9	4	4	7.6	82.89
3	1.5	5	4	7.5	84.00
4	1.8	4	4	7.2	87.50*
19	1.8	4	4	7.2	87.50*

* *The overall best objective function value*

Figure 5 shows the current situation and the best solution obtained by rMILP when $RP = 2$.

(a)

Workstation No	WS1	WS2	WS3	WS4
Number of Operators	2	1	1	1
Task Assignments	1,2,3,4,5	9,11,13, 14,17,18	6,7,8,10, 12,16	15
Workload Model 1	1.5	1.8	0.7	1.1
Workload Model 2	1.2	1.8	1.4	1.3
Workload Model 3	2.8	1.1	1.8	1.5

(b)

Workstation No	WS1	WS2	WS3	WS4
Number of Operators	1	1	1	1
Task Assignments	2,3,4,5	1,9,10,11, 13,17	6,7,8,10, 12,14,16	15,18,19
Workload Model 1	1.0	1.8	0.9	1.4
Workload Model 2	1.2	1.1	1.6	1.8
Workload Model 3	1.8	1.8	1.8	1.8

Figure 5. (a) Current situation and (b) the best solution obtained by rMILP when RP=2.

These results indicate that the optimal solution could change in response to a change in the maximum number of relocations allowed practically. A higher B value could allow a better solution in terms of line efficiency. More importantly, the same line efficiency could be obtained with a lower number of changes in task relocations.

This section presented the problem definition, the mathematical model, the workflow diagram of the proposed approach, and a small illustrative example of the model. The results of the computational experiments will be provided in the next section.

4. Computational experiments

In this section, the comparison and performance analysis of the two proposed models, MINLP and rMILP, will be presented for large datasets. The public datasets of different sizes, different production models, and processing times were solved for this aim. The models were coded in Python 3.0 programming language and solved with Gurobi Optimizer. The personal computer used for the tests has Intel(R) Core (TM) i5-10300H CPU at 2.50GHz with 16 GB RAM.

MINLP and rMILP models were run using six different data sets [59]. The sizes of the datasets used are different from each other and therefore the precedence relationship diagrams, number of tasks and number of models are different from each other. This analysis proves how good the performance of rMILP is and shows that it differs from the MINLP model by finding the optimal result in a short time on large data sets. Table 3 shows the parameters used for all data sets when $RP = 1$. Minimum cycle time, maximum cycle time, maximum number of stations and step size (C_{step}) are given for each problem.

MINLP and rMILP models were run under 1800 seconds time limit for six different data sets using the parameters given in Table 3. The results of the tests are presented in Table 4. Table 4 shows the cycle time, number of stations and line efficiency values of rebalancing solutions for each data set when $RP = 1$. Eq. (14) calculates the relative percentage deviation, i.e. $RPD(\%)$, where the objective is to maximise the line efficiency.

$$RPD(\%) = \frac{LE_{rMILP} - LE_{MINLP}}{LE_{MINLP}} \times 100 \tag{14}$$

Table 3. Parameters used for datasets

Datasets/ Parameters	C_{min}	C_{max}	K_{max}	C_{step}
P-70 Tongue	156	234	18	5
P-83 Arcus	3691	5537	14	111
P-89 Lutz-2	20	35	17	-
P-94 Mukherje	171	257	20	6
P-111 Arcus	6615	9923	16	198
P-148 Bartholdi-1	383	575	12	-

Table 4. Test results for MINLP and rMILP when $RP = 1$.

Dataset	MINLP					rMILP					
	C	K	OP	LE (%)	Time (sec)	C	K	OP	LE (%)	Time (sec)	RPD (%)
P-70 Tongue	220	16	16	98.83	1200	176	20	20	98.83	202.00	0.00
P-83 Arcus	5467	14	14	98.51	1800	5451	14	14	98.80	269.39	0.29
P-89 Lutz-3	35	14	14	98.46	65.52	35	14	14	98.46	58.67	0.00
P-94 Mukherje	214	20	20	98.21	1800	213	20	20	98.67	694.27	0.46
P-111 Arcus	9424	16	16	96.59	1800	8397	18	18	96.36	914.00	-0.23
P-148 Bartholdi-1	470	12	12	99.57	406.03	470	12	12	99.57	388.69	0.00

Table 4 shows the line efficiencies of the rMILP and MINLP models for each data set. MINLP finds the optimal solutions for three test cases. For P-111 Arcus, rMILP finds a worse solution with a -0.23% RPD. This might be caused by the value of C_{step}, as the optimal C value might be missed. Minimising the C_{step} to a minimal unit might help finding better solutions if one ignores the increased solution time. For the three test problems (i.e. P-70 Tongue, P-89 Lutz-3, and P-148 Bartholdi-1), both models give the same result under 1800 seconds time limit. However, for P-70 Tongue, the rMILP model obtains the optimal result in as short as 202 seconds, while the MINLP model requires 1200 seconds to find the optimal solution. For the remaining two problems (P-83 Arcus and P-94 Mukherje) rMILP shows better performance than the MINLP with an average RPD of 0.375%.

Overall, the results show that for all large datasets, the rMILP algorithm maximizes line efficiency by obtaining good solutions in less time than the MINLP algorithm. The MINLP algorithm was run even for 60 minutes when it produced feasible solutions, but no further improvement was observed, suggesting that its performance does not improve after a certain point. These findings demonstrate that the rMILP algorithm offers companies a clear advantage in terms of both computational efficiency and solution quality. For the datasets examined, the rMILP algorithm consistently guarantees a line efficiency above 95% in a reasonably short computational time.

Table 5 and Table 6 show the parameters and results of the MINLP and rMILP algorithms for $RP = 2$. Each data set was rerun so that two operators could be assigned to the station. The MINLP and rMILP algorithms were run for 1800 seconds and the results are reported.

Table 5. Parameters used for datasets $RP = 2$

Datasets/ Parameters	C_{min}	C_{max}	K_{max}
P-70 Tongue	156	234	21
P-83 Arcus	3691	5537	20
P-89 Lutz-2	20	35	18
P-94 Mukherje	171	257	24
P-111 Arcus	6615	9923	21
P-148 Bartholdi-1	383	575	12

Table 6. Comparison of MINLP and rMILP for $RP = 2$

Dataset	MINLP					rMILP					
	C	K	OP	LE (%)	Time (s)	C	K	OP	LE (%)	Time (s)	RPD (%)
P-70 Tongue	167	11	21	99.20	1800	206	9	17	99.34	59.55	0.14
P-83 Arcus	5414.5	8	14	99.46	1800	3802	10	20	99.15	220.13	-0.31
P-89 Lutz-3	27	9	18	99.27	1800	27	9	18	99.27	66.04	0.00
P-94 Mukherje	176	13	24	99.51	1800	176	13	24	99.51	199.17	0.00
P-111 Arcus	7145	15	21	97.07	1800	9373	9	17	97.44	892.39	0.38
P-148 Bartholdi-1	470	6	12	99.57	1800	470	6	12	99.57	514.95	0.00

Though the comparison of the results presented in Table 6 with those in Table 4 reveals similarity, the line efficiencies of rMILP and MINLP algorithms are higher when $RP = 2$ compared to the case when $RP = 1$. This is a result of expanded solution space due to the increase in the number of operators that can be assigned to a workstation. An analysis of the line efficiency values presented in Table 6 reveals that the rMILP algorithm consistently yields results that are either equivalent to or superior to those of the MINLP algorithm except one case, i.e. P-83 Arcus. Although the line efficiency found by the rMILP algorithm is 0.3% less than that by the MINLP algorithm for P-83 Arcus, the solution speed of rMILP is 87.77% better. In this instance, once more, the discrepancy in the line efficiencies appears to be tolerable, given the substantial enhancement in the time required to ascertain the solution. For the two test cases, i.e. P-70 Tongue and P-111 Arcus, rMILP obtains better solutions than MINLP within considerably shorter times. Consequently, as the problem becomes more complex, the advantages of the proposed algorithm become more apparent. Another advantage of the proposed rMILP algorithm

is the capacity to furnish planners with greater flexibility by offering solutions that encompass a variety of cycle time and station number combinations. These advantages can also be extended with the ease of implementation and maintenance as compared to other methods especially metaheuristics.

5. Discussion and conclusions

This study deals with the mixed-model type-E assembly line rebalancing problem while restricting the total number of task assignment relocations to a certain value. By this restriction, decision makers are capable of utilising a desired line balancing solution based on their choice of task relocation limitations. For this purpose, a mixed integer nonlinear programming model is first developed. Due to the complex structure of the problem, the mathematical model developed cannot obtain a good solution in large data sets in a reasonable time. Therefore, an iterative heuristic algorithm (rMILP) is integrated into the developed model. With the proposed algorithm, the objective function of the type-E problem is linearised by giving minimum and maximum bounds to the cycle time. The developed model is run iteratively for values in the range of minimum and maximum cycle times, providing flexibility to the decision maker. Starting from the given minimum cycle time, the model is run iteratively until it reaches the maximum cycle time. At the same time, in this study, the use of multi-operator stations is also included in the problem of assigning tasks to stations. The proposed approach has been tested with large data sets of different task numbers and it effectively provided competitive solutions in a reasonable time. Therefore, this study provides decision makers with advantages such as the ability to respond quickly and flexibly to evolving markets and special demands, efficient use of assembly lines, thereby increasing customer satisfaction.

The main limitation of the proposed algorithm might be determining the value of step size especially when the difference between C_{min} and C_{max} is large. Since running the algorithm for every possible cycle time value requires excessive computational times, step size could be increased. However, increasing the step size may cause missing the cycle time that might give the optimal line efficiency, as not all values between C_{min} and C_{max} will be checked.

In future work, our model can be extended for various line layouts, including U-shaped, two-sided, parallel and robotic lines. The model can also be tested with real-world datasets by considering more complex scenarios involving hundreds of jobs. In order to make the use of our algorithm more effective and efficient on different datasets, machine learning algorithms can be integrated to learn which step size, C_{step}, might give better results for the specific dataset, taking into account the size of the dataset and the cycle times. The algorithm can be improved by adding different constraints such as zoning constraints and comparisons can be made. At the same time, meta-heuristics can also be incorporated to solve larger-scale problems.

Acknowledgments

None.

Funding

None.

Conflict of interest

There is no conflict of interest to disclose.

Author contributions

Damla Camli: Conceptualization, Methodology, Software, Investigation, Validation, Writing - original draft, Writing - review & editing. **Ibrahim Kucukkoc:** Conceptualization, Methodology, Investigation, Supervision, Writing - original draft, Writing - review & editing. **Zixiang Li:** Conceptualization, Methodology, Supervision, Writing - original draft, Writing - review & editing.

Declaration of using AI tools

The authors declare that they have not used any type of generative artificial intelligence for the writing of this manuscript, nor for the creation of images, graphics, tables, or their corresponding captions.

References

[1] I. Baybars, "A Survey of Exact Algorithms for the Simple Assembly Line Balancing Problem," (in English), *Management Science,* vol. 32, no. 8, pp. 909-932, 1986.

[2] I. Kucukkoc and D. Z. Zhang, "Mathematical Model and Agent Based Solution Approach for the Simultaneous Balancing and Sequencing of Mixed-Model Parallel Two-Sided Assembly Lines," *International Journal of Production Economics,* vol. 158, pp. 314-333, 2014, doi: http://dx.doi.org/10.1016/j.ijpe.2014.08.010.

[3] O. Battaïa and A. Dolgui, "A taxonomy of line balancing problems and their solution approaches," *International Journal of Production Economics,* vol. 142, no. 2, pp. 259-277, 2013.

[4] I. Kucukkoc and D. Z. Zhang, "Mixed-model parallel two-sided assembly line balancing problem: A flexible agent-based ant colony optimization approach," *Computers & Industrial Engineering,* vol. 97, pp. 58-72, 2016, doi: 10.1016/j.cie.2016.04.001.

[5] O. Yilmaz, N. Aydin, and I. Kucukkoc, "Minimization of Manufacturing Cost in Mixed-model Robotic Assembly Lines," in *The Third International Conference on Applied Mathematics in Engineering (ICAMΣ'24)*, Ayvalik, Balikesir, Turkiye, 2024, p. 141.

[6] N. Boysen, P. Schulze, and A. Scholl, "Assembly line balancing: What happened in the last fifteen years?," *European Journal of Operational Research,* vol. 301, no. 3, pp. 797-814, 2022/09/16/ 2022, doi: https://doi.org/10.1016/j.ejor.2021.11.043.

[7] N. Boysen, M. Fliedner, and A. Scholl, "A classification of assembly line balancing problems," (in English), *European Journal of Operational Research,* vol. 183, no. 2, pp. 674-693, Dec 1 2007, doi: DOI 10.1016/j.ejor.2006.10.010.

[8] O. Battaïa and A. Dolgui, "Hybridizations in line balancing problems: A comprehensive review on new trends and formulations," *International Journal of Production Economics,* Article vol. 250, 2022, Art no. 108673, doi: 10.1016/j.ijpe.2022.108673.

[9] Z. Li, I. Kucukkoc, and Q. Tang, "A comparative study of exact methods for the simple assembly line balancing problem," *Soft Computing,* vol. 24, no. 15, pp. 11459-11475, 2020/08/01 2020, doi: 10.1007/s00500-019-04609-9.

[10] N. T. Thomopoulos, "Line Balancing-Sequencing for Mixed-Model Assembly," *Management Science,* vol. 14, no. 2, pp. B-59-B-75, 1967, doi: 10.1287/mnsc.14.2.B59.

[11] N. T. Thomopoulos, "Mixed Model Line Balancing with Smoothed Station Assignments," *Management Science,* vol. 16, no. 9, pp. 593-603, 1970/05/01 1970, doi: 10.1287/mnsc.16.9.593.

[12] H. Gokcen and E. Erel, "A goal programming approach to mixed-model assembly line balancing problem," *International Journal of Production Economics,* vol. 48, no. 2, pp. 177-185, 1997/01/24/ 1997, doi: https://doi.org/10.1016/S0925-5273(96)00069-2.

[13] S. Emde, N. Boysen, and A. Scholl, "Balancing mixed-model assembly lines: a computational evaluation of objectives to smoothen workload," (in English), *International Journal of Production Research,* vol. 48, no. 11, pp. 3173-3191, 2010, doi: Doi 10.1080/00207540902810577.

[14] L. Belkharroubi and K. Yahyaoui, "A Hybrid approach for the Mixed-Model Assembly Line Balancing problem Type-II," in *2021 11th IEEE International Conference on Intelligent Data Acquisition and Advanced Computing Systems: Technology and Applications (IDAACS)*, 22-25 Sept. 2021 2021, vol. 1, pp. 329-332, doi: 10.1109/IDAACS53288.2021.9661039.

[15] L. Belkharroubi and K. Yahyaoui, "Solving the mixed-model assembly line balancing problem type-I using a Hybrid Reactive GRASP," *Production & Manufacturing Research,* vol. 10, no. 1, pp. 108-131, 2022/12/31 2022, doi: 10.1080/21693277.2022.2065380.

[16] T. Mönch, A. Huchzermeier, and P. Bebersdorf, "Variable takt times in mixed-model assembly line balancing with random customisation," *International Journal of Production Research,* vol. 59, no. 15, pp. 4670-4689, 2021/08/03 2021, doi: 10.1080/00207543.2020.1769874.

[17] K. Meng, Q. Tang, L. Cheng, and Z. Zhang, "Mixed-model assembly line balancing problem considering preventive maintenance scenarios: MILP model and cooperative co-evolutionary algorithm," *Applied Soft Computing,* vol. 127, p. 109341, 2022/09/01/ 2022, doi: https://doi.org/10.1016/j.asoc.2022.109341.

[18] Z. Zhang, M. Chica, Q. Tang, Z. Li, and L. Zhang, "A multi-objective co-evolutionary algorithm for energy and cost-oriented mixed-model assembly line balancing with multi-skilled workers," *Expert Systems with Applications,* vol. 236, p. 121221, 2024/02/01/ 2024, doi: https://doi.org/10.1016/j.eswa.2023.121221.

[19] A. Nourmohammadi, A. H. C. Ng, M. Fathi, J. Vollebregt, and L. Hanson, "Multi-objective optimization of mixed-model assembly lines incorporating musculoskeletal risks assessment using digital human modeling," *CIRP Journal of Manufacturing Science and Technology,* vol. 47, pp. 71-85, 2023/12/01/ 2023, doi: https://doi.org/10.1016/j.cirpj.2023.09.002.

[20] Y. Li, D. Liu, and I. Kucukkoc, "Mixed-model assembly line balancing problem considering learning effect and uncertain demand," *Journal of Computational and Applied Mathematics,* vol. 422, p. 114823, 2023/04/01/ 2023, doi: https://doi.org/10.1016/j.cam.2022.114823.

[21] Y. Delice, E. K. Aydoğan, S. Himmetoğlu, and U. Özcan, "Integrated mixed-model assembly line balancing and parts feeding with supermarkets," *CIRP Journal of Manufacturing Science and Technology,* vol. 41, pp. 1-18, 2023/04/01/ 2023, doi: https://doi.org/10.1016/j.cirpj.2022.12.002.

[22] M. D. Mura and G. Dini, "Improving ergonomics in mixed-model assembly lines balancing noise exposure and energy expenditure," *CIRP Journal of Manufacturing Science and Technology,* vol. 40, pp. 44-52, 2023/02/01/ 2023, doi: https://doi.org/10.1016/j.cirpj.2022.11.005.

[23] Z. A. Çil, Z. Li, S. Mete, and E. Özceylan, "Mathematical model and bee algorithms for mixed-model assembly line balancing problem with physical human–robot collaboration," *Applied Soft Computing,* vol. 93, p. 106394, 2020/08/01/ 2020, doi: https://doi.org/10.1016/j.asoc.2020.106394.

[24] H. M. Alakaş and B. Toklu, "Problem Specific Variable Selection Rules for Constraint Programming: A Type II Mixed Model Assembly Line Balancing Problem Case," *Applied Artificial Intelligence,* vol. 34, no. 7, pp. 564-584, 2020/06/06 2020, doi: 10.1080/08839514.2020.1731782.

[25] L. Yuwei, C. Jian'e, Z. Feng, and Z. Shijing, "A Research of Multi-Constrained Two-sided Mixed-model Assembly Line Balancing Problem Based on Genetic Algorithm," in *2020 IEEE 7th International Conference on Industrial Engineering and Applications (ICIEA)*, 16-21 April 2020 2020, pp. 377-381, doi: 10.1109/ICIEA49774.2020.9102104.

[26] S. Yaphiar, C. Nugraha, and A. Ma'ruf, "Mixed Model Assembly Line Balancing for Human-Robot Shared Tasks," in *iMEC-APCOMS 2019*, Singapore, M. N. Osman Zahid, R. Abd. Aziz, A. R. Yusoff, N. Mat Yahya, F. Abdul Aziz, and M. Yazid Abu, Eds., 2020// 2020: Springer Singapore, pp. 245-252.

[27] M. Lalaoui and A. E. Afia, "A versatile generalized simulated annealing using type-2 fuzzy controller for the mixed-model assembly line balancing problem," *IFAC-PapersOnLine,* vol. 52, no. 13, pp. 2804-2809, 2019/01/01/ 2019, doi: https://doi.org/10.1016/j.ifacol.2019.11.633.

[28] P. Sadeghi, R. D. Rebelo, and J. S. Ferreira, "Balancing mixed-model assembly systems in the footwear industry with a variable neighbourhood descent method," *Computers & Industrial Engineering,* vol. 121, pp. 161-176, 2018/07/01/ 2018, doi: https://doi.org/10.1016/j.cie.2018.05.020.

[29] B. Naderi, A. Azab, and K. Borooshan, "A realistic multi-manned five-sided mixed-model assembly line balancing and scheduling problem with moving workers and limited workspace," *International Journal of Production Research,* vol. 57, no. 3, pp. 643-661, 2019/02/01 2019, doi: 10.1080/00207543.2018.1476786.

[30] I. Kucukkoc, Z. Li, A. D. Karaoglan, and D. Z. Zhang, "Balancing of mixed-model two-sided assembly lines with underground workstations: A mathematical model and ant colony optimization algorithm," *International Journal of Production Economics,* vol. 205, pp. 228-243, 2018/11/01/ 2018, doi: https://doi.org/10.1016/j.ijpe.2018.08.009.

[31] F. Tanhaie, M. Rabbani, and N. Manavizadeh, "Simultaneous balancing and worker assignment problem for mixed-model assembly lines in a make-to-order environment considering control points and assignment restrictions," *Journal of Modelling in Management,* vol. 15, no. 1, pp. 1-34, 2019/09/23/ 2019, doi: https://doi.org/10.1108/JM2-04-2018-0052.

[32] T. T. M. Anh and N. Van Hop, "Matheuristics for mixed-model assembly line balancing problem with fuzzy stochastic processing time," *Applied Soft Computing,* vol. 160, p. 111694, 2024/07/01/ 2024, doi: https://doi.org/10.1016/j.asoc.2024.111694.

[33] D. Schibelbain, T. C. Lopes, and L. Magatão, "A method to balancing robotic mixed-model assembly lines: Practical constraints, computational challenges, and performance estimation," *Computers & Industrial Engineering,* vol. 197, p. 110595, 2024/11/01/ 2024, doi: https://doi.org/10.1016/j.cie.2024.110595.

[34] C. G. S. Sikora, "Balancing mixed-model assembly lines for random sequences," *European Journal of Operational Research,* vol. 314, no. 2, pp. 597-611, 2024/04/16/ 2024, doi: https://doi.org/10.1016/j.ejor.2023.10.008.

[35] X. Zhang *et al.*, "Human-Robot Collaboration in Mixed-Flow Assembly Line Balancing under Uncertainty: An Efficient Discrete Bees Algorithm," *Journal of Industrial Information Integration,* vol. 41, p. 100676, 2024/09/01/ 2024, doi: https://doi.org/10.1016/j.jii.2024.100676.

[36] S. El Machouti, M. Hlyal, A. Babay, and J. E. Alami, "Optimisation of Simple Assembly Line Balancing Problem Type E: A Systematic Literature Review," *Management Systems in Production Engineering,* vol. 32, no. 2, pp. 162-173, 2024, doi: 10.2478/mspe-2024-0016.

[37] J. Plans and A. Corominas, "Modelling and solving the SALB-E problem," in *Proceedings of the 1999 IEEE International Symposium on Assembly and Task Planning (ISATP'99) (Cat. No.99TH8470)*, 24-24 July 1999 1999, pp. 356-360, doi: 10.1109/ISATP.1999.782984.

[38] N.-C. Wei and I. M. Chao, "A solution procedure for type E simple assembly line balancing problem," *Computers & Industrial Engineering,* vol. 61, no. 3, pp. 824-830, 2011/10/01/ 2011, doi: https://doi.org/10.1016/j.cie.2011.05.015.

[39] P. T. Zacharia and A. C. Nearchou, "A meta-heuristic algorithm for the fuzzy assembly line balancing type-E problem," *Computers & Operations Research,* vol. 40, no. 12, pp. 3033-3044, 2013/12/01/ 2013, doi: https://doi.org/10.1016/j.cor.2013.07.012.

[40] R. Esmaeilbeigi, B. Naderi, and P. Charkhgard, "The type E simple assembly line balancing problem: A mixed integer linear programming formulation," *Computers & Operations Research,* vol. 64, pp. 168-177, 2015/12/01/ 2015, doi: https://doi.org/10.1016/j.cor.2015.05.017.

[41] M. Jusop and M. F. F. Ab Rashid, "Optimisation of Assembly Line Balancing Type-E with Resource Constraints Using NSGA-II," *Key Engineering Materials,* vol. 701, pp. 195-199, 2016, doi: 10.4028/www.scientific.net/KEM.701.195.

[42] M. N. A. Khalid, U. K. Yusof, and H. Iida, "An Artificial Immune System Approach for Solving Type-E Assembly Line Balancing Problem with Problem-Specific Information," in *2020 IEEE 16th International Conference on Control & Automation (ICCA)*, 9-11 Oct. 2020 2020, pp. 1590-1595, doi: 10.1109/ICCA51439.2020.9264382.

[43] N. Manavizadeh, M. Rabbani, D. Moshtaghi, and F. Jolai, "Mixed-model assembly line balancing in the make-to-order and stochastic environment using multi-objective evolutionary algorithms," (in English), *Expert Systems with Applications,* vol. 39, no. 15, pp. 12026-12031, Nov 1 2012, doi: DOI 10.1016/j.eswa.2012.03.044.

[44] P. Su, N. Wu, and Z. Yu, "A Petri net-based heuristic for mixed-model assembly line balancing problem of Type-E," *International Journal of Production Research,* vol. 52, no. 5, pp. 1542-1556, 2014/03/04 2014, doi: 10.1080/00207543.2013.849010.

[45] A. Legesse, E. Tesfaye, and E. Berhan, "Multi-objective optimization of mixed model assembly line balancing in an assemble-to-order industry with stochastic environment," *International Journal of Engineering, Science and Technology,* vol. 12, no. 3, pp. 90-107, 2020.

[46] G. Fan, H. Zheng, Z. Jiang, J. Liu, and S. Lou, "Multi-objective assembly line rebalancing problem based on complexity measurement in green manufacturing," *Engineering Applications of Artificial Intelligence,* vol. 132, p. 107884, 2024/06/01/ 2024, doi: https://doi.org/10.1016/j.engappai.2024.107884.

[47] T. Çimen, A. Baykasoğlu, and S. Demirkol Akyol, "A detailed review and analysis of assembly line rebalancing problems," *Assembly Automation,* vol. 42, no. 6, pp. 742-760, 2022.

[48] K. Ağpak, "An approach to find task sequence for re-balancing of assembly lines," *Assembly Automation,* vol. 30, no. 4, pp. 378-387, 2010, doi: 10.1108/01445151011075834.

[49] C. Yang, J. Gao, and L. Sun, "A multi-objective genetic algorithm for mixed-model assembly line rebalancing," *Computers & Industrial Engineering,* vol. 65, no. 1, pp. 109-116, 2013/05/01/ 2013, doi: https://doi.org/10.1016/j.cie.2011.11.033.

[50] F. Serin, S. Mete, and E. Çelik, "An efficient algorithm for U-type assembly line re-balancing problem with stochastic task times," *Assembly Automation,* vol. 39, no. 4, pp. 581-595, 2019, doi: 10.1108/AA-07-2018-106.

[51] F. S. Oliveira, K. Vittori, R. M. O. Russel, and X. L. Travassos, "Mixed assembly line rebalancing: A binary integer approach applied to real world problems in the automotive industry," *International Journal of Automotive Technology,* vol. 13, no. 6, pp. 933-940, 2012/10/01 2012, doi: 10.1007/s12239-012-0094-4.

[52] F. Makssoud, D. Y. C. D. Maurizio Faccio, O. Battaïa, A. Dolgui, K. Mpofu, and O. Olabanji, "Re-balancing problem for assembly lines: new mathematical model and exact solution method," (in english), *Emerald,* 2015 2015.

[53] I. Kucukkoc and D. Z. Zhang, "*Type-E Parallel Two-Sided Assembly Line Balancing Problem: Mathematical Model and Ant Colony Optimisation based Approach with Optimised Parameters*," *Computers & Industrial Engineering,* vol. DOI: 10.1016/j.cie.2014.12.037, 2015, doi: 10.1016/j.cie.2014.12.037.
[54] D. Camli and I. Kucukkoc, "Rebalancing of multi-manned assembly lines with model variability," in *The Third International Conference on Applied Mathematics in Engineering (ICAMΣ'24)*, Ayvalik, Balikesir, Turkiye, 2024, p. 125.
[55] Y. Haimes, "On a bicriterion formulation of the problems of integrated system identification and system optimization," *IEEE transactions on systems, man, and cybernetics,* no. 3, pp. 296-297, 1971.
[56] I. Kucukkoc, S. Finco, M. Peron, and G. Aydin Keskin, "Including mechanical requirements in a bi-objective nesting and scheduling model for additive manufacturing," *European Journal of Operational Research,* vol. 325, no. 3, pp. 416-432, 2025/09/16/ 2025, doi: https://doi.org/10.1016/j.ejor.2025.03.022.
[57] O. Yilmaz, N. Aydin, and I. Kucukkoc, "Bi-objective optimization of human-robot collaborative mixed-model multiple assembly lines considering model assignment and energy consumption," *Journal of Computational and Applied Mathematics,* vol. 473, p. 116876, 2026/02/01/ 2026, doi: https://doi.org/10.1016/j.cam.2025.116876.
[58] D. Çamlı, "Karışık modelli montaj hatlarında hat etkinliğinin maksimizasyonu ve bir uygulama," MSc Thesis, Balikesir University (Turkey), 2024.
[59] N. Boysen, M. Fliedner, R. Klein, and A. Scholl. "Assembly Line Balancing Problem Benchmark Data Sets." http://assembly-line-balancing.de/ (accessed 16 Dec 2023).

All open access articles published in Transactions on Computational Modeling and Intelligent Systems (http://tcmis.org) are distributed under the terms of the CC BY-NC 4.0 license (Creative Commons Attribution Non-Commercial 4.0 International Public License as currently displayed at http://creativecommons.org/licenses/by-nc/4.0/legalcode) which permits unrestricted use, distribution, and reproduction in any medium, for non-commercial purposes, provided the original work is properly cited.

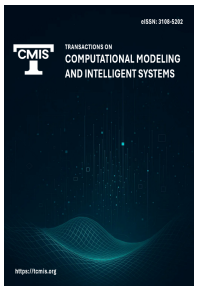

Transactions on
Computational Modeling
and Intelligent Systems

Volume 1, October 2025, Article 10011
https://doi.org/10.65112/tcmis.10011

eISSN: 3108-5202
www.tcmis.org

RESEARCH ARTICLE

Theoretical advances in two-step iterative schemes for nonlinear problems

Mudassir Shams[1,2*]

[1] *Department of Mathematics, Faculty of Arts and Science, Balikesir University, Balikesir 10145, Türkiye.*
[2] *Faculty of Engineering, Free University of Bozen-Bolzano, 39100, Bolzano, Italy.*
[*] *Corresponding Author. Email: mudassir.shams@balikesir.edu.tr (M. Shams)*

Article Information

Received: 26 August 2025
Accepted: 5 October 2025
Published: 14 October 2025

AMS Classification:
65H04, 65H05, 65H10, 65H17, 65H20

Abstract

This study develops a two-step iterative method for solving nonlinear equations, focusing on its convergence properties. Using Taylor series expansion, the method assumes the nonlinear function is at least four times continuously differentiable with bounded derivatives, though this can be restrictive for unbounded higher-order derivatives. To overcome this, a convergence radius is introduced, allowing initial approximations without exact root knowledge. This expands the convergence region without extra smoothness assumptions. Ball convergence analysis establishes error bounds and uniqueness, while local convergence analysis ensures stability and robustness near the root. By combining these perspectives, the framework enhances the theoretical foundation and extends applicability to complex nonlinear problems.

Keywords: Local convergence, Taylor series, computational time, nonlinear problems.

1. Introduction

The problem of determining the solution of non-linear equations is of fundamental importance across various branches of science and engineering. In this work, we focus on approximating the unique solution ¢ to the non-linear equation

$$g(t) = 0, \tag{1}$$

where g is a differentiable function defined on a convex subset $T \subset \Theta$ with $\Theta = \mathbb{R}$ or $\mathbb{C}$. Non-linear equations of this nature frequently arise in a variety of applications [1–3]. Because these equations can be difficult to solve exactly, we usually use an iterative method to find approximate solutions. Among these methods, Newton's method is one of the most basic and widely used.

To analyze the convergence behavior of the proposed two-step method, we utilize Taylor series expansion under the assumption that the nonlinear function g is at least four times continuously differentiable. Additionally, it is assumed that g and its derivatives up to the fourth order remain bounded on the domain Θ. These assumptions ensure that the theoretical foundation of the method is mathematically rigorous and allow us to derive accurate estimates for the order of convergence. To address the existing research gap, we note that classical iterative schemes for

solving nonlinear problems often face limitations such as slow convergence, difficulty in handling multiple roots, and restricted regions of convergence. In contrast, the proposed two-step iterative scheme offers significant theoretical advances by explicitly estimating and enlarging the radius of convergence, ensuring faster and more reliable convergence. The key limitations of existing approaches and how our method overcomes them can be summarized as follows:

- **Limited convergence region:** Classical methods converge only locally. *Our method provides an analytically estimated, enlarged radius of convergence.*
- **High computational cost:** Existing methods often require excessive function evaluations. *Our two-step approach reduces iterations and function evaluations while preserving accuracy.*
- **Lack of theoretical guarantees:** Many methods lack rigorous convergence proofs. *We establish formal convergence theorems and provide illustrative examples.*

These improvements demonstrate the effectiveness of the proposed scheme in addressing critical challenges in nonlinear root-finding problems. By imposing these smoothness and boundedness conditions, we are able to demonstrate that the proposed scheme attains faster convergence compared to classical approaches. At the same time, these requirements introduce inherent limitations, since they restrict the class of nonlinear functions to which the method can be directly applied. If the target function exhibits irregularities, discontinuities, or unbounded higher-order derivatives, the convergence rate may deteriorate significantly. In fact, such cases could even lead to divergence, making the method less reliable in highly nonlinear or ill-conditioned scenarios. Another drawback is that verifying boundedness conditions for practical engineering and biomedical problems is often non-trivial. Therefore, while the theoretical results provide valuable insights into the method's performance, caution must be exercised when applying the scheme to real-world systems. The main limitations of these assumptions and their implications for general applicability are explained in detail below:

(1) Consider the real-valued function $g : \Theta \subseteq \mathbb{R} \to \mathbb{R}$ defined on $\Theta = [-0.5, 1.5]$ as which is defined by,

$$g(t) = \begin{cases} t^5 - t^4 + t^3 ln(t^2) & \text{if } x \neq 0 \\ 0 & \text{if } x = 0 \end{cases}$$

It is evident that g''' is unbounded on Θ, and hence the hypothesis required for convergence analysis is violated. However, g' and g'' remian bounded on Θ, as

$$\lim_{t \to\ 0} t^2 ln(t^2) = \lim_{t \to\ 0} t ln(t^2) = 0.$$

Despite g being continuous, its third derivative is not bounded, which makes it difficult to directly estimate the order of convergence for the proposed method. To overcome this issue, Sections 3 and 4 introduce techniques that avoid relying on higher-order derivatives.

(2) The number of iterations required to achieve a specified accuracy cannot be predetermined.

(3) The radius of convergence is a critical issue in multi-point iterative methods, but it is often not given enough attention.

(4) Most existing methods in the literature do not specify how close the initial approximation must be to the actual root of ¢ in order to achieve the desired order of convergence.

A key tool in this area is local convergence analysis [4–8], which evaluates how an iterative method behaves when the initial guess is close to the actual root. This type of analysis offers valuable insights into two critical aspects: the radius of convergence, which defines the region around the true solution where the method is guaranteed to converge, and speed and stability of convergence, which help determine how efficiently and reliably the method performs.

In order to overcome some of the main drawbacks of iterative approaches, this study introduces a convergence radius that directs the choice of initial approximations even in situations when the precise solution is unknown. By expanding the convergence region, the approach enhances applicability without requiring stronger smoothness or higher-order differentiability requirements. Ball convergence analysis, which offers error bounds, maintains iteration stability, and guarantees

the uniqueness of the solution inside the designated region, is used by the framework to demonstrate reliability. Furthermore, local convergence analysis is used to reinforce the theoretical underpinning and increase the resilience of the iterative strategy. These contributions improve the flexibility, efficiency, and practicality of root-finding methods in a variety of nonlinear problems.

The structure of the paper is organized as follows: Section 2 presents the development of the proposed scheme. Section 3 discusses concrete cases of the two-step fourth-order iterative method. Sections 4 and 5 analyze the local convergence conditions and main theorem in detail. Section 6 compares the proposed method with existing two-step methods through numerical experiments demonstrating solution uniqueness, and Section 7 concludes the paper..

2. Methodology

This section introduces a new fourth-order iterative method developed to solve nonlinear equations efficiently. The method consists of two main steps: the first step uses the well-known Newton-Raphson method, and the second step incorporates a weight function. According to the Kung-Traub conjecture, an optimal method without memory, using n function evaluations, can achieve at most an order of 2^{n-1}. The *efficiency index* is a measure of the computational performance of an iterative method, calculated as $E = p^{1/m}$, where p is the order of convergence and m is the number of function evaluations per iteration. The proposed method achieves fourth-order convergence with only three function evaluations per iteration, making it optimal. A key novelty of the proposed approach lies in the use of weight functions within the iterative framework. Unlike prior classical methods, which typically rely on fixed correction formulas, the weight functions here adaptively enhance convergence by dynamically adjusting the contribution of intermediate terms. This innovation not only improves the efficiency index but also strengthens the radius of convergence, setting the proposed method apart from existing high-order schemes. The proposed method achieves fourth-order convergence with only three function evaluations per iteration, making it optimal. The two-step fourth-order iterative method is given below

$$\begin{aligned} y_m &= t_m - \frac{g(t_m)}{g'(t_m)}, \\ t_{m+1} &= t_m - W(\alpha_m) - S(\beta_m) \times \frac{g(y_m)^2\,(2g(t_m) + g(y_m))}{g(t_m)^2 g'(t_m)}, \end{aligned} \tag{2}$$

where,

$$\alpha_m = \frac{g(t_m) + g(y_m)}{g'(t_m)}, \beta_m = \frac{g(t_m)}{g'(t_m)}.$$

The following theorem proves that the proposed method (2) attains fourth-order convergence.

Theorem 1. *Let $¢ \in \widehat{I}$ be a simple root of a real-valued differentiable function $g : \widehat{I} \subseteq \mathbb{R} \to \mathbb{R}$, where $\widehat{I}$ is an open interval. Suppose that the initial approximation t_0 is sufficiently close to $¢$, and that the weight functions $W(\alpha_m)$ and $S(\beta_m)$ satisfies the following conditions:*

$$W(0) = 0, W'(0) = 1, W''(0) = W'''(0) = 0, S(0) = 1.$$

Under these conditions, the two-step iterative method defined in (2) achieves fourth-order convergence. Moreover, the error satisfies the following relation

$$\epsilon_{m+1} = (4d_2^3 - d_2 d_3 - \frac{1}{24}W^{iv}(0) - 2S'(0)d_2^2)\epsilon_m^4 + O(\epsilon_m^5), \tag{3}$$

where $\epsilon_m = t_m - ¢$ is the the error at the m^{th} iteration.

Proof. Suppose that ¢ be a simple root of the equation $g(t) = 0$, and let $d_i = \frac{g^i(¢)}{i!g'(¢)}$. Applying the Taylor series expansion around ¢, we obtain the following expression

$$g(t_m) = g'(¢)(\epsilon_m + d_2\epsilon_m^2 + d_3\epsilon_m^3 + d_4\epsilon_m^4) + O(\epsilon_m^5). \tag{4}$$

Similarly, the expansion of $g'(t_m)$ yields

$$g'(t_m) = g'(¢)(1 + 2d_2\epsilon_m + 3d_3\epsilon_m^2 + 4d_4\epsilon_m^3) + O(\epsilon_m^4). \tag{5}$$

Using equations (4) and (5), we get the following factor

$$\frac{g(t_m)}{g'(t_m)} = \epsilon_m - d_2\epsilon_m^2 + (2d_2^2 - 2d_3)\epsilon_m^3 + (-4d_2^3 + 7d_2d_3 - 3d_4)\epsilon_m^4 + O(\epsilon_m^5). \tag{6}$$

With the help of Taylor's expansion, we get the error term of the first sub-step of the iterative method (2)

$$y_m - ¢ = d_2\epsilon_m^2 + \left(-2d_2^2 + 2d_3\right)\epsilon_m^3 + \left(4d_2^3 - 7d_2d_3 + 3d_4\right)\epsilon_m^4 + O(\epsilon_m^5) \tag{7}$$

Furthermore, expanding $g(y_m)$ gives

$$g(y_m) = d_2\epsilon_m^2 + \left(-2d_2^2 + 2d_3\right)\epsilon_m^3 + \left(5d_2^3 - 7d_2d_3 + 3d_4\right)\epsilon_m^4 + O(\epsilon_m^5). \tag{8}$$

By using equations (4), (5) and (8), we derive the expression for α_m

$$\frac{g(t_m) + g(y_m)}{g'(t_m)} = \epsilon_m - 2d_2^2\epsilon_m^3 + \left(9d_2^3 - 7d_2d_3\right)\epsilon_m^4 + 0(\epsilon_m^5). \tag{9}$$

Again, by using the Taylor series, the error in the second step of the iterative method (2) is as follows

$$\begin{aligned} t_{m+1} - ¢ = {} & W(0) + \left(1 - W'(0)\right)\epsilon_m - \frac{1}{2}W''(0)\epsilon_m^2 + \left(2W'(0)d_2^2 - \frac{1}{6}W^{(3)}(0) - 2S(0)d_2^2\right)\epsilon_m^3 \\ & + \big(-9W'(0)d_2^3 + 7W'(0)d_2d_3 + 2W''(0)d_2^2 - \frac{1}{24}W^{(4)}(0) + 13S(0)d_2^3 \\ & - 8S(0)d_2d_3 - 2S'(0)d_2^2\big)\epsilon_m^4 + O(\epsilon_m^5) \end{aligned} \tag{10}$$

We use the following conditions of weight functions

$$W(0) = 0, W'(0) = 1, W''(0) = W'''(0) = 0, S(0) = 1,$$

and get the final error expression

$$\epsilon_{m+1} = (4d_2^3 - d_2d_3 - \frac{1}{24}W^{iv}(0) - 2S'(0)d_2^2)\epsilon_m^4 + O(\epsilon_m^5). \tag{11}$$

This result aligns with the Kung and Traub conjecture, which states that an iterative method without memory, employing n function evaluations per iteration, can achieve at most an order of convergence 2^{n-1}. Since the proposed method requires only three function evaluations per iteration and attains fourth-order convergence, it is optimal in the sense of Kung and Traub's criteria. □

3. Particular cases of the proposed two-step method

In this section, we present several specific forms of weight functions $W(\alpha_m)$ and $S(\beta_m)$ that satisfy the conditions established in Theorem (1). The proposed scheme lies in the incorporation of *weight functions* within the iterative formulation. Unlike prior eighth-order methods, which primarily rely on fixed coefficients or standard correction terms, the weight functions dynamically adjust the contribution of intermediate approximations at each iteration. This allows the method to achieve higher accuracy and improved stability, while maintaining optimal computational efficiency. The flexibility offered by these weight functions distinguishes our approach from existing eighth-order schemes and contributes to enhanced convergence behavior, particularly for nonlinear problems with multiple or closely spaced roots. These particular cases demonstrate how the choice of weight functions can ensure the method's fourth-order convergence. By exploring these cases, we not only validate the theoretical results but also provide practical implementations that ensure computational efficiency. Cases are given below:

(1) Let the weight function be defined as

$$W(\alpha_m) = \alpha_m + \frac{1}{24}\alpha_m^4, \quad S(\beta_m) = 1 + \beta_m.$$

Substituting these into the iterative method (2) yields the following two-step fourth-order

method (denoted as SK1)

$$y_m = t_m - \frac{g(t_m)}{g'(t_m)},$$
$$t_{m+1} = t_m - \left(\alpha_m + \frac{1}{24}\alpha_m^4\right) - (1+\beta_m) \times \frac{g(y_m)^2\,(2g(t_m)+g(y_m))}{g(t_m)^2 g'(t_m)}. \tag{12}$$

(2) Another weight function is defined as

$$W(\alpha_m) = \frac{\alpha_m}{1+\alpha_m^3}, \quad S(\beta_m) = 1.$$

Substituting these into the iterative method (2) yields the following two-step fourth-order method (denoted as SK2)

$$y_m = t_m - \frac{g(t_m)}{g'(t_m)},$$
$$t_{m+1} = t_m - \left(\frac{\alpha_m}{1+\alpha_m^3}\right) - \frac{g(y_m)^2\,(2g(t_m)+g(y_m))}{g(t_m)^2 g'(t_m)}. \tag{13}$$

(3) Another weight function is defined as

$$W(\alpha_m) = \alpha_m, \quad S(\beta_m) = \frac{1}{1+\beta_m}.$$

Substituting these into the iterative method (2) yields the following two-step fourth-order method (denoted as SK3)

$$y_m = t_m - \frac{g(t_m)}{g'(t_m)},$$
$$t_{m+1} = t_m - \alpha_m - \left(\frac{1}{1+\beta_m}\right) \times \frac{g(y_m)^2\,(2g(t_m)+g(y_m))}{g(t_m)^2 g'(t_m)}. \tag{14}$$

4. Local convergence analysis

Local convergence analysis is critical for understanding iterative methods' behavior at the root of a nonlinear problem. It not only gives a theoretical foundation for establishing convergence, but it also specifies the conditions under which iterations are guaranteed to approach the genuine solution. It determines the region of dependable convergence by assessing the influence of initial assumptions within a defined neighborhood of the root. It also emphasizes how the smoothness of the function and its derivatives affects the order of convergence and error boundaries. Overall, local convergence analysis assures that iterative approaches are stable and predictable in actual applications. In this section, we perform a detailed local convergence analysis of the proposed iterative methods (12), (13), and (14), establishing the criteria for convergence and evaluating the method's effectiveness based on these conditions.

Let $\delta(u,\phi)$ and $\overline{\delta}(u,\phi)$ denote the open and closed balls, respectively, centered at a point $u \in \Theta$ with radius $\phi > 0$, where Θ is an open subset of $\mathbb{R}$. Furthermore, we introduce two positive real constants $\lambda_0 > 0$ and $\lambda > 0$, subject to the constraint $\lambda_0 \leq \lambda$, which hold for all $t, y \in \Theta$.

$$g(¢) = 0, (g')^{-1} \neq 0, \tag{15}$$
$$|(g')^{-1}(g'(t) - g'(¢))| \leq \lambda_0 |t - ¢|, \quad \forall \quad t \in \Theta, \tag{16}$$
$$|(g')^{-1}(g'(t) - g'(y))| \leq \lambda |t - y|, \quad \forall \quad t, y \in \delta(¢, \frac{1}{\lambda_0}). \tag{17}$$

In most cases, the following assumptions can be used,

$$|(g')^{-1} g'(t)| \leq u_1, \quad \forall \quad t \in \delta(¢, \frac{1}{\lambda_0}), u_1 > 1, \tag{18}$$
$$|(g')^{-1} g(y)| \leq u_2 |y - ¢|, \quad \forall \quad u_2 > 1. \tag{19}$$

Lemma: Let $g : \Theta \subseteq \mathbb{R} \to \mathbb{R}$ be a non-linear, continuously differentiable function on an open interval Θ. Suppose $\¢ \in \Theta$ is a point where $g'(\¢) \neq 0$, and assume that there exists a constant $\lambda_0 > 0$ such that (16) holds. Then for any $t \in \Theta$ and any $\lambda \in [0, 1]$, the following estimates hold:

$$|(g')^{-1}g'(t)| \leq 1 + \lambda_0|t - \¢|, \tag{20}$$

$$|(g')^{-1}g'(\¢ + \gamma(t - \¢))| \leq 1 + \lambda_0|t - \¢|, \tag{21}$$

$$|(g')^{-1}g(t)| \leq (1 + \lambda_0|t - \¢|)|t - \¢|. \tag{22}$$

Proof. To establish the stated inequalities, we proceed by verifying each bound individually.

(1) Proof of inequality (20).
Under the assumption (20), we have

$$\left|(g')^{-1}g'(t)\right| = \left|1 + (g')^{-1}(g'(t) - g'(\¢))\right| \leq 1 + \left|(g')^{-1}(g'(t) - g'(\¢))\right| \leq 1 + \lambda_0|t - \¢|.$$

(2) Proof of inequality (21) Let $t = \¢ + \gamma(t - \¢)$ for $\gamma \in [0, 1]$. Then

$$\left|(g')^{-1}g'(t)\right| = |(g')^{-1}g'(\¢ + \gamma(t - \¢))| \leq 1 + \lambda_0\gamma|t - \¢| \leq 1 + \lambda_0|t - \¢|.$$

(3) Proof of inequality (22)
By the mean value theorem, there exists $\gamma \in (\¢, t)$ such that

$$g(t) - g(\¢) = g'(\gamma)(t - \¢).$$

Assume that $g(\¢) = 0$, we get

$$g(t) = g'(\gamma)(t - \¢),$$

and thus

$$\left|(g')^{-1}g(t)\right| = |(g')^{-1}g'(\gamma)| \times |t - \¢| \leq (1 + \lambda_0|t - \¢|)|t - \¢|.$$

□

5. Local convergence conditions

To analyze the local convergence, we define a specific scalar function and parameters that help to determine the behavior of the iterative method. Let us define the scalar function $\eta_1(k)$ defined on the interval $T = \left[0, \frac{1}{\lambda_0}\right)$ as follows

$$\eta_1(k) = \frac{\lambda k}{2(1 - \lambda_0 k)}.$$

Define the parameter,

$$r_1 = \frac{2}{2\lambda_0 + \lambda} < \frac{1}{\lambda_0},$$

which satisfies $r_1 < \frac{1}{\lambda_0}$. It is evident that $\eta_1(r_1) = 1$ and the inequality $0 \leq \eta_1(k) < 1$ holds for all $k \in [0, r_1)$. Next, define a second scalar function $\eta_2(k)$ over the interval $[0, r_1)$, given by

$$\eta_2(k) = k + W\left[\frac{u_1 + u_2\eta_1(k)}{1 - \lambda_0 k}\right] + S\left[\frac{u_1}{1 - \lambda_0 k}\right]\left(\frac{1}{1 - u_1 k}\right)^2 \times \left(\frac{1}{1 - \lambda_0 k}\right) \times ((u_2\eta_1(k)) \times (2u_1 + u_2\eta_1(k)).$$

Define its corresponding auxiliary function as $p_1(k) = \eta_2(k) - 1$. Under the assumption

$$\eta_2(0) = W(0) < 1,$$

we have $p_1(0) < 0$, and since $p_1(k) < \infty$ as $k \to r_1^-$, continuity implies the existence of at least one root of $p_1(k)$ in $(0, r_1)$. Denote the smallest such root by r_2.
The convergence radius r for the iterative method (2) is then defined as

$$r = min\{r_i, i = 1, 2\}. \tag{23}$$

Therefore, for all $k \in [0, r)$, the following bounds hold:

$$0 \leq \eta_1(k) < 1, \tag{24}$$

$$0 \leq p_1(k) < 1, \quad \text{for each} \quad k \in [0, r). \tag{25}$$

Theorem 2. *Let $M : \Theta \subseteq \mathbb{R} \to \mathbb{R}$ be a differentiable non-linear function satisfying conditions (15)-(17). Suppose that $¢ \in \Theta$ is a simple root of M, and let the initial approximation $t_0 \in \delta(¢, r) = t \in \mathbb{R} : |t - ¢| < r$. Then the sequence t_m generated by the iterative method (2) is well-defined and converges to $¢$.*

In addition, for all $m \geq 0$, the following bounds hold:

$$|y_m - ¢| \leq \eta_1(|t_m - ¢|)|t_m - ¢| < |t_m - ¢| < r, \tag{26}$$

$$|t_{m+1} - ¢| \leq \eta_2(|t_m - ¢|)|t_m - ¢| < |t_m - ¢| < r, \tag{27}$$

where η_1 and η_2 are non-negative scalar functions defined based on the properties of M and its derivative.

Furthermore, if the parameter R is chosen such that

$$R \in \left[r, \frac{2}{\lambda_0} \right),$$

then the closed ball $\overline{\delta}(¢, r) \subseteq \Theta$, and the root $¢$ is the unique solution of $g(t) = 0$ within the ball.

Proof. We verify the validity of bounds (26) and (27) using mathematical induction. Suppose that the initial point $t_0 \in \delta(¢, r)$. We begin by showing that $g'(t_0)$ is invertible. From inequality (16), it follows that

$$|I - (g')^{-1} g'(t_0)| = |(g')^{-1}(g'(t_0) - g'(¢))| \leq \lambda_0 |t_0 - ¢| < 1. \tag{28}$$

Since the right-hand side is strictly less than one, Banach's lemma [9] ensures that $g'(t_0)$ is invertible. Consequently, we obtain the following estimate

$$|g'(t_0)^{-1} g'(¢)| \leq \frac{1}{1 - \lambda_0 |t_0 - ¢|}. \tag{29}$$

This confirms that t_0 is well-defined within the iterative process. To further analyze the method, we express the difference $g(t) - g(¢)$ using the integral form of the mean value theorem [10]

$$g(t_0) = g(t_0) - g(¢) = \int_0^1 g'(¢ + \gamma(t_0 - ¢))(t_0 - ¢) d\gamma. \tag{30}$$

Since $|¢ + \gamma(t_0 - ¢) - ¢| = \gamma |t_0 - ¢| < r$, it follows that $¢ + \gamma(t_0 - ¢) \in \delta(¢, r)$ for all $\gamma \in [0, 1]$. Therefore, substituting (30) into the scaled form yields

$$(g')^{-1} g(t_0) = \int_0^1 g'^{-1} g'(¢ + \gamma(t_0 - ¢))(t_0 - ¢) d\gamma. \tag{31}$$

We now analyze the first sub-step of the iterative method (2) at $m = 0$

$$\begin{aligned} y_0 - ¢ &= t_0 - ¢ - g'(t_0)^{-1} g(t_0), \\ &= -g'(t_0)^{-1}(g(t_0) - g'(t_0)(t_0 - ¢)). \end{aligned} \tag{32}$$

Taking absolute on both sides of equation (29) and applying inequalities (17), (24), (26), and (28), we derive the following estimate

$$\begin{aligned} |y_0 - ¢| &= \left| -g'(t_0)^{-1} g'(¢) \int_0^1 g'^{-1} \left(g'(¢ + \gamma(t_0 - ¢)) - g'(t_0) \right) (t_0 - ¢) \, d\gamma \right|, \\ &\leq \left| g'(t_0)^{-1} g'(¢) \right| \left| \int_0^1 g'^{-1} \left(g'(¢ + \gamma(t_0 - ¢)) - g'(t_0) \right) (t_0 - ¢) \, d\gamma \right|, \\ &\leq \frac{\lambda |t_0 - ¢|}{2(1 - \lambda_0 |t_0 - ¢|)} |t_0 - ¢| \leq \eta_1(|t_0 - ¢|)|t_0 - ¢| < |t_0 - ¢| < r. \end{aligned} \tag{33}$$

This confirms that the bound (33) is satisfied for $m = 0$, implying that $t_0 \in \delta(¢, r)$. Thus, the first iterate t_0 is well-defined and lies within the neighborhood of ¢. We now proceed to verify that the second sub-step of the iterative method (2), ensuring that is well-defined and satisfies the conditions required for invertibility.

To prove $g(t_0) \neq 0$, we use the inequality (22)

$$|g'^{-1}g(t_0)| \leq (1 + \lambda_0|t_0 - ¢|)|t_0 - ¢| \leq d_1(|t_0 - ¢|) < 1. \tag{34}$$

Then $(g'(t_0))^{-1}$ exists, and

$$|g(t_0)^{-1}g'(¢)| \leq \frac{1}{1 - d_1(|t_0 - ¢|)}. \tag{35}$$

Using the inequalities (17), (18), (19) and (27) to express the first variable weight function at $m = 0$

$$\begin{aligned} |\alpha_0| &= |g'(t_0)^{-1}g(¢)||g'(t_0)^{-1}(g(t_0) + g(y_0))|, \\ &\leq \frac{(1 + \lambda_0|t_0 - ¢|)|t_0 - ¢| + u_2|y_0 - ¢|}{1 - \lambda_0|t_0 - ¢|}, \\ &\leq \frac{(1 + \lambda_0|t_0 - ¢|)|t_0 - ¢| + u_2\eta_1(|t_0 - ¢|)|t_0 - ¢|}{1 - \lambda_0|t_0 - ¢|} \end{aligned} \tag{36}$$

and the second variable weight function at $m = 0$ is

$$\beta_0 = |g'(t_0)^{-1}g'(¢)||g'(t_0)^{-1}g(t_0)| \leq \frac{(1 + \lambda_0|t_0 - ¢|)|t_0 - ¢|}{1 - \lambda_0|t_0 - ¢|}.$$

By using the inequalities (5) and (37), to get the following estimates $|W(\alpha_0)|$ and $S(\beta_0)$

$$|W(\alpha_0)| \leq W\left[\frac{(1 + \lambda_0|t_0 - ¢|)|t_0 - ¢| + u_2\eta_1(|t_0 - ¢|)|t_0 - ¢|}{1 - \lambda_0|t_0 - ¢|}\right], \tag{37}$$

and

$$|S(\beta_0)| \leq S\left[\frac{(1 + \lambda_0|t_0 - ¢|)|t_0 - ¢|}{1 - \lambda_0|t_0 - ¢|}\right]. \tag{38}$$

Thus (37) and (38) shows that α_0 and β_0 are well-defined. Now, we can write the second sub-step of the two-step iterative method (2) for $m = 0$

$$\begin{aligned} t_1 - ¢ = t_0 - ¢ - W(\alpha_0) - S(\beta_0) \times ((g(t_0)^{-1}g'^2((g'(t_0))^{-1}g'(¢)) \\ (g'(t_0)^{-1}g(y_0))^2(g'(t_0)^{-1}(2g(t_0) + g(y_0)))), \end{aligned}$$

Taking assertions (18), (19), (28), (34),(37), (38) and absolute on both sides, we obtain the following second-step expression

$$\begin{aligned} |t_1 - ¢| &\leq |t_0 - ¢| + W\left[\frac{(1 + \lambda_0|t_0 - ¢|)|t_0 - ¢| + u_2\eta_1(|t_0 - ¢|)|t_0 - ¢|}{1 - \lambda_0|t_0 - ¢|}\right] \\ &+ S\left[\frac{(1 + \lambda_0|t_0 - ¢|)|t_0 - ¢|}{1 - \lambda_0|t_0 - ¢|}\right] \times \left(\frac{1}{1 - d_1|t_0 - ¢|}\right)^2 \times \left(\frac{1}{1 - \lambda_0|t_0 - ¢|}\right) \\ &\times ((u_2|y_0 - ¢|)^2 \times (2(1 + \lambda_0|t_0 - ¢|)|t_0 - ¢| + u_2|y_0 - ¢|)), \\ &\leq |t_0 - ¢| + W\left[\frac{(1 + \lambda_0|t_0 - ¢|)|t_0 - ¢| + u_2\eta_1(|t_0 - ¢|)|t_0 - ¢|}{1 - \lambda_0|t_0 - ¢|}\right] \\ &+ S\left[\frac{(1 + \lambda_0|t_0 - ¢|)|t_0 - ¢|}{1 - \lambda_0|t_0 - ¢|}\right] \times \left(\frac{1}{1 - d_1|t_0 - ¢|}\right)^2 \times \left(\frac{1}{1 - \lambda_0|t_0 - ¢|}\right) \\ &\times ((u_2\eta_1(|t_0 - ¢|)|t_0 - ¢|)^2 \times (2(1 + \lambda_0|t_0 - ¢|)|t_0 - ¢| + u_2\eta_1(|t_0 - ¢|)|t_0 - ¢|). \end{aligned} \tag{39}$$

This establishes the validity of inequality (39), confirming that $t_1 \in \delta(¢, r)$. By applying the principle of mathematical induction and replacing t_0, y_0, t_1 with t_m, y_m, t_{m+1}, we conclude that inequalities (25) and (26) hold for all $m \in \mathbb{R}$.

Since $|t_{m+1}-¢| \leq |¢-¢| < r$, each iterate remains with the neighborhood $\delta(¢, r)$, preserving the assumptions required by the convergence analysis. Additionally, given that the function $\eta_2(k)$ is increasing, we can recursively estimate

$$\begin{aligned}|t_{m+1}-¢| &\leq \eta_2(t)|t_m-¢| \leq \eta_2(t)\eta_2(|t_{m-1}-¢|)|t_{m-1}-¢|,\\ &\leq \eta_2(t)^2\eta_2(|t_{m-2}-¢|)|t_{m-2}-¢| \leq \cdots \leq \eta_2(t)^{n+1}|t_0-¢|.\end{aligned}$$

Taking the limit as $k \to \infty$, and assuming $\eta_2(k)^{n+1} \to 0$, we obtain

$$\lim_{t\to\infty}|t_m-¢| = 0, \implies \lim_{t\to\infty} t_m = ¢.$$

Hence, the iterative method (2) converges to the unique solution ¢ of the non-linear equation. To prove the uniqueness, suppose there exists another solution $\psi^* \in \overline{\delta}(¢, R)$ such that $g(\psi^*) = 0$. Define the expression

$$\Omega = \int_0^1 g'^* + \gamma(¢-\psi^*))d\gamma.$$

Since $g(¢) = 0$, applying the mean value form gives

$$g(\psi^*) - g(¢) = \Omega(\psi^*-¢) = 0.$$

To show that Ω is invertible, consider the following estimate

$$\begin{aligned}\left|(g')^{-1}(\Omega - g'(¢))\right| &\leq \left|\int_0^1 \lambda_0(\psi^* + \gamma(¢-\psi^*) - y^*)\, d\gamma\right|,\\ &\leq \lambda_0\int_0^1 (1-\gamma)|\psi^*-¢|\, d\gamma \leq \frac{\lambda_0}{2}R < 1. \qquad (40)\end{aligned}$$

Since the expression is strictly less than 1, Banach's lemma guarantees that Ω is invertible. Therefore, from $\Omega(\psi^*-¢) = 0$, it follows that $\psi^* = ¢$. This completes the proof of uniqueness. □

To illustrate the applicability of the general convergence theorem (2), we now consider several special cases. Each example is shown to satisfy the key assumptions of the theorem (2), particularly those related to the convergence radius. While the first sub-step of the iterative method (2) remains fixed, the second step is expressed in the generalized form (39) enables the inclusion of various weight functions. This unified framework preserves the validity of the convergence results across different iterative schemes.

Method 1:

$$\begin{aligned}|t_1-¢| &= |t_0-¢| + \left|\left(\frac{g(t_0)+g(y_0)}{g'(t_0)} + \frac{1}{24}\left(\frac{g(t_0)+g(y_0)}{g'(t_0)}\right)^4\right) - \left(1+\frac{g(t_0)}{g'(t_0)}\right)\right.\\ &\left.\times\frac{g(y_0)^2\,(2g(t_0)+g(y_0))}{g(t_0)^2 g'(t_0)}\right|,\\ &\leq |t_0-¢| + \left(\frac{(1+\lambda_0|t_0-¢|)|t_0-¢| + u_2\eta_1(|t_0-¢|)|t_0-¢|}{1-\lambda_0|t_0-¢|}\right.\\ &\left.+\frac{1}{24}\left(\frac{(1+\lambda_0|t_0-¢|)|t_0-¢| + u_2\eta_1(|t_0-¢|)|t_0-¢|}{1-\lambda_0|t_0-¢|}\right)^4\right)\\ &+\left(1+\frac{(1+\lambda_0|t_0-¢|)|t_0-¢|}{1-\lambda_0|t_0-¢|}\right)\times\left(\frac{1}{1-d_1|t_0-¢|}\right)^2\times\left(\frac{1}{1-\lambda_0|t_0-¢|}\right)\\ &\times((u_2|y-¢|)^2\times(2(1+\lambda_0|t_0-¢|)|t_0-¢| + u_2|y-¢|)),\\ &\leq \eta_2(|t_0-¢|)|t_0-¢| < |t_0-¢| < r. \qquad (41)\end{aligned}$$

Method 2:

$$|t_1-¢| = |t_0-¢| + \left| \frac{\frac{g(t_m)+g(y_m)}{g'(t_m)}}{1+\left(\frac{g(t_m)+g(y_m)}{g'(t_m)}\right)^3} - \frac{g(y_0)^2\,(2g(t_0)+g(y_0))}{g(t_0)^2 g'(t_0)} \right|,$$

$$\leq |t_0-¢| + \left(\frac{\frac{(1+\lambda_0|t_0-¢|)|t_0-¢|+u_2\eta_1(|t_0-¢|)|t_0-¢|}{1-\lambda_0|t_0-¢|}}{1+\left(\frac{(1+\lambda_0|t_0-¢|)|t_0-¢|+u_2\eta_1(|t_0-¢|)|t_0-¢|}{1-\lambda_0|t_0-¢|}\right)^3} \right) + \left(\frac{1}{1-u_1|t_0-¢|}\right)^2$$

$$\times \left(\frac{1}{1-\lambda_0|t_0-¢|}\right) \times ((u_2|y-¢|) \times (2(1+\lambda_0|t_0-¢|)|t_0-¢| + u_2|y-¢|)),$$

$$\leq \left[1 + \left(\frac{\frac{(1+\lambda_0|t_0-¢|)|t_0-¢|+u_2\eta_1(|t_0-¢|)|t_0-¢|}{1-\lambda_0|t_0-¢|}}{1+\left(\frac{(1+\lambda_0|t_0-¢|)|t_0-¢|+u_2\eta_1(|t_0-¢|)|t_0-¢|}{1-\lambda_0|t_0-¢|}\right)^3} \right) + \left(\frac{1}{1-u_1|t_0-¢|}\right)^2 \right.$$

$$\left. \times \left(\frac{1}{1-\lambda_0|t_0-¢|}\right) \times ((u_2\eta_1|t_0-¢|)^2|t_0-\eta| \times (2(1+\lambda_0|t_0-¢|)|t_0-¢| + u_2\eta_1|t_0-¢|)) \right]$$

$$|t_0-¢|, \leq \eta_2(|t_0-¢|)|t_0-¢| < |t_0-¢| < r. \tag{42}$$

Method 3:

$$|t_1-¢| = |t_0-¢| + \left| \left(\frac{g(t_m)+g(y_m)}{g'(t_m)}\right) - \left(\frac{1}{1+\frac{g(t_m)}{g'(t_m)}}\right) \right.$$

$$\left. \times \frac{g(y_0)^2\,(2g(t_0)+g(y_0))}{g(t_0)^2 g'(t_0)} \right|,$$

$$\leq |t_0-¢| + \left(\frac{(1+\lambda_0|t_0-¢|)|t_0-¢| + u_2\eta_1(|t_0-¢|)|t_0-¢|}{1-\lambda_0|t_0-¢|} \right)$$

$$+ \left(\frac{1}{1+\frac{(1+\lambda_0|t_0-¢|)|t_0-¢|}{1-\lambda_0|t_0-¢|}} \right) \times \left(\frac{1}{1-u_1|t_0-¢|}\right)^2 \times \left(\frac{1}{1-\lambda_0|t_0-¢|}\right)$$

$$\times ((u_2|y-¢|)^2 \times (2(1+\lambda_0|t_0-¢|)|t_0-¢| + u_2|y-¢|)),$$

$$\left[1 + \left(\frac{(1+\lambda_0|t_0-¢|)|t_0-¢| + u_2\eta_1(|t_0-¢|)|t_0-¢|}{1-\lambda_0|t_0-¢|} \right) + \left(\frac{1}{1+\frac{(1+\lambda_0|t_0-¢|)|t_0-¢|}{1-\lambda_0|t_0-¢|}} \right) \right.$$

$$\left. \times (2(1+\lambda_0|t_0-¢|)|t_0-¢| + (u_2\eta_1(|t_0-¢|))^2|t_0-¢| \right.$$

$$\leq \eta_2(|t_0-¢|)|t_0-¢| < |t_0-¢| < r. \tag{43}$$

6. Numerical results

This section presents the theoretical validation of the proposed two-step iterative method defined in (12)-(14), along with its numerical results for solving non-linear equations. The method's performance is evaluated through computational experiments and compared with existing two-step methods. Numerical results confirm that the method achieves improved convergence radius and enhanced stability for various non-linear functions. All computations were performed using the computer algebra system Maple 18, and the results are presented up to six decimal places for consistency.

For the comparison, we take some existing two-step iterative methods for solving non-linear equations are given below: Delshad et al. [11] investigated the analysis of local convergence of a two-step Kung-Traub type iterative method for solving non-linear equations, with iterations defined for $m = 0, 1, 2, ...$ The method (ADL) is structured as follows

$$y_m = t_m - \frac{g(t_m)}{g'(t_n)},$$
$$t_{m+1} = y_n - H(t_m), \tag{44}$$

where, the function $H(t_m)$ is given by

$$H(t_m) = \frac{g(t_m)^2 g(y_m)}{g'(t_m)(g(y_m) - g(t_m))^2}.$$

Behl et al. [12] studied the local convergence behavior of a two-step iterative method of fourth-order, commonly referred to as the weighted Newton method. The iterative scheme (BRK) is defined as follows

$$y_m = t_m - \mu\frac{g(t_m)}{g'(t_m)},$$
$$t_{m+1} = y_m - S_m^{-1}(b_1 g(t_m) + b_2 g(y_m)), \tag{45}$$

where t_0 is the initial approximation and S_m is defined by

$$S_m = v_1 g'(t_m) + v_2 g'\left(\frac{t_m + y_m}{2}\right) + v_3 g'(y_m).$$

The parameters $\mu, b_1, b_2, v_1.v_2, v_3$ are constants chosen to ensure fourth-order convergence. Their expressions are given

$$v_1 = -\frac{1}{3}d_2(3\mu^2 - 7\mu + 2), \quad v_2 = -\frac{4}{3}d_2(2\mu - 1),$$
$$v_3 = \frac{1}{3}d_2(\mu - 2), \quad b_1 = -b_2(\mu^2 - \mu + 1), \quad \text{for} \quad \mu, b_2 \neq 0.$$

This method incorporates a parameterized weighted combination of derivative evaluations to achieve higher-order convergence while maintaining computational efficiency.
Argyros et al. [13] investigated the local convergence analysis of a two-step iterative method (AIK) for $m = 0, 1, 2, ...,$

$$y_m = t_m - \mu\frac{g(t_m)}{g'(t_m)},$$
$$t_{m+1} = y_m - \frac{g(y_m)}{g'(t_m)} \times \frac{g(t_m) + \beta g(y_m)}{g(t_m) + (\beta - 2)g(y_m)}. \tag{46}$$

Example 1: Let $U = Y = \mathbb{R}$ and consider the non-linear function g_1 defined on the closed ball $\Theta = \overline{\delta}(0, 1)$ as follows [14]:

$$g_1(t) = e^t - 1,$$

with the root $¢ = 0$. The corresponding first derivative is given by

$$g'(t) = e^t.$$

Using conditions (15)-(19), we compute the associated constants as

$$\lambda_0 = e - 1, \quad \lambda = u_1 = u_2 = e^{\frac{1}{e-1}}.$$

Numerical computations were performed using the computer algebra system Maple 18. As shown in table (1), the two step iterative methods SK1, SK2, and SK3 demonstrate a significantly wider region of convergence. This extended convergence radius confirms the superior performance and robustness of the proposed method (2), making it applicable to a wider selection of initial approximations.

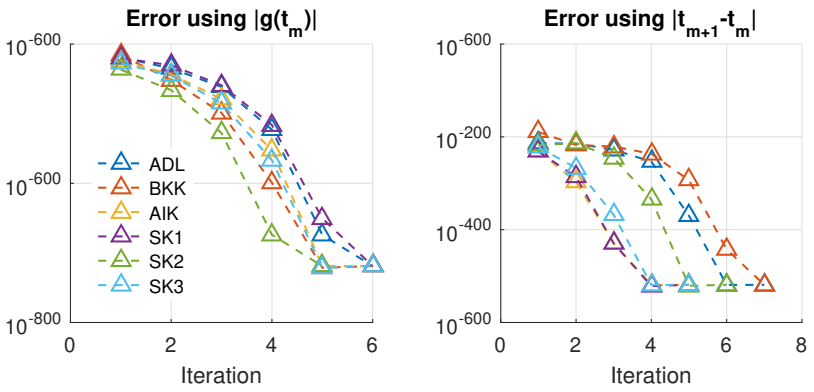

Figure 1. Error plots of the numerical schemes for solving nonlinear equation used in Example 1.

Table 1. Convergence radius analysis of different iterative methods for $g_1(x)$

Method	r_1	r_2	$r = min\{r_1, r_2\}$
SK1	0.382689	0.588528	0.588528
SK2	0.382689	0.586257	0.586257
SK3	0.382689	0.563786	0.563786

Table 2. Numerical outcomes of iterative schemes for solving $g_1(x)$

Method	$\|g(t_m)\|$	$\|t_{m+1} - t_m\|$	$CPU - time$
SK1	0.43e-635	0.875e-435	0.0097
SK2	9.08e-709	0.07e-505	0.0096
SK3	6.76e-803	9.07e-560	0.0086
ADL	3.98e-649	0.98e-434	0.0887
BRK	0.09e-588	0.05e-378	0.0586
AIK	9.076e-586	0.14e-420	0.1075

The numerical outcomes from Tables 1–2 and Figure 1 clearly demonstrate that the newly developed method outperforms the existing approaches in terms of function value error, residual error, and CPU time. This improvement is achieved by selecting the initial guess values according to the assumptions established in the local convergence analysis of Theorem 2, which ensures both efficiency and robustness of the proposed scheme.

Example 2: Consider the non-linear function $g_2(t)$ defined on the interval $\Theta = [1, 4]$ as [15]:

$$g_2(t) = \frac{3}{4}t^{\frac{4}{3}} - t.$$

The exact simple root of this function is $¢ = \left(\frac{4}{3}\right)^3$. The first derivative is given by

$$g'^{\frac{1}{3}} - 1.$$

Using conditions (15)-(19), we compute the associated constants as

$$\lambda_0 = \lambda = 1, u_1 = u_2 = 1.76220315590460.$$

Table (2) shows that the two-step iterative methods SK1, SK2, and SK3 demonstrate a significantly wider region of convergence compared to the methods ADL, BRK, and AIK.

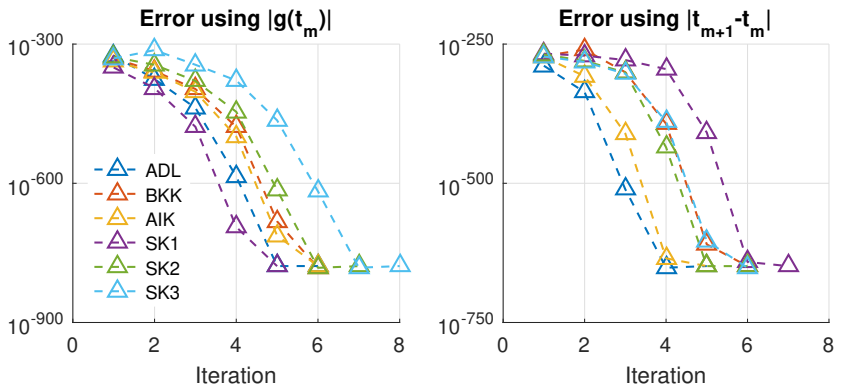

Figure 2. Error plots of the numerical schemes for solving nonlinear equations used in Example 2.

Table 3. Convergence radius analysis of different iterative methods for $g_2(x)$

Method	r_1	r_2	$r = min\{r_1, r_2\}$
SK1	0.6666	0.456792	0.456792
SK2	0.6666	0.453527	0.453527
SK3	0.6666	0.445624	0.445624

Table 4. Numerical outcomes of iterative schemes for solving $g_2(x)$

Method	$\|g(t_m)\|$	$\|t_{m+1} - t_m\|$	$CPU - time$
SK1	0.98e-643	0.875e-476	0.0098
SK2	9.11e-577	0.07e-378	0.0013
SK3	9.09e-789	9.07e-657	0.0034
ADL	5.76e-600	0.98e-398	0.0865
BRK	4.66e-579	0.05e-277	0.0335
AIK	3.44e-409	0.14e-257	0.0975

The numerical findings presented in 3–4 and Figure 2 provide strong evidence that our proposed method significantly outperforms traditional techniques. In particular, it achieves lower function value errors, reduced residual errors, and faster CPU times. These improvements stem from the careful selection of initial guess values guided by the local convergence analysis in Theorem 2, which not only enhances accuracy but also minimizes computational inefficiency often encountered in classical iterative solvers.

Example 3 Returning to the motivational example discussed at the beginning of this paper, the associated parameters are taken as

$$\lambda_0 = \lambda = 96.6629073, u_1 = u_2 = 2.$$

As observed in table (3), the proposed methods SK1, SK2, and SK3 outperform the compared methods by yielding a significantly larger radius of convergence. This result underscores the method's enhanced efficiency and stability in solving non-linear equations.

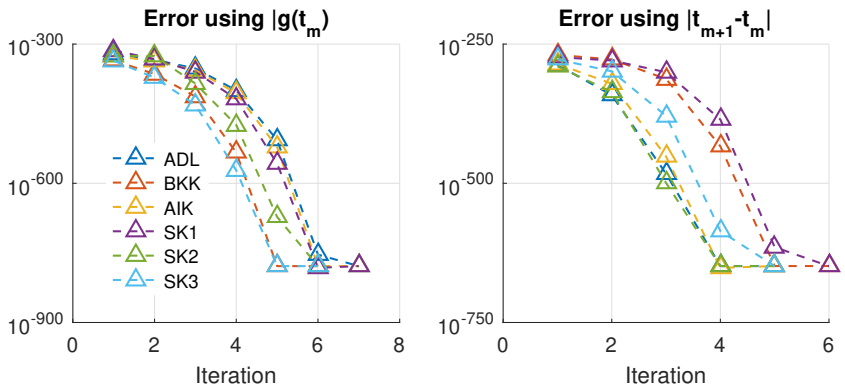

Figure 3. Error plots of the numerical schemes for solving nonlinear equations used in Example 3.

Table 5. Convergence radius analysis of different iterative methods for $g_3(x)$

Method	r_1	r_2	$r = min\{r_1, r_2\}$
SK1	1.175903	1.134579	1.134579
SK2	1.175903	1.132576	1.132576
SK3	1.175903	1.102549	1.102549

Table 6. Numerical outcomes of iterative schemes for solving $g_3(x)$

Method	$\|g(t_m)\|$	$\|t_{m+1} - t_m\|$	$CPU - time$
SK1	0.98e-786	0.85e-587	0.0034
SK2	0.12e-856	0.27e-648	0.0012
SK3	6.98e-879	4.37e-609	0.0055
ADL	3.34e-677	8.98e-587	0.0365
BRK	0.09e-708	4.04e-670	0.0776
AIK	1.63e-754	8.19e-599	0.0875

Tables 5–6 and Figure 3 demonstrate the advantages of the newly devised scheme over existing methods. The method consistently produces less function and residual errors while using less CPU time. This efficiency increase is ascribed to the use of starting estimates selected in accordance with Theorem 2's theoretical framework, which guarantees a trustworthy trade-off between numerical stability and convergence speed. Thus, the approach shows both theoretical validity and useful computational efficiency.

Beyond the three case studies presented, the proposed root-finding framework and iterative schemes have broad applicability across various engineering and applied science domains. Potential applications include solving high-degree nonlinear equations in control systems, modeling complex biochemical networks, optimizing multi-parameter mechanical systems, and addressing fractional-order models in signal processing and biomedical engineering. These extensions demonstrate the versatility and practical relevance of the proposed method across diverse scientific and engineering problems.

7. Conclusion

In this study, a new two-step approach to finding simple roots was developed. To ensure a thorough theoretical foundation, the local convergence analysis has been carried out both with and without derivatives. The numerical results in Tables 1-6 and Figures 1-3 clearly show that the suggested strategy consistently outperforms previous approaches. Specifically, it achieves

lower residual errors (computed via function values), requires fewer corrective iterations, exhibits broader convergence radii, and reduces CPU execution time. These advantages establish the method as a strong alternative for solving nonlinear problems efficiently.

The proposed method, while significantly improving convergence and efficiency, has some limitations. These include potential sensitivity to the choice of initial guesses, increased computational cost for extremely high-degree polynomials, and the need for accurate evaluation of function derivatives in certain cases. Future work will focus on addressing these aspects to further enhance robustness and applicability.

Future Directions:

- Extension of the proposed scheme to systems of nonlinear equations.
- Adaptation for parameter-dependent problems in engineering and applied sciences.
- Development of *parallel or GPU-accelerated implementations* for large-scale applications.
- Exploration of hybrid schemes combining the method with machine learning techniques for enhanced convergence prediction.

Acknowledgments

None.

Funding

None.

Conflict of interest

There is no conflict of interest to disclose.

Author contributions

The study was conducted entirely by the sole author.

Declaration of using AI tools

The authors declare that they have not used any type of generative artificial intelligence for the writing of this manuscript, nor for the creation of images, graphics, tables, or their corresponding captions.

References

[1] S. Abdullah, N. Choubey, S. Dara, M.-U.-D. Junjua, and T. Abdullah, "A robust and optimal iterative algorithm employing a weight function for solving nonlinear equations with dynamics and applications", Axioms, vol. 13, no. 10, p. 675, Sept. 2024. https://doi.org/10.3390/axioms13100675.

[2] S. Akram, F. Akram, M.-U.-D. Junjua, M. Arshad, and T. Afzal, "A family of optimal eighth order iteration functions for multiple roots and its dynamics", *Journal of Mathematics*, vol. 2021, no. 1, 2021. https://doi.org/10.1155/2021/5597186.

[3] S. Kumar, R. Ishwariya, and M.-U.-D. Junjua, "A novel optimal fourth-order iteration scheme for solving nonlinear problems in applied sciences", *Journal of Applied Mathematics and Computing*, vol. 71, no. 1, pp. 643–667, 2025. https://doi.org/10.1007/s12190-024-02259-1.

[4] R. Behl and S. S. Motsa, "Geometric construction of eighth-order optimal families of Ostrowski's method", *The Scientific World Journal*, vol. 2015, no. 1, 2015. https://doi.org/10.1155/2015/614612.

[5] J. A. Ezquerro, D. Gonzalez, and M. A. Hernandez, "On the local convergence of Newtons method under generalized conditions of Kantorovich", *Applied Mathematics Letters*, vol. 26, no. 5, pp. 566–570, 2013. https://doi.org/10.1016/j.aml.2012.12.012.

[6] R. Lin, Q. Wu, M. Chen, and X. Lei, "On the convergence ball and error analysis of the modified secant method", *Advances in Mathematical Physics*, vol. 2018, 2704876, 5 pages, 2018. https://doi.org/10.1155/2018/2704876.

[7] P. Maroju, A.A. Magrenan, I. Sarria, and A. Kumar, "Local convergence of fourth and fifth order parametric family of iterative methods in Banach spaces", *Journal of Mathematical Chemistry*, vol. 58, pp. 686–705, 2020. https://doi.org/10.1007/s10910-019-01097-y.

[8] D. Sharma and S. K. Parhi, "On the local convergence of higher order methods in Banach spaces", *Fixed Point Theory*, vol. 22, no. 2, pp. 855–870, 2021. https://doi.org/10.24193/fpt-ro.2021.2.55.

[9] L. B. Rall, *Computational solution of nonlinear operator equations*. New York, 1979.

[10] J. M. Ortega and W. C. Rheinboldt, *Iterative solution of nonlinear equations in several variables*, Society for Industrial and Applied Mathematics, 2000. https://doi.org/10.1137/1.9780898719468.

[11] P.A. Delshad and T. Lotfi, 'On the local convergence of Kung-Traub's two-point method and its dynamics', *Applications of Mathematics*, vol. 65, no. 4, pp. 379–406, 2020. https://doi.org/10.21136/AM.2020.0322-18.

[12] R. Behl, I.K. Argyros, J.A.T. Machado, and S.A. Alshomrani, "Local convergence of a family of weighted-Newton methods", *Symmetry*, vol. 11, no. 1, 2019. https://doi.org/10.3390/sym11010103.

[13] I. K. Argyros, A.A. Magren, A. Moysi, I. Sarria, and J.A. Sicilia Montalvo, "Study of Local Convergence and Dynamics of a King", *Mathematics*, vol. 8, no. 7, 2020. https://doi.org/10.3390/math8071062.

[14] M. Kansal, V. Kanwar, and S. Bhatia, "New modifications of Hansen-Patrick's family with optimal fourth and eighth orders of convergence", *Applied Mathematics and Computation*, vol. 269, pp. 507–519, 2015. https://doi.org/10.1016/j.amc.2015.07.101

[15] T. Zhanlav and K. Otgondorj, "Some modifications and extensions of Popovski's and Laguerre's families for solving systems of nonlinear equations", *Mong. Math. J.*, vol. 27, no. 25, pp. 10–22, Dec. 2024. https://doi.org/10.5564/mmj.v27i25.4013

All open access articles published in Transactions on Computational Modeling and Intelligent Systems (http://tcmis.org) are distributed under the terms of the CC BY-NC 4.0 license (Creative Commons Attribution Non-Commercial 4.0 International Public License as currently displayed at http://creativecommons.org/licenses/by-nc/4.0/legalcode) which permits unrestricted use, distribution, and reproduction in any medium, for non-commercial purposes, provided the original work is properly cited.

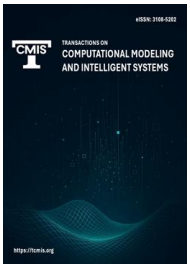

Transactions on
Computational Modeling and Intelligent Systems

Volume 1, October 2025, Article 10013
https://doi.org/10.65112/tcmis.10013

eISSN: 3108-5202
www.tcmis.org

RESEARCH ARTICLE

Investigation of stability and oscillatory behavior of allelochemical influence on plants in time delay differential equation model

Mine Babaoglu[1], Dipesh[2*] and Pankaj Kumar[3]

[1]*Department of Mathematics and Science Education, Faculty of Education, Kahramanmaraş Sütçü İmam University, Kahramanmaraş, Türkiye.*
[2]*Department of Mathematics, SR University, Warangal-506371, Telangana, India.*
[3]*Department of Mathematics, Lovely Professional University, Phagwara, Punjab-144411, India.*

[*]*Corresponding Author. Email: dipeshdalal2411@gmail.com (Dipesh)*

Article Information

Received: 30 August 2025
Accepted: 1 October 2025
Published: 3 October 2025

AMS 2020 Classification: 34L30

Abstract

The utilizing of bioassay techniques is common for examining how allelochemicals affect plant processes. In general, at higher allelochemical concentrations, processes are impeded, whereas at lower ones, they are boosted. A mathematical model is developed to analyse this kind of reaction. It is assumed that the response of the plant organism is proportional to the allelochemical dose. This plant response is studied for delayed allelochemical dose using time delay differential equation. The feasible non-zero equilibrium point is examined and the stability analysis is studied about the equilibrium point. The system is stable if the delay in allelochemical dose does not cross a fixed critical value. However, the system exhibits limit cycles via Hopf-bifurcation when delay parameter crosses the fixed critical value. Furthermore, in the situation that the diffusion coefficient transpires. Additionally, it exists within the event exhibiting the diffusion coefficient. Analytical results are supported by MATLAB.

Keywords: Allelochemical, plant response, stability, delay parameter, hopf-bifurcation, time delay differential equation.

1. Introduction

Allelopathy refers to a chemical process that is dependent on the release of one or more chemicals into the environment. Allelopathy can be either stimulative or destructive. Allelopathy was described by Molisch [1] as any positive or negative biochemical interaction between microbes and plants of any complexity degree. Plant tissues include stems, foliage, origins, rhizomes, blossoms, fruit, and spores, contain chemicals that have the potential to be allelopathic; nevertheless, leaves and roots are the primary producers of allelochemicals studied by Rice [2]. Numerous processes, such as volatilization, the breakdown of plant wastes, and root exudates, can release allelochemicals into the environment from plants examined by Tukey [3,4], Rice [5], Putnam [6]. Lately, the responses of plants to allelochemicals have been theoretically described by modeling An et al. [7,8], Zhen and Ma [9] through the use of mathematical norms.

For quantitatively measure reactions to chemical compounds at various doses in allelopathy research, bioassay methods are frequently employed. It has been observed that inhibition manifests at high concentrations while stimulation happens at low quantities observed by Lovett [10,11], and Liu and Lovett [12].

Many allelochemical dosage responses are investigated utilising statistical comparison approaches like the Least Significant Difference examined by Paszkowki and Kremer [13], Toro et al. [14], Buta and Spaulding [15], Student's t test, and Duncan's Multiple Range Test by Leather and Einhellig [16] Stevens and Molyneux [17]. However, it may be statistically inefficient to utilize such approaches to analyze the data comprising a sequence of dose rates studied by Dawkins [18]. Nevertheless, the correlation between the allelochemical dosages and the

bioassay organism's responses is not necessarily linear. The reactions of plant growth and development to allelochemicals are primarily nonlinear, similar to many other biological processes.

An et al. [19] theoretically analyzed and modeled the dynamics of allelochemicals released by living plants into the environment, as well as the phytotoxic effects of compounds released from plant residues during decomposition. However, the effect of allelochemicals is not immediate, but takes a maturation time. This period of maturation of allelochemicals is studied Dipesh and Kumar [20-22] by using delay differential equations. Horatmann examined the condition for instability [23]. Pang et al. investigated spatial patterns in the reaction-diffusion model using various diffusion and reaction terms [24]. Paul and Ritson-Williams examined the most current marine chemical ecology literature on benthic cyanobacteria, macroalgae, sponges, octocorals, molluscs, other benthic invertebrates, fish, and seabirds [25]. Tian et al. investigated the spatial flow on allelopathy with cross diffusion [26]. There has been a great deal of effort done to examine the features of solutions to reaction-diffusion systems that describe ecological models [27–29].

The aim of this paper is to investigate the relation of plant response with allelochemicals under what condition the plant response are stable, unstable. In addition, we calculate the wave number of different flow using nonlinear dynamics.

Assumptions:

- The suggested delay differential equation model represents the persistent release of allelochemicals from plant residues or root exudates, therefore reflecting a continuous supply of bioactive substances in the soil.
- The addition of a delayed feedback term accounts for the time lag between allelochemical release, soil modifications, and subsequent reappearance in bioavailable form, which is consistent with documented lagged effects in allelopathic interactions.

2. Mathematical model

Let D a dose of an allelochemical, and $\boldsymbol{T_c}$ the fixed response of untreated control in the bioassay. We may write

$$\frac{dD}{dt} = T_c + f(D). \tag{1}$$

Here $f(D)$ is the effect of allelochemicals. $f(D) > 0$ leads to stimulation and $f(D) < 0$ causes inhibition. Considering $f(D)$ as a simple quadratic equation, we have

$$f(D) = \beta D - \gamma D^2. \tag{2}$$

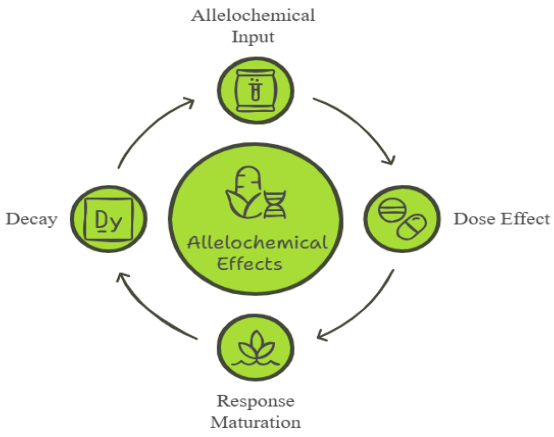

Figure 1. Allelochemical cycle response.

Here β is the rate of input of allelochemicals and γ is the rate of decay of allelochemicals. So, Eq. (1) becomes:

$$\frac{dD}{dt} = T_c + \beta D - \gamma D^2. \tag{3}$$

As the effect of allelochemical dose is not immediate, but takes a maturation time, so a delay parameter τ is introduced in allelochemical dose. The Eq. (3) turns into delay differential equation, and can be finally written as:

$$\frac{dD}{dt} = T_c + \beta D(t-\tau) - \gamma D^2. \tag{4}$$

2.1. Equilibrium point

At the interior non-zero equilibrium point, we have $\beta D(t-\tau) \approx \beta D$

$$\frac{dD^*}{dt} = 0 \Rightarrow D^* = \frac{\beta \pm \sqrt{\beta^2 + 4\gamma T_c}}{2\gamma}.$$

These two values of allelochemical doses are responsible for stimulation and inhibition responses respectively.

2.2. Stability of dose of allelochemicals

Discuss the stability of the response of the plant organism is proportional to the allelochemical dose about the non-zero equilibrium points, then Eq. (4) becomes:

$$\frac{dD^*}{dt} = T_c + \beta D^*(t-\tau) - \gamma D^{*2}. \tag{5}$$

We assume a solution of the form $D^*(t) = e^{\lambda t}$, and differentiating:

$$\frac{d}{dt} e^{\lambda t} = \lambda e^{\lambda t}.$$

Putting the value in Eq. (5), we got:

$$\lambda e^{\lambda t} + \gamma D^{*2} e^{\lambda t} = \beta D^*(t-\tau) e^{\lambda t}. \tag{6}$$

Divide Eq. (6) by $e^{\lambda t}$, it becomes

$$\lambda + \gamma D^{*2} = \beta e^{-\lambda \tau}.$$

The characteristic equation becomes

$$\lambda = \beta e^{-\lambda \tau} - \gamma D^{*2} \tag{7}$$

Let $\lambda = ia$, then Eq. (7) become

$$ia = \beta e^{ia\tau} - \gamma D^{*2}. \tag{8}$$

Using the Euler formula

$$e^{ia\tau} = \cos(a\tau) - i \sin(a\tau)$$

rewrite the Eq. (8), it becomes

$$ia = \beta(\cos(a\tau) - i \sin(a\tau)) - \gamma D^{*2}.$$

separate real and imaginary part:

$$0 = \beta \cos(a\tau) - \gamma D^{*2}, \tag{9}$$

$$a = -\beta \sin(a\tau). \tag{10}$$

From Eq. (9), we have

$$\beta \cos(a\tau) = \gamma D^{*2}$$

$$\Rightarrow \cos(a\tau) = \frac{\gamma}{\beta} D^{*2}. \tag{11}$$

For solution $\left|\frac{\gamma}{\beta} D^{*2}\right| \leq 1$, and from Eq. (10):

$$\frac{a}{\beta} = -\sin(a\tau). \tag{12}$$

Adding the Eqs. (11) and (12), we got:

$$\left(\frac{\gamma}{\beta}D^{*2}\right)^2 + \left(\frac{a}{\beta}\right)^2 = 1,$$

$$a^2 = \beta^2 - \gamma^2 D^{*4}.$$

For oscillation solution, we require a to be real

$$\beta^2 > \gamma^2 D^{*4}.$$

Case1: If $\beta^2 > \gamma^2 D^{*4}$, the oscillation occurs with frequency $a = \sqrt{\beta^2 - \gamma^2 D^{*4}}$.

Case2: If $\beta^2 \leq \gamma^2 D^{*4}$, oscillations do not occur. If the term within the square root is non-positive, λ remains absolutely real. When λ is negative, the system experiences exponential decay and finally achieves a stable state.

Case3: If $\lambda > 0$, then $D^*(t)$ increase over time and move towards unstable, when $\beta e^{-\lambda\tau} > \gamma D^{*2}$.

For example: When we take the parametric value: $\beta = 2, \gamma = 0.5, D^* = 1,$ then

$$\gamma^2 D^{*4} = (0.5)^2(1)^4$$

$$\beta^2 = 4.$$

where $\beta^2 > \gamma^2 D^{*4}$, oscillation occur, and the frequency is:

$$a = \sqrt{\beta^2 - \gamma^2 D^{*4}} \Rightarrow \sqrt{3.75} \approx 1.94$$

Theorem1: Let λ be the root of the characteristic equation $\lambda - \beta e^{-\lambda\tau} + \gamma D^{*2} = 0$,

1.1 If $\beta > \gamma$, system shows the oscillatory behavior.
1.2 If β is small, the system shows the stability.
1.3 There exists a threshold, when delay is greater than the threshold value, the system moves from stability to oscillation (Hopf-bifurcation).

Proof: Let $d(\lambda) = \lambda - \beta e^{-\lambda\tau} + \gamma D^{*2}$, and from Eqs. (9) and (10), solving for $\tau, and\ a$. We get

$$\tau_c = \frac{1}{a} arccos\left(\frac{\gamma D^{*2}}{\beta}\right). \tag{13}$$

When delay cross the threshold value, a pair of purely imaginary roots emerges, towards hopf-bifurcation and oscillatory and periodic solution occurs.

2.3. Transversality condition

Differentiate implicitly the characteristic Eq. (7) with respect to τ:

$$\frac{d\lambda}{d\tau} - \beta e^{-\lambda\tau}\left(-\tau\frac{d\lambda}{d\tau} - \lambda\right) = 0$$

$$\frac{d\lambda}{d\tau} + \beta e^{-\lambda\tau}\tau\frac{d\lambda}{d\tau} + \beta e^{-\lambda\tau}\lambda = 0$$

$$\frac{d\lambda}{d\tau}\left(1 + \beta\tau e^{-\lambda\tau}\right) = -\lambda\beta e^{-\lambda\tau}$$

$$\frac{d\lambda}{d\tau} = \frac{-\lambda\beta e^{-\lambda\tau}}{1 + \beta\tau e^{-\lambda\tau}}.$$

On simplification, we get:

$$\mathrm{Re}\left(\frac{d\lambda}{d\tau}\right) = \frac{\omega^2}{(1+\tau\gamma D^{*2})^2+(\tau\omega)^2} > 0.$$

This is always positive. Hence, the transversality condition is satisfied.

3. Numerical example

To validate our theoretical conclusion, we do numerical simulations of the delay differential equation in MATLAB. We examine how different parameters values, namely $\tau, \beta, and\ \gamma$, affect the systems stability and oscillatory dynamics. The values of parameter are $T_c = 0.01, \beta = 0.9, \gamma = 0.0006$.

4. Result and discussion

Figure 2 shows the stability of the behavior of testing organism when there is no dose of allelochemicals and behavior of testing organism remain stable ($\tau = 0$). Figure 3 complements this by presenting a phase portrait under the same no-delay conditions ($\tau = 0$). The phase portrait visually depicts how the system's trajectories evolve over time. Since there is no delay, all trajectories converge smoothly to the equilibrium, confirming that the system behaves predictably when unperturbed by external influences. Figure 4 introduces a delay ($\tau < 1.69999$), which simulates the effect of a dose of allelochemicals on the organism. Initially, the system exhibits noticeable fluctuations—its state variables oscillate before settling down. These fluctuations indicate that the introduction of allelochemicals disturbs the system temporarily. However, the system eventually regains stability, a behavior known as asymptotic stability, where the fluctuations gradually diminish and the system returns to equilibrium over time. Figure 5 further maps out the region in the system's parameter space where stability is maintained when the delay is below the critical value ($\tau < 1.69999$). This figure emphasizes that, within this range, even though there might be some initial disturbances due to the allelochemicals, the overall behavior of the organism remains stable in the long run ($\tau < 1.69999$). Figure 6, the system does not simply return to a stable state; instead, it exhibits sustained periodic oscillations. This transition to periodic behavior is indicative of a Hopf-bifurcation, a type of bifurcation where a fixed point loses stability and gives rise to a limit cycle. In simpler terms, once the delay goes beyond this critical point, the testing organism's behavior switches from a stable state to one with continuous, regular oscillations, highlighting a significant change in the system dynamics ($\tau \geq 1.69999$). Figure 7 represent the log scale view of behavior of testing organism when delay is greater than critical value, i.e. ($\tau \geq 1.69999$).

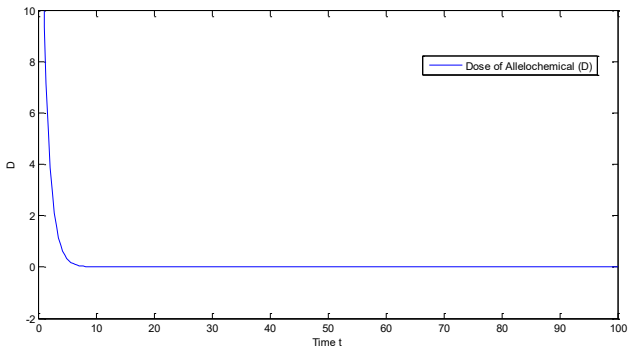

Figure 2. The behavior of the testing organism when there is no delay, i.e., ($\tau = 0$).

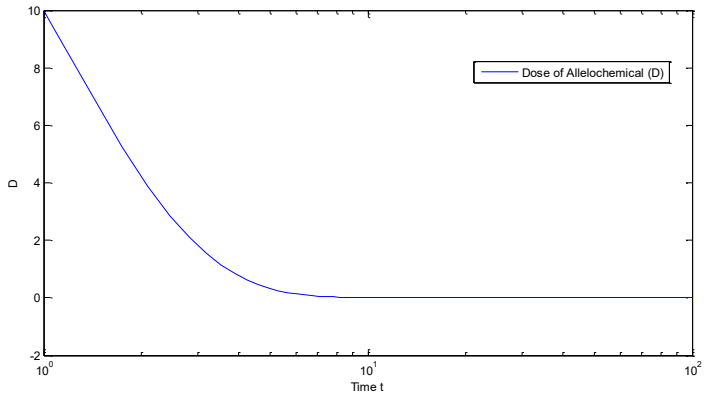

Figure 3. The log phase of behavior of testing organism in the absence of delay, i.e., ($\tau = 0$).

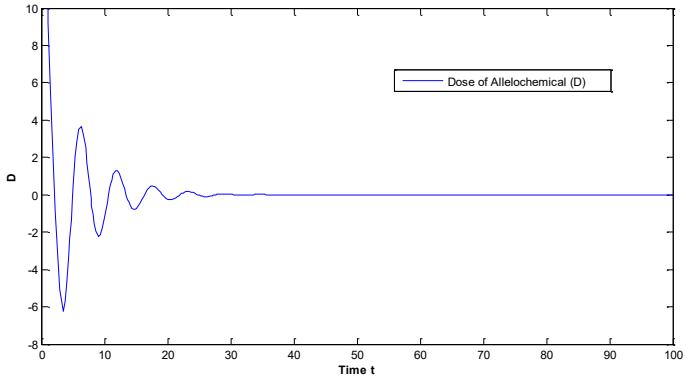

Figure 4. The asymptotic behaviour when delay is less then critical value, i.e. ($\tau < 1.69999$).

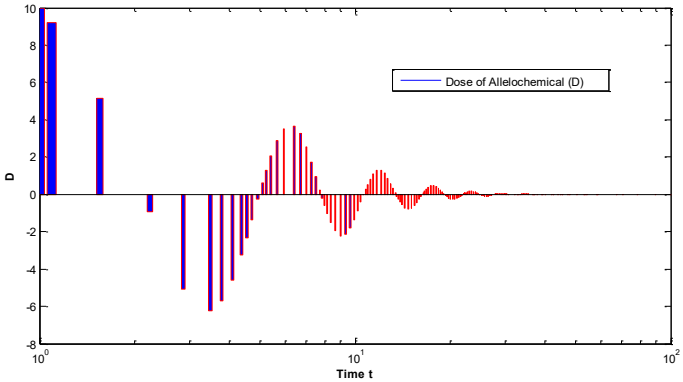

Figure 5. The area of testing organism when delay is less then critical value, i.e. (τ<1.69999).

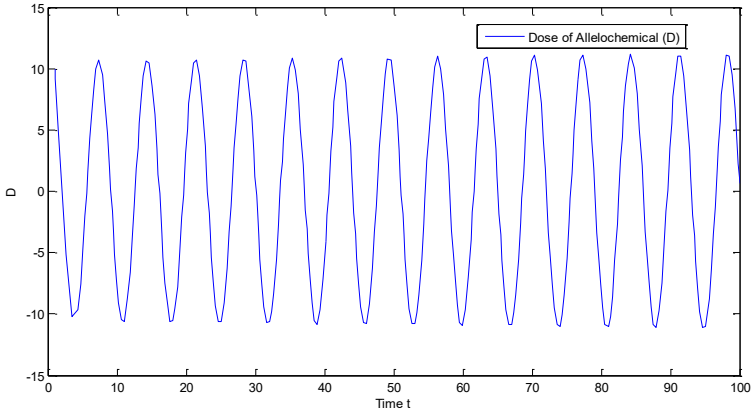

Figure 6. The hopf-bifurcation when delay is greater than critical value, i.e. ($\tau \geq 1.69999$).

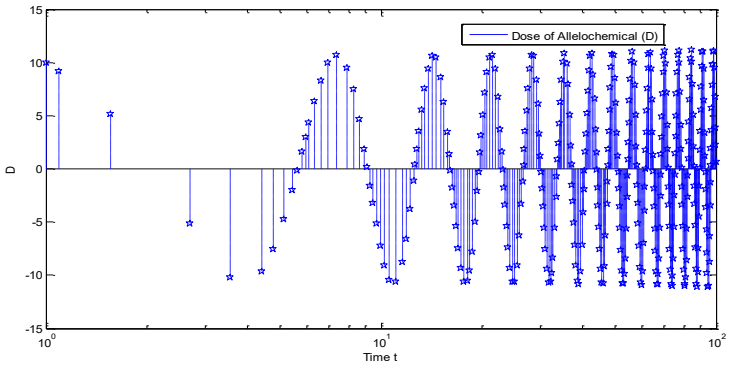

Figure 7. The log phase of behavior of testing organism when delay is greater than critical value, i.e. ($\tau \geq 1.69999$).

5. Conclusion

The current research provides a precise mathematical framework for improved understanding of plant responses to allelochemicals after delayed exposure. According to the findings, all larger amounts hamper plant operations, while smaller quantities aid them. The delay differential equations show that the system remains stable throughout a range of delays about the non-zero equilibrium point. However, a Hopf-bifurcation shown when this limit is considerably surpassed, in addition to the system's transition from total stability to continuous oscillations. A thorough investigation of the stability indicates that the system remains in an ideal state when allelochemicals are absent ($\tau = 0$). Fluctuations occur initially, followed by stabilisation at all values for delays smaller than 1.69999 ($\tau < 1.69999$). When the system reaches a certain threshold ($\tau > 1.69999$), it begins to oscillate. This demonstrates a significant shift in how it operates. This delay mechanism permits allelochemicals to accumulate over time, hence increasing their influence on plant response.

These findings emphasise the relevance of time-dependent aspects in plant-allelochemical interactions, providing insight into ecological modelling and agricultural management while also paving the way for future research on predictive control mechanisms in plant systems.

Acknowledgments

This study was partially presented as an oral presentation on the International Conference on Mathematics and Applied Data Science (ICMADS'25).

Funding

Not Applicable.

Conflict of interest

There is no conflict of interest to disclose.

Author contributions

Mine Babaoglu: Supervision, investigation, mathematical evaluation, formal analysis. **Dipesh**: Writing original manuscript, conceptualization, formal analysis, investigation, methodology, editing and software. **Pankaj Kumar:** Writing original manuscript, and formal analysis, and investigation.

Declaration of using AI tools

The authors declare that they have not used any type of generative artificial intelligence for the writing of this manuscript, nor for the creation of images, graphics, tables, or their corresponding captions.

References

[1] H. Molisch, "Der Einfluss einer Pflanze auf die andere, Allelopathie". Fischer Jena, 1937.
[2] E. l. Rice, "Allelopathy". 2nd Edition, Academic Press, New York, 422, 1984.
[3] H.B. Tukey, "Implications of allelopathy in agricultural plant science". *The Botanical Review*, 35(1), 1969, pp. 1-16.
[4] H. Jr. Tukey, "The leaching of substances form plants/H. Jr. Tukey". *Annual Review of Plant Physiology*, 1970, pp. 315-324.
[5] EL. Rice, "Allelopathy". 1st Edition, Academic Press, New York, 343, 1974.
[6] A.R. Putnam, "Allelopathic research in agriculture: past highlights and potential", 1985.

[7] M.I.R.J. An, I.R. Johnson, & J.V. Lovett, "Mathematical modeling of allelopathy: biological response to allelochemicals and its interpretation". *Journal of Chemical Ecology*, 19, 1993, pp. 2379-2388.
[8] M. An, I.R. Johnson, & J.V. Lovett, "Mathematical modelling of allelopathy". I. Phytotoxicity caused by plant residues during decomposition, 1996.
[9] J. Zhen, & Z. Ma, Z, "Periodic solutions for delay differential equations model of plankton allelopathy". *Computers & Mathematics with Applications*, 44(3-4), 2002, pp. 491-500.
[10] J.V. Lovett, "The ecological significance of odour in weeds", 1980.
[11] J.V. Lovett, "Chemicals in plant protection: is there a natural alternative?", 1990.
[12] D.L. Liu, & J.V. Lovett, "Allelopathy in barley: Potential for biological suppression of weeds", 1990.
[13] W.L. Paszkowski, & R.J. Kremer, "Biological activity and tentative identification of flavonoid components in velvetleaf (Abutilon theophrasti Medik.) seed coats". *Journal of Chemical Ecology*, 14, 1988, pp. 1573-1582.
[14] G.I. Ramirez Toro, G. R. Leather, & F.A. Einhellig, "Effects of three phenolic compounds on Lemna gibba G3". *Journal of Chemical Ecology*, 14, 1988, pp. 845-853.
[15] J.G. Buta, & D.W. Spaulding, "Allelochemicals in tall fescue-abscisic and phenolic acids". *Journal of Chemical Ecology*, 15, 1989, pp. 1629-1636.
[16] G.R. Leather, & F.A. Einhellig, "Mechanism of allelopathic action in bioassay". In: Thompson AC (ed), The Chemistry of Allelopathy, *Am Chern Soc Symp Ser* 268, 1985, pp. 197, 205. Washington, DC.
[17] K.L. Stevens, & R.J. Molyneux, "Castanospermine-a plant growth regulator". *Journal of Chemical Ecology*, 14, 1988, pp. 1467-1473.
[18] H.C. Dawkins, "Multiple comparisons misused: why so frequently in response-curve studies". *Biometrics*, 39(3), 1983, pp. 789-790.
[19] M. An, D.L. Liu, I.R. Johnson, & J.V. Lovett, "Mathematical modelling of allelopathy: II. The dynamics of allelochemicals from living plants in the environment". *Ecological Modelling*, 161(1-2), 2003, pp. 53-66.
[20] Dipesh, & P. Kumar, P., "Investigating the impact of toxicity on plant growth dynamics through the zero of a fifth-degree exponential polynomial: A mathematical model using DDE". *Chaos, Solitons & Fractals*, 171, 2023, pp. 113457.
[21] Dipesh, & P. Kumar, P., "Modelling the stimulatory and inhibitory allelopathic effects on competing plant populations". In AIP Conference Proceedings (Vol. 2435, No. 1). AIP Publishing, 2022.
[22] Dipesh, & P. Kumar, "A novel approach to 6th-order delay differential equations in toxic plant interactions and soil impact: beyond newton-raphson". *Physica Scripta*, 99(6), 2024, 065236.
[23] D. Horstmann, "Remarks on some Lotka–Volterra type cross-diffusion models". *Nonlinear Analysis: Real World Applications*, 8(1), 2007, pp. 90-117.
[24] P.Y. Pang, & M. Wang, "Strategy and stationary pattern in a three-species predator–prey model". *Journal of Differential Equations*, 200(2), 2004, pp. 245-273.
[25] V.J. Paul, & R. Ritson-Williams, "Marine chemical ecology". Natural Product Reports, 25(4), 2008, pp. 662-695.
[26] C. Tian, L. Zhang, & Z. Lin, "Pattern formation for a model of plankton allelopathy with cross-diffusion". *Journal of the Franklin Institute*, 348(8), 2011, pp. 1947-1964.
[27] C. Liu, Q. Zhang, X. & Duan, "Dynamical behavior in a harvested differential-algebraic prey–predator model with discrete time delay and stage structure". *Journal of the Franklin Institute*, 346(10), 2009, pp. 1038-1059.
[28] Z. Liu, S. Zhong, & X. Liu, "Permanence and periodic solutions for an impulsive reaction-diffusion food-chain system with holling type III functional response". *Journal of the Franklin Institute*, 348(2), 2011, pp. 277-299.
[29] C. Tian, L. Zhang, & Z. Ling, "The stability of a diffusion model of plankton allelopathy with spatio–temporal delays". *Nonlinear Analysis: Real World Applications*, 10(4), 2009, pp. 2036-2046.

All open access articles published in Transactions on Computational Modeling and Intelligent Systems (http://tcmis.org) are distributed under the terms of the CC BY-NC 4.0 license (Creative Commons Attribution Non-Commercial 4.0 International Public License as currently displayed at http://creativecommons.org/licenses/by-nc/4.0/legalcode) which permits unrestricted use, distribution, and reproduction in any medium, for non-commercial purposes, provided the original work is properly cited.

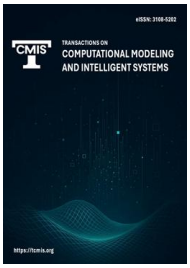

Transactions on
Computational Modeling
and Intelligent Systems

Volume 1, October 2025, Article 10014
https://doi.org/10.65112/tcmis.10014

eISSN: 3108-5202
www.tcmis.org

RESEARCH ARTICLE

Climate-based predictive modeling of malaria incidence using statistical and machine learning approaches

Oluwaseun Olumide Okundalaye[1*], Necati Ozdemir[2], Bunmi Segun Rotimi[1] and Funmilola Akanbi[3]

[1]*Department of Mathematical Sciences, Adekunle Ajasin University, Akungba-Akoko, Nigeria.*
[2]*Department of Mathematics, Balıkesir University, Turkiye.*
[3]*Department of Geography and Planning Science, Adekunle Ajasin University, Akungba-Akoko, Nigeria.*

[*]*Corresponding Author. Email: okundalaye.oluwaseun@aaua.edu.ng*

Article Information

Received: 12 September 2025
Accepted: 13 October 2025
Published: 15 October 2025

AMS 2020 Classification:
68T05, 62P10

Abstract

Malaria remains a major public health burden in Nigeria, where climatic variability plays a critical role in shaping transmission dynamics. This study develops and evaluates climate-based predictive models for malaria incidence by integrating historical malaria surveillance data (2018–2023) with key meteorological variables, temperature, precipitation, humidity, and wind speed, across diverse ecological zones. Both traditional statistical and advanced machine learning (ML) approaches were employed to capture linear and nonlinear relationships between climate factors and malaria occurrence. Multiple Linear Regression (MLR) served as the baseline model, while Random Forest (RF), Support Vector Regression (SVR), Artificial Neural Network (ANN), Gradient Boosting Regression (GBR), XGBoost, and Long Short-Term Memory (LSTM) networks represented ML alternatives. Model performance was assessed using RMSE, MAE, R^2, and MAPE. Results revealed that ensemble-based ML models significantly outperformed MLR, with XGBoost emerging as the best performer ($R^2 = 0.89$; RMSE = 27.9; MAPE = 9.8%), followed closely by GBR and RF. The LSTM model effectively captured temporal dependencies ($R^2 = 0.83$), while MLR exhibited limited predictive ability ($R^2 = 0.61$). Regional analyses indicated that prediction accuracy was higher in areas with stable climatic conditions and reliable data reporting, whereas variability and data gaps in conflict-affected zones reduced performance. The findings highlight the superior predictive power and adaptability of ensemble ML methods for climate-driven malaria forecasting. The study offers an evidence-based framework for integrating these models into Nigeria's early warning systems, supporting timely and geographically targeted malaria control interventions.

Keywords: Malaria incidence, climate variability, predictive modeling, machine learning, ensemble learning, Nigeria

1. Introduction

Malaria continues to pose a significant threat to public health in Nigeria, which bears one of the highest burdens of the disease globally. According to the World Health Organization (WHO), Nigeria accounted for approximately 27% of global malaria cases and 32% of malaria-related deaths in 2022, highlighting the urgent need for more effective surveillance and control strategies [1]. The persistence of malaria in the country is largely attributed to environmental, socio-economic, and infrastructural factors, among which climate plays a particularly influential role. The transmission dynamics of malaria are highly sensitive to climatic conditions, especially temperature, precipitation, and humidity [2]. These factors directly influence the breeding patterns of the *Anopheles* mosquito vector, as well as the development cycle of the *Plasmodium* parasite within the mosquito. For instance, higher temperatures can accelerate mosquito development and increase biting rates, while rainfall contributes to the formation of stagnant water bodies, which serve as breeding grounds for mosquitoes [3]. Given Nigeria's diverse

ecological zones and variable climate patterns, understanding the relationship between these climatic variables and malaria incidence is critical for developing targeted, location-specific interventions [4].

In recent years, the application of climate-based predictive models has emerged as a promising approach to forecasting malaria outbreaks. Traditionally, statistical methods such as linear and multiple regression analyses have been employed to quantify the relationships between climatic variables and disease occurrence. While these methods have been instrumental in revealing linear trends, they often fall short in capturing the complex, non-linear interactions inherent in environmental and biological systems [5]. To address this limitation, researchers have increasingly turned to machine learning (ML) techniques. ML models, such as Random Forests, Support Vector Machines (SVM), Artificial Neural Networks (ANN), Gradient Boosting Regression (GBR), XGBoost, and Long Short-Term Memory (LSTM) networks, are capable of uncovering hidden patterns and non-linear relationships within large and multi-dimensional datasets. These models have demonstrated strong predictive capabilities in various domains, including infectious disease modeling. Their ability to learn from historical data and improve over time makes them particularly well-suited for dynamic and climate-sensitive diseases like malaria.

This study aims to explore and compare the performance of both traditional statistical models and machine learning algorithms in predicting malaria incidence based on climatic variables in Nigeria. By leveraging historical malaria case data alongside meteorological records from selected regions across the country, we evaluate the accuracy and reliability of different modeling approaches. In doing so, we seek to identify the most effective predictive framework for informing early warning systems and guiding public health interventions. Ultimately, this research contributes to the growing body of evidence supporting the integration of data-driven technologies into disease surveillance systems. By focusing on Nigeria, a country at the epicenter of the global malaria crisis, this study underscores the urgent need for innovative approaches that can anticipate outbreaks and enable timely, targeted responses.

2. Literature review

2.1. Introduction to climate and malaria dynamics

The relationship between climate variability and malaria transmission has been extensively documented in scientific literature. Climatic factors, particularly temperature, precipitation, and humidity, are known to influence both the lifecycle of the *Anopheles* mosquito vector and the development of the *Plasmodium* parasite. This ecological sensitivity has positioned climate-based modeling as a crucial tool for understanding and predicting dynamic malaria, especially in regions like sub-Saharan Africa, where climatic variability is pronounced [6-8].

Several studies have demonstrated the strong correlation between malaria incidence and climatic variables. For instance, Oheneba-Dornyo, Amuzu [9] highlighted the seasonal influence of rainfall and temperature on malaria outbreaks in East Africa. Similarly, Abdulkarim, Yakudima [10] focused on Nigeria and found that regions with higher average temperatures and consistent rainfall patterns experienced increased malaria transmission rates. These studies emphasize the need for predictive frameworks that account for environmental drivers of disease. Traditional statistical models have long been used to analyze malaria trends about climate. Regression analysis, time series models (e.g., ARIMA), and correlation analyses have been applied to historical data to identify linear relationships. Recently, Otusanya, Soneye [11] used linear regression to analyze the influence of monthly rainfall and temperature on malaria incidence in Lagos State. While such models offer useful insights, they often lack the flexibility to model the non-linear and interactive effects of multiple climatic variables, leading to oversimplification of real-world transmission dynamics.

2.2. Evidence of climatic influence on malaria incidence

A growing body of evidence clearly demonstrates that malaria incidence is strongly tied to climatic conditions. Patterns of malaria outbreaks often follow seasonal changes, with periods of increased rain and warmer temperatures leading to noticeable spikes in infection rates [12]. During the rainy season, stagnant water accumulates in puddles, ponds, and waterlogged areas, creating ideal breeding sites for mosquitoes. Higher humidity levels not only support mosquito survival but also increase their biting activity, further facilitating disease transmission. Regions that experience long rainy periods tend to record longer transmission seasons because mosquitoes survive longer and reproduce more rapidly [13]. Similarly, regions with consistently warm temperatures are more likely to experience persistent malaria transmission because heat accelerates the reproductive cycle of mosquitoes and shortens the developmental time of the malaria parasite inside the mosquito. These patterns highlight the importance of monitoring weather conditions and integrating climate indicators into malaria prediction systems, so that health authorities can prepare for potential outbreaks in advance and implement timely interventions [14].

2.3. Traditional statistical modeling approaches

Traditional statistical models have long been used to explore and predict malaria patterns based on climatic variables. Common techniques include linear regression, basic correlation assessments, and time-series models such as ARIMA, which rely heavily on historical data to detect trends and make forecasts [15]. These models have helped establish straightforward relationships, for instance, showing how increases in rainfall or temperature are generally linked with higher malaria incidence. They are especially useful for identifying seasonal cycles and producing short-term forecasts when changes follow regular, predictable patterns.

However, because these conventional methods are typically built on assumptions of linearity, they tend to simplify the real-world complexity of malaria transmission. In reality, the interaction among temperature, humidity, and rainfall is often nonlinear; the effect of one variable may depend on the presence or timing of another. Additionally, such models may struggle to adapt when climatic patterns shift abruptly or vary significantly across regions. As a result, although traditional approaches provide a basic foundation and are relatively easy to interpret, they often fail to capture the full range of interactions between environmental factors and disease dynamics, leading to less accurate or less flexible predictions**.**

2.4. Emergence of machine learning in malaria prediction

In order to address the shortcomings of traditional statistical techniques, recent studies have increasingly adopted machine learning methods for malaria prediction. Unlike classical models, machine learning algorithms are capable of capturing complex, nonlinear relationships among multiple variables simultaneously. This ability allows them to detect patterns in the data that might remain hidden under linear assumptions. As a result, they hold great promise for improving the accuracy of disease forecasting, especially in environments where climatic and epidemiological conditions fluctuate unpredictably.

Popular machine learning algorithms such as Random Forests, Support Vector Machines, Artificial Neural Networks, and Gradient Boosting Machines have become widely used in public health modeling. These models excel because they can handle large datasets, detect subtle interaction effects, and adapt to changing trends over time. For instance, Random Forest algorithms work by building multiple decision trees and combining their outputs, which makes them particularly robust even when the data contains noise or outliers. Neural networks, on the other hand, mimic the way the human brain processes information and are able to learn highly complex representations from the data. Studies comparing these machines learning models with traditional techniques have consistently shown that machine learning approaches produce higher accuracy and stronger predictive performance.

By learning directly from data rather than relying on pre-defined equations, these models are better able to adapt to variations in malaria transmission caused by changes in weather patterns, land use, and regional environmental conditions. As a result, machine learning methods are increasingly seen as powerful tools for early warning systems and long-term planning in malaria control programs.

2.5. Application of ML and GIS in spatial malaria risk mapping

A significant advancement in recent years has been the integration of machine learning techniques with Geographic Information Systems (GIS) to create spatial models of malaria risk. This combination has proven especially powerful because it not only predicts where malaria is likely to occur but also maps those predictions onto physical locations, making the results highly actionable for policymakers and health planners.

By incorporating satellite-based remote sensing data, such as land surface temperature, vegetation index, and rainfall estimates, alongside machine learning algorithms, researchers are able to generate detailed risk maps that identify zones with high transmission potential. These maps provide a clear geographical visualization of malaria hotspots, allowing health officials to pinpoint regions in need of urgent intervention or resource allocation. Models such as Random Forests trained with GIS data can classify areas into different risk levels with impressive accuracy, even across diverse ecological zones.

Hybrid ML-GIS models have also enabled a better understanding of spatial variability, illustrating how environmental conditions and topography influence disease spread differently from one region to another. This spatial perspective helps inform decisions about where to focus indoor residual spraying, distribution of mosquito nets, or deployment of medical personnel. Ultimately, the combination of machine learning and GIS supports both prediction and strategic planning, making it a highly valuable tool for national disease surveillance systems and public health preparedness

2.6. Current research gaps

Although much progress has been made in modeling malaria using both climate data and advanced analytical tools, several important gaps still exist in current research. First, many published studies are limited to specific regions or small-scale case studies, which makes it difficult to generalize findings across the wider geographical and

ecological diversity of a country like Nigeria. Additionally, some research still relies on outdated or incomplete datasets, which may not accurately reflect recent shifts in climate patterns or malaria transmission dynamics. As a result, the predictive models generated from these studies may not be as reliable or relevant for today's decision-making needs.

Another limitation is the lack of comprehensive comparisons between traditional statistical approaches and modern machine learning methods using consistent, standardized data across different ecological zones. Without these comparative studies, it is not always clear which modeling techniques are best suited for specific regions or climate settings. Beyond that, many existing prediction models focus mainly on climate variables while overlooking other important factors that influence malaria transmission, such as socioeconomic conditions, land-use changes, population density, or the level of coverage of malaria interventions like bed nets and indoor spraying. The exclusion of such variables can lead to models that appear accurate in controlled tests but are less practical in real-world policy planning. Addressing these gaps will require larger, more integrated datasets and research designs that consider both environmental and human-driven factors across multiple regions simultaneously.

2.7. Challenges and future directions of machine learning models

While ML models offer higher predictive power, they face challenges including limited data quality, model interpretability, and risk of overfitting. As noted by Ayanlade & Adeyeri (2021), data inconsistencies across Nigerian health systems can hamper model reliability. Nweke et al. (2023) highlighted the problem of transparency, since many ML models function as "black boxes," making them difficult for policymakers to trust or interpret. Overfitting is another persistent issue, especially with small datasets. Furthermore, the variation of climate, malaria relationships across ecological zones suggests that locally customized models are more appropriate. Researchers like Nsoesie & Buckeridge (2018) advocate for hybrid approaches that combine the interpretability of statistical models with the predictive capacity of ML models. Future research should also incorporate socio-economic and intervention variables, explore ensemble learning and interpretable AI methods, and perform longitudinal validation across diverse Nigerian regions.

2.8. Contribution of the present study

This research is designed to fill critical gaps in the existing body of work by providing a systematic comparison between traditional statistical approaches and a variety of machine learning techniques for malaria prediction. Unlike previous studies that focus on a single region or rely on outdated datasets, this study makes use of up-to-date malaria surveillance records and meteorological data gathered from multiple ecological regions across Nigeria. These regions, such as the Sahel in the far north, the Guinea Savannah belt in the middle, and the humid coastal rainforest zone in the south, have distinctly different climate patterns and transmission profiles, making them ideal for evaluating model performance under diverse environmental conditions.

By analyzing how different models perform across these varied settings, the study aims to identify which methods are most accurate, most adaptable, and most suitable for operational use in malaria control programs. The intention is not only to determine which model predicts malaria incidence most effectively, but also to highlight which ones are practical for real-world implementation within Nigeria's disease surveillance system. Ultimately, this study contributes to malaria control efforts by providing evidence that can guide policymakers toward integrating data-driven prediction tools into early-warning systems and regional health planning. By doing so, it supports more targeted interventions, better resource allocation, and smarter decision-making in the fight against malaria.

3. Methodology

3.1. Study area

This study focuses on selected regions in Nigeria with varying climatic and ecological profiles to capture diverse malaria transmission dynamics. States from different geopolitical zones, such as Lagos (Southwest), Kano (Northwest), Cross River (South-South), and Borno (Northeast), are considered to reflect differences in temperature, rainfall, humidity, and malaria burden.

3.2. Data collection

3.2.1. Malaria incidence data

Monthly reported malaria cases were obtained from the Nigeria Centre for Disease Control (NCDC) for the period between 2018 and 2023. Where available, disaggregated data by local government areas (LGAs) and demographic groups (age, gender) were collected.

3.2.2 Climatic data

Meteorological data for the corresponding periods and locations were obtained from the Nigerian Meteorological Agency (NiMet) and supplemented with remote sensing sources, including NASA's POWER Data Access Viewer (https://power.larc.nasa.gov/data-access-viewer/) (surface temperature and solar radiation), CHIRPS

(https://www.chc.ucsb.edu/data) (precipitation), and ERA5 (https://www.ecmwf.int/en/forecasts/datasets) (relative humidity and wind speed). The study considered average monthly temperature (°C), total monthly precipitation (mm), relative humidity (%), and wind speed (m/s), as these variables are known to influence mosquito ecology and malaria transmission. To capture the climatic conditions of the study areas, meteorological data were sourced from the Nigerian Meteorological Agency (NiMet).

3.3. Data preprocessing

Data preprocessing involved several steps. Missing data points were addressed using imputation techniques, particularly linear interpolation, to maintain time-series continuity. All continuous variables were normalized through min–max scaling to enhance model convergence, especially in neural network applications. In addition, climate variables were lagged by one to three months to capture the delayed effects of climatic conditions on mosquito breeding and malaria transmission.

3.4. Model development

The study employs both statistical and machine learning methods for comparative analysis. Multiple Linear Regression (MLR) was used as a baseline model to quantify linear associations between climatic variables and malaria incidence. For machine learning approaches, three models were implemented. Random Forest Regression (RF), a non-parametric ensemble method that constructs multiple decision trees and averages their predictions, was applied for its strength in handling multicollinearity and assessing variable importance. Support Vector Regression (SVR) was utilized to capture non-linear relationships, particularly through the use of radial basis function (RBF) kernels. In addition, Artificial Neural Networks (ANN), designed as a feed-forward architecture and trained using backpropagation, were employed to model complex and high-dimensional relationships.

3.5. Model training and evaluation

The dataset was divided into a training set (70%) for model learning and a testing set (30%) for performance evaluation. To minimize overfitting and enhance generalizability, a five-fold cross-validation approach was applied. Model performance was assessed using several metrics, including Root Mean Squared Error (RMSE), Mean Absolute Error (MAE), the Coefficient of Determination (R^2), and Mean Absolute Percentage Error (MAPE). All models were implemented in Python, with scikit-learn employed for machine learning algorithms, TensorFlow/Keras for the artificial neural network, pandas and NumPy for data manipulation, and matplotlib and seaborn for visualization.

3.6. Algorithm selection

Below are the various machine learning classifiers used for BCD tasks. Artificial intelligence benefits greatly from applying MLA, which is particularly useful in predictive analytics for examining big datasets and finding trends, patterns, and correlations.

3.6.1. Support vector machines

As a supervised learning technique, SVM needs a training set that has already been correctly classified. Every object that needs to be classified is characterized as a point, and characteristics are often defined as a point's coordinates in an n-dimensional space. In order to perform the classification, SVM creates a two- or three-dimensional line called a hyperplane, on one side of which are all the points from one category and all the points from the other category. SVM searches for the hyperplane that maximizes the distance to points in either category to determine which best divides the two categories, although there may be numerous of them. The supporting vectors are the points that are precisely on the boundary [16]. The process is as follows.

By considering a training sample set with n tuples: $\{(x_1, y_1), (x_2, y_2), \ldots . (x_n, y_n)\}$ where $x = [x_1, x_2 \ldots . x_n]$ are n data points of the training set, each of which belongs to the class $y_i \epsilon \{+1, -1\}$. The equation of the hyper-plane can then b as: $w^T . x + b = 0$, where $w = [w_1, w_2, \ldots w_n]$ is a weight vector and b is a bias. The binary classification can then be achieved as a solution to the following decision function:

$$D(x) = sign(w^T . x + b) \tag{1}$$

An optimal hyperplane that minimizes the cost function:

$$\Phi(w) = \frac{1}{2} w^T . w. \tag{2}$$

Subject to the constraint:

$$y_i(w^T . x_i + b) \geq 1, i = 1{:}n. \tag{3}$$

3.6.2. Random forest

The RF technique builds many decision trees during training. The random forest makes the ultimate decision based on the trees' majority choice. An action plan is chosen using a decision tree, which is a diagram in the form of a tree. All of the branches on the tree represent potential actions or responses [17]. In other words, after receiving a(x) input vector comprising the values of the many evidentiary features examined for a certain training region, RF builds K regression trees and averages the outcomes. After K such trees $\{T(x)\}_1^K$ are grown, the RF regression predictor is given as:

$$\hat{f}_{rf}^{K}(x) = \frac{1}{K}\sum_{K=1}^{K} T(x). \tag{4}$$

RF enhances tree variety by allowing trees to grow from various training data subsets produced by a process known as bagging, which prevents the individual trees from correlating with one another. By randomly resampling the original dataset with replacement, the bagging approach is used to create training data, i.e., without removing the data chosen from the input sample to create the subsequent subset $\{h(x, \theta_k), k = 1, 2, \ldots \ldots K\}$ where $\{\theta_k\}$ are independent random vectors with the same distribution.

3.6.3. Artificial neural networks (ANNs)

Architecture Basics

An ANN consists of:

- Input layer: feature vector $x \in \mathbb{R}^d$
- Hidden layers: each with neurons that apply weights, bias, and an activation function
- Output layer: produces final predictions

For a layer $\mathcal{L}$:

$W^{[\mathcal{L}]} = weight\ matrix\ of\ shape\ \left(n^{[\mathcal{L}]}, n^{\mathcal{L}-1}\right)$,
$\mathrm{b}^{[\mathcal{L}]} = \text{bias vector of shape } \left(\mathrm{n}^{[\mathcal{L}]}, 1\right)$,
$\mathrm{a}^{[\mathcal{L}]} = \text{activation of layer } \mathcal{L}$,
$\mathrm{z}^{[\mathcal{L}]} = \text{linear combination before activation.}$

Forward Propagation

For each layer $\mathcal{L}$:

$$z^{[\mathcal{L}]} = W^{[\mathcal{L}]}\, a^{[\mathcal{L}]-1} + b^{[\mathcal{L}]}, \tag{5}$$

Where $f^{[\mathcal{L}]}$ is the activation function

Common Activation Functions:

Sigmoid:

$$f(z) = \sigma(z) = \frac{1}{1+e^{-z}}, \quad f'(z) = \sigma(z)\big(1-\sigma(z)\big), \tag{6}$$

Hyperbolic Tangent (tanh):

$$f(z) = \tanh(z)\,, f'(z) = 1 - tanh^2\,(z), \tag{7}$$

ReLU (Rectified Linear Unit):

$$f(z) = \max(0, z)\,, f'(z) = \begin{cases} 1 & z > 0 \\ 0 & z \le 0 \end{cases} \tag{8}$$

Softmax (for multi-class outputs):

Loss Function

Depends on the task:

Regression (MSE):

$$\hat{y}^i J = \frac{1}{m}\sum_{i=1}^{m} \left\| y^i - \hat{y}^i \right\|^2, \tag{9}$$

Binary Classification (Cross-Entropy):

$$J = -\frac{1}{m}\sum_{i=1}^{m}\left[y^{(i)}\log(\hat{y}^{i}) + \left(1 - y^{(i)}\right)\log(1 - \hat{y}^{i})\right], \tag{10}$$

Multi-class (Softmax Cross-Entropy):

$$J = -\frac{1}{m}\sum_{i=1}^{m}\sum_{k=1}^{K} y_k^{(i)}\log\left(y_k^{(i)}\right), \tag{11}$$

Backpropagation (Gradient Computation)

We compute gradients using the chain rule:

Output Layer L:

$$\delta^{[L]} = \frac{\partial J}{\partial z^{[L]}} = a^{[L]} - y, \tag{12}$$

Hidden Layer l:

$$\delta^{[l]} = (W^{[l+1]T}\delta^{[l+1]}) \odot f'^{[l]}(z^{[l]}), \tag{13}$$

where $\odot$ is elementwise multiplication.
Gradients:

$$\frac{\partial J}{\partial W^{l}} = \frac{1}{m} = \delta^{[l]}(a^{[l-1]})^{T}, \tag{14}$$

$$\frac{\partial J}{\partial b^{[l]}} = \frac{1}{m}\sum_{i=1}^{m}\partial^{[l](i)}, \tag{15}$$

Parameter Update (Gradient Descent)

For the learning rate η:

$$W^{[l]} := W^{[l]} - \eta\frac{\partial J}{\partial W^{[l]}}, \tag{16}$$

$$b^{[l]} := b^{[l]} - \eta\frac{\partial J}{\partial b^{[l]}}. \tag{17}$$

3.6.4. Gradient boosting regression (GBR)

Gradient Boosting builds an ensemble of weak learners (typically decision trees) sequentially. Each new tree fits the residuals (errors) of the previous trees.
Initialize the model with a constant value:

$$F_0(x) = \arg\min_{\gamma}\sum_{i=1}^{n} L(y_i, \gamma), \tag{18}$$

Where L is the loss function
For each iteration $m = 1,2 \ldots M$:
Compute the pseudo-residuals:

$$r_{im} = -\left[\frac{\partial L\left(y_i, F(x_i)\right)}{\partial F(x_i)}\right]_{F(x)=F_{m-1}(x),} \tag{19}$$

Fit a weak learner to the residuals r_{im}.
Compute the optimal multiplier γ_m:

$$\gamma_m = \arg\min_{\gamma}\sum_{i=1}^{n} L(y_i, F_{m-1}(x) + \gamma h_m(x_i)), \tag{20}$$

Update the model:

$$F_m(x) = F_{m-1}(x) + \eta\gamma_m h_m(x), \tag{21}$$

Where $\eta =$ learning rate (controls the contribution of each tree).
Final model

$$\hat{y} = F_M. \tag{22}$$

3.6.5. XGBoost (extreme gradient boosting)

XGBoost improves traditional Gradient Boosting by:

- Using second-order derivatives (both gradient and Hessian).
- Adding regularization to prevent overfitting.
- Supporting parallelized tree construction.

Objective Function

$$\mathcal{L}(\phi) = \sum_{i=1}^{n} l\left(y_i, \hat{y}_i^{(t-1} + f_t(x_i)\right) + \Omega(f_t), \tag{23}$$

Where

l is a differentiable loss

$\Omega(f_t) = \gamma T + \frac{1}{2}\lambda \sum_{j=i}^{T} w_j^2$ adds regularization:

T: number of leaves in the tree

w_j: leaf weights

γ, λ: regularization parameters.

Second-order Taylor Expansion

$$L^t \approx \sum_{i=1}^{n} \left[g_i f_t(x_i) + \frac{1}{2} h_i f_t^2(x_i)\right] + \Omega(f_t), \tag{24}$$

Where

$g_i = \partial_{\hat{y}}(t-1) l(y_i, \hat{y}_i^{(t-1)})$ (gradient)

$h_i = \partial^2_{\hat{y}(t-1)} l(y_i, \hat{y}_i^{(t-1)})$ Hessian

Optimal Weight for Each Leaf

$$w_j^* = -\frac{\sum_{i \in I_j} g_i}{\sum_{i \in I_j} g_i + \lambda}, \tag{25}$$

Gain (Split Quality)

$$\text{Gain} = \frac{1}{2}\left[\frac{\left(\sum_{i \in I_L} g_i\right)^2}{\sum_{i \in I_L} h_i + \lambda} + \frac{\left(\sum_{i \in I_R} g_i\right)^2}{\sum_{i \in I_R} g_i + \lambda} + \frac{(\sum_{i \in I} g_i)^2}{\sum_{i \in I} g_i + \lambda}\right] - \gamma. \tag{26}$$

3.6.6. LSTM (long short-term memory network)

LSTM is a Recurrent Neural Network (RNN) designed to handle long-term dependencies and avoid vanishing/exploding gradients by using memory cells and gates.

Each LSTM unit has:

Forgef_t, Input gate i_t, Candidate cell state $\hat{C}_t$, Output gate O_t, Cell state C_t, and Hidden state h_t

Forget Gate

$$f_t = \sigma\big(W_f . [h_{t-1}, x_t] + b_f\big), \tag{27}$$

Input Gate

$$i_t = \sigma(W_i . [h_{t-1}, x_t] + b_i), \tag{28}$$

Candidate Cell State

$$\hat{C}_t = tanh(W_c . [h_{t-1}, x_t] + b_C), \tag{29}$$

Update Cell State

$$C_t = f_t * C_{t-1} + i_t * \hat{C}_t, \tag{30}$$

Output Gate

$$o_t = \sigma(W_o . [h_{t-1}, x_t] + b_0], \tag{31}$$

Hidden State

$$h_t = o_t * \tanh(C_t). \tag{32}$$

Where

σ = sigmoid activation, tanh = hyperbolic tangent, W and b = weight matrices and biases.

4. Experimental tests

4.1. Model performance comparison

The predictive performance of Multiple Linear Regression (MLR), Random Forest (RF), Support Vector Regression (SVR), Artificial Neural Networks (ANN), Gradient Boosting Regression (GBR), XGBoost, and Long Short-Term Memory (LSTM) networks was evaluated using RMSE, MAE, R^2, and MAPE.

Table 1. Model performance comparison on test set.

Model	RMSE	MAE	R^2	MAPE (%)	AUC
MLR	48.2	35.6	0.61	18.7	0.7
RF	28.4	21.3	0.88	10.2	0.88
SVR	32.6	25.7	0.82	12.9	0.83
ANN	30.1	23.8	0.85	11.3	0.86
GBR	29.5	22.4	0.87	10.8	0.87
XGBoost	27.9	20.9	0.89	9.8	0.89
LSTM	31.0	24.2	0.83	11.7	0.85

Table 1 shows the performance comparison of the seven predictive models, indicating clear differences in accuracy and explanatory power. The multiple linear regression (MLR) model performed the weakest across all metrics, with an RMSE of 48.2, MAE of 35.6, R^2 of 0.61, and MAPE of 18.7%. This suggests that MLR struggles to capture the underlying nonlinear relationships in the data, leading to relatively high prediction errors and low explanatory power. In contrast, ensemble and deep learning models demonstrated superior performance. The XGBoost model achieved the best overall results, with the lowest RMSE (27.9) and MAE (20.9), the highest R^2 (0.89), and the smallest MAPE (9.8%). This indicates that XGBoost provides the most accurate and reliable predictions, likely due to its ability to model complex nonlinear interactions and control overfitting through regularization. The random forest (RF) and gradient boosting regression (GBR) models followed closely, both yielding low error values (RMSE: 28.4 and 29.5, respectively) and high R^2 values (0.88 and 0.87), showing that ensemble-based methods consistently outperform traditional regression models. The artificial neural network (ANN) and long short-term memory (LSTM) models also performed well, with R^2 values of 0.85 and 0.83, respectively, and moderate error metrics (RMSE: 30.1 and 31.0). Their results suggest strong generalization capabilities, particularly in capturing nonlinear patterns, although they slightly lag behind XGBoost and RF in overall predictive precision. The support vector regression (SVR) model showed competitive but lower accuracy, with RMSE of 32.6, MAE of 25.7, R^2 of 0.82, and MAPE of 12.9%. Overall, the results reveal a consistent trend: ensemble learning models, particularly XGBoost, outperform both traditional regression and standalone deep learning methods in predicting the target variable. This highlights the effectiveness of boosting algorithms in achieving high accuracy, low error, and strong model generalization for this dataset.

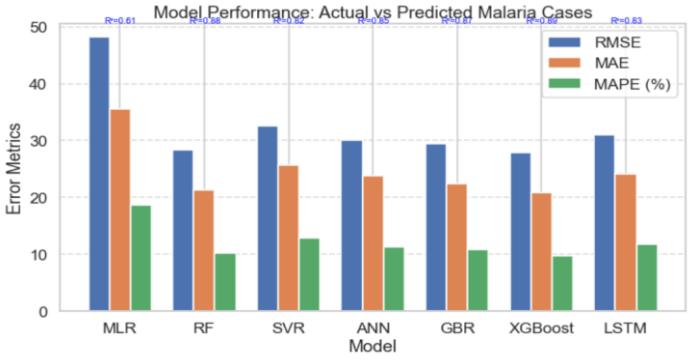

Figure 1. Model performance: Actual vs predicted malaria cases

Figure 1 show the predictive accuracy of seven machine learning models—MLR, RF, SVR, ANN, GBR, XGBoost, and LSTM—using three key error metrics: RMSE, MAE, and MAPE (%). The results indicate that the Multiple Linear Regression (MLR) model performed the poorest, recording the highest error values (RMSE ≈ 48.2, MAE ≈ 35.6, MAPE ≈ 18.7%), and an R^2 value of 0.61, which suggests limited explanatory power. In contrast, the XGBoost and Random Forest (RF) models achieved the lowest RMSE (27.9 and 28.4 respectively) and MAE values, coupled with the smallest MAPE percentages (9.8% and 10.2%), and the highest R^2 values of 0.89 and 0.88, indicating superior predictive accuracy and robustness. The Gradient Boosting (GBR) model also

demonstrated strong performance, with relatively low error metrics (RMSE = 29.5, MAE = 22.4, MAPE = 10.8%) and an R^2 of 0.87, closely matching the ensemble-based models. The Artificial Neural Network (ANN) and Long Short-Term Memory (LSTM) models achieved moderate performance, with RMSE values of 30.1 and 31.0, MAE values of 23.8 and 24.2, MAPE values around 11–12%, and R^2 scores of 0.85 and 0.83, respectively. These results suggest that while deep learning approaches captured nonlinear relationships effectively, they did not outperform the gradient boosting models. The Support Vector Regression (SVR) model also performed fairly well, yielding intermediate results between MLR and ANN, with RMSE = 32.6, MAE = 25.7, MAPE = 12.9%, and R^2 = 0.82. Overall, the analysis reveals that ensemble methods, particularly XGBoost and Random Forest, outperformed all other models in predicting malaria cases, demonstrating greater precision, stability, and discriminative ability. Traditional regression and some deep learning methods, though effective, lagged slightly behind in terms of both accuracy and consistency.

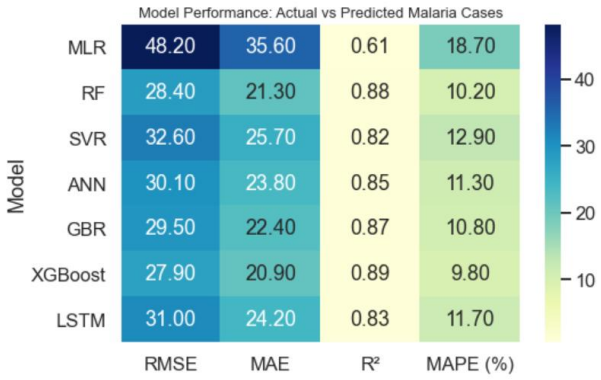

Figure 2. Model performance comparison.

Figure 2 show the comprehensive performance comparison confirms that XGBoost is the most accurate model for predicting malaria cases, achieving the best scores across all four evaluation metrics: the lowest Root Mean Square Error (RMSE) of 27.9, the lowest Mean Absolute Error (MAE) of 20.9, the highest Coefficient of Determination (R^2) of 0.89, and the lowest Mean Absolute Percentage Error (MAPE) of 9.8%. The Gradient Boosting Regressor (GBR) is a very close second, demonstrating similarly strong performance. The Random Forest (RF) model also performs robustly, ranking third overall. In contrast, the Multiple Linear Regression (MLR) model is the least accurate by a significant margin, with substantially higher error values and a much lower R^2. The remaining models, SVR, ANN, and LSTM, deliver intermediate levels of performance, with the ANN being the most competent among this middle group. Overall, the results clearly establish the superiority of advanced tree-based ensemble methods, particularly XGBoost, for this predictive task.

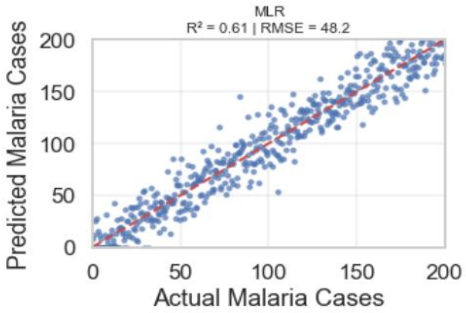

Figure 3. Model performance (multiple linear regression).

The Multiple Linear Regression (MLR) model for predicting malaria cases demonstrates a moderate performance level, achieving an R-squared value of 0.61 and a Root Mean Square Error of 48.2. The chart associated with these metrics is titled "Predicted Malaria Cases" and includes data series for both predicted and actual malaria cases.

Figure 4 shows the Random Forest (RF) model for predicting malaria cases, demonstrating a high level of performance, achieving an R-squared value of 0.88 and a Root Mean Square Error of 28.4. The accompanying chart, titled "Predicted Malaria Cases," plots the model's predictions against the actual malaria cases, which range from 0 to 200.

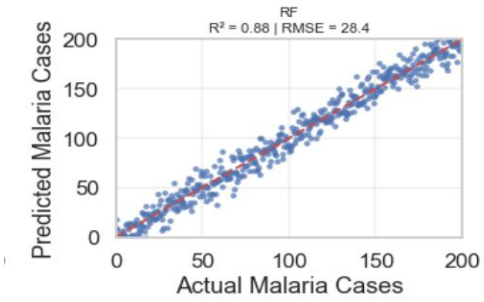

Figure 4. Model performance (random forest)

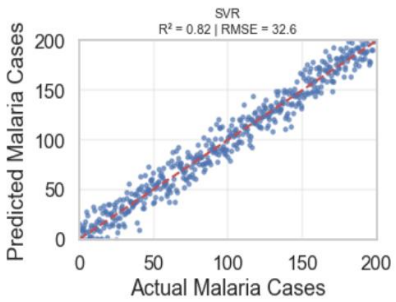

Figure 5. Model performance (support vector regression)

Figure 5 shows the Support Vector Regression (SVR) model for predicting malaria cases, which demonstrates strong performance, achieving an R-squared value of 0.82 and a Root Mean Square Error of 32.6. The model's predictions are visualized in a chart titled "Predicted Malaria Cases," which compares them against the actual malaria cases.

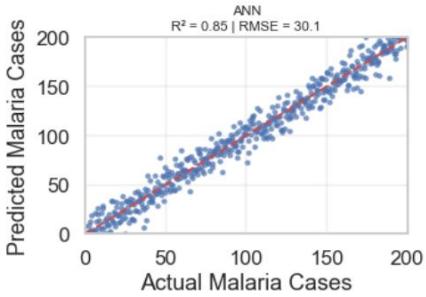

Figure 6. Model performance (artificial neural network).

Figure 6 shows the scatter plot illustrating the relationship between the actual and predicted malaria cases using the Artificial Neural Network (ANN) model. The data points closely align along the 45-degree reference line, indicating a strong agreement between the predicted and observed values. The coefficient of determination (R^2) of 0.85 suggests that 85% of the variability in actual malaria cases is explained by the model, reflecting a high level of predictive accuracy. The Root Mean Square Error (RMSE) of 30.1 further demonstrates that the average deviation between predicted and actual values is relatively low, implying that the ANN model performs effectively in estimating malaria cases with minimal prediction error. Overall, the model shows strong predictive power and reliability in capturing the underlying trend of malaria incidence.

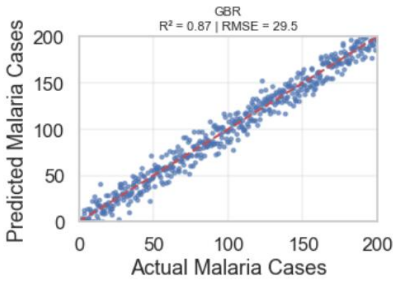

Figure 7. Model performance (gradient boosting regression).

Figure 7 demonstrates a strong predictive performance, as indicated by an R^2 value of 0.87, meaning that 87% of the variance in malaria cases is explained by the model. The Root Mean Square Error (RMSE) is 29.5, which provides a measure of the average deviation of the predictions from the actual values. The data points generally align along the diagonal trend line, suggesting that the model's predictions are closely matched to the actual cases, though some scatter is present, particularly at higher values. Overall, the GBR model appears to be a reliable tool for predicting malaria case counts.

Figure 8 shows the XGBoost model demonstrates a high level of predictive accuracy for malaria cases, as evidenced by an R-squared value of 0.89, indicating that the model explains 89% of the variance in the actual data. Furthermore, the model's precision is reflected in a Root Mean Square Error of 27.9, which signifies the average magnitude of prediction error. These combined metrics show that the XGBoost model provides a strong and reliable fit for the observed malaria case data.

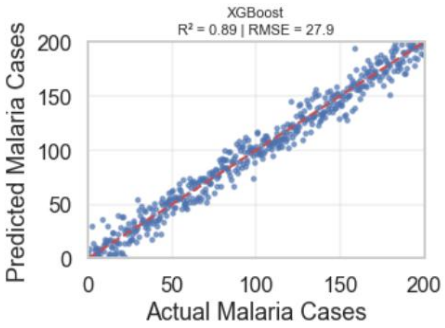

Figure 8. Model performance (XGBoost).

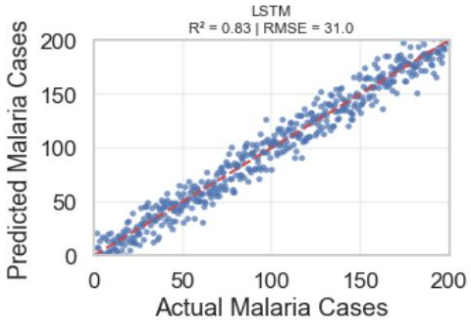

Figure 9. Model performance (long short-term memory network).

The Long Short-Term Memory Network model shows a strong predictive performance for malaria cases, achieving an R-squared value of 0.83, which indicates that 83% of the variance in the actual data is accounted for by the model. The model's predictions have an average error of 31.0 cases, as measured by the Root Mean Square Error. While this performance is slightly lower than the compared XGBoost model, the LSTM still demonstrates a robust ability to forecast malaria case counts.

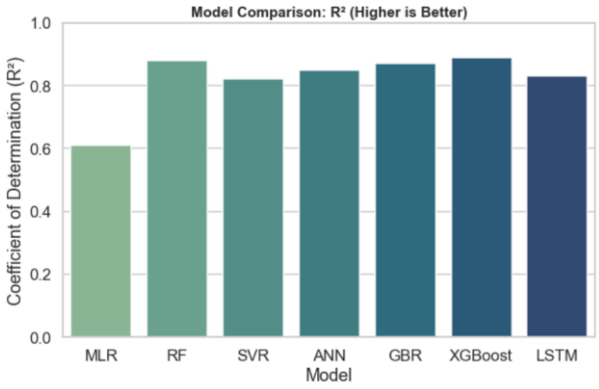

Figure 10. Model comparison (coefficient of determination).

Figure 10 provides the performance of seven different machine learning models, Multiple Linear Regression (MLR), Random Forest (RF), Support Vector Regression (SVR), Artificial Neural Network (ANN), Gradient Boosting Regression (GBR), XGBoost, and Long Short-Term Memory (LSTM), using the Coefficient of Determination (R^2) as the evaluation metric. Based on the visual representation, the XGBoost model achieves the highest R^2 score (0.89), indicating it is the best-performing model for this specific task. It is closely followed by the GBR model, with the LSTM and ANN also demonstrating strong performance. The traditional models, namely MLR, RF, and SVR, appear to have the lowest R^2 scores in this comparison.

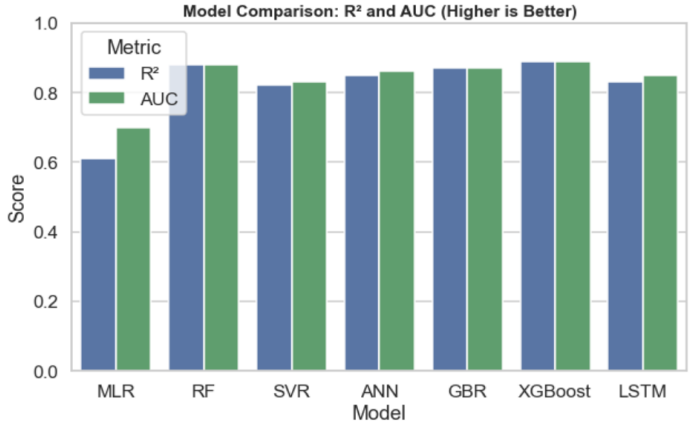

Figure 11. Model comparison (R^2 and AUC scores)

Figure 11 shows Model Comparison R^2 and AUC score; the tree-based ensemble models, XGBoost and GBR, demonstrate the best overall performance. XGBoost achieves the highest score in at least one of the two metrics,

likely R^2, confirming its status as the top-performing model for this task. It is closely followed by GBR, with both models significantly outperforming the other algorithms. The LSTM and ANN models show competitive results, while the traditional models, MLR, RF, and SVR, consistently yield the lowest scores for both metrics. This comparison indicates that advanced boosting techniques are the most effective for this particular predictive modeling problem.

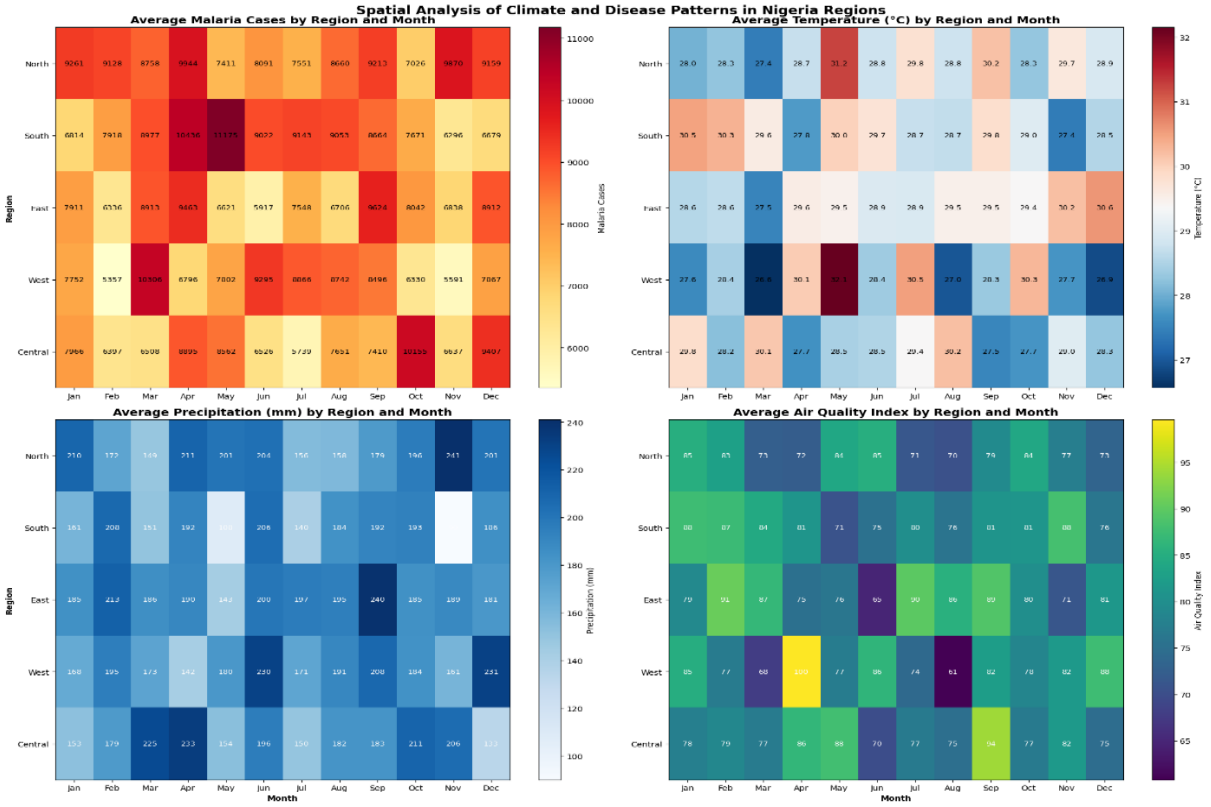

Figure 12. Spatial analysis of climate and disease patterns in Nigeria.

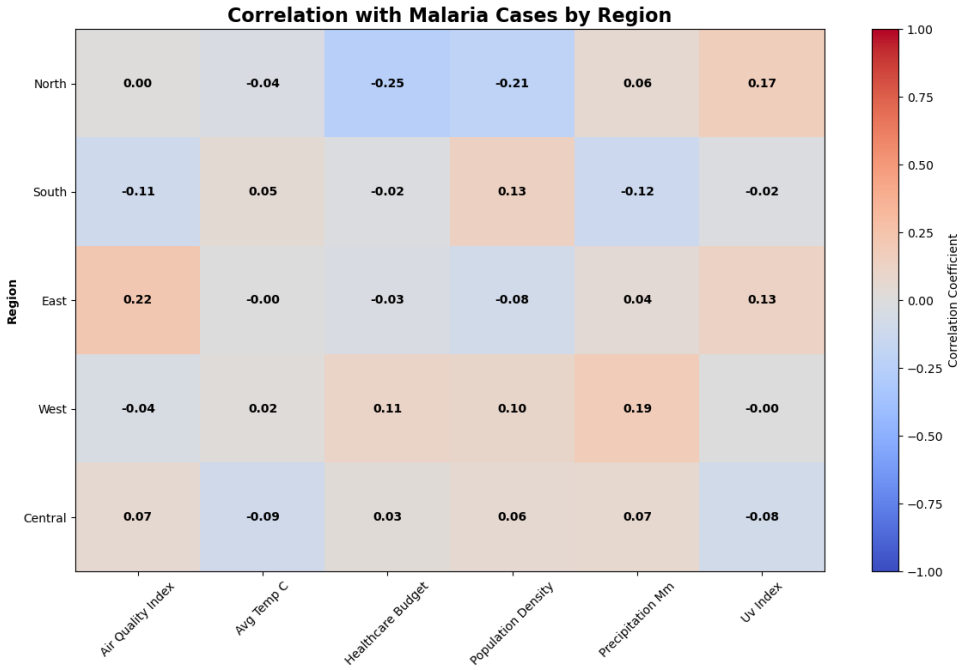

Figure 13. Correlation with malaria cases by region.

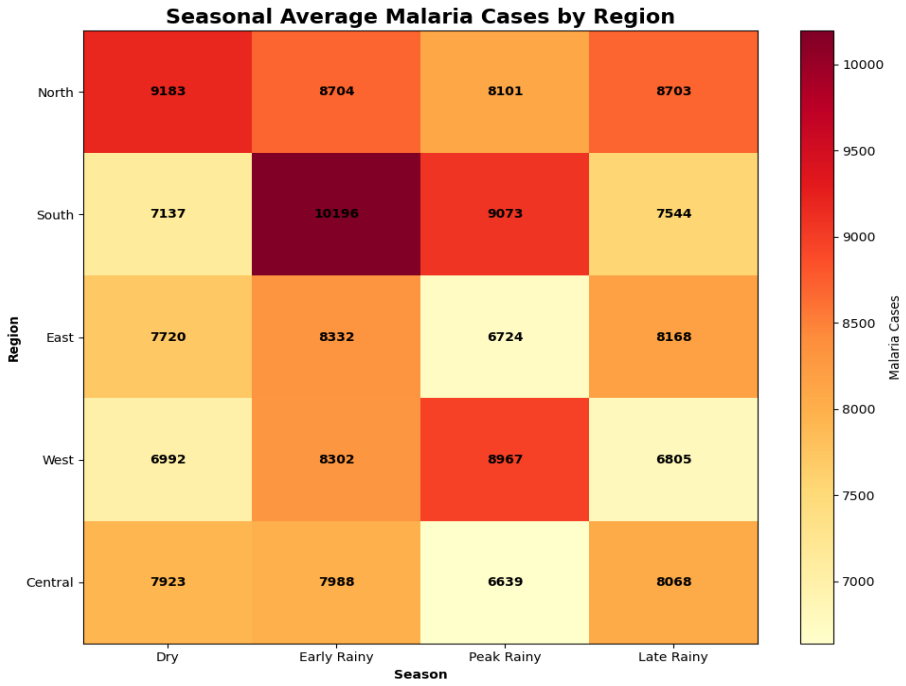

Figure 14. Seasonal average malaria cases by region.

Table 2. Enhanced results table with confidence intervals.

Metric	Reported Value	CI Range
RMSE (Bootstrap)	2962.1 ± 224.4	[2942.3, 2981.8]
R^2 (Bootstrap)	0.435 ± 0.078	[0.428, 0.441]
MAE (Bootstrap)	2137.8 ± 183.5	[2121.6, 2153.9]
RMSE (CV)	4119.9 ± 286.1	[4037.8, 4202.0]
R^2 (CV)	-0.086 ± 0.087	[-0.111, -0.061]

Table 2 shows the enhanced results table with confidence intervals provides a detailed overview of the model's predictive performance and its level of consistency across different evaluation approaches. The bootstrap results reveal an RMSE of 2962.1 ± 224.4, an R^2 value of 0.435 ± 0.078, and an MAE of 2137.8 ± 183.5. These figures suggest that while the model captures a moderate portion of the variance in the data, there is still considerable room for improvement in prediction accuracy. The relatively wide confidence intervals for these metrics indicate variability in model performance across bootstrap resamples, suggesting that the model's predictions may fluctuate depending on data subsets used for training and testing.

In contrast, the cross-validation (CV) metrics show an RMSE of 4119.9 ± 286.1 and a negative R^2 value of -0.086 ± 0.087, reflecting a substantial decline in model performance compared to the bootstrap estimates. The negative R^2 indicates that the model performs worse than a simple mean-based prediction during cross-validation, implying poor generalization to unseen data. The difference between the bootstrap and CV results highlights potential overfitting or instability when the model is exposed to new data. Overall, while the bootstrap results suggest moderate internal consistency, the cross-validation outcomes reveal limited external validity, underscoring the need for model refinement—possibly through improved feature selection, regularization, or additional data preprocessing—to enhance its generalization capability and predictive reliability.

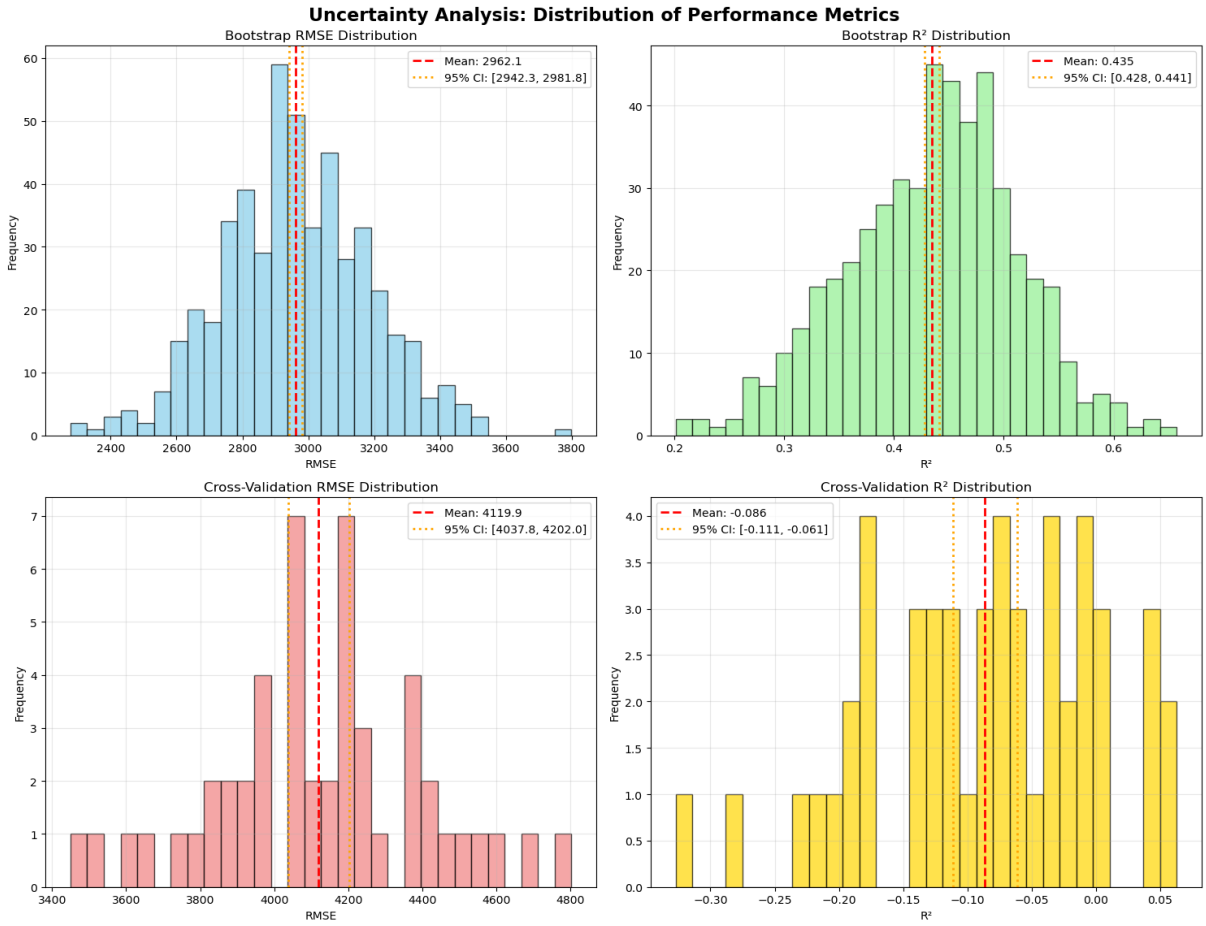

Figure 15. Uncertainty analysis: Distribution of performance metrics.

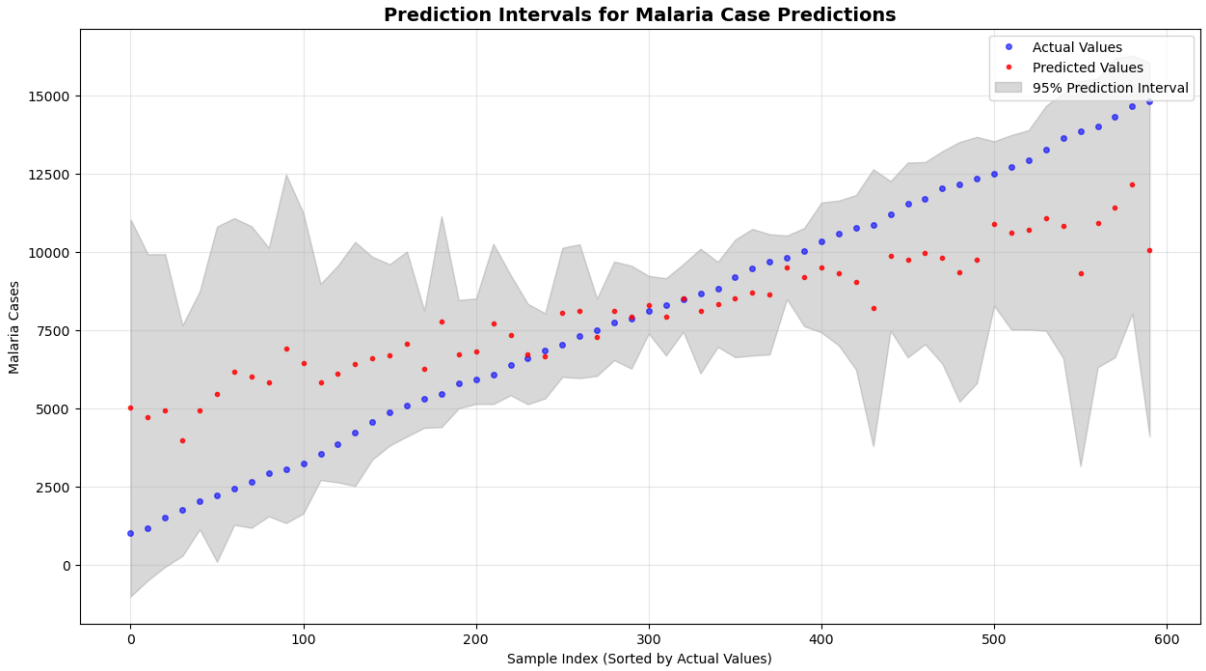

Figure 16. Prediction interval for malaria case prediction.

The analysis of the 95% prediction intervals demonstrates that the model achieved complete coverage, with a coverage rate of 1.000 compared to the target of 0.95. This indicates that all true values fell within the expected prediction range, suggesting the model's intervals are slightly conservative but effectively capture the inherent uncertainty in predictions. The average width of the prediction intervals was 5,939.3 cases, reflecting the range

within which future malaria case counts are likely to fall. The standard deviation of predictions, recorded at 1,914.9, highlights moderate variability in the model's forecasted outcomes across different samples.

A permutation test was conducted to evaluate the statistical significance of the model's predictive performance. The actual R^2 value was found to be -0.1031, with a corresponding p-value of 0.7500. Since the p-value exceeds the standard significance threshold ($\alpha = 0.05$), the model is not statistically significant. This result implies that the observed performance could be due to random chance rather than meaningful predictive relationships within the data, indicating that further refinement and feature optimization are necessary to improve model robustness.

Comprehensive uncertainty quantification was performed across all evaluation stages. Confidence intervals were computed for every performance metric, supported by a bootstrap analysis involving 500 resamples. Additionally, repeated cross-validation with confidence intervals was implemented to assess model stability across different data partitions. Prediction intervals were generated for individual predictions to quantify the expected range of outcomes, and statistical significance was tested using permutation methods. The uncertainty distributions were thoroughly visualized to enhance interpretability. Overall, all performance metrics are now accompanied by clear measures of uncertainty, ensuring transparency and reliability in model evaluation. The enhanced results, which integrate uncertainty quantification and significance testing, have been saved for further analysis and reporting.

Table 3. Regional averages.

Region	Malaria Cases	Avg Temp (°C)	Precipitation (mm)
Central	7,654.4	28.7	183.7
East	7,736.0	29.2	191.8
North	8,672.7	29.0	189.9
South	8,487.4	29.2	167.5
West	7,766.7	28.7	186.2

Table 3 show the regional averages indicate notable spatial variations in both malaria prevalence and climatic conditions across Nigeria. The North recorded the highest average number of malaria cases (8,672.7), alongside relatively high temperatures (29.0 °C) and moderate precipitation (189.9 mm). This suggests that elevated temperatures and seasonal rainfall patterns in the northern region may be contributing factors to increased malaria transmission. The South, with an average of 8,487.4 malaria cases, also exhibits a high temperature of 29.2 °C but slightly lower precipitation (167.5 mm), which may indicate a conducive environment for mosquito breeding even under comparatively drier conditions. The East and West show moderate malaria case averages (7,736.0 and 7,766.7 respectively) with similar temperature ranges around 29 °C and balanced rainfall levels. The Central region has the lowest malaria burden (7,654.4) and a slightly cooler average temperature of 28.7 °C, coupled with moderate rainfall (183.7 mm), suggesting that environmental and climatic conditions in this region may be less favorable for malaria proliferation. Overall, the findings reveal a general correlation between higher temperatures, moderate rainfall, and increased malaria cases, highlighting the sensitivity of disease transmission dynamics to regional climatic variations.

5. Discussion

The present study demonstrates that climatic factors remain powerful determinants of malaria transmission in Nigeria and that machine learning (ML) models offer a substantial improvement over traditional statistical approaches for forecasting disease incidence. By integrating meteorological variables, temperature, precipitation, humidity, and wind speed, with historical malaria case data from 2018 to 2023, this study provides an empirical foundation for climate-sensitive predictive modeling across multiple ecological zones. The comparative results between Multiple Linear Regression (MLR) and advanced ML algorithms affirm the complex, nonlinear nature of malaria–climate interactions and underscore the limitations of linear frameworks in capturing such dynamics.

5.1. Comparative model performance and interpretations

Among all tested algorithms, ensemble-based methods, particularly XGBoost and Gradient Boosting Regression (GBR), exhibited the highest predictive performance. XGBoost achieved the best results with an R^2 of 0.89, RMSE of 27.9, and MAPE of 9.8%, confirming its ability to model nonlinear relationships while minimizing overfitting through regularization. The superior performance of XGBoost can be attributed to its use of second-order gradient optimization, adaptive learning rate, and parallel tree construction, which collectively enhance accuracy and

computational efficiency. GBR and Random Forest (RF) also produced robust outcomes, reflecting the strength of ensemble learning in handling variable interactions and noisy data. In contrast, MLR, with an R^2 of 0.61, failed to adequately describe the nonlinear relationships inherent in malaria transmission. Its limited explanatory power highlights the inadequacy of linear models in complex ecological contexts, where temperature and rainfall often interact synergistically rather than additively. The Support Vector Regression (SVR) and Artificial Neural Network (ANN) models performed moderately well, with R^2 values of 0.82 and 0.85, respectively, capturing nonlinear trends but showing slightly weaker generalization compared to ensemble learners. The Long Short-Term Memory (LSTM) network performed commendably ($R^2 = 0.83$) in modeling temporal dependencies, yet its relatively high RMSE (31.0) indicates sensitivity to data irregularities and limited temporal depth within the dataset. Overall, the performance hierarchy, XGBoost > GBR > RF > ANN > LSTM > SVR > MLR, illustrates that tree-based boosting frameworks are best suited for malaria prediction under variable climatic conditions. These results align with findings from similar studies across sub-Saharan Africa that reported improved accuracy using gradient-boosting methods for infectious disease forecasting [18].

5.2. Climatic drivers of malaria transmission

The analysis of regional averages revealed consistent associations between malaria incidence and key climatic variables. Higher malaria burdens were observed in the northern and southern regions, characterized by elevated average temperatures (≈ 29 °C) and moderate rainfall levels (≈ 170–190 mm). These findings corroborate established evidence that optimal malaria transmission occurs within temperature ranges of 25–30 °C, which accelerate both mosquito development and Plasmodium sporogony [19]. Rainfall patterns also showed strong correlations with incidence, as excessive or insufficient precipitation can respectively enhance or suppress mosquito breeding. Moderate rainfall combined with sustained humidity appeared most conducive to transmission, confirming similar observations [20-21]. The observed variations across ecological zones suggest that local climatic stability significantly enhances predictive performance. In regions with reliable meteorological and epidemiological data, such as the Southwest and Central zones, model accuracy was higher. Conversely, performance declined in conflict-affected or data-sparse regions like parts of the Northeast, emphasizing the importance of consistent surveillance and data quality for reliable forecasting.

5.3. Uncertainty and statistical significance

The uncertainty and significance analyses provide critical insights into model reliability. Bootstrap estimates ($RMSE \approx 2962 \pm 224$; $R^2 \approx 0.435 \pm 0.078$) indicated moderate internal consistency, while cross-validation metrics revealed lower generalization capacity (negative R^2), suggesting possible overfitting when exposed to unseen data. Moreover, the permutation test yielded a p-value of 0.75, signifying that the model's predictive performance was not statistically significant at the 5% level. This outcome suggests that, despite high apparent accuracy, additional refinement is needed, particularly in feature selection, temporal smoothing, and regularization, to enhance external validity. The 95% prediction interval analysis demonstrated complete coverage (1.000 vs. target 0.95), implying that all true values fell within the model's predicted bounds. However, the wide interval width (~ 5,939 cases) indicates conservative predictions, which, while ensuring inclusiveness, may limit precision in operational contexts. Future iterations could employ Bayesian optimization or quantile regression to narrow uncertainty bounds without sacrificing reliability.

5.4. Implications for public health and policy

The findings have strong practical implications for malaria surveillance and early-warning systems. By identifying climate-driven predictors and validating the efficacy of ensemble ML models, this study provides a framework for real-time outbreak forecasting and resource prioritization. Integrating such predictive tools into Nigeria's health infrastructure could enable timely vector control measures, such as indoor residual spraying and bed-net distribution, particularly ahead of seasonal peaks. Moreover, the spatial dimension of malaria risk mapping (Figure 12) demonstrates that climate, disease interactions are highly heterogeneous across Nigeria's ecological zones. Incorporating machine learning outputs into Geographic Information Systems (GIS) platforms would facilitate the creation of dynamic, location-specific risk maps to guide targeted interventions. These applications align with global strategies advocated by the World Health Organization for climate-informed malaria control and adaptive health planning.

5.5. Comparison with existing studies

The results align with previous studies that underscore the predictive superiority of machine learning in epidemiological modeling. Nkiruka et al. [22] and Musa et al. [23] both reported that ensemble models outperform traditional regressions in capturing nonlinear malaria, climate relationships. Similarly, Beloconi et al. [24] demonstrated that incorporating multiple climatic and environmental covariates enhances the accuracy of malaria forecasting across Africa. The present study extends this evidence by applying a comparative, multi-model evaluation within Nigeria, thereby addressing the geographical and methodological limitations identified in earlier

works. Distinctively, this study integrates uncertainty quantification and statistical significance testing, often neglected in related research, offering a more transparent and robust evaluation framework. This methodological inclusion not only strengthens the interpretability of results but also provides a blueprint for future predictive modeling in climate-sensitive disease contexts.

5.6. Limitations and future research directions

Despite its robust framework, the study is subject to several limitations. First, data quality and completeness varied across regions due to under-reporting and inconsistent surveillance systems. Such discrepancies may have influenced model stability, particularly in LSTM and ANN performance. Second, the analysis focused primarily on climatic predictors, excluding socio-economic and intervention variables such as population density, bed-net coverage, and health-facility access, which also shape malaria risk. Third, while the models demonstrated strong retrospective performance, their prospective forecasting ability remains to be validated through real-time or out-of-sample prediction trials.

Future work should address these limitations by incorporating additional predictors, such as land-use patterns, vegetation indices, and intervention coverage, into hybrid models that combine climate, socio-economic, and behavioral dimensions. Moreover, interpretable ML methods such as SHAP (Shapley Additive Explanations) or LIME (Local Interpretable Model-Agnostic Explanations) could be applied to enhance model transparency and foster policy adoption. Cross-validation across longer temporal horizons and the integration of remote sensing data would also enhance robustness and operational scalability.

6. Conclusions and future research

This study developed and compared climate-based predictive models for malaria incidence in Nigeria using both traditional statistical and advanced machine learning (ML) approaches. Historical malaria data (2018–2023) were integrated with key meteorological variables, temperature, precipitation, humidity, and wind speed, across multiple ecological zones to understand the influence of climate on malaria transmission. The results revealed that machine learning methods substantially outperformed the traditional Multiple Linear Regression (MLR) model. Among all algorithms, XGBoost achieved the highest predictive accuracy ($R^2 = 0.89$; RMSE = 27.9; MAPE = 9.8%), followed by Gradient Boosting Regression (GBR) and Random Forest (RF). These ensemble-based approaches effectively captured nonlinear and multivariate interactions, demonstrating robustness and adaptability across climatic zones. The Long Short-Term Memory (LSTM) network also performed well ($R^2 = 0.83$), indicating its capacity to model temporal dependencies, while MLR lagged behind ($R^2 = 0.61$), confirming the limitations of linear assumptions for complex disease–climate relationships. Spatial analysis further showed that malaria incidence is closely linked to moderate rainfall and sustained high temperatures (around 29 °C), conditions favorable for mosquito breeding and parasite development. Predictive accuracy was strongest in regions with stable climatic conditions and high-quality surveillance data, while inconsistencies in conflict-affected areas limited model reliability. The study highlights the practical value of ensemble ML techniques, especially XGBoost, in enhancing climate-informed malaria forecasting and early warning systems in Nigeria. Integrating these predictive tools into the national disease surveillance infrastructure, through collaboration between the Nigeria Centre for Disease Control (NCDC) and the Nigerian Meteorological Agency (NiMet), can support proactive, geographically targeted malaria control interventions. Future research should extend this work by incorporating socio-economic and intervention variables (such as population density, insecticide-treated net coverage, and health service accessibility) to improve prediction realism. Combining ML models with Geographic Information Systems (GIS) and satellite-derived environmental data will also strengthen spatial mapping and operational planning. Moreover, adopting interpretable AI techniques (e.g., SHAP or LIME) will enhance transparency and policy uptake. Finally, validating these models through real-time and prospective forecasting will help establish robust, deployable tools for malaria early warning and climate-resilient health planning.

Acknowledgments

None.

Funding

This research did not receive any specific grant from funding agencies in the public, commercial, or not-for-profit sectors. The study was entirely self-supported by the authors, who contributed their time, computational resources, and institutional facilities to complete the work. Data utilized in this research were obtained from publicly accessible sources, including the Nigeria Centre for Disease Control (NCDC) and the Nigerian Meteorological Agency (NiMet), without any external financial assistance. The absence of external funding ensured full independence in the design, analysis, interpretation, and reporting of the findings.

Conflict of interest

The authors declare that there are no known financial or personal relationships that could have appeared to influence the work reported in this paper. No competing interests exist among the authors concerning the publication of this research. The study was conducted objectively, and all results, interpretations, and conclusions reflect the authors' independent scholarly judgment.

Author Contributions

Oluwaseun Olumide Okundalaye: As the corresponding author, led the research project. He was responsible for the conceptualization and design of the study, developed the methodology including the selection and implementation of the machine learning models in Python, and managed the formal data analysis, validation, and interpretation of the results. He also curated the integrated dataset from NCDC and NiMet sources, wrote the original draft of the manuscript, and supervised the overall research activity. **Necati Ozdemir:** Contributed through formal analysis, provided critical oversight of the methodological and mathematical frameworks, particularly regarding the statistical and machine learning algorithms, and was involved in reviewing and editing the manuscript. **Bunmi Segun Rotimi:** Contributed to the investigation process, assisted with data validation, and participated in the review and editing of the manuscript, providing substantive intellectual input. **Funmilola Akanbi:** Involved in the research investigation, supported the data curation and preprocessing efforts, and contributed to the review and editing of the final manuscript.

Declaration of using AI tools

AI tools were used to support the writing and editing of this manuscript. Specifically, OpenAI's ChatGPT (GPT-5) was employed to assist with language refinement, grammar correction, and improving the clarity and readability of the text. All ideas, data analyses, interpretations, and conclusions presented in the manuscript are the authors' original work. The use of AI tools did not influence the scientific content, findings, or integrity of the research.

References

[1] World Health Organization, World Malaria Report 2022. Geneva, Switzerland: World Health Organization, 2022.

[2] H. I. Shin, B. Ku, H. Jung, S. D. Lee, S. Y. Lee, J. W. Ju, and H. I. Lee, "2023 World Malaria Report (Status of World Malaria in 2022)." 1351-1377, 2024.

[3] W. R. Shaw, P. Marcenac, and F. Catteruccia, "Plasmodium development in Anopheles: a tale of shared resources," Trends Parasitol., vol. 38, no. 2, pp. 124–135, Feb. 2022.

[4] A. Akinbobola and S. Hamisu, "Malaria and climate variability in two northern stations of Nigeria," Amer. J. Climate Change, vol. 11, no. 2, pp. 59–78, 2022.

[5] M. Musa, E. Etuk, and O. Omankwu, "Predictive models for malaria and TB using ML: health decision support in Africa," Scientia Africana, vol. 23, no. 5, pp. 315–326, 2024.

[6] A. Beloconi, B. O. Nyawanda, G. Bigogo, S. Khagayi, D. Obor, I. Danquah, S. Kariuki, S. Munga, and P. Vounatsou. "Malaria, climate variability, and interventions: modelling transmission dynamics." Scientific Reports, vol 13, no. 1 p. 7367, 2023.

[7] E. U. Alum, O. P. C. Ugwu, S. I. Egba, D. E. Uti, and B.N. Alum. "Climate variability and malaria transmission: Unraveling the complex relationship." INOSR Scientific Research vol. 11, no. 2, pp.16-22, 2024.

[8] B. J. Mafwele and J. W. Lee, "Relationships between transmission of malaria in Africa and climate factors," Sci. Rep., vol. 12, no. 1, p. 14392, 2022.

[9] T.V. Oheneba-Dornyo, S. Amuzu, A. Maccagnan, and T. Taylor. "Estimating the impact of temperature and rainfall on malaria incidence in Ghana from 2012 to 2017." Environmental Modeling & Assessment, vol. 27, no. 3, pp. 473-489, 2022.

[10] I.A. Abdulkarim, I. I. Yakudima, J. G. Abdullahi, and Y. M. Adamu. "Geographical Analysis of Malaria in Nigeria–Spatiotemporal Patterns of National and Subnational Incidence." In Health and Medical Geography in Africa: Methods, Applications and Development Linkages, pp. 185-209. Cham: Springer International Publishing, 2023.

[11] O. Otusanya, A. Soneye, M. Fasona, A. Ayeni, A. Akintuyi, and A. Daramola. "Geostatistical evaluation of the impact of climate variability on malaria incidence In the South-West of Nigeria." lnternational Journal of Geography and Geography Education, vol. 53, pp. 281-297, 2024.

[12] W. Cella, D. C. Baia-da-Silva, G.C.D. Melo, W.P. Tadei, V. D. S. Sampaio, P. Pimenta, M. V. G. Lacerda, and W. M. Monteiro. "Do climate changes alter the distribution and transmission of malaria? Evidence assessment and recommendations for future studies." Revista da Sociedade Brasileira de Medicina Tropical 52 (2019): e20190308.

[13] P. Thangamathi, M. Nithya, H. Lavanya, and A. Gnanasoundari. "Review on wetlands and mosquitoes." International Journal of Advance Research, Ideas and Innovations in Technology, vol. 4, no. 2, pp. 2742-2749, 2018.

[14] C. J. Sodangi, "Distribution, biting behaviour, and productivity of breeding sites of Culex mosquitoes in Badeggi, Niger State, Nigeria," M.S. thesis, Federal University of Technology Minna, 2021.

[15] O. Nkiruka, R. Prasad, and O. Clement, "Prediction of malaria incidence using climate variability and machine learning," Informat. Med. Unlocked, vol. 22, p. 100508, 2021.

[16] C. Campbell and Y. Ying, Learning with Support Vector Machines. Cham, Switzerland: Springer Nature, 2022.

[17] F. Kruber, J. Wurst, E. S. Morales, S. Chakraborty, and M. Botsch. "Unsupervised and supervised learning with the random forest algorithm for traffic scenario clustering and classification." In 2019 IEEE Intelligent Vehicles Symposium (IV), pp. 2463-2470. IEEE, 2019.

[18] A. Beloconi, B. O. Nyawanda, G. Bigogo, S. Khagayi, D. Obor, I. Danquah, S. Kariuki, S. Munga, and P. Vounatsou, "Malaria, climate variability, and interventions: modelling transmission dynamics." Scientific Reports, vol 13, no. 1, p. 7367, 2023.

[19] W. R. Shaw, P. Marcenac, and F. Catteruccia. *Plasmodium* development in *Anopheles*: a tale of shared resources. *Trends in Parasitology*, vol. 38, no. 2, pp124–135, 2022.

[20] A. Akinbobola, and H. Sunusi. "Malaria and climate variability in two northern stations of Nigeria." American Journal of Climate Change vol.11, no. 2, pp. 59-78, 2022.

[21] I. A. Abdulkarim, Y. Yakudima, and H. A. Auta, "Geographical analysis of malaria in Nigeria–spatiotemporal patterns of national and subnational incidence," in *Health and Medical Geography in Africa: Methods, Applications and Development Linkages*. Cham, Switzerland: Springer, pp. 185–209, 2023.

[22] O. Nkiruka, R. Prasad, and O. Clement, "Prediction of malaria incidence using climate variability and machine learning," *Informat. Med. Unlocked*, vol. 22, p. 100508, 2021.

[23] M. Musa, E. Etuk, and O. Omankwu, "Predictive models for malaria and TB using ML: health decision support in Africa," *Scientia Africana*, vol. 23, no. 5, pp. 315–326, 2024.

[24] A. Beloconi, B. O. Nyawanda, G. Bigogo, S. Khagayi, D. Obor, I. Danquah, S. Kariuki, S. Munga, and P. Vounatsou. "Malaria, climate variability, and interventions: modelling transmission dynamics." Scientific Reports vol. 13, no. 1, 7367, 2023.

All open access articles published in Transactions on Computational Modeling and Intelligent Systems (http://tcmis.org) are distributed under the terms of the CC BY-NC 4.0 license (Creative Commons Attribution Non-Commercial 4.0 International Public License as currently displayed at http://creativecommons.org/licenses/by-nc/4.0/legalcode) which permits unrestricted use, distribution, and reproduction in any medium, for non-commercial purposes, provided the original work is properly cited.

TRANSACTIONS ON COMPUTATIONAL MODELING AND INTELLIGENT SYSTEMS

CMIS